

https://dspace.org/

A quantitative analysis of alteration in the Carbon Leader Reef in the West Wits Line Goldfield: an application of Shortwave Infrared Reflectance Spectroscopy

Eliot, Adrienne

2020

https://hdl.handle.net/10539/31396

Downloaded from a DSpace repository. https://dspace.org/



UNIVERSITY OF THE
WITWATERSRAND,
JOHANNESBURG

A quantitative analysis of alteration in the Carbon Leader Reef in the West Wits Line Goldfield: An application of Shortwave Infrared Reflectance Spectroscopy

A thesis submitted to the Faculty of Science, University of the Witwatersrand, Johannesburg, in the fulfilment of the requirements for the degree of Master of Science

Adrienne Eliot

312624
ABEliot@AngloGoldAshanti.com

Supervisor: Professor Gillian Drennan; Gillian.Drennan@wits.ac.za; 011 717 6570
Co-supervisor: Professor Gordon Cooper; Gordon.Cooper@wits.ac.za; 011 717 6608

February 2020

Declaration

I declare that this dissertation is my own, unaided work. It is being submitted for the Degree of Master of Science at the University of the Witwatersrand, Johannesburg. It has not been submitted before for any degree or examination at any other university.

_____

Adrienne Brooke Eliot
Student # 312624

This _____ day of _____ 2020.

Acknowledgements

Foremost I would like to thank my two supervisors, Professor Gillian Drennan and Professor Gordon Cooper for their guidance and patience whilst undertaking my research over the past few years. It has been a long road to complete my postgraduate studies however it would not have been possible without their assistance.

AngloGold Ashanti Limited are thanked for providing data and samples, as well as for sponsoring the processing of samples used for this research. I would also like to extend my gratitude to Phil Harris and the team at TerraCore Geospectral Imaging, particularly to Khano Mushiana, who assisted with the processing of the spectral data as well as provided feedback and input on my spectral findings.

To my AngloGold Ashanti colleagues who worked with me at TauTona Mine prior to its closure in 2017, please know that it is because of you that I chose not to give up hope and to finish my thesis. TauTona Mine will always be a soft spot for me, and the extended family I gained from working there is irreplaceable. To Caroline Pienaar and Tarryn Flitton, thank you for your input and advice whilst finishing up my research. All those coffee breaks at the office seem worth it now.

Finally, I would like to thank my family as well as my husband for their love and support. Mom, you inspire me to always be better and challenge myself. This thesis was probably my biggest challenge yet but with your constant support and bribery with G&Ts at the end of a long day, I can finally say that I have done it! To dad and James, thank you for making things easier by just being you. Laughter really is the best medicine and without it, I would have been very lost. To my husband, Christiaan, thank you for being my “rock” in uncertain times. You have been my biggest cheerleader whilst I’ve been completing my thesis, and for this I am forever grateful. Now you can watch TV with the sound on again…

Abstract

Alteration within the Witwatersrand Basin has been of great interest and widely researched for many years with a focus on depositional and post-depositional processes that lead to the occurrence of the alteration. Numerous methodologies are used to investigate alteration of orebodies globally however hyperspectral scanning is a relatively new methodology that is gradually being introduced to determine the mineralogical characteristics of borehole core and hand specimens. Spectral scanning is quicker than using conventional and time-consuming methods such as petrological studies and geochemical analyses.

A quantitative analysis of alteration within the Carbon Leader Reef in the AngloGold Ashanti West Wits Line Goldfield was carried out using several methodologies including macroscopic observations, petrology, geochemical analyses, gold assay as well as shortwave infrared reflectance spectroscopy (hyperspectral scanning). These methodologies were undertaken to better understand alteration and the associated gold grade across the West Wits Line (comprising Savuka Mine in the west, TauTona Mine in the east and Mponeng Mine south of Savuka and TauTona Mines). The immediate overlying hangingwall and underlying footwall units were also investigated.

A comparison of the methodologies confirmed that more than one alteration event has occurred. This was noticeable in thin section and was verified by means of spectral scanning. A combination of rounded grains including gold, pyrite, chromite, uraninite and zircon were noted throughout the Carbon Leader Reef as well as within the hangingwall/footwall units and were suggestive of a detrital origin. Euhedral grains of tourmaline and pyrite were noted in a few of the reef samples representative of the north-east to central areas of the West Wits Line. Euhedral pyrite grains were seen in samples where pyrite had recrystallised and developed on the outer edges of a pre-existing detrital pyrite grain. Rounded to sub-rounded inclusions of gold and chalcopyrite within euhedral pyrite grains were also observed in thin section, suggestive of a secondary origin for the recrystallised pyrite, gold and chalcopyrite. Rutile that has undergone hydrothermal alteration results in the forming of leucoxene. Anhedral to

euhedral grains of leucoxene were noted throughout the Carbon Leader Reef samples, further confirming that (secondary) hydrothermal alteration has taken place.

Carbon (masses/flyspeck) was often noted to occur within the reef associated with leucoxene and rutile, and in a few samples associated with detrital gold and uraninite. Carbon was also noted to occur, infilling fractures or veinlets within uraninite grains. The close association of carbon with detrital uraninite grains suggests remobilisation of carbon has occurred. Carbon infilling fractures within uraninite grains suggests the carbon was introduced after the deposition of the uraninite grains.

The spectral scanning data revealed variations in the alteration mineralogy. In most of the samples there was a dominant alteration mineral, with lesser amounts of different alteration products cross-cutting each facies type. This suggested that the alteration involved complex processes, possibly related to multiple injections of fluid phases during post-depositional fluid fluxes through the sedimentary package. This also suggested that several hydrothermal fluid (alteration) events may have taken place to alter the mineralogy of the host rock over a period of time. The rounded clasts within the samples suggest transportation from a source area has occurred. Following deposition, several pulses of hydrothermal fluids through time altered the mineralogy of the host rock, allowing for the formation of secondary mineral phases such as rutile, tourmaline and recrystallised pyrite.

At the AngloGold Ashanti West Wits Line, a Carbon Leader Reef facies model based on three facies types (the No. 1 Facies, No. 2 Facies and No. 3 Facies) is used to differentiate between sedimentological variations as well as the occurrence of carbon within the Carbon Leader Reef. The facies model however does not provide much information on the mineralisation within the Carbon Leader Reef. As a result, the Carbon Leader Reef estimation domain model was developed and implemented by AngloGold Ashanti at its West Wits Line. The estimation domain model encompasses Carbon Leader Reef mineralogical characteristics, alteration mineralogy, sedimentology facies, structural influences as well as trend analyses with the variations of grade and channel width. The estimation domain model however does not account for the occurrence or absence of carbon within the Carbon Leader Reef. The current

research findings suggest that variations in the mineralogy of the Carbon Leader Reef do not align fully with the Carbon Leader Reef facies model nor with the Carbon Leader Reef estimation domain model.

A new Carbon Leader Reef facies model, specific to the West Wits Line, has been proposed to include a No. 3 Facies sub-type. The No. 3 Facies sub-type was based on samples that did not align fully with the No. 3 Facies definitions (i.e. samples with a thin basal carbon seam and/or higher than average gold grades of the No. 3 Facies). The samples used within this research also indicated that the TauTona, Driefontein and Peggy estimation domains need to be re-evaluated and revised on a continuous basis as more information becomes available.

Using the results from the various methodologies applied in this research, three major alteration zones have been identified based on alteration styles including: pyrophyllitic alteration, chloritisation and sericitic alteration. The pyrophyllitic alteration zone was based on pyrophyllite as a major alteration mineral and extended from the north-eastern to the southern portion of TauTona Mine. The chloritisation zone, based on a combination of chlorite and chloritoid as the major alteration minerals, extended across the West Wits Line from east to west. The sericitic alteration zone, based on sericitic muscovite as a major alteration mineral, exhibited was similar distribution range to that covered to the chloritisation zone, however, it extended further north-east and further south than the chloritisation zone.

The pyrophyllitic alteration zone was noted to coincide with the Pretorius Fault Zone. The zone of chloritisation was noted to coincide with frequent, smaller faults and fewer intrusions, and the sericitic alteration zone was noted to coincide with a frequent occurrence of intrusions with lesser faults. Based on geothermometric techniques, an estimated timeline for alteration was proposed. It was suggested that the Pretorius Fault Zone pre-dates the occurrence of the smaller and more frequent faulting events with fewer intrusions. The youngest events correspond to abundant intrusions associated with lesser faulting. Overall, this suggested that the intrusions are younger than the faults across the West Wits Line, with the Pretorius Fault Zone having occurred before the smaller faults and associated intrusions.

Spectral scanning was able to assist in determining alteration within the host rock as reliably as petrological and geochemical analyses. However, spectral scanning could not accurately predict gold grade within the Carbon Leader Reef or the hangingwall and footwall units. Spectral scanning presents accurate results, and this contributes to the easy identification of sedimentological contacts where macroscopic observations are not as obvious. Analysis of the alteration within the Carbon Leader Reef, as well as the hangingwall and footwall units, showed that there was very little correlation between alteration type and the associated gold grade. The presence of organic matter (i.e. carbon) in samples is commonly noted to affect the spectral scanning outcomes. Additional research should be carried out using a reef, such as the Ventersdorp Contact Reef, that is non-carbon bearing to determine if there is a correlation between alteration type and associated gold, where the presence of carbon cannot influence the alteration readings of the spectral scans.

The presence of carbon and/or uraninite within the host rock, however, was a consistent indicator for the presence of gold grade. Based on these results, it could be concluded that favourable gold grade is independent of the type of alteration and is more dependent on the presence of carbon and/or uraninite within the host rock.

Table of Contents

DECLARATION ..... **i**
ACKNOWLEDGEMENTS ..... **ii**
ABSTRACT ..... **iii**

LIST OF FIGURES **3**
LIST OF TABLES **12**
LIST OF APPENDICES **18**
LIST OF ABBREVIATIONS **19**

1 INTRODUCTION **20**
1.1 LOCATION OF THE RESEARCH AREA 22
1.2 GEOLOGY OF THE RESEARCH AREA 23
1.3 THE WITWATERSRAND BASIN 24
1.3.1 Gold Mineralisation 24
1.3.2 Tectonic Setting 26
1.3.3 Mineralogy and Alteration 27
1.4 LOCAL STRATIGRAPHY 28
1.5 THE CARBON LEADER REEF 30
1.6 REFLECTANCE SPECTROSCOPY 35
1.6.1 Introduction to the Reflectance Spectroscopy of Minerals 35
1.6.2 Short-wave Infrared Spectroscopy 36
1.6.3 Case Studies 42
1.7 AIMS 44
1.8 OBJECTIVES 44

2 METHODOLOGY **46**
2.1 MACROSCOPIC OBSERVATIONS AND PHOTOGRAPHY 48
2.2 PETROLOGY 50
2.3 GEOCHEMICAL ANALYSES 50
2.4 GOLD ASSAY 51
2.5 SPECTRAL SCANNING AND PROCESSING OF BOREHOLES AND TOMBSTONES 52
2.6 GEOLOGICAL MODELLING 64

3 RESULTS 64
3.1 MACROSCOPIC OBSERVATIONS 64
3.1.1 Hangingwall Descriptions 65
3.1.2 Footwall Descriptions 67
3.1.3 Carbon Leader Reef Descriptions 70
3.1.4 Discussion 81
3.2 PETROGRAPHIC OBSERVATIONS 86
3.2.1 Hangingwall Descriptions 86
3.2.2 Footwall Descriptions 92
3.2.3 Carbon Leader Reef Descriptions 97
3.2.4 Discussion 107
3.3 GEOCHEMICAL & GOLD ASSAY ANALYSES 115
3.3.1 Geochemical & Gold Assay Results (Hangingwall & Footwall samples) 115
3.3.2 Geochemical & Gold Assay Results (Carbon Leader Reef samples) 123
3.3.3 Discussion 145
3.4 SPECTRAL SCANNING OBSERVATIONS 151
3.4.1 Spectral Scanning Results (Tombstone samples) 152
3.4.2 Spectral Scanning Results (Borehole samples) 162
3.4.3 Discussion 173
3.5 GEOLOGICAL MODELLING OF THE CARBON LEADER REEF 177
3.5.1 Alteration Models of the Carbon Leader Reef 177
3.5.2 Discussion 185
4 INTEGRATIVE DISCUSSION 191
5 CONCLUSION 210
6 RECOMMENDATIONS 212
7 REFERENCES 214
8 APPENDICES 221

LIST OF FIGURES

Figure 1.1: A geological representation of the location of the research area on the Witwatersrand Basin (encircled) (Dankert and Hein, 2010). 23

Figure 1.2: A stratigraphic column of the Witwatersrand Supergroup (modified after Guy et al., 2010). 29

Figure 1.3: Graphical representation of the Carbon Leader Reef facies types across the AngloGold Ashanti West Wits Line (In-house Report, 2017). 31

Figure 1.4: Schematic diagram of the Carbon Leader Reef facies model proposed by Fletcher (2009) (adapted from In-house Report, 2008). 32

Figure 1.5: Carbon Leader Reef estimation domain model comprising the Savuka, Blyvooruitzicht, Peggy, TauTona and Driefontein estimation domains. The various domains are separated by red lines and the gold value in cm.g/t is colour-coded (warmer colours/shades of red indicate higher gold values, and the cooler colours/shades of blue indicate lower gold values, Burnett et al., 2015). 33

Figure 1.6: The electromagnetic spectrum showing the varying spectral ranges (modified after Kerr et al., 2011). 35

Figure 1.7: (a) An absorption feature in a kaolinite short-wave infrared spectrum; (b) A zoomed-in view of the feature (modified after Thompson et al. (1999)). 38

Figure 1.8: A plot of a known spectrum and an image spectrum (modified after Kruse et al., 1993; Harris Geospatial Solutions, 2018b). 40

Figure 1.9: A stacked plot of spectra representing different minerals. Chlorite and pyrophyllite are two minerals of interest for the purpose of this research (Kerr et al., 2011). 41

Figure 1.10: A stacked plot of spectra representing Fe-rich clinochlore and Mg-rich clinochlore. Note the steeper slope of the Fe-rich spectrum from 1 300 to 1 900 nm (Thompson et al., 1999). 42

Figure 1.11: (a) Map showing sample location as well as the main alteration mineral found within each sample; (b) Map showing the two main alteration types in the area (taken from Crósta, 2010). 43

Figure 2.1: (a) the sisuROCK® was used to spectrally scan a total of 36 boreholes (Specim Spectral Imaging Ltd., 2015); (b) the TerraSpec® was used to spectrally scan a total of 18 tombstones (Malvern Panalytical Ltd., 2019). . 52

Figure 2.2: Examples of image outputs (from a left (L) to right (R) direction) generated for the Red-Green-Blue camera and spectral data: (a) Natural colour image; (b) Enhanced infrared image; (c) Spectral facies image; (d) Spectral index image (Adapted from Harris, 2006b, p.158) 55

Figure 2.3: Mean depth spectral profiles against the pyrophyllite, sericite, chlorite and chloritoid feature extractions. Sample 22 is used above, where the spectral profiles for the Brown-Orange Argillaceous Zone (BOAZ), No. 2A and No. 2B Facies, Pale Pebbly Quartzite (PPQ) and footwall (FW) are seen. A borehole log to show the relative depth of the borehole and the sedimentological unit(s) underlies the spectral profiles. 63

Figure 3.1: Close-up of the cubic pyrite (py) grains and pyrite stringers seen in the easternmost areas at TauTona Mine within the hangingwall (HW) quartzite. Floating clasts of chert (cht) and quartz (qtz) were also noted within the hangingwall quartzite – Sample 20. 65

Figure 3.2: Greenish discolouration (area of possible chloritisation) of the hangingwall (HW) quartzite closer to the No. 1 Facies-hangingwall contact. Pyrite (py) on foresets was seen in between bedding-parallel bluish-grey bands in the hangingwall quartzite – Sample 28. 65
Figure 3.3: (a) A 14 mm thick quartz (qtz) vein cutting the hangingwall (HW) quartzite. The vein was truncated at the No. 1 Facies upper contact with the hangingwall quartzite and did not extend to the footwall (FW) quartzite – Sample 5; (b) Scattered clasts (poor pebble lag) in the hangingwall quartzite proximal to the No. 1 Facies contact – Sample 14. 66
Figure 3.4: An under-developed pebble lag comprising various quartz (qtz) clasts above the No. 2B Facies contact within the hangingwall (HW) quartzite. Pyrite (py) along foresets was visible, as are small areas of possible chloritisation within the hangingwall quartzite – Sample 23. 66
Figure 3.5: (a) A poorly developed footwall pebble band (FWPB) in the footwall (FW) quartzite unit underlying the No. 1 Facies and hangingwall (HW) quartzite units – Sample 4; (b) A thin carbon seam separates the footwall quartzite and internal quartzite (IQ) units – Sample 12. 67
Figure 3.6: A poorly developed footwall pebble band (FWPB) hosting milky and smoky quartz (qtz) clasts alongside chert (cht) pebbles in the footwall (FW) quartzite unit. There was a noted colour variation in the footwall quartzite above and below the footwall pebble band – Sample 20. 68
Figure 3.7: Footwall pebble band (FWPB) with possible chloritisation of some milky quartz (qtz) clasts. Smoky quartz clasts as well as interstitial pyrite (py) was also noted within the footwall pebble band – Sample 20. 68
Figure 3.8: A well-developed footwall pebble band (FWPB) with predominantly smoky and milky quartz (qtz) clasts set within a dark greenish-grey matrix. Interstitial pyrite (py) occured between the clasts – Sample 34. 69
Figure 3.9: Angular chert (cht) clasts floating within a coarse-grained greenish-grey footwall (FW) quartzite. Very fine-grained rounded disseminated pyrite (py) grains were visible within the footwall quartzite – Sample 34. 69
Figure 3.10: Greenish-grey argillaceous footwall (FW) quartzite with small floating clasts of rounded smoky quartz (qtz) and elongated to angular chert (cht) – Sample 23. 70
Figure 3.11: Discolouration (darkening) of the footwall (FW) quartzite closer to the No. 2A Facies. Floating clasts of smoky quartz (qtz) are also noted within the footwall quartzite – Sample 44. 70
Figure 3.12: Floating chert (cht), smoky and milky quartz (qtz) clasts scattered across a gritty-textured footwall (FW) quartzite – Sample 48. 70
Figure 3.13: Matrix-supported No. 1 Facies overlying the footwall (FW) quartzite and underlying the hangingwall (HW) quartzite unit. The No. 1 Facies had an alternating dark grey and light grey matrix with varying sizes and types of quartz (qtz) clasts – Sample 24. 71
Figure 3.14: Matrix-supported No. 1 Facies with a siliceous internal quartzite (IQ) and an underlying carbon seam, separating the reef package from the footwall (FW) quartzite. A 5 mm thick quartz vein (QV) was seen cutting the hangingwall (HW) quartzite overlying the reef package – Sample 32. 72

Figure 3.15: Matrix-supported No. 1 Facies with possible chloritisation overlying the footwall (FW) quartzite unit. The hangingwall (HW) was seen draping over the underlying clasts of the reef package – Sample 33..... 73
Figure 3.16: (a) Carbon Leader Reef No. 2 Facies overlying the footwall (FW) quartzite with distinct No. 2A and No. 2B Facies flanking either side of the Pale Pebbly Quartzite (PPQ). Overlying the No. 2B Facies was a Brown-Orange Argillaceous Zone (BOAZ) – Sample 2; (b) No. 2A Facies intersection with overlying hangingwall (HW) quartzite – Sample 11. 74
Figure 3.17: No. 2B Facies with milky quartz (qtz) clasts and possibly a quartz clast that has undergone chloritisation, overlain by a Brown-Orange Argillaceous Zone (BOAZ) with pyrite (py) along foresets – Sample 31. 74
Figure 3.18: Greenish discolouration of the No. 2A Facies with possible chloritisation of some of the quartz (qtz) clasts. Rounded disseminated pyrite (py) grains occur interstitially between the quartz clasts – Sample 31. 75
Figure 3.19: Matrix-supported No. 2A Facies with interstitial disseminated pyrite (py) between milky and smoky quartz (qtz) clasts. The No. 2A Facies was overlain by a Pale Pebbly Quartzite (PPQ) with floating quartz clasts – Sample 22. 76
Figure 3.20: Pale Pebbly Quartzite (PPQ) intersection within the No. 2 Facies. The Pale Pebbly Quartzite had rounded disseminated grains of pyrite (py) as well as pyrite along foresets – Sample 35. 76
Figure 3.21: Alteration of the Pale Pebbly Quartzite (PPQ) within the No. 2 Facies package may be due to oxidation of sulphides. Occasional clasts of smoky and milky quartz (qtz) were seen within a pyrite lag – Sample 23. 76
Figure 3.22: Clast-supported No. 2B Facies flanked by a Pale Pebbly Quartzite (PPQ) and a Brown-Orange Argillaceous Zone (BOAZ) of quartzite. The discolouration within the No. 2B Facies may be due to oxidation of the sulphides within the core – Sample 23. 77
Figure 3.23: A Brown-Orange Argillaceous Zone (BOAZ) intersection of the No. 2 Facies package showing the variations in colour. Rounded disseminated pyrite (py) grains were seen within the quartzite – Sample 35. 77
Figure 3.24: A poorly developed intersection of the No. 3 Facies overlying the footwall (FW) quartzite. The No. 3 Facies had very fine-grained rounded pyrite along foresets. A slight discolouration was noted on the outer edges of the pyrite along foresets. The No. 3 Facies was overlain by the hangingwall (HW) quartzite – Sample 21..... 78
Figure 3.25: A close-up of the footwall (FW)-reef contact of the No. 3 Facies. Discolouration was noted on the edges of pyrite along foresets and may be due to oxidation of sulphides or chloritisation within the core – Sample 21. 79
Figure 3.26: A close-up of a thin carbon seam at the base of the No. 3 Facies, separating the footwall (FW) quartzite and the reef band. Fine grains of rounded disseminated pyrite (py) occurred within the carbon seam. Milky quartz (qtz) clasts were visible within the No. 3 Facies – Sample 25..... 79
Figure 3.27: Greenish discolouration of the matrix within the No. 3 Facies. Possible chloritisation of a milky quartz (qtz) clast was noted within the reef, as well as a concentration of disseminated rounded pyrite grains nearer to the base of the No. 3 Facies – Sample 25. 80

Figure 3.28: Floating clasts of milky and smoky quartz, hosted within an area dense with disseminated pyrite (py) grains within the overlying hangingwall (HW) quartzite – Sample 26. 80
Figure 3.29: (a) Alternating matrix-supported and clast-supported bands within the No. 3 Facies, underlying a siliceous hangingwall (HW) quartzite and overlying a coarse-grained argillaceous footwall (FW) quartzite – Sample 16; (b) Clasts were absent from the No. 3 Facies in Sample 17 however there was a very thin carbon seam separating the reef from the footwall quartzite – Sample 17. 81
Figure 3.30: (a) Typical mineral assemblage of the hangingwall unit overlying the Carbon Leader Reef comprising quartz (Qtz), pyrophyllite (Prl), muscovite (Ms) and chlorite (Chl) – Sample 1, viewed in cross-polarised transmitted light. The major mineral assemblage seen in (a) was noted across all the hangingwall samples, regardless of facies type, with the exception of Sample 4 overlying the No. 1 Facies where there was an absence of chlorite; (b) Chloritoid (Ctd) was also seen throughout all of the hangingwall samples (across all facies types) – Sample 11, viewed in cross-polarised transmitted light; (c) A single detrital zircon (Zr) grain enclosed within a chloritoid (Ctd) lath alongside a rounded detrital pyrite (Py) grain, hosted between quartz (Qtz) clasts and within a pyrophyllite (Prl)-muscovite (Ms) matrix – Sample 5, viewed in cross-polarised transmitted light. Zircon was noted within hangingwall samples that were overlying the No. 1 and the No. 3 Facies; (d) A euhedral columnar grain of tourmaline (Tour) between quartz (Qtz) clasts within the hangingwall quartzite - Sample 10, viewed in plane-polarised transmitted light. 87
Figure 3.31: (a) A rounded grain of chromite (Cr) in the hangingwall quartzite. The grain occurs interstitially between quartz (Qtz) clasts and within a pyrophyllite (Prl) and muscovite (Ms) matrix – Sample 14, viewed in reflected light; (b) A rounded grain of uraninite (Ur) observed to be in association with detrital pyrite (Py), pentlandite (Pent) and leucoxene (Lxn) – Sample 4, viewed in reflected light. 88
Figure 3.32: (a) A carbon (C) mass is found in this sample. Leucoxene (Lxn) was commonly found in the hangingwall samples, as were grains of pyrite (Py). It appears that rounded pyrite has been overgrown by secondary pyrite – Sample 15, viewed in reflected light; (b) A small gold (Au) grain occurring alongside a recrystallised pyrite (Py) grain. Chloritoid (Ctd) laths were noted within the matrix – Sample 4, viewed in reflected light; (c) A small gold (Au) grain is seen alongside a rounded pyrite (Py) grain hosting pyrrhotite (Po) veinlets. Chloritoid (Ctd) laths were noted within the matrix - Sample 9, viewed in reflective light. 89
Figure 3.33: (a) Monocrystalline quartz (Qtz) clasts constitute the bulk mineralogy within the footwall quartzite. Pyrophyllite (Prl) and muscovite (Ms) occur interstitially between the quartz (Qtz) clasts – Sample 2, viewed in cross-polarised transmitted light; (b) A large pyrophyllite (Prl) grain surrounded by a very fine sericitic muscovite (Ms) and chlorite matrix, occurring interstitially between clasts of quartz (Qtz). Muscovite appears to be replacing pyrophyllite. Grains of pyrite (Py) were noted within the polished thin section – Sample 14, viewed in cross-polarised transmitted light. 92
Figure 3.34: (a) Pyrophyllite (Prl) and muscovite (Ms) both occurred as very fine matrix material and were not easily distinguishable from one another however a few pyrophyllite (Prl) grains were noted to be coarser.

Chloritoid (Ctd) laths were also seen within the fine-grained matrix occurring interstitially between quartz (Qtz) clasts – Sample 6, viewed in cross-polarised transmitted light; (b) Angular to columnar tourmaline (Tour) grains were seen in some of the footwall samples, occurring between quartz (Qtz) clasts and within a pyrophyllite (Prl) and muscovite (Ms) matrix – Sample 2, viewed in cross-polarised transmitted light; (c) Rutile (Rut) was seen to be associated with leucoxene (Lxn) in all of the footwall samples. Chloritoid (Ctd) laths were noted within the matrix – Sample 9, viewed in reflected light; (d) A grain of gersdorffite (Gdf) occurring within a footwall sample. In this microphotograph it is seen with a chalcopyrite (Cpy) overgrowth – Sample $4^{(b)}$, viewed in reflected light. 93

Figure 3.35: (a) A grain of gold (Au) enclosed by gersdorffite (Gdf). Rutile (Rut) and/or leucoxene (Lxn) was also seen proximal to a gold grain in the uppermost right corner of the microphotograph. An anhedral gold grain is seen in the bottom left portion of the microphotograph – Sample 18, viewed in reflected light; (b) Gold (Au) associated with carbon (C) and uraninite (Ur) in the footwall sample – Sample 19, viewed in reflected light. 96

Figure 3.36: (a) Pyrophyllite (Prl) and sericitic muscovite (Ms)-rich matrix occurred interstitially between quartz (Qtz) clasts. Chloritoid (Ctd) laths and detrital pyrite (Py) grains were noted – Sample 21, viewed in cross-polarised transmitted light; (b) Pyrophyllite (Prl) grains noted in some instances were coarser than the muscovite grains. Chloritoid (Ctd) laths could be seen together with detrital pyrite (Py) between quartz (Qtz) clasts – Sample 27, viewed in cross-polarised transmitted light; (c) More quartz (Qtz) clasts with less pyrophyllite and muscovite (Ms) were seen alongside rounded pyrite (Py) - Sample 20, viewed in cross-polarised transmitted light. 98

Figure 3.37: (a) A mass of secondary leucoxene (Lxn) surrounded by euhedral to rounded (detritral) pyrite (Py) grains. Gold (Au) occurs with rounded pyrite (Py) grains within the matrix as well as with leucoxene (Lxn) – Sample 2, viewed in reflected light; (b) Rutile (Rut) and leucoxene (Lxn) occurred together within the sample. Gold (Au) occurred as inclusions within the anhedral pyrite (Py) grain as well as within the matrix – Sample 23, viewed in reflected light. 102

Figure 3.38: (a) Anhedral gersdorffite (Gdf) with gold (Au) inclusions and gold micro-nuggets within the matrix of the reef – Sample 2, viewed in reflected light; (b) Uraninite (Ur) grains with carbon (C) masses, with gold (Au) rimming the carbon masses and occurring in infilling fractures in rounded rounded pyrite. Leucoxene (Lxn) is noted within the uppermost right corner adjacent to (fly-speck) carbon nodules – Sample 4, viewed in reflected light; (c) A carbon (C) nodule (fly-speck carbon) associated with leucoxene (Lxn) and gold (Au). A pyrite (Py) grain was noted within the matrix of the reef – Sample 10, viewed in reflected light; (d) Leucoxene (Lxn) occurring together with carbon (C) and gold (Au). The gold occurs as micro-nuggets within the matrix of the reef – Sample 8, viewed in reflected light. 103

Figure 3.39: Ternary diagrams comparing the phyllosilicate concentrations of the hangingwall (HW), footwall (FW) and reef samples: (a) Pyrophyllite (Prl), chlorite (Chl) and muscovite (Ms) plot showing higher amounts of chlorite within the hangingwall samples. The footwall samples have lower muscovite content with higher pyrophyllite. The reef samples have variable muscovite content with lower chlorite; (b) Carbon Leader Reef facies comparison for pyrophyllite (Prl), chlorite (Chl) and muscovite (Ms) with the No. 1 and No. 3 Facies having higher chlorite and

muscovite content than in the No. 2 Facies; (c) The sum of pyrophyllite (Prl) and muscovite (Ms), chlorite (Chl) and chloritoid (Ctd) plot indicating lower chloritoid content and higher amounts of chlorite within the hangingwall samples in comparison to the footwall sample; (d) Carbon Leader Reef facies comparison for the sum of pyrophyllite (Prl) and muscovite (Ms), chlorite (Chl) and chloritoid (Ctd) with the chloritoid content variable for all facies types (Ternary plot template used for all diagrams: Warnsloh, 2015). 108

Figure 3.40: Gold grade-trace element plot of the hangingwall samples. The strongest correlation noted within in the hangingwall samples was gold grade against U_3O_8, followed by gold grade against U and gold grade against Pb. Hangingwall Samples 1 to 19 are plotted above. The markers are annotated by sample number. 116

Figure 3.41: Gold grade-oxide plot of the hangingwall samples. Hangingwall Samples 1 to 19 are plotted above. The markers are annotated by sample number. 118

Figure 3.42: Gold grade-trace element plot of the footwall samples, inclusive of the extreme outlying gold grades for Samples 18 and 19. The markers are annotated by sample number. 120

Figure 3.43: Gold grade-trace element plot, exclusive of the extreme outlying gold grades. The strongest correlation noted within in the footwall samples is gold grade against Th, followed by gold grade against U and gold grade against U_3O_8. Footwall Samples 1 to 19 are plotted above. The markers are annotated by sample number. 121

Figure 3.44: (a) Gold grade-oxide plot of the footwall samples. Correlations are not immediately noted between gold grade and the major oxides as the very high-grade Samples 18 and 19 are skewing the data; (b) Gold grade-oxide plot of the footwall samples, exclusive of the extreme outlying gold grades. Footwall Samples 1 to 17 are plotted above. The markers are annotated by sample number. 122

Figure 3.45: Gold grade-U plot of the Carbon Leader Reef (tombstone and borehole) samples. The highest gold grade was noted to occur within Sample 8 (311.0 g/t) and lies within the No. 3 Facies. The highest concentration of uranium was noted within Sample 13 (5746 ppm) and lies within the No. 1 Facies. The markers are annotated by sample number. 124

Figure 3.46: Gold grade (g/t) and U (ppm) comparison for all the Carbon Leader Reef tombstone and boreholes samples. The higher gold grades correspond to higher U concentrations, with favourable gold grades seen predominantly in the No. 1 and No. 3 Facies. 127

Figure 3.47: (a) Gold grade (g/t) and U + Th (ppm) plot of the Carbon Leader Reef (tombstone) samples. The strongest correlation between gold grade and U + Th was seen in the No. 2 Facies (R^2=0.9038); (b) Gold grade (g/t) and U_3O_8 (ppm) plot of the Carbon Leader Reef (tombstone) samples. The strongest correlation between gold grade and U_3O_8 was seen in the No. 2 Facies (R^2= 0.9011). The markers are annotated by sample number. 128

Figure 3.48: Gold grade (g/t) and Pb (ppm) plot of the Carbon Leader Reef (tombstone and borehole) samples. The strongest correlation between gold grade and Pb was noted within the No. 2 Facies (R^2=0.7529). The markers are annotated by sample number. 129

Figure 3.49: Gold grade (g/t) and total carbon (%) plot of the Carbon Leader Reef (tombstone and borehole) samples. The strongest correlation between gold grade and carbon was noted for the No. 3 Facies (R^2=0.6044), followed by the No. 1 Facies (R^2=0.0777). Sample 11 was the only sample from the No. 2 Facies with carbon concentration above the lower detection limit of 0.01%. The markers are annotated by sample number. 131
Figure 3.50: (a) Gold grade (g/t) and Ag (ppm) plot of the Carbon Leader Reef (tombstone and borehole) samples. The strongest correlation between gold grade and Ag was noted within the No. 3 Facies (R^2=0.9534); (b) Gold grade (g/t) and Ni (ppm) plot of the Carbon Leader Reef (tombstone and borehole) samples. The strongest correlation between gold grade and Ni was noted within the No. 2 Facies (R^2=0.6715). The markers are annotated by sample number. 133
Figure 3.51: (a) Gold grade (g/t) and Co (ppm) plot of the Carbon Leader Reef (tombstone and borehole) samples. The correlations were similar across the facies types, with No. 2 Facies having the strongest correlation between gold grade and Co concentration (R^2=0.4464); (b) Co (ppm) and Ni (ppm) plot of the Carbon Leader Reef (tombstone and borehole) samples. The No. 1 Facies was noted to have the strongest correlation between the trace elements, suggestive of a different depositional environment of pyrite and/or different type(s) of pyrite in comparison to the No. 2 and No. 3 Facies of the Carbon Leader Reef. The markers are annotated by sample number. 135
Figure 3.52: Gold grade (g/t) and Ba (ppm) plot of the Carbon Leader Reef (tombstone and borehole) samples. The No. 1 Facies was noted to have the strongest correlation (R^2=0.6428) and the No. 2 Facies was noted to have the weakest (non-existent) correlation (R^2=0.0142) between gold grade and Ba concentration. The markers are annotated by sample number. 136
Figure 3.53: Gold grade (g/t) and Cu (ppm) plot of the Carbon Leader Reef (tombstone and borehole) samples. The strongest correlation was noted within the No. 2 Facies (R^2=0.5954). The highest Cu concentration was seen in Sample 18 (230 ppm) at a gold grade of 173.0 g/t. The markers are annotated by sample number. 137
Figure 3.54: Gold grade (g/t) and Fe_2O_3 (%) plot of the Carbon Leader Reef (tombstone and borehole) samples. The No. 3 Facies was noted to have the strongest correlation (R^2=0.7442). The markers are annotated by sample number. 138
Figure 3.55: Gold grade (g/t) and Al_2O_3 (%) plot of the Carbon Leader Reef (tombstone and borehole) samples. The highest %Al_2O_3 was noted within Sample 8 (10.10%) within the No. 3 Facies. The markers are annotated by sample number. 140
Figure 3.56: Gold grade (g/t) and TiO_2 (%) plot of the Carbon Leader Reef (tombstone and borehole) samples. The highest %TiO_2 was noted within Sample 13 (0.62%) within the No. 1 Facies. The markers are annotated by sample number. 141
Figure 3.57: Gold grade (g/t) and CaO (%) plot of the Carbon Leader Reef (tombstone and borehole) samples. %CaO relative to the gold grade shows there was very little to no association. The markers are annotated by sample number. 142

Figure 3.58: Gold grade (g/t) and MgO (%) plot of the Carbon Leader Reef (tombstone and borehole) samples. The strongest correlation between gold grade and %MgO was noted within the No. 2 Facies (R^2=0.5861). The No. 3 Facies had the weakest (non-existent) correlation (R^2=0.0002). The markers are annotated by sample number. . 143
Figure 3.59: Gold grade (g/t) and K_2O (%) plot of the Carbon Leader Reef (tombstone and borehole) samples. The poorest (non-existent) correlation between gold grade and %K_2O was noted within the No. 1 Facies (R^2=0.0839). 144
Figure 3.60: Gold grade (g/t) and Cr_2O_3 (%) plot of the Carbon Leader Reef (tombstone and borehole) samples. The No. 2 Facies was noted to have the highest correlation between gold grade and %Cr_2O_3 (R^2=0.5401). The No. 1 Facies had the poorest correlation (non-existent) between gold grade and %Cr_2O_3 (R^2=0.0016). The markers are annotated by sample number. 145
Figure 3.61: The average gold assay and trace element analyses for the hangingwall, footwall, Carbon Leader Reef average, No. 1 Facies, No. 2 Facies and No. 3 Facies. The data labels above the plotted bars indicate the highest average concentrations for the Carbon Leader Reef units. 148
Figure 3.62: The average major element compositions for the hangingwall, footwall, Carbon Leader Reef average, No. 1 Facies, No. 2 Facies and No. 3 Facies. The data labels above the plotted bars indicate the highest average element oxide concentrations for the various units. 149
Figure 3.63: (a) Spectral mean depths (nm) of pyrophyllite (Prl), sericite (Ser), chlorite (Chl) and chloritoid (Ctd) of the hangingwall units overlying the Carbon Leader Reef in west-east section across TauTona Mine, plotted against gold grade (g/t); (b) Spectral mean depths (nm) of pyrophyllite (Prl), sericite (Ser), chlorite (Chl) and chloritoid (Ctd) of the footwall units underlying the Carbon Leader Reef in west-east section across TauTona Mine, plotted against gold grade (g/t). 153
Figure 3.64: Spectral mean depths (nm) of pyrophyllite (Prl), sericite (Ser), chlorite (Chl) and chloritoid (Ctd) of the Carbon Leader Reef units in west-east section across TauTona Mine, plotted against gold grade (g/t). 156
Figure 3.65: Spectral mean depth (nm) profiles against the pyrophyllite, sericite, chlorite and chloritoid feature extractions – Sample 30. The profiles include the underlying footwall (FW) unit and the overlying hangingwall (HW) unit. A borehole log to show the relative depth of the borehole and the sedimentological unit(s) underlies the spectral profiles. 164
Figure 3.66: Spectral mean depth (nm) profiles against the pyrophyllite, sericite, chlorite and chloritoid feature extractions for (a) Sample 65 - the profiles include the Green Bar (GB), Rice Pebble Marker (RPM), hangingwall (HW) and footwall (FW); (b) Sample 42 – the profiles include the Rice Pebble Marker (RPM), hangingwall (HW), Brown-Orange Argillaceous Zone (BOAZ), Pale Pebbly Quartzite (PPQ) and footwall (FW). A borehole log to show the relative depth of the borehole and the sedimentological unit(s) underlies the spectral profiles. 166
Figure 3.67: Spectral mean depth (nm) profiles against the pyrophyllite, sericite, chlorite and chloritoid feature extractions for (a) Sample 64 - the profiles include the Green Bar (GB), Rice Pebble Marker (RPM), hangingwall (HW), internal quartzite (IQ) and footwall (FW); (b) Sample 20 – the profiles include the hangingwall (HW), Brown-

Orange Argillaceous Zone (BOAZ), Pale Pebbly Quartzite (PPQ) and footwall (FW). A borehole log to show the relative depth of the borehole and the sedimentological unit(s) underlies the spectral profiles. 170
Figure 3.68: Sample locations for tombstone and borehole reef intersections relative to the Carbon Leader Reef facies type (In House Report, 2017). 177
Figure 3.69: Three main types of alteration were noted for the reef intersections across the West Wits Line used within this research: pyrophyllitic alteration, sericitic alteration and chloritisation. 180
Figure 3.70: Sample locations for tombstone and borehole reef intersections relative to the current structure model of the Carbon Leader Reef (In House Report, 2017). 184
Figure 3.71: The proposed alteration model for the Carbon Leader Reef across the West Wits Line. Sericitic alteration had no definite trend and occurred across the mines; chloritisation occurred across all the mines however it extends further west than the sericitic alteration zone; pyrophyllitic alteration was concentrated on the north-eastern to the south-eastern and south portion of TauTona Mine. 185
Figure 3.72: West to east section of the gold grades of the samples versus the major alteration groups. Pyrophyllitic alteration was predominant in the eastern portion of the West Wits Line suggesting these samples are proximal to the main (hydrothermal) fluid source. The samples were noted to have sericitic alteration in the western portions of the West Wits Line. The markers are annotated with a sample number. 187
Figure 3.73: Three main types of alteration were noted for the reef intersections across the West Wits Line used within this research: pyrophyllitic alteration, sericitic alteration and chloritisation. Samples with discrepancies against the Carbon Leader Reef facies model are displayed in red and are annotated with a sample number. 188
Figure 3.74: Proposed change to the Carbon Leader Reef facies model currently implemented at the West Wits Line. The No. 3 Facies sub-type includes samples with a thin basal carbon seam and/or higher than average gold grades for Carbon Leader Reef No. 3 Facies. Samples with discrepancies against the Carbon Leader Reef facies model are displayed in red and are annotated with a sample number. 189
Figure 3.75: Three main types of alteration were noted for the reef intersections across the West Wits Line used within this research: pyrophyllitic alteration, sericitic alteration and chloritisation. Samples with discrepancies against the estimation domain model are displayed in red and are annotated with a sample number. 190

LIST OF TABLES

Table 1.1: A summary of the various absorption features for the spectral regions and their respective wavelengths (Brown *et al*., 2004; Clark, 1995; Clark, 1999; Hauff, 2001, p.2; Kerr *et al*., 2011). 36

Table 2.1: Borehole and tombstone samples and the methodologies undertaken per sample for the purpose of this research. 47

Table 2.2: An example of core logging undertaken for all 49 boreholes. Sample 34 is used below. 48

Table 2.3: An example of the sedimentological descriptions made for 19 tombstones. Sample 19 is used below. . 49

Table 2.4: Performance specifications for the short-wave infrared and Red-Green-Blue cameras on the sisuROCK® (Specim Spectral Imaging Ltd., 2013) and for the short-wave infrared camera on the TerraSpec® spectrometer (ASD Inc., 2008, p.3; Malvern Panalytical Ltd., 2019). 53

Table 2.5: A summary of the main image outputs from the Red-Green-Blue camera and spectral data (Harris, 2006b). 57

Table 2.6: A spectral facies image as well as spectral responses to the pyrophyllite, sericite, chlorite and chloritoid feature extractions (i.e. the spectral index images) in a tombstone, scanned with a TerraSpec® spectrometer. Sample 1 is used below, where the spectral image outcomes for the hangingwall (HW), No. 1 Facies and footwall (FW) are seen. Cooler colours (shades of dark purple and blue) indicate a low response to the feature extraction, and warmer colours (shades of green, orange and red) indicate a moderate to high response to the feature extraction 59

Table 2.7: A spectral facies image as well as spectral responses to the pyrophyllite, sericite, chlorite and chloritoid feature extractions (i.e. the spectral index images) in a borehole, scanned with sisuROCK® spectrometer. Sample 22 is used below, where the spectral image outcomes for the Brown-Orange Argillaceous Zone (BOAZ), No. 2A and No. 2B Facies, Pale Pebbly Quartzite (PPQ) and footwall (FW) are seen. Cooler colours (shades of dark purple and blue) indicate a low response to the feature extraction, and warmer colours (shades of green, orange and red) indicate a moderate to high response to the feature extraction. 61

Table 2.8: Spectral mean depths against the pyrophyllite, sericite, chlorite and chloritoid feature extractions for a tombstone sample, scanned with a TerraSpec® spectrometer. Sample 1 is used below. 62

Table 3.1: A summary of the borehole and tombstone samples that are representative of the Carbon Leader Reef No. 1 Facies (21 samples in total). 71

Table 3.2: A summary of the borehole and tombstone samples that are representative of the Carbon Leader Reef No. 2 Facies (30 samples in total). 73

Table 3.3: A summary of the borehole and tombstone samples that are representative of the Carbon Leader Reef No. 3 Facies (17 samples in total). 78

Table 3.4: A summary of the noted alteration styles and unusual observations in some samples. Samples not included in the table below did not have notable alteration or unusual macroscopic observations however, the macroscopic observations can be referred to in Appendix 2: Macroscopic Observations. A red-yellow-green colour

scale highlights the varying gold grades (red = high gold grade; yellow = intermediate gold grade; green = low gold grade). N/D: not determined. 85

Table 3.5: The modal abundance of 19 hangingwall (tombstone) samples. The modal abundance comprises % content (where applicable) for: quartz (Qtz), pyrophyllite (Prl), muscovite (Ms), chlorite (Chl), chromite (Cr), pyrite (Py), rutile (Rut) and leucoxene (Lxn), chloritoid (Ctd), zircon (Zr), pyrrhotite (Po), carbon (C), gersdorffite (Gdf), chalcopyrite (Cpy), tourmaline (Tour), pentlandite (Pent) and uraninite (Ur). *Gold (Au) appears as a trace element in most of the samples – the gold grade (g/t) determined by fire assay has been included. Samples 4, 9, 10, 14, 15, 16, 18 and 19 were noted to have a gold grade greater than 1 g/t. Minerals noted to have a trace amount are denoted by Tr. Where no detail is included this indicates the mineral was not present within the polished thin section and/or XRD analysis. [(a)] Determined by means of XRD analysis as they were not seen within the polished thin section. 91

Table 3.6: The modal abundance of 20 hangingwall (tombstone) samples. The modal abundance comprises % content (where applicable) for: quartz (Qtz), pyrophyllite (Prl), muscovite (Ms), chlorite (Chl), chromite (Cr), pyrite (Py), rutile (Rut) and leucoxene (Lxn), chloritoid (Ctd), zircon (Zr), pyrrhotite (Po), carbon (C), gersdorffite (Gdf), chalcopyrite (Cpy), tourmaline (Tour), uraninite (Ur) and gold (Au). *Gold (Au) appears as a trace element in all the samples – the gold grade (g/t) determined by fire assay has been included. Samples 9[(b)], 10, 11, 12, 15, 18 and 19 were noted to have a gold grade greater than 1 g/t. Minerals noted to have a trace amount are denoted by Tr. Where no detail is included this indicates the mineral was not present within the polished thin section and/or XRD analysis. [(a)] Determined by means of XRD analysis as they were not seen within the polished thin section. [(b)] Footwall pebble band samples. 95

Table 3.7: The modal abundance of 37 Carbon Leader Reef (tombstone and borehole) samples. The modal abundance comprises % content (where applicable) for: quartz (Qtz), pyrophyllite (Prl), muscovite (Ms), chlorite (Chl), chromite (Cr), pyrite (Py), rutile (Rut) and leucoxene (Lxn), chloritoid (Ctd), zircon (Zr), pyrrhotite (Po), carbon (C), gersdorffite (Gdf), chalcopyrite (Cpy), tourmaline (Tour), uraninite (Ur), bornite (Bor), hematite (Hem) and gold (Au). *Gold (Au) appears in all the reef samples – the gold grade (g/t) determined by fire assay has been included. Minerals noted to have a trace amount are denoted by Tr. Where no detail is included this indicates the mineral was not present within the polished thin section and/or XRD analysis. [(a)] Determined by means of XRD analysis as they were not seen within the polished thin section. [(b)] Pale Pebbly Quartzite (PPQ) unit for Sample 2. [(c)] No. 2A Facies for Sample 2. [(d)] Internal Quartzite (IQ) for Sample 15. 99

Table 3.7 - continued: The modal abundance of 37 Carbon Leader Reef (tombstone and borehole) samples. The modal abundance comprises % content (where applicable) for: quartz (Qtz), pyrophyllite (Prl), muscovite (Ms), chlorite (Chl), chromite (Cr), pyrite (Py), rutile (Rut) and leucoxene (Lxn), chloritoid (Ctd), zircon (Zr), pyrrhotite (Po), carbon (C), gersdorffite (Gdf), chalcopyrite (Cpy), tourmaline (Tour), uraninite (Ur), bornite (Bor), hematite (Hem) and gold (Au). *Gold (Au) appears in all the reef samples – the gold grade (g/t) determined by fire assay has been included. Minerals noted to have a trace amount are denoted by Tr. Where no detail is included this

indicates the mineral was not present within the polished thin section and/or XRD analysis. [a] Determined by means of XRD analysis as they were not seen within the polished thin section. 100

Table 3.8: Microscopic observations for all reef samples. A red-yellow-green colour scale highlights the varying gold grades (red = high gold grade; yellow = intermediate gold grade; green = low gold grade). 112

Table 3.9: The geochemical analyses and gold assay results of hangingwall Samples 1 to 19. The trace elements (ppm) include: U, Ni, Th, Pb, U_3O_8 and Ba. The major oxides (%) include: Fe_2O_3, K_2O, MgO, TiO_2, Al_2O_3, Na_2O. The remaining trace elements and major oxides have been included in Appendix 4: Geochemical Analyses and Gold Assay. The oxides, U, Th and U_3O_8 were determined by XRF. Ni, Pb and Ba were determined by ICP-OES. Gold grade (g/t) was determined by fire assay. Five hangingwall samples were noted to have a higher than average (1.4 g/t) gold grade: Sample 4 (1.4 g/t), Sample 9 (3.9 g/t), 10 (2.7 g/t), 14 (2.5 g/t) and 19 (8.0 g/t). Gold was seen occurring alongside detrital pyrite in thin section for Sample 9. Samples 10, 14 and 19 had no gold noted in thin section, however it was noted that gold occurred alongside a recrystallised pyrite grain in Sample 4. *Below the lower detection limit. 117

Table 3.10: The geochemical analyses and gold assay results of footwall Samples 1 to 19. The trace elements (ppm) include: U, Ni, Th, Pb, U_3O_8 and Ba. The major oxides (%) include: Fe_2O_3, K_2O, MgO, TiO_2, Al_2O_3, Na_2O. The oxides, U, Th and U_3O_8 were determined by means of XRF. Ni, Pb and Ba were determined by means of ICP-OES. Gold grade (g/t) was determined by fire assay. The remaining trace elements and major oxides have been included in Appendix 4: Geochemical Analyses and Gold Assay. Two footwall samples were noted to have a high-grade gold: Sample 18 (135.0 g/t) and Sample 19 (26.8 g/t). A grain of gold was seen enclosed by gersdorffite in Sample 18 and gold was seen to be associated with both carbon and uraninite in Sample 19. [a] Footwall pebble band samples; *Below the lower detection limit. 119

Table 3.11: The geochemical analyses for trace elements and gold assay results of all the Carbon Leader Reef (tombstone and borehole) samples. Ag was determined by means of AAS. Total Sulphur and Carbon were determined by LECO Carbon and Sulphur Analysis. U, U_3O_8 and Th were determined by means of XRF and the remaining trace elements As, Ba, Co, Cu, Ni, Pb and Zn were determined by ICP-OES. Gold grade (g/t) was determined by fire assay. [a] Total Sulphur/Carbon; [b] Pale Pebbly Quartzite (PPQ) for Sample 2; [c] No. 2B Facies for Sample 2; [d] Internal Quartzite (IQ) for Sample 15; [e] 0.01% for Samples 1 to 19; 0.05% for Samples 20 to 34; [f] 10 ppm for Samples 1 to 19; 8 ppm for Samples 20 to 34; [g] 50 ppm for Samples 1 to 19; 30 ppm for Samples 20 to 34; [h] 2 ppm for Samples 1 to 19; 10 ppm for Samples 20 to 24; [i] 30 ppm for Samples 1 to 19; 20 ppm for Samples 20 to 34; I/S: Insufficient Sample; N/D: Not Determined; *Below the lower detection limit. 125

Table 3.11 - continued: The geochemical analyses for trace elements and gold assay results of all the Carbon Leader Reef (tombstone and borehole) samples. Ag was determined by means of AAS. Total Sulphur and Carbon were determined by LECO Carbon and Sulphur Analysis. U, U_3O_8 and Th were determined by means of XRF and the remaining trace elements As, Ba, Co, Cu, Ni, Pb and Zn were determined by ICP-OES. Gold grade (g/t) was determined by fire assay. [a] Total Sulphur/Carbon; [b] Pale Pebbly Quartzite (PPQ) for Sample 2; [c] No. 2B Facies for

Sample 2; [d] Internal Quartzite (IQ) for Sample 15; [e] 0.01% for Samples 1 to 19; 0.05% for Samples 20 to 34; [f] 10 ppm for Samples 1 to 19; 8 ppm for Samples 20 to 34; [g] 50 ppm for Samples 1 to 19; 30 ppm for Samples 20 to 34; [h] 2 ppm for Samples 1 to 19; 10 ppm for Samples 20 to 24; [i] 30 ppm for Samples 1 to 19; 20 ppm for Samples 20 to 34; I/S: Insufficient Sample; N/D: Not Determined; *Below the lower detection limit. 126

Table 3.12: The geochemical analyses for major oxides and gold assay results of all the Carbon Leader Reef (tombstone and borehole) samples. All the major oxides were determined by means of XRF. Gold grade (g/t) was determined by fire assay. [a] Loss on ignition (LOI); [b] Pale Pebbly Quartzite (PPQ) for Sample 2; [c] No. 2B Facies for Sample 2; [d] Internal Quartzite (IQ) for Sample 15; *Below the lower detection limit. 139

Table 3.13: A spectral facies image as well as spectral responses to the pyrophyllite, sericite, chlorite and chloritoid feature extractions for Sample 3 – including the hangingwall (HW), footwall (FW) and a footwall pebble band (FWPB). The legend for the spectral facies image has been included below the images. Cooler colours (shades of dark purple and blue) indicate a low response to the feature extraction, and warmer colours (shades of green, orange and red) indicate a moderate to high response to the feature extraction. 157

Table 3.14: Spectral mean depths (nm) against the pyrophyllite, sericite, chlorite and chloritoid feature extractions as well as gold grade (g/t) for comparison – Sample 3. 158

Table 3.15: A spectral facies image as well as spectral responses to the pyrophyllite, sericite, chlorite and chloritoid feature extractions for Sample 11 – including the hangingwall (HW) and footwall (FW). The legend for the spectral facies image has been included below the images. Cooler colours (shades of dark purple and blue) indicate a low response to the feature extraction, and warmer colours (shades of green, orange and red) indicate a moderate to high response to the feature extraction. 159

Table 3.16: Spectral mean depths (nm) against the pyrophyllite, sericite, chlorite and chloritoid feature extractions as well as gold grade (g/t) for comparison – Sample 11. 160

Table 3.17: A spectral facies image as well as spectral responses to the pyrophyllite, sericite, chlorite and chloritoid feature extractions for Sample 8 – including the hangingwall (HW) and the footwall (FW). The legend for the spectral facies image has been included below the images. Cooler colours (shades of dark purple and blue) indicate a low response to the feature extraction, and warmer colours (shades of green, orange and red) indicate a moderate to high response to the feature extraction. 160

Table 3.18: Spectral mean depths (nm) against the pyrophyllite, sericite, chlorite and chloritoid feature extractions as well as gold grade (g/t) for comparison – Sample 8. 161

Table 3.19: A spectral facies image as well as spectral responses to the pyrophyllite, sericite, chlorite and chloritoid feature extractions for Sample 30 – including the Green Bar (GB), Rice Pebble Marker (RPM), hangingwall (HW) and footwall (FW). The legend for the spectral facies image has been included below the images. Cooler colours (shades of dark purple and blue) indicate a low response to the feature extraction, and warmer colours (shades of green, orange and red) indicate a moderate to high response to the feature extraction. 163

Table 3.20: A spectral facies image as well as spectral responses to the pyrophyllite, sericite, chlorite and chloritoid feature extractions for Sample 65 – including the hangingwall (HW) and the footwall (FW). The legend for the spectral facies image has been included below the images. Cooler colours (shades of dark purple and blue) indicate a low response to the feature extraction, and warmer colours (shades of green, orange and red) indicate a moderate to high response to the feature extraction. 165
Table 3.21: A spectral facies image as well as spectral responses to the pyrophyllite, sericite, chlorite and chloritoid feature extractions for Sample 42 – including the Rice Pebble Marker (RPM), hangingwall (HW), Brown-Orange Argillaceous Zone (BOAZ), Pale Pebbly Quartzite (PPQ) and the footwall (FW). The legend for the spectral facies image has been included below the images. Cooler colours (shades of dark purple and blue) indicate a low response to the feature extraction, and warmer colours (shades of green, orange and red) indicate a moderate to high response to the feature extraction. 168
Table 3.22: A spectral facies image as well as spectral responses to the pyrophyllite, sericite, chlorite and chloritoid feature extractions for Sample 64 – including the hangingwall (HW), internal quartzite (IQ) and the footwall (FW). The legend for the spectral facies image has been included below the images. Cooler colours (shades of dark purple and blue) indicate a low response to the feature extraction, and warmer colours (shades of green, orange and red) indicate a moderate to high response to the feature extraction. 169
Table 3.23: Spectral scanning output observations for all the reef samples (excluding Samples 4, 29, 33 and 34 that were not spectrally scanned). A red-yellow-green colour scale highlights the varying gold grades (red = high gold grade; yellow = intermediate gold grade; green = low gold grade). N/D: not determined. 176
Table 3.24: Overall findings of the various methodologies (including macroscopic observations, microscopic observations, geochemical analyses and spectral observations) were used to assign samples to an appropriate alteration group and to create an alteration model based on the major alteration groups. For the spectral observations, findings were ranked on a low, moderate (mod) and high response to a particular feature extraction. The feature extractions used for this research included pyrophyllite (prl), sericite (ser), chlorite (chl) and chloritoid (ctd). The gold grades used within this table are a combination of the gold grades reported for the purpose of this research, and in the absence of gold grade for the borehole samples, the gold assay grade of the borehole sample done prior to the commencement of this research was used. [(a)] No. 2A Facies; [(b)] No. 2B Facies; [(c)] No. 2A/2B Facies; [(d)] No. 2A and No. 2B Facies average. The samples are arranged from west to east across the West Wits Line. 178
Table 3.24 – continued: Overall findings of the various methodologies (including macroscopic observations, microscopic observations, geochemical analyses and spectral observations) were used to assign samples to an appropriate alteration group and to create an alteration model based on the major alteration groups. For the spectral observations, findings were ranked on a low, moderate (mod) and high response to a particular feature extraction. The feature extractions used for this research included pyrophyllite (prl), sericite (ser), chlorite (chl) and chloritoid (ctd). The gold grades used within this table are a combination of the gold grades reported for the purpose of this research, and in the absence of gold grade for the borehole samples, the gold assay grade of the

borehole sample done prior to the commencement of this research was used. [(a)] No. 2A Facies; [(b)] No. 2B Facies; [(c)] No. 2A/2B Facies; [(d)] No. 2A and No. 2B Facies average. The samples are arranged from west to east across the West Wits Line. 179
Table 3.25: Samples noted with discrepancies against the Carbon Leader Reef facies model definitions (Fletcher, 2009; Muller, 1991) and/or the estimation domain model definitions (Burnett *et al*., 2015). 182
Table 3.25 – continued: Samples noted with discrepancies against the Carbon Leader Reef facies model definitions (Fletcher, 2009; Muller, 1991) and/or the estimation domain model definitions (Burnett *et al*., 2015). 183

LIST OF APPENDICES

Appendix 1: Sample Locality Map

Appendix 2: Macroscopic Observations

Appendix 3: Microscopic Observations

Appendix 4: Geochemical Analyses and Gold Assay

Appendix 5: Tombstone Spectral Profiles

Appendix 6: Tombstone Spectral Images

Appendix 7: Borehole Spectral Profiles

Appendix 8: Borehole Spectral Images

LIST OF ABBREVIATIONS

%	percent or percentage
<	less than
>	greater than
°C	degrees Celcius
AAS	Atomic Absorption Spectroscopy
Au	gold
BH	Borehole
BOAZ	Brown-Orange Argillaceous Zone
Bor	bornite
C	carbon
ca.	circa (approximately)
Chl	chlorite
Cht	chert
cm	centimetre
cm.g/t	(gold) value reported in centimetre grams per tonne
Cpy	chalcopyrite
Cr	chromite
Ctd	chloritoid
D	Deflection (with reference to boreholes; usually followed by a number) or depth
DPH	Development Pilot Hole (also: nomenclature used in AngloGold Ashanti's borehole identities)
E	east (used in the sample identifications)
et al.	et alia (and others)
FW	footwall
FW HM	Full Width at Half Maximum
FWPB	Footwall pebble band
g/t	(gold) grade reported in grams per tonne
Ga	Giga-annum
GB	Green Bar
GBH	Geological Borehole (also: nomenclature used in AngloGold Ashanti's borehole identities)
Gdf	gersdorffite
Hem	hematitie
HW	hangingwall
I/S	insufficient sample
ICP-OES	Inductively Coupled Plasma Optical Emission Spectrometry
IQ	Internal Quartzite
kg	kilogram
LECO	Company name
LIB	Long Inclined Borehole (also: nomenclature used in AngloGold Ashanti's borehole identities)
LOI	Loss on ignition
Ltd.	Limited
LVB	Long Vertical Borehole (also: nomenclature used in AngloGold Ashanti's borehole identities)
Lxn	leucoxene
m	metre
Ma	Mega-annum
MC	missing core
mm	millimetre
MPO	Mponeng (used in the sample identifications)
Ms	muscovite
N/D	not determined
NE	north-east (used in the sample identifications)
nm	nanometre
No. 1 Facies	Carbon Leader Reef No. 1 Facies
No. 2 Facies	Carbon Leader Reef No. 2 Facies
No. 2A Facies	Carbon Leader Reef No. 2A Facies
No. 2B Facies	Carbon Leader Reef No. 2B Facies
No. 3 Facies	Carbon Leader Reef No. 3 Facies
p.	page (used with textbook references)
Po	pyrrhotite
ppm	parts per million
PPQ	Pale Pebbly Quartzite
Prl	pyrophyllite
Py	pyrite
Qtz	quartz
QV	quartz vein
R	correlation coefficient
R_b	band centre reflectance
R_c	spectral continuum
RPM	Rice Pebble Marker
Rse	Raise (also: nomenclature used in AngloGold Ashanti's naming of underground areas)
Rut	rutile
S	south (used in the sample identifications)
Ser	sericite
SGS	is followed by South Africa ((Pty) Ltd.) in this research and refers to a registered company name
SW	south-west (used in the sample identifications)
Tour	tourmaline
Tr	trace (amount)
TS	tombstone
UD	Ultra-Deep (also: nomenclature used in AngloGold Ashanti's borehole identities)
Ur	uraninite
W	west (used in the sample identifications)
Wze	Winze (also: nomenclature used in AngloGold Ashanti's naming of underground areas)
XRD	X-ray Diffraction
XRF	X-ray Fluorescence
Zr	zircon
λ	wavelength

1 INTRODUCTION

Mineralisation variations within the Witwatersrand Basin are studied to better understand the depositional and post-depositional processes within the Basin. Alteration that has occurred due to structural influences and fluid movement is furthermore an important aspect of understanding mineralisation within the Basin.

The purpose of this research was to potentially create a valuable exploration model for the Carbon Leader Reef currently mined at the West Wits Line portion of the Witwatersrand Basin, owned by AngloGold Ashanti Ltd. (hereinafter referred to as AngloGold Ashanti). The aim of this project was to explore aspects of spectral data coupled with petrological and geochemical data to better understand the various mineralisation zones, as well as alteration styles across the West Wits Line comprising Savuka, TauTona and Mponeng Mines. As of the end of 2017 both Savuka and TauTona Mines were placed on care and maintenance, with smaller sections at these mines being moved under the management of Mponeng Mine. The Carbon Leader Reef is the dominant economic horizon mined at Savuka and TauTona Mines and is the secondary economic horizon to the Ventersdorp Contact Reef at Mponeng Mine. The Carbon Leader Reef forms the basis of this project.

A total of 49 borehole reef intersections across the West Wits Line and 19 underground samples (referred to as tombstones i.e. representative samples comprising of reef, with approximately 10 cm of footwall and hangingwall either side of the reef, that have been removed from mined-out areas underground) collected from TauTona Mine were made available by AngloGold Ashanti for the purpose of this research.

Prior to the commencement of this research, 36 of the 49 boreholes and 18 of the 19 tombstones were scanned for spectral analysis. The remaining 13 boreholes and 1 tombstone were not spectrally scanned however macroscopic observations were carried out for these samples (boreholes and the tombstone), and microscopic observations as well as geochemical analyses were carried out for the tombstone sample. All the data made available by AngloGold Ashanti was used in this research and in the absence of one or more methodologies, the

relationships were inferred based on the proximity of the samples as well as similarity of the samples in terms of macroscopic observations and spectral outcomes.

A hyperspectral core imager (Specim's sisuROCK®) was used to spectrally scan the boreholes and a hand-held spectrometer (the TerraSpec®) was used to scan the tombstones. The spectral scanning of both the boreholes and tombstones was supervised by Mr. P. Linton and was carried out at the AngloGold Ashanti Geoscience Technical Offices based in Carletonville prior to the commencement of this research. The raw spectral data from the spectral analyses for the boreholes as well as the already processed data for the tombstones was made available by AngloGold Ashanti for the purpose of this research.

The spectral data for each borehole included a small portion of footwall, hangingwall and the entire Carbon Leader Reef portion, and in some instances extended further into the hangingwall units (Rice Pebble Marker and the Green Bar). Although the initial stages of spectral scanning had been completed, the raw spectral data had not yet been processed nor interpreted for the boreholes. Processing of the raw spectral data for the boreholes was carried out by TerraCore Geospectral Imaging by means of in-house spectral processing software to produce visual image displays as well as digital data files (refer to Chapter 2.5).

The tombstone spectral images extended from the immediate footwall, to the Carbon Leader Reef, through to the immediate hangingwall. The previously processed data for the tombstones, including visual image displays and digital data files, were readily available and provided by AngloGold Ashanti for interpretation.

The interpretation of the processed spectral data for both the tombstones and boreholes was carried out independently as part of this research, with input from Mr. K. Mushiana from TerraCore Geospectral Imaging.

The interpreted spectral data was compared with geochemical results, petrological analyses as well as gold assays for 15 boreholes and 19 tombstone samples. The additional methodologies were used as a means of confirming the spectral data responses. The geochemical analyses (XRF, XRD, ICP-OES, LECO analysis and atomic absorption spectroscopy), cutting of thin sections, gold assays and photographs of the tombstone samples were carried out by SGS

South Africa prior to the commencement of this research. The geochemical results (61 samples), gold assays (61 samples) as well as photographs (19 tombstones) of the footwall, Carbon Leader Reef and hangingwall portions for each of the tombstones, and a total of 84 polished thin sections (of which 23 were footwall, 38 were Carbon Leader Reef and 23 were hangingwall thin sections) were made available by AngloGold Ashanti.

Although 49 boreholes were made available for macroscopic viewing and observations, only 15 reef intersections were able to be sampled for geochemical analyses and used for the cutting of polished thin sections. This was due to legal restrictions in place with regards to the usage of stored gold-bearing exploration boreholes by AngloGold Ashanti. Borehole core was geologically and structurally logged, photographed, cut to size, marked for thin sections and sent to SGS South Africa on commencement of this study. XRF analyses were carried out for the footwall, Carbon Leader Reef and hangingwall portions for all 15 boreholes (45 samples in total). The same geochemical analyses done for the tombstone samples, as well as polished thin sections were only carried out on the Carbon Leader Reef portion of the boreholes (15 reef samples). The polished thin sections, geochemical and assay results for all the samples were made available by AngloGold Ashanti.

A comparison of the collected data from AngloGold Ashanti, for both the boreholes and the tombstones, was undertaken as part of this research to recognise any relationships and/or trends with regards to the spectral, geochemical and petrological results. The spectral data for the boreholes and the tombstones were also compared to establish differences or similarities between the datasets (and the different scanning techniques used). Using a combination of the results, geological modelling was carried out to create an exploration model with the intended purpose to supplement the exploration of the Carbon Leader Reef continuously underway at Mponeng Mine.

1.1 LOCATION OF THE RESEARCH AREA

The area of interest for this project lies along the West Wits Line Goldfield near Carletonville, southwest of Johannesburg, South Africa. The research area lies within the Witwatersrand Basin, as seen in Figure 1.1.

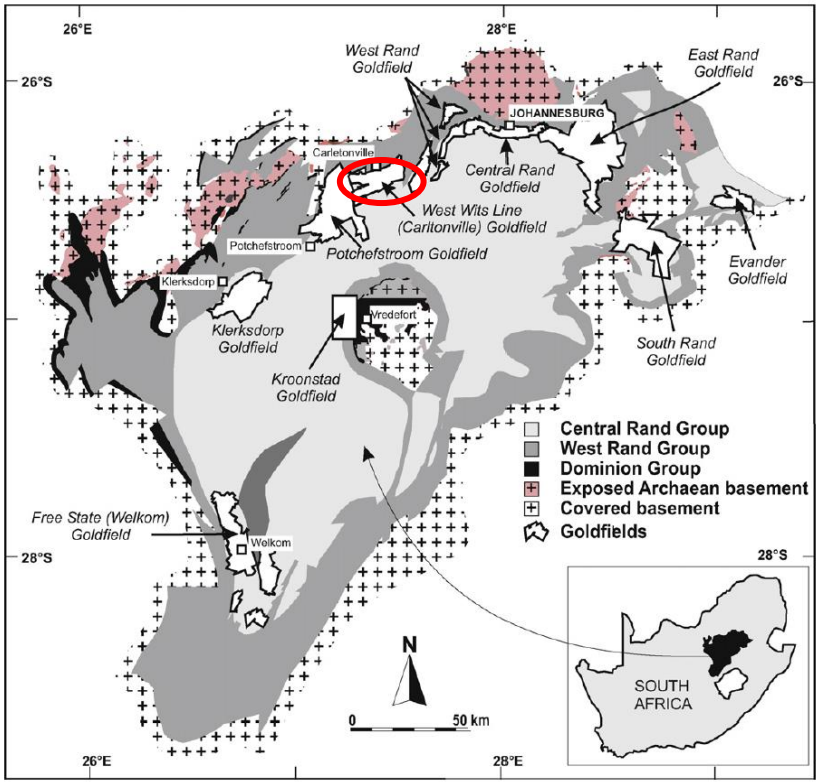

***Figure 1.1**: A geological representation of the location of the research area on the Witwatersrand Basin (encircled) (Dankert and Hein, 2010).*

1.2 GEOLOGY OF THE RESEARCH AREA

Between 2.99 and 2.78 Ga, the Witwatersrand Basin was deposited over the Kaapvaal Craton in South Africa (Guy *et al*., 2014; Depiné *et al*., 2013). The Witwatersrand Basin is one of the largest and richest gold deposits in the world and is also host to a major uranium resource (Depiné *et al*., 2013; Jolley *et al*., 2004; Meier *et al*., 2009; Simanovich, 2009). The Basin rests upon a basement characterised by granitoid rocks, greenstone belts as well as clastic sediments, volcaniclastic deposits and lavas of the Dominion Group (Agangi *et al*., 2015; Beach and Smith, 2007; Guy *et al*., 2014). The Basin hosts the Mesoarchean Witwatersrand Supergroup (Agangi *et al*., 2015; Depiné *et al*., 2013; Guy *et al*., 2014; Phillips and Powell, 2015).

The Witwatersrand Supergroup comprises the West Rand Group, which is overlain by the Central Rand Group (Agangi *et al*., 2015; Depiné *et al*., 2013; Guy *et al*., 2010; Simanovich, 2009). The West Rand Group (ca. 2.99 to 2.91 Ga, Kositcin and Krapež, 2004) is made up dominantly of shale sediments, with occasional units of banded iron formation and

conglomerates, indicating a shallow marine to fluvio-deltaic depositional setting affected by post-rifting thermal subsidence (Depiné *et al*., 2013; Guy *et al*., 2014; Guy *et al*., 2010). The Central Rand Group (ca. 2.90 to 2.78 Ga, Kositcin and Krapež, 2004) comprises coarse-grained fluvio-deltaic sedimentary rocks that were likely deposited within a foreland basin setting (Depiné *et al*., 2013; Guy *et al*., 2014; Phillips and Powell, 2015). Conglomerates can be found in both the West Rand and Central Rand Groups, however more gold and higher grades of gold are found within the Central Rand Group (Depiné *et al*., 2013; Guy *et al*., 2010).

Within the Central Rand Group lie several gold-bearing conglomerates, including the focus of this project, the Carbon Leader Reef (Depiné *et al*., 2013; Grove and Harris, 2010; Guy *et al*., 2010; McCarthy, 2006). The Carbon Leader Reef is a uraninite-bearing conglomerate (Depiné *et al*., 2013; Grove and Harris, 2010) which consists of three distinct facies types (Fletcher, 2009; Muller, 1991) and is further discussed in Chapter 1.5.

The Ventersdorp Supergroup, characterised by flood basalts of the Klipriviersberg Group, as well as volcanics and clastic sediments of the Platberg and Pniel Groups, overlies the Witwatersrand Supergroup (Meier *et al*., 2009; Simanovich, 2009). The Ventersdorp Contact Reef marks the base of the Ventersdorp Supergroup, separating the Ventersdorp and Witwatersrand Supergroups (Tucker *et al.*, 2016).

1.3 THE WITWATERSRAND BASIN

1.3.1 Gold Mineralisation

The origin of the Witwatersrand mineralisation remains one of the most debated topics in economic geology despite several proposed models of origin that have been investigated over the years (Frimmel, 2014).

Mineralisation within the Witwatersrand Basin is represented by several models of origin (Drennan and Robb, 2006; Grove and Harris, 2010; Mathur *et al*., 2013; Phillips and Law, 2000; Phillips and Powell, 2011). The main models include the (unmodified) placer model, a modified placer model and a hydrothermal model of origin (Grove and Harris 2010; Mathur *et al*., 2013;

Phillips and Law, 2000). The placer model, originally proposed by Mellor (1916), suggests that the deposition of gold occurred at the same time as the sediments i.e. the gold is detrital (Mathur *et al*., 2013). The mineral compositions were derived from the weathering of greenstone belts (ca. 3.10 to 2.90 Ga) located north and west of the Basin (Grove and Harris, 2010; Mathur *et al*., 2013). Controls on the gold mineralisation are based on the source area as well as sorting of sediments (Phillips and Law, 2000).

The placer model was then challenged by Graton (1930), who suggested that gold was introduced during infiltration of post-depositional hydrothermal fluids (Barnicoat *et al*., 1997; Frimmel, 1997b; Frimmel *et al*., 2005). Precipitation of gold and other minerals was influenced by fluid pathways as well as the geochemistry of the host rocks (Phillips and Law, 2000; Law and Phillips, 2005). Hydrothermal fluid migration has been related to several events that occurred distally from the Basin, such as Ventersdorp volcanism, regional metamorphism due to the Vredefort impact, or the emplacement of the Bushveld Complex (Frimmel *et al*., 1999; Frimmel *et al*., 2005; Kositcin and Krapež, 2004).

The development of the modified placer model combines both the placer and hydrothermal models agreeing that the gold was detrital as suggested by Mellor (1916), however the original mineral composition was not retained but rather modified by post-depositional hydrothermal fluids (Frimmel *et al*., 2005; Phillips and Law, 2000). Positions of the gold grains are reflective of deposition and the gold movement occurred within hydrocarbon-bearing fluids ranging from centimetre-scale to larger scale faults, bedding planes as well as unconformities following burial (Drennan and Robb, 2006). Controls on gold distribution are based on the source area and sediment sorting (Phillips and Law, 2000) as well as the characteristics of post-depositional fluids (Drennan and Robb, 2006).

Other proposed genetic models for the Basin mineralisation include a sedimentary-exhalative model where gold sources are along the Basin margin (Hutchinson and Viljoen, 1987) and a syngenetic microbially-mediated model proposed by Mossman *et al*. (1999, 2008). Frimmel and Hennigh (2015) further proposed that the precipitation of gold in the Mesoarchean was due to the introduction of oxygen into a predominantly reducing atmosphere by means of

photosynthesis, thus providing a favourable setting for gold to dissolve in meteoric as well as shallow sea water. Precipitation of the gold occurred along the surface of oxygen-producing microbes, allowing for the deposition of microbially-mediated gold over an extensive area, some of which has since been preserved in thin carbon seams (Frimmel and Hennigh, 2015).

Nwaila *et al*. (2017) more recently investigated shales within the Mesoarchean Witwatersrand Supergroup with the results suggesting the sediments within the West Rand Group were sourced from varying basement rock types and were not exposed to tectonic rejuvenation. It was further suggested that the sediments within the Central Rand Group, in contrast to the West Rand Group, originated from several sources and underwent extreme changes within the geometry of the Basin (Nwaila *et al.*, 2017). This was similar to the findings of Frimmel and Hennigh (2015) and Heinrich (2015). Additionally, it was proposed that the origin of the Central Rand Group sediments was initially greenstone-dominated and changed to a more granite-dominated setting as a result of syn-depositional uplift and erosion of granitoids (Nwaila *et al.*, 2017).

1.3.2 Tectonic Setting

The Witwatersrand Basin formed in an Andean-style collisional setting during the Archaen (Jolley *et al*., 1999; Jolley *et al*., 2004; Robb and Robb, 1998). Prior to deposition of the Witwatersrand Supergroup, the Dominion Group underwent rifting (Beach and Smith, 2007; Phillips and Law, 2000; Robb and Robb, 1998). The sediments of the lower West Rand Group were deposited during a post-Dominion rift thermal subsidence phase (Beach and Smith, 2007; Robb and Robb, 1998). The upper parts of the West Rand Group, as well as the Central Rand Group, were deposited within a foreland basin setting (Beach and Smith, 2007; Phillips and Law, 2000). Deposition of the Witwatersrand sediments is characterised by varying stratigraphic thicknesses as well as syn-sedimentary folding, faulting and independently moving fault blocks, indicating a compressional setting (McCarthy, 1994; Robb and Robb, 1998).

During the outpouring of the Klipriviersberg lavas the compressional setting changed to extensional (McCarthy, 1994; Robb and Robb, 1998). During this extensional setting, pre-

existing reverse faults were inverted to normal faults and in some instances half-grabens were developed (McCarthy, 1994; Phillips and Law, 2000; Robb and Robb, 1998). Simultaneously the Platberg Group, characterised by synrift and post-rift sequences, was deposited (Beach and Smith, 2007).

Deposition of the Transvaal Supergroup followed minor events of compression and inversion in the upper Platberg Group (Beach and Smith, 2007). The Transvaal succession underwent post-depositional deformation resulting in large-scale folding as well as faulting (Robb and Robb, 1998). This deformation is suggested to be as a result of the Vredefort impact which was the concluding major effect on the Witwatersrand Basin (Grove and Harris, 2010; McCarthy, 1994; Robb and Robb, 1998).

1.3.3 Mineralogy and Alteration

The Witwatersrand Basin has been affected by regional greenschist facies metamorphic conditions (300 - 400°C) at pressures of approximately 3 kbar allowing for definitive mineral assemblages to be recognised within the Basin (Frimmel, 1994; Hayward *et al*., 2005; Meier *et al*., 2009; Phillips and Powell, 2011; Vidal *et al*., 2007). Within the gold-bearing conglomerates of the Central Rand Group the typical mineralogy comprises a mixture of sulphides, heavy minerals and non-metallic minerals, including quartz, pyrite, chromite, uraninite, sphalerite, zircon, chlorite, muscovite, rutile and gold (Agangi *et al*., 2015; Jolley *et al*., 2004; Hayward *et al*., 2005; Phillips and Powell, 2011; Simanovich, 2009).

Gold-bearing conglomerates are made up of rounded pebbles whereas less auriferous conglomerates contain varying shapes and sizes of pebbles (Simanovich, 2009). Another relationship that can be noted is that the higher the packing density (compaction) of pebbles and sorting in conglomerates, the higher the mineralisation and gold content (Phillips and Powell, 2011; Simanovich, 2009).

In terms of correlation between minerals, gold has been closely associated with the presence of pyrite and uraninite (Phillips and Powell, 2015; Simanovich, 2009). There is also a gold-hydrocarbon-uranium relationship that exists within the Witwatersrand Basin (Agangi *et al*.,

2015; Depiné *et al*., 2013; Drennan and Robb, 2006; Phillips and Powell, 2015). According to Mossman *et al.* (2008), as much as 40% of the gold within the Witwatersrand Basin is associated with hydrocarbons. Hydrocarbon is noted to occur as fly-speck carbon or as a basal hydrocarbon seam within several of the major reefs in the Basin, including the Carbon Leader Reef, the Basal Reef and the Vaal Reef (England *et al*., 2001). The Carbon Leader Reef is one of the richest gold-bearing hydrocarbon seams in the Central Rand Group (Mossman *et al.*, 2008). As with the origin of the Witwatersrand Basin, there are many models and theories that may explain the gold-hydrocarbon-uranium relationship, as well as the relationship between gold and pyrite.

Alteration assemblages found within the Central Rand Group (possibly due to the interaction of hydrothermal fluids) commonly reveal the presence of pyrophyllite, chloritoid, chlorite and muscovite (Law and Phillips, 2005). Nearer to fault zones and major faulting quartz veining can be found within the varying reef horizons as well as the occurrence of phyllonites marking the base/top of the reef (Jolley *et al*., 2004; Law and Phillips, 2005). Pyrophyllite-rich sediments are also commonly found around fault planes, and intrusions (dykes and sills) that also utilise these fault planes (Phillips and Law, 1994). Wallrock alteration is also found close to faults (Phillips and Law, 1994).

1.4 LOCAL STRATIGRAPHY

Figure 1.2, modified after Guy *et al*. (2010), shows a stratigraphic profile through the Witwatersrand Supergroup within the Witwatersrand Basin. The stratigraphic profile is applicable across the research area and includes the localities of the Ventersdorp Contact Reef, Carbon Leader Reef as well as the North Leader Reef. This project focuses on the Carbon Leader Reef and its immediate surrounding geology i.e. hangingwall and footwall. Consequently, only the Johannesburg Subgroup from the Central Rand Group as well as the Jeppestown Subgroup from the West Rand Group will be discussed. Within the Johannesburg Subgroup lies Maraisburg Quartzite which is dark-grey in colour and medium-grained (Fletcher, 2009). Overlying Maraisburg Quartzite is the North Leader Reef which forms part of the Johannesburg Subgroup within the Central Rand Group (McCarthy, 2006).

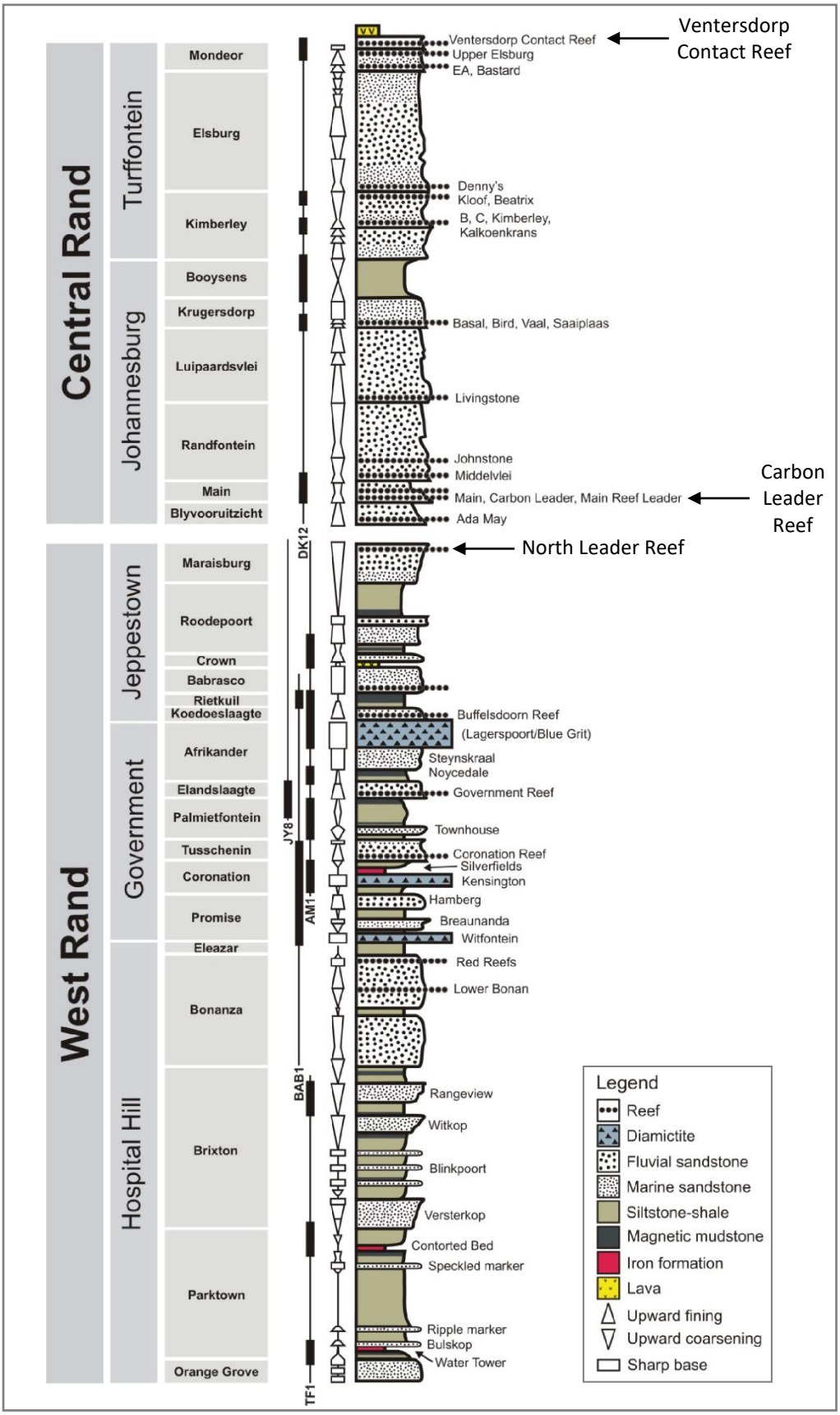

***Figure 1.2**: A stratigraphic column of the Witwatersrand Supergroup (modified after Guy et al., 2010).*

The North Leader Reef lies unconformably above the Maraisburg Quartzite and has an abundance of sulphides, as well as a concentration of disseminated pyrite surrounding black chert and smoky/white quartz pebbles (Fletcher, 2009; Frimmel and Minter, 2002). The North Leader Reef is overlain by an argillaceous Blyvooruitzicht Quartzite which forms the footwall of the Carbon Leader Reef (Fletcher, 2009; McCarthy, 2006). The footwall is fine- to medium-grained and displays an olive-green colour, accompanied by visible cross-bedding and pebble bands (Fletcher, 2009). The Carbon Leader Reef overlies the footwall and is further discussed in Chapter 1.5.

The hangingwall of the Carbon Leader Reef is a semi-siliceous, fine- to medium-grained, blue-grey quartzite displaying cross-bedding in some instances, as well as quartz veining which appears to be more common within the hangingwall than in the footwall of the Carbon Leader Reef (Fletcher, 2009). The hangingwall is overlain by a Rice Pebble Marker that is distinctively gritty with black chert and white quartz pebbles that resemble grains of rice (Fletcher, 2009). A brown-green chloritoid-rich siltstone overlies the Rice Pebble Marker and is referred to as the Green Bar, which is a reliable marker used in the identification of the Carbon Leader Reef (Fletcher, 2009; McCarthy, 2006). The Main Quartzites, described as light-grey, fine-grained and siliceous, overlie the Green Bar (Fletcher, 2009; Grove and Harris, 2010).

1.5 THE CARBON LEADER REEF

The Carbon Leader Reef is a uraninite-bearing conglomerate comprising quartz pebbles, pyrite, gold, hydrocarbon and heavy minerals such as chromite and zircon (Depiné *et al*., 2013; Grove and Harris, 2010; Muller, 1991). Metamorphic silicates typically found within the Carbon Leader Reef include chlorite, chloritoid, pyrophyllite and white mica (Depiné *et al*., 2013; Grove and Harris, 2010). The Carbon Leader Reef mined at the West Wits Line consists of three distinct facies types (Figure 1.3):

(1) Carbon Leader Reef with a carbon seam (No. 1 Facies): characterised by a hydrocarbon seam typically 1 to 20 mm thick at the base of the conglomerate - which is less than 0.1 m thick itself (Fletcher, 2009; Muller, 1991). This type of facies is laterally extensive and hosts higher gold grades than the other facies types because of a gold-

hydrocarbon-uranium relationship commonly recognised within the Witwatersrand Basin (Agangi *et al*., 2015; Depiné *et al*., 2013; Drennan and Robb, 2006; Phillips and Powell, 2015).

(2) Carbon Leader Reef with multiple conglomerates (No. 2 Facies): consisting of an interbedded conglomerate-quartzite sequence (Muller, 1991). This facies type is commonly greater than 0.5 m thick and has varying/inconsistent gold grades with very little carbon (Muller, 1991; Phillips and Law, 2000).

(3) Carbon Leader Reef single conglomerate (No. 3 Facies): typically made up of one conglomerate unit less than 0.3 m thick (Fletcher, 2009; Muller, 1991). This facies type is also laterally continuous and hosts high and persistent gold grades (Muller, 1991). The single conglomerate has smaller amounts of hydrocarbons than the No. 1 Facies which typically occurs as "fly-speck" carbon rather than an actual seam (Depiné *et al*., 2013; Fletcher, 2009; Janisch, 1986; Phillips and Law, 2000).

Figure 1.3 illustrates the locations of the different facies types across the West Wits Line, specifically at Mponeng, TauTona and Savuka Mines.

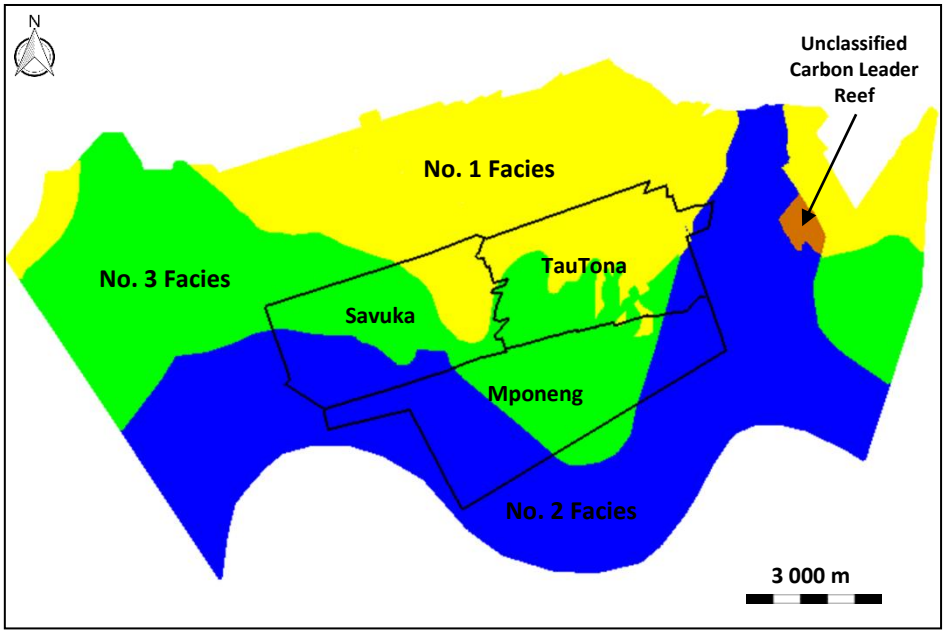

***Figure 1.3**: Graphical representation of the Carbon Leader Reef facies types across the AngloGold Ashanti West Wits Line (In-house Report, 2017).*

Currently there is a Carbon Leader Reef facies type that does not fit into the descriptions above, and as a result remains unclassified possibly because there is a No. 1 and 2 Facies overlap (see Figures 1.3 and 1.4). The unclassified portion does not, however, influence the research area and/or samples that were taken, and falls beyond the scope of this project.

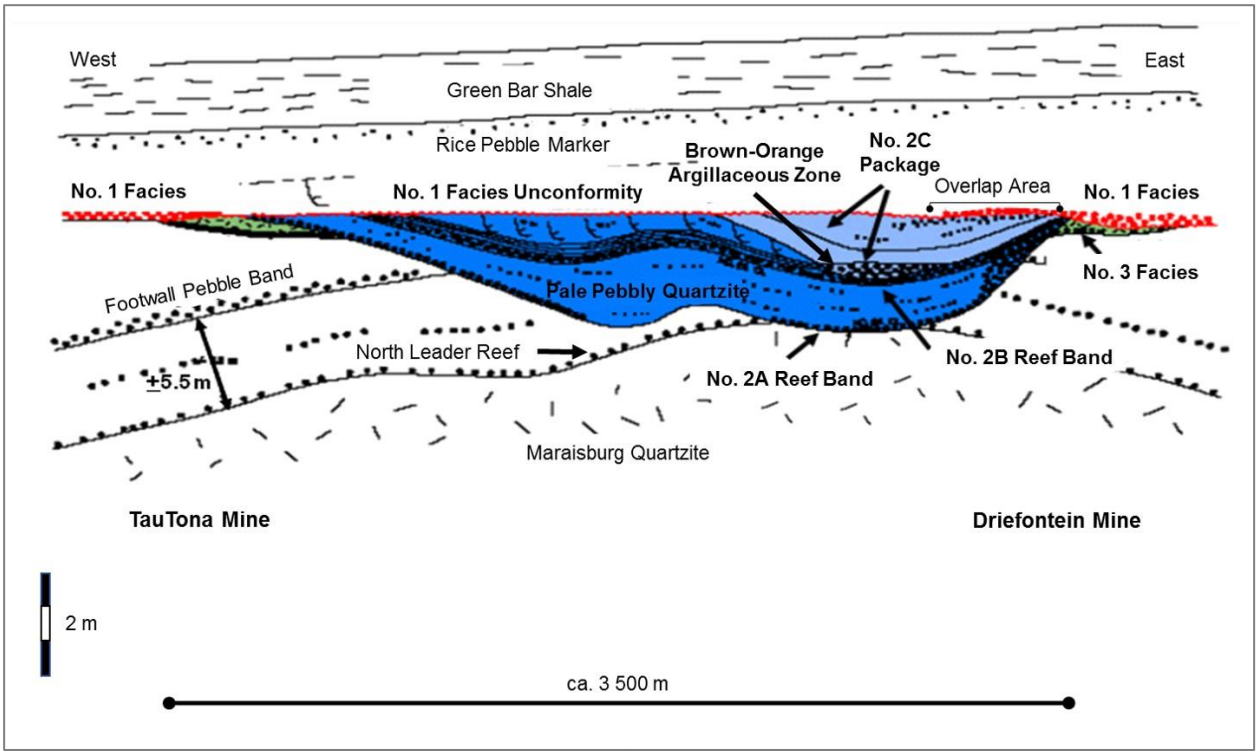

***Figure 1.4**: Schematic diagram of the Carbon Leader Reef facies model proposed by Fletcher (2009) (adapted from In-house Report, 2008).*

Although the facies have been delineated into separate types there are not definite boundaries between facies – i.e. there is a transition from one facies to the next (Muller, 1991). This transition was noted by Phillips and Law (2000) where the Carbon Leader Reef changes from a single reef unit in the northern portions of the Basin to multiple conglomeratic reefs in the south, southeast and southwest regions. Figure 1.4 shows a schematic cross-section (cutting the Witwatersrand Basin from west to east) of the Carbon Leader Reef facies model.

According to Fletcher (2009), the burial of the North Leader Reef combined with the formation of the Blyvooruitzicht Quartzite, led to the forming of the Carbon Leader Reef. The No. 3 Facies was deposited in conglomerate form on an unconformity that was formed as a result of erosion of the west Witwatersrand area (In-house Report, 2004a). The No. 2 Facies was formed by the

reworking of the No. 3 Facies and is divided into 5 units: No. 2A Reef Band (basal unit), Pale Pebbly Quartzite, No. 2B Reef Band, Brown-Orange Argillaceous Zone and the No. 2C Unit (another quartzite) which lies at the top of the package (Fletcher, 2009). Deposition of the No. 1 Facies occurred due to erosional processes and reworking of the No. 2 and No. 3 Facies, i.e. the No. 1 Facies is the actual Carbon Leader Reef and the No. 2 and No. 3 Facies are precursors to the Carbon Leader Reef (In-house Report, 2004a).

The Carbon Leader Reef facies model is based on sedimentological changes across the West Wits Line and is not able to provide much information on the mineralisation within the Carbon Leader Reef. As a result, there was development of an estimation domain model that encompasses Carbon Leader Reef mineralogical characteristics, alteration mineralogy, sedimentology facies, structural influences as well as trend analyses with the variations of grade and channel width (Burnett *et al*., 2015). The estimation domain model however does not account for the occurrence or absence of carbon within the Carbon Leader Reef. The estimation model can be seen in Figure 1.5.

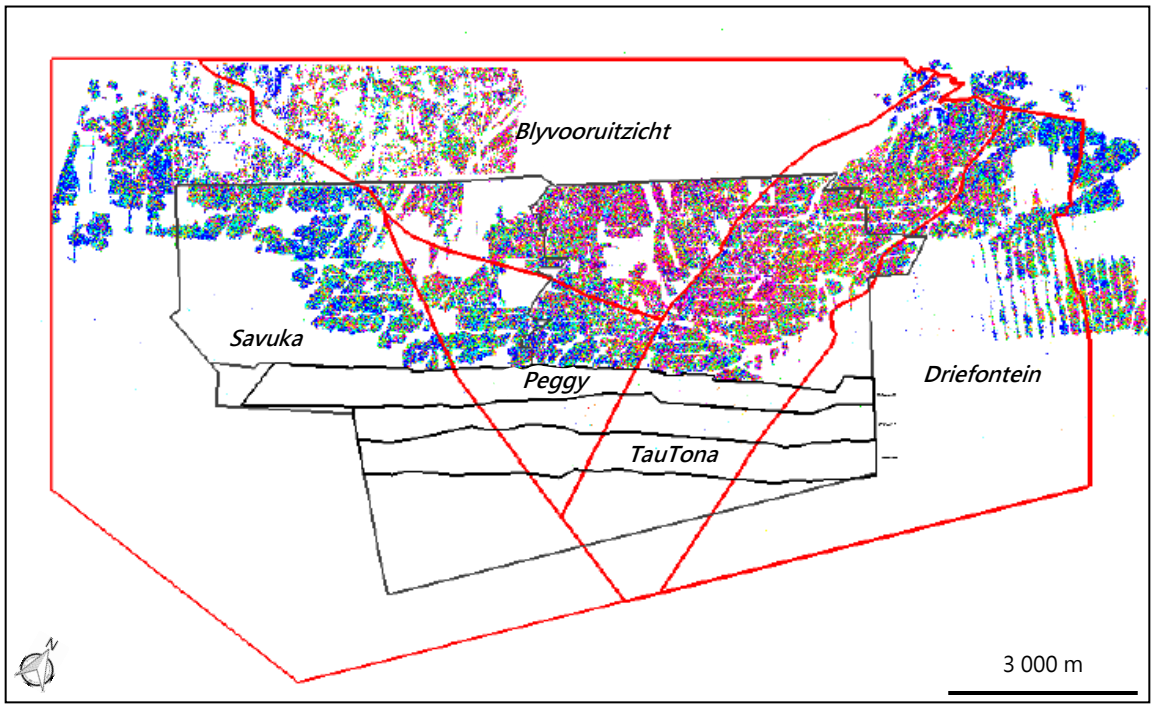

***Figure 1.5**: Carbon Leader Reef estimation domain model comprising the Savuka, Blyvooruitzicht, Peggy, TauTona and Driefontein estimation domains. The various domains are separated by red lines and the gold value in cm.g/t is colour-coded (warmer colours/shades of red indicate higher gold values, and the cooler colours/shades of blue indicate lower gold values, Burnett et al., 2015).*

The gold value (cm.g/t) referred to in the various estimation domains factors in both the thickness of the reef (cm) and the grade (g/t).

The estimation domain model comprises five estimation domains:

- *Savuka estimation domain*: the Carbon Leader Reef within this estimation domain is typically a polymictic, multi-banded, matrix-supported conglomerate (greater than 0.3 m in thickness) with low gold values. This estimation domain has the lowest hydrothermal alteration compared to the others, with an elevated occurrence of chlorite and sericite (Burnett *et al*., 2015).
- *Blyvooruitzicht estimation domain*: the Carbon Leader Reef is a thin (less than 0.1 m), single-banded, oligomictic, clast-supported conglomerate with high gold values. There is an excess of hydrothermal alteration within the reef, dominated by the presence of pyrophyllite (Burnett *et al*., 2015).
- *Peggy estimation domain*: averaging at 0.25 m in thickness the reef alternates between single and multiple bands, is polymictic and matrix-supported with intermediate gold values. The purpose of this estimation domain is to separate lower gold values in the south-western areas of TauTona and the south-east areas of Savuka from higher gold values in the northern and eastern portions of the mines (Burnett *et al*., 2015).
- *TauTona estimation domain*: the reef is characterised by alternating single and multiple bands, and is oligomictic, clast-supported, with some instances of internal quartzite, averaging 0.2 m in thickness and has relatively high gold values. In the north-east area there is a high amount of hydrothermal alteration, indicated by a dominance of pyrophyllite, which decreases to intermediate alteration in the south-west area, indicated by an abundance of chloritoid (Burnett *et al*., 2015).
- *Driefontein estimation domain*: similar to the Savuka estimation domain the reef is typically polymictic, multi-banded, matrix-supported (greater than 0.3 m in thickness) with erratic medium to high gold values in the north-east area. High hydrothermal alteration can be noted in the north with pyrophyllite dominant in the north-west, and chlorite dominant in the north-east (Burnett *et al*., 2015).

1.6 REFLECTANCE SPECTROSCOPY

1.6.1 Introduction to the Reflectance Spectroscopy of Minerals

The study of light that has been emitted, reflected or scattered from a solid, liquid or gas is called spectroscopy (Clark, 1999). Spectrometers are used to identify minerals in altered rocks and variations in mineral compositions, ultimately assisting in the understanding of the formation of ore deposits, noting alteration patterns and helping to locate the ore (Crósta, 2010; Thompson *et al*., 1999). The capability of a spectrometer is dependent on the spectral range, spectral bandwidth, spectral sampling as well as the signal-to-noise ratio (Clark, 1999). Visible/Infrared Reflectance Spectrometers are able to use electromagnetic radiation with wavelengths in the range of 350 nm to 2 500 nm, which is separated into three (wavelength) ranges: visible light, near-infrared and short-wave infrared (Kerr *et al*., 2011; Clark, 1999). Often visible light and near-infrared are combined into a visible-near infrared range (Clark, 1999). Figure 1.6 depicts the electromagnetic spectrum in which the varying ranges of visible light (390 to 750 nm), near-infrared (600 to 1 300 nm) and short-wave infrared (1 300 to 2 500 nm) can be seen (Kerr *et al*., 2011; Brown *et al*., 2004; Hauff, 2001, p.2; Zhang *et al*., 2001).

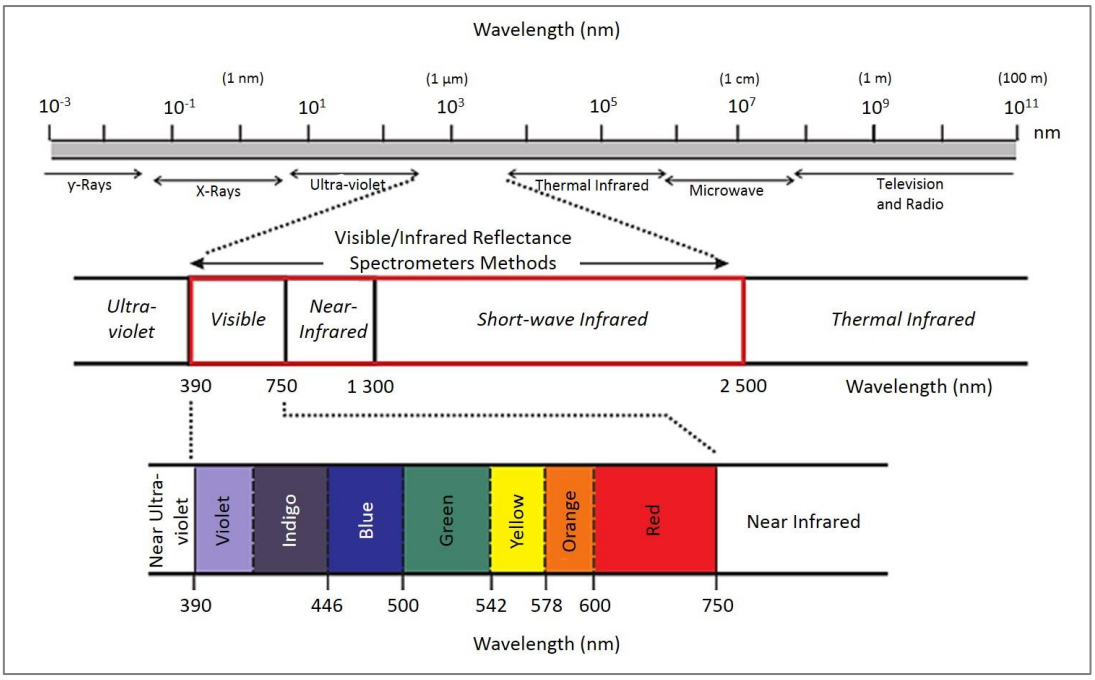

***Figure 1.6**: The electromagnetic spectrum showing the varying spectral ranges (modified after Kerr et al., 2011).*

Absorption in the spectra of material is caused by two general processes: electronic and vibrational processes (Clark, 1999). Absorption features of the ranges as well as their respective process are summarised in Table 1.1.

Table 1.1: A summary of the various absorption features for the spectral regions and their respective wavelengths (Brown *et al*., 2004; Clark, 1995; Clark, 1999; Hauff, 2001, p.2; Kerr *et al*., 2011).

Absorption Feature	Process	Wavelength Range	Spectral Region
Generation of colour variation in minerals, linked to transition metals	Electronic	390 to 750 nm	Visible
Charge transfer absorption where the absorption of a photon results in the movement of an electron between ions	Electronic	1 to 750 nm	Ultra-violet/Visible
Presence of ions in the mineral (i.e. crystal field effects) allowing for the identification of rare-earth elements	Electronic	390 to 1 300 nm	Visible/Near-Infrared
Water and hydroxyl where the water molecule has fundamental vibrations and frequencies shift due to hydrogen bonding in liquid water – associated with hydrothermal alteration zones	Vibrational	1 300 to 2 500 nm	Short-wave Infrared
Carbonates due to several vibrational modes of the CO_3^{-2} ion	Vibrational	600 to 2 500 nm	Near-Infrared/Short-wave Infrared

Absorption features may not be unique to a given mineral however a combination of features can be used to identify a mineral (Kerr *et al*., 2011).

1.6.2 Short-wave Infrared Spectroscopy

This project focused on short-wave infrared spectroscopy as its spectral range (1 300 to 2 500 nm) is rich in mineral spectral signatures and is, as a result, the most effective range for geological analyses (Specim Spectral Imaging Ltd., 2015, Thompson *et al*., 1999).

Short-wave infrared spectroscopy detects energy within molecular bonds due to vibrational processes (Brown *et al*., 2004; Clark, 1999; Thompson *et al*., 1999). With reference to Figure 1.6 and Table 1.1, these molecular bonds are able to stretch and bend within the 1 300 to 2 500 nm range of the electromagnetic spectrum (Brown *et al*., 2004; Clark, 1999; Hauff, 2001, p.2; Thompson *et al*., 1999).

Short-wave infrared spectroscopy is used specifically for evaluating the distribution of alteration mineral assemblages, and short-wave infrared field spectrometers help to consistently map alteration throughout a mineralised ore deposit (Kerr *et al*., 2011; Thompson *et al*., 1999). By using a short-wave infrared method both substitution of elements, and changes in crystallinity or paragenesis in the minerals is possible to pinpoint (Hauff, 2001, p.1; Zhang *et al*., 2001). This method is also useful in the examination of weathered surfaces and weathering profiles (Hauff, 2001, p.2).

As summarised in Table 1.1, short-wave infrared is predominantly sensitive to certain molecules including (but not limited to) OH, H_2O, CO_3^{-2} and NH_4, as well as cation-OH bonds (Clark, 1999; Hauff, 2001, p.3; Thompson *et al*., 1999). This allows for the identification of clay minerals, OH-bearing minerals, hydroxides, iron oxides, pyrophyllite, carbonates and chlorites (Clark, 1999; Hauff, 2001, p.2; Thompson *et al*., 1999; Zhang *et al*., 2001).

Characteristically several absorption features can be seen in a short-wave infrared spectrum (Thompson *et al*., 1999). As seen in Figure 1.7, an absorption feature is made up of various aspects including the hull, wavelength position, depth, full height width and half-width maximum (Thompson *et al*., 1999). The continuum curve is a convex hull and connects the highest parts of the spectrum with straight line segments using a convex hull algorithm (Harris Geospatial Solutions, 2018c; Mielke *et al*., 2015).

In a two-dimensional convex hull problem there is a multiset (*S*) of points (*p*) where each point is assigned its own Cartesian co-ordinates (*p.x, p.y*) in a plane (Gamby and Katajainen, 2018). The convex hull *H* (*S*) of *S* is determined by enclosing all the points of *S* and creating a boundary (i.e. creating the smallest convex polygon containing *S*) (Gamby and Katajainen, 2018; Kao and Knott, 1990).

The continuum is the background absorption onto which absorption features are applied to and its application is required prior to extraction of spectral features (Clark, 1999, p.53; Harris, 2006b, p.214, van der Meer, 2004). A sloping continuum causes an apparent shift (i.e. background illumination) in the lowest reflectance of the spectrum (Clark, 1999, p.53; Harris, 2006b, p.216).

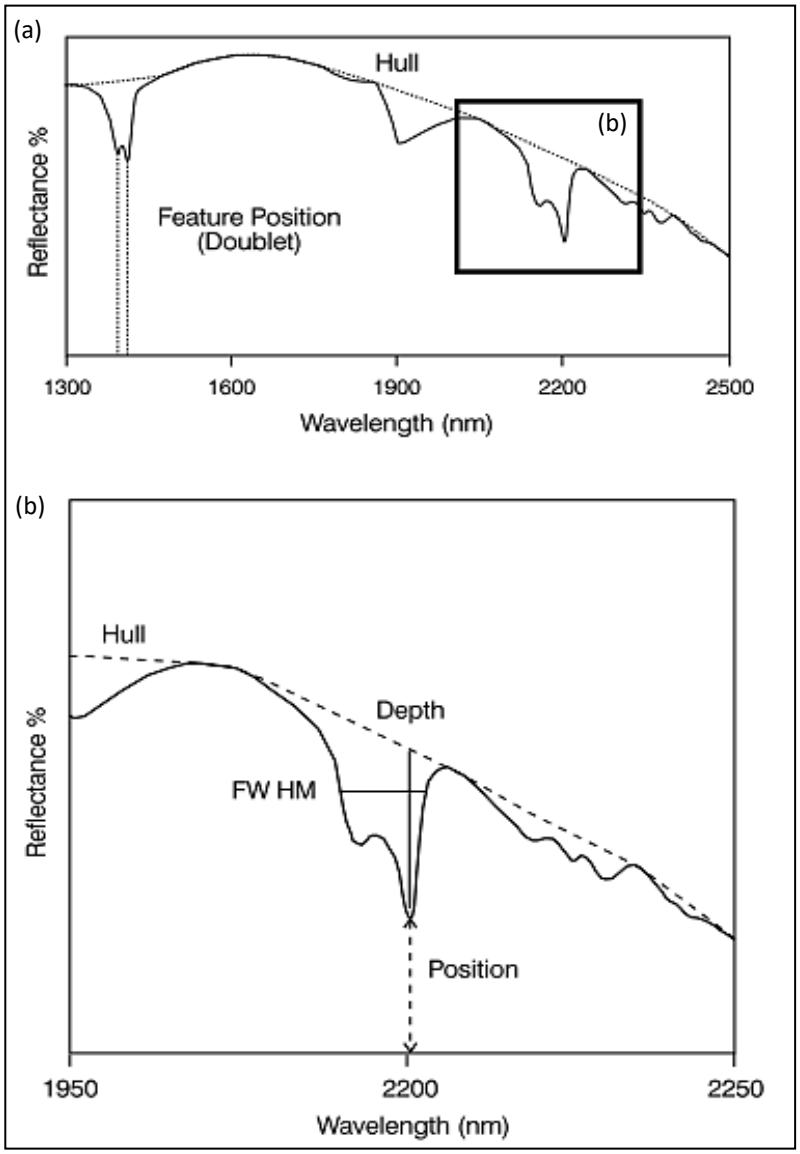

Figure 1.7*: (a) An absorption feature in a kaolinite short-wave infrared spectrum; (b) A zoomed-in view of the feature (modified after Thompson et al. (1999)).*

In a spectrum with a sloping continuum, a hull quotient correction is carried out to remove the background illumination within the hyperspectral data which allows for scaling of the spectra to 100% where the spectral curve approaches the continuum (Clark, 1999, p.53; Harris, 2006b, p.216, Mielke *et al.*, 2015; van der Meer, 2004).

A hull quotient correction is applied to reduce absorption effects not related to mineralogy (i.e. light scattering, surface roughness and particle-size effects) (Dalm and Buxton, 2018). To apply a hull quotient correction, the convex hull of the spectra needs to be calculated and then used

to divide the reflectance on each wavelength band of the spectra to produce a continuum-removed (also referred to as corrected) spectra (Dalm and Buxton, 2018). Continuum-removed spectra are used primarily for the Spectral Feature Fitting method (Harris Geospatial Solutions, 2018c).

The depth of an absorption feature is related to the abundance of the mineral within the sample as well as the grain size (Clark, 1999, p.53, van der Meer, 2004). The greater the depth, the greater the abundance of the mineral within the sample (van der Meer, 2004). Grain size influences the absorption-band depth as the amount of scattered light and the absorption by a grain is dependent on grain size i.e. smaller grains have more surface reflections and larger grains have greater internal paths where photons may be absorbed (Clark, 1999, p.53; van der Meer, 2004). As a result, reflectance decreases with an increase in the size of the grain (van der Meer, 2004). To determine the depth (D) of an absorption feature there needs to be reflectance values at the band centre (R_b) as well as the value of spectral continuum at the same wavelength (R_c): $D = (R_c-R_b)/R_c$ (Clark, 1999; Murphy, 2015). This allows for the depth of the feature to be scaled to the brightness of the spectrum that exists at that wavelength (Murphy, 2015). The width of an absorption feature is referred to as the full width at half maximum (FW HM) and is defined as the wavelength width at the 50% response level of the function (Clark, 1999; Hauff, 2001).

The creation of hyperspectral imagery, i.e. the hull and feature depth, is an automated process in which either a Spectral Angle Mapper method or a Spectral Feature Fitting method is used (Harris Geospatial Solutions, 2018b). The Spectral Angle Mapper method is a classification method used to compare image spectra (raw data) from known spectra (Harris Geospatial Solutions, 2018b). Known spectra are collected and stored within spectral libraries in the form of binary files that contain both spectra and associated wavelengths, and these are used for comparison with the image spectra (Kruse *et al.*, 1993).

The Spectral Angle Mapper method calculates the spectral angle between the two spectra, treating them as vectors within an *n*-dimensional spectral space where *n* also refers to the

number of bands (Figure 1.8, Kruse *et al*., 1993; Harris, 2006a; Harris Geospatial Solutions, 2018b).

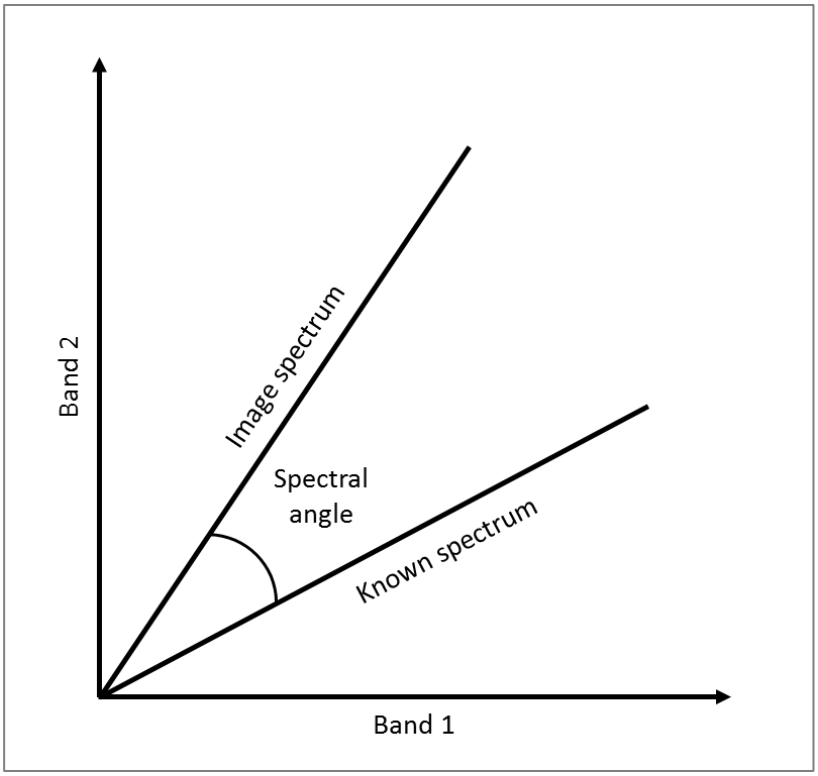

Figure 1.8*: A plot of a known spectrum and an image spectrum (modified after Kruse et al., 1993; Harris Geospatial Solutions, 2018b).*

From this Spectral Angle Mapper method, a classification image is created (Harris Geospatial Solutions, 2018b). The classification image assigns each pixel to a class that is representative of one of the materials within the spectral library (Harris Geospatial Solutions, 2018b). With each pixel in the input image, the classification image chooses a (known) spectrum that has the smallest spectral angle i.e. the best match to a given material for each pixel (Kruse *et* al., 1993; Harris, 2006a; Harris Geospatial Solutions, 2018b).

Spectral Feature Fitting is an absorption feature-based method and is used to match image (pixel) spectra to known spectra and evaluates the physical shape of the spectral signatures (Harris, 2006a; Harris Geospatial Solutions, 2018b). To be able to achieve the best fit with the least amount of error it is necessary to select the narrowest spectral range that contains an entire absorption feature (Harris Geospatial Solutions, 2018b). The Spectral Feature Fitting method determines a scale factor, dependent on the size of spectral features, that can match

the known spectrum to the pixel spectrum (Harris Geospatial Solutions, 2018b). A band-by-band, least squares fit between each known spectrum and the pixel spectra is performed, producing a root mean squared image for each known spectrum (Harris, 2006a; Harris Geospatial Solutions, 2018b). Pixels with a high scale factor and a low root mean square fit are considered to be closely matching (Harris, 2006a).

Depending on the character of the spectrum profile, intensity/shape of absorption troughs and wavelength positions, minerals are identified (Figure 1.9, Thompson *et al*., 1999).

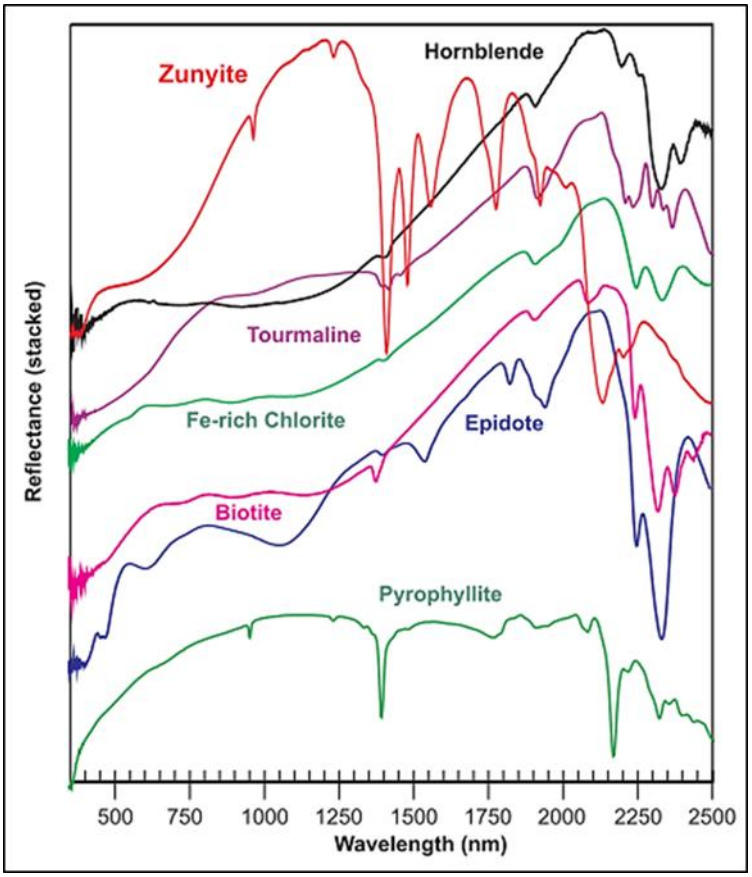

Figure 1.9*: A stacked plot of spectra representing different minerals. Chlorite and pyrophyllite are two minerals of interest for the purpose of this research (Kerr et al., 2011).*

The spectral curve and absorption features are influenced by grain size, degree of sample orientation, overall reflectivity, water content (both surface and interlayered), contaminants (such as organic matter), data collection as well as instrument parameters (Hauff, 2001, p.2; Thompson *et al*., 1999). Shifts in wavelength positions as well as changes to the hull shape are often indicators of variations within the mineral chemistry (Brown *et al*., 2004; Kerr *et al*., 2011;

Hauff, 2001, p.2; Thompson *et al*., 1999). For example, the presence of iron within most minerals displays a strong positive slope from 1 300 to 1 900 nm (Thompson *et al*., 1999). This is clearly depicted in Figure 1.10 where spectra from both Mg-rich and Fe-rich clinochlore can be seen and compared, with the Fe-rich chlorite displaying a much steeper slope than the Mg-rich chlorite (Thompson *et al*., 1999). Quality spectral interpretation is dependent greatly on observations and descriptions of colour, textures, veining, fractures and weathering states of the samples used (Thompson *et al*., 1999).

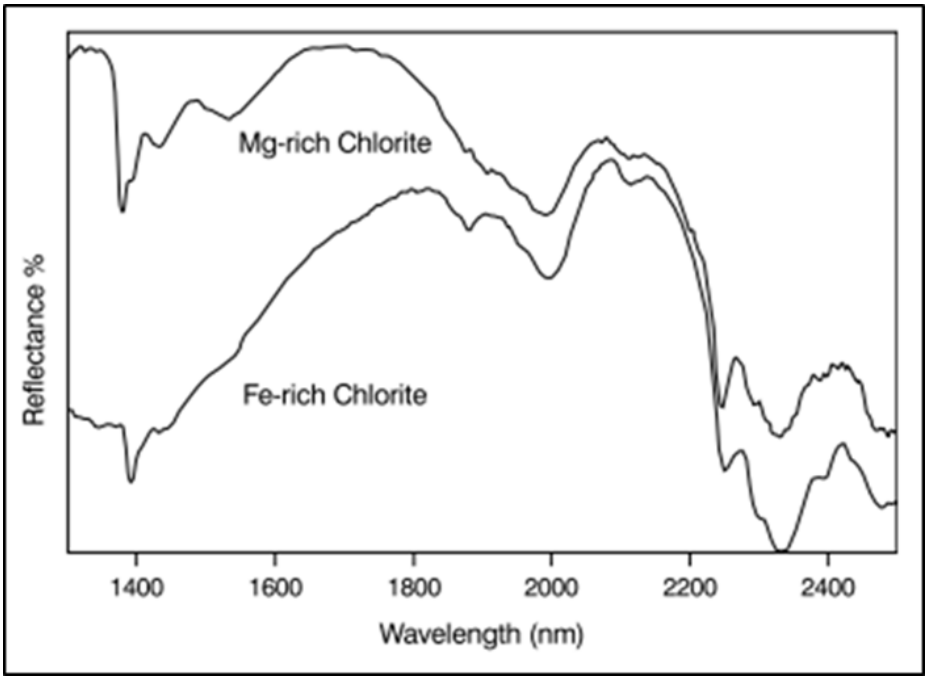

***Figure 1.10**: A stacked plot of spectra representing Fe-rich clinochlore and Mg-rich clinochlore. Note the steeper slope of the Fe-rich spectrum from 1 300 to 1 900 nm (Thompson et al., 1999).*

1.6.3 Case Studies

A study by Crósta (2010) of the El Salvador Porphyry in Northern Chile used reflectance spectroscopy to characterise hydrothermal alteration mineralogy and zoning to create a map of the spatial distribution of the alteration minerals as well as a map of the main alteration types. Crósta (2010) used the spectral reflectance results (measured in a lab) to compile the maps (Figure 1.11). The varying minerals identified within the samples characterised two main alteration zones (Crósta, 2010). The argillic alteration zone included minerals smectite, illite, dickite and alunite, and the advanced argillic alteration zone contained illite, alunite and

kaolinite (Crósta, 2010). This separation in the alteration results revealed that there is an inner zone of argillic alteration which is surrounded by a zone of advanced argillic alteration (Crósta, 2010).

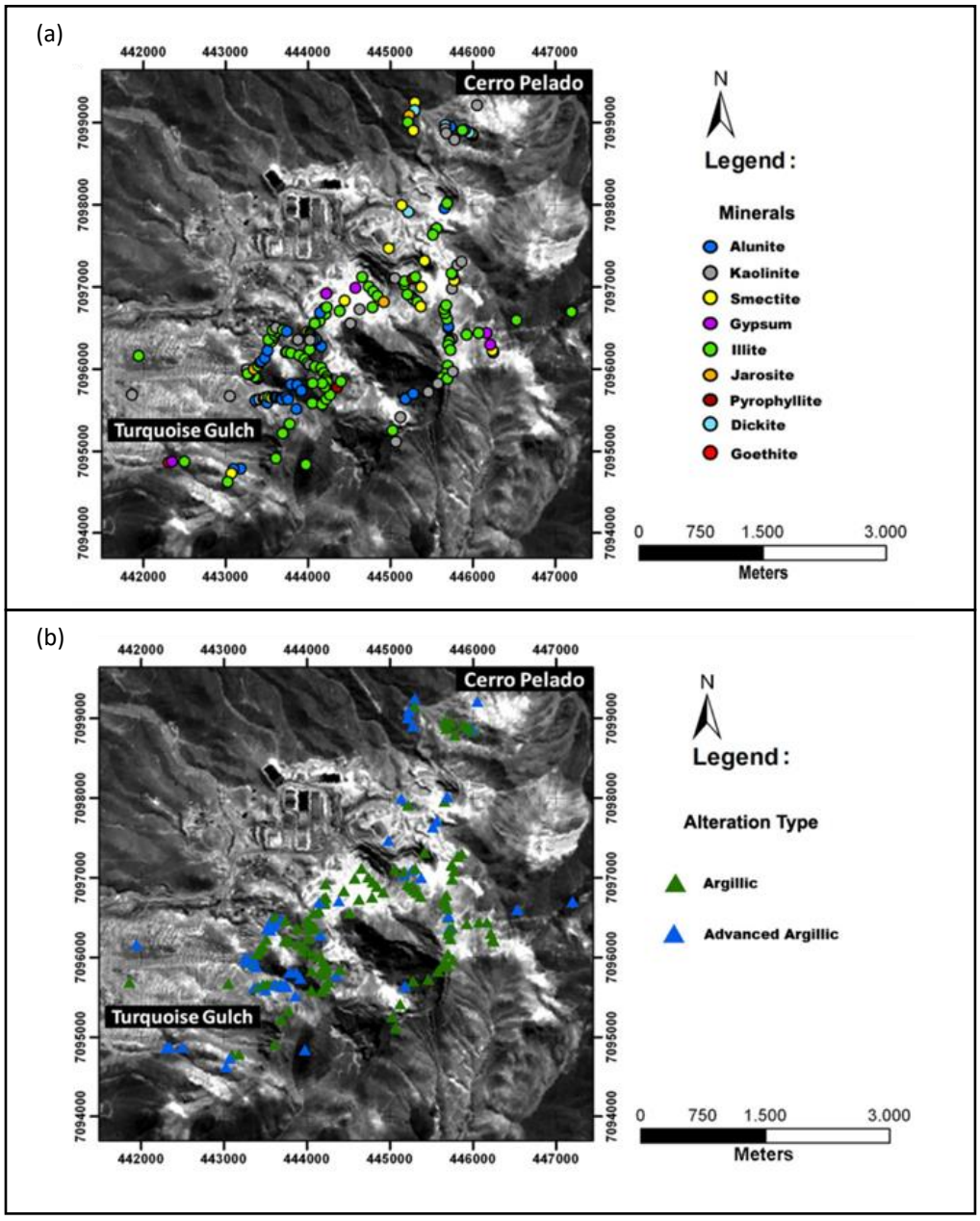

***Figure 1.11**: (a) Map showing sample location as well as the main alteration mineral found within each sample; (b) Map showing the two main alteration types in the area (taken from Crósta, 2010).*

The mapping of the different alteration zones using reflectance spectroscopy helped to better understand the geological processes (i.e. alteration) that lead to the formation of the El

Salvador Porphyry deposit (Crósta, 2010). This allowed for the development of a new deposit model which could be further used in exploration surveys (Crósta, 2010).

A similar procedure was followed by Thompson *et al*., (1999), with the exception of a handheld spectrometer being used. High- and low-sulphidation epithermal gold deposits in Peru were investigated (Thompson *et al*., 1999). Alteration minerals found within one of the high-sulphidation deposits included alunite, dickite, pyrophyllite, diaspora, smectite, kaolinite, illite and quartz, and were used to determine alteration zone patterns (Thompson *et al*., 1999). Within the low-sulphidation deposits the alteration patterns were characterised by calcite-replacement within quartz veins that grade outward in the host rock to zones of illite, illite-smectite and illite/smectite-chlorite (Thompson *et al*., 1999). Data collected within this case study was used to identify major alteration zones and contributed to the understanding of the various systems that were being explored (Thompson *et al*., 1999).

1.7 AIMS

The aim of this project was to explore the aspects of spectral data, including spectral images and spectral profiles, coupled with petrological and geochemical data to better understand the various Carbon Leader Reef mineralisation zones as well as alteration across the AngloGold Ashanti West Wits Mines.

1.8 OBJECTIVES

In order to investigate the alteration within the Carbon Leader Reef (specifically at the West Wits Mines) and to create a potentially valuable exploration model for the Carbon Leader Reef currently mined at the West Wits Mines, the following objectives were to be met:

- Borehole (geological and structural) logging of 49 boreholes made available by AngloGold Ashanti. The borehole logging could be used to identify macroscopic variations in alteration across the mines as well as alteration proximal to structural influences such as faults and intrusions.

- Sampling of 15 boreholes made available by AngloGold Ashanti, to undergo geochemical analyses (including XRF, XRD and ICP-OES), gold assaying (reef samples only) and to be cut for polished thin sections (reef samples only). The geochemical analyses could be used to supplement the findings of the spectral data and to confirm the presence or absence of the minerals identified by means of the spectral scanning.
- Processing of raw spectral data for a total of 36 boreholes provided by AngloGold Ashanti, with the assistance of TerraCore Geospectral Imaging. The processing of the raw data was an important step in the spectral scanning process, particularly in understanding the various algorithms used in creating the outputs and how the various outputs could be interpreted.
- Independent interpretation of the processed spectral data (18 tombstones and 36 boreholes) for the purpose of this study, with input from Mr. K. Mushiana from TerraCore Geospectral Imaging. The interpretation of the spectral data could be useful in creating a valuable alteration model for the West Wits Mines.
- Using the collected spectral data, geochemical results, gold assays and thin sections made available by AngloGold Ashanti to undertake petrological and geochemical analyses to determine the relationship (if any) between the interpreted spectral data, geochemical and petrological data. Spectral scanning is a relatively new methodology that needs to be supplemented with trusted methodologies such as petrology and geochemical analyses.
- To identify lateral changes in mineralogy/alteration/gold grades across the AngloGold Ashanti West Wits Line area, with a focus on the Carbon Leader Reef. Understanding the lateral changes across Savuka, TauTona and Mponeng Mines could be useful in creating a valuable model that considers the aspects of mineralogy, alteration as well as gold grade.
- To develop an alteration model using the results acquired from the above objectives i.e. create alteration ‘zones’ that group areas with characteristically similar alteration, to potentially help understand the geological processes that lead to the formation of the deposit.

2 METHODOLOGY

The localities of 49 borehole reef intersections and 19 tombstone samples used for this research can be found in Appendix 1: Sample Locality Map. The samples are plotted according to their X and Y co-ordinates (two-dimensionally). The Carbon Leader Reef facies and estimation domain model (previously discussed in Chapter 1.5) have been included in the map of the sample locations, as have the West Wits Line mine boundaries.

Out of the 49 boreholes that were made available for macroscopic viewing and observations, only 15 reef intersections were able to be sampled for geochemical analyses and used for the cutting of polished thin sections. This was mainly due to legal restrictions in place with regards to the usage of stored gold-bearing exploration boreholes by AngloGold Ashanti.

Although not all the borehole reef intersections that were scanned and logged were sampled, the borehole reef intersections that were sampled are near those that were not sampled. For example, when referring to borehole GBH 1000 D0, the 'D0' indicates that this was the initial "parent" hole drilled in the area (In-house Report, 1998). Borehole GBH 1000 D1 indicates the first deflection from the parent hole. Several more deflections are recorded for GBH 1000 and are created using a deflection wedge in the hole that is being drilled. It is important to note that in some of the borehole reef intersections the presence of carbon was minimal, or carbon was absent. This is due to high pressure water used during the drilling process of the boreholes which very often washes out the softer carbon within the sample. It should also be noted that the borehole and tombstone samples were split vertically (for geochemical analyses and thin section cutting) and as a result what is noted in one methodology/analysis may not necessarily be seen in the other.

The tombstone samples were only collected at TauTona Mine (refer to Appendix 1: Sample Locality Map). As a result, a comparison of the tombstones could only be made with boreholes from TauTona Mine. This comparison was then used to infer relationships with the boreholes from Savuka Mine and Mponeng Mine. Table 2.1 summarises the various methodologies carried out per borehole and tombstone sample.

Table 2.1: Borehole and tombstone samples and the methodologies undertaken per sample for the purpose of this research.

Sample ID		Sample Type	Unit	Macroscopic Analysis	Microscopic Analysis			Geochemical Analyses & Gold Assay			Spectral Analysis	
					Footwall	Reef	Hangingwall	Footwall	Reef	Hangingwall	Spectral Scans	Spectral Profiles
1	94-94 E1	Tombstone	No. 1 Facies	x	x (2)	x (2)	x (1)	x	x	x	x	x
2	99-94 E2	Tombstone	No. 2 Facies	x	x (1)	x (3)	x (1)	x	x	x	x	x
3	104-88 W6	Tombstone	No. 1 Facies	x	x (1)	x (2)	x (1)	x	x	x	x	x
4	105-86 E2	Tombstone	No. 1 Facies	x	x (2)	x (1)	x (2)	x	x	x		
5	112-83 W3	Tombstone	No. 1 Facies	x	x (1)	x (1)	x (1)	x	x	x	x	x
6	112-83 W4	Tombstone	No. 1 Facies	x	x (1)	x (2)	x (2)	x	x	x	x	x
7	114-78 E1	Tombstone	No. 1 Facies	x	x (1)	x (2)	x (1)	x	x	x	x	x
8	120-55 W4	Tombstone	No. 3 Facies	x	x (1)	x (1)	x (1)	x	x	x	x	x
9	120-77 S1	Tombstone	No. 3 Facies	x	x (2)	x (2)	x (1)	x	x	x	x	x
10	96-94 E2	Tombstone	No. 1 Facies	x	x (1)	x (2)	x (2)	x	x	x	x	x
11	100-92 Wze	Tombstone	No. 2 Facies	x	x (1)	x (2)	x (1)	x	x	x	x	x
12	104-88 E1A	Tombstone	No. 1 Facies	x	x (1)	x (2)	x (1)	x	x	x	x	x
13	104-88 W7	Tombstone	No. 1 Facies	x	x (2)	x (2)	x (1)	x	x	x	x	x
14	109-87 E2	Tombstone	No. 1 Facies	x	x (1)	x (2)	x (1)	x	x	x	x	x
15	112-84 RSE	Tombstone	No. 1 Facies	x	x (1)	x (2)	x (2)	x	x	x	x	x
16	120-55 NE7	Tombstone	No. 3 Facies	x	x (1)	x (3)	x (1)	x	x	x	x	x
17	120-55 W5	Tombstone	No. 3 Facies	x	x (1)	x (2)	x (1)	x	x	x	x	x
18	120-55 W7	Tombstone	No. 3 Facies	x	x (1)	x (3)	x (1)	x	x	x	x	x
19	120-70 W1	Tombstone	No. 3 Facies	x	x (1)	x (2)	x (1)	x	x	x	x	x
20	DPH 3883	Borehole	No. 2 Facies	x		x (1)		XRF only	x	XRF only		x
21	DPH 4057	Borehole	No. 3 Facies	x		x (1)		XRF only	x	XRF only		x
22	GBH 1000 D6	Borehole	No. 2 Facies	x		x (1)		XRF only	x	XRF only	x	x
23	GBH 2788	Borehole	No. 2 Facies	x		x (1)		XRF only	x	XRF only		x
24	GBH 3763	Borehole	No. 1 Facies	x		x (1)		XRF only	x	XRF only		x
25	GBH 3844	Borehole	No. 3 Facies	x		x (1)		XRF only	x	XRF only		x
26	GBH 3845	Borehole	No. 3 Facies	x		x (1)		XRF only	x	XRF only		x
27	GBH 4003	Borehole	No. 1 Facies	x		x (1)		XRF only	x	XRF only		x
28	GBH 6000	Borehole	No. 1 Facies	x		x (1)		XRF only	x	XRF only		x
29	GBH 6001	Borehole	No. 3 Facies	x		x (1)		XRF only	x	XRF only		
30	GBH 6003	Borehole	No. 1 Facies	x		x (1)		XRF only	x	XRF only	x	x
31	GBH 6004	Borehole	No. 2 Facies	x		x (1)		XRF only	x	XRF only		x
32	GBH 6014	Borehole	No. 1 Facies	x		x (1)		XRF only	x	XRF only		x
33	GBH 6028	Borehole	No. 1 Facies	x		x (1)		XRF only	x	XRF only		
34	GBH 6036	Borehole	No. 1 Facies	x		x (1)		XRF only	x	XRF only		
35	GBH 1000 D0	Borehole	No. 2 Facies	x							x	x
36	GBH 1000 D1	Borehole	No. 2 Facies	x							x	x
37	GBH 1000 D2	Borehole	No. 2 Facies	x							x	x
38	GBH 1000 D4	Borehole	No. 2 Facies	x							x	x
39	GBH 1000 D5	Borehole	No. 2 Facies	x							x	x
40	GBH 1000 D7	Borehole	No. 2 Facies	x							x	x
41	GBH 1000 D8	Borehole	No. 2 Facies	x							x	x
42	GBH 1000 D9	Borehole	No. 2 Facies	x							x	x
43	GBH 1000 D10	Borehole	No. 2 Facies	x							x	x
44	GBH 1000 D11	Borehole	No. 2 Facies	x							x	x
45	GBH 6008	Borehole	No. 1 Facies	x							x	
46	LIB 120 SW1 D0	Borehole	No. 3 Facies	x							x	
47	LVB 18 D0	Borehole	No. 3 Facies	x							x	
48	LVBI D2	Borehole	No. 2 Facies	x							x	x
49	LVBI D5	Borehole	No. 2 Facies	x							x	x
50	LVBI D7	Borehole	No. 2 Facies	x							x	x
51	LVBI D10	Borehole	No. 2 Facies	x							x	x
52	LVBK D3	Borehole	No. 2 Facies	x							x	x
53	LVBL D2	Borehole	No. 2 Facies	x							x	x
54	MPO LIB 2 D2	Borehole	No. 3 Facies	x							x	
55	MPO LIB 3 D2	Borehole	No. 3 Facies	x							x	
56	MPO LIB 3 D3	Borehole	No. 3 Facies	x							x	
57	UD 2 D0	Borehole	No. 2 Facies	x							x	
58	UD 2 D2	Borehole	No. 2 Facies	x							x	x
59	UD 5 D0	Borehole	No. 2 Facies	x							x	x
60	UD 13 D0	Borehole	No. 3 Facies	x							x	
61	UD 15 D1	Borehole	No. 2 Facies	x							x	
62	UD 25 D11	Borehole	No. 2 Facies	x							x	x
63	UD 32 D8	Borehole	No. 2 Facies	x							x	
64	UD 33 D15	Borehole	No. 3 Facies	x							x	x
65	UD 36 D4	Borehole	No. 1 Facies	x							x	x
66	UD 36 D7	Borehole	No. 1 Facies	x							x	
67	UD 37 D1	Borehole	No. 2 Facies	x							x	
68	UD 37 D5	Borehole	No. 2 Facies	x							x	
Total Number of Samples:				*68*	*19*	*34*	*19*	*34*	*34*	*34*	*54*	*51*
(Number of Polished Thin Sections)				*N/A*	*23*	*53*	*23*	*N/A*				

2.1 MACROSCOPIC OBSERVATIONS AND PHOTOGRAPHY

A total of 49 borehole were geologically and structurally logged, with a focus on the immediate footwall quartzite, Carbon Leader Reef and the hangingwall quartzite overlying the reef (Appendix 2: Macroscopic Observations). Sedimentological descriptions were recorded in the focus area (Table 2.2) noting mineralogy, grain size, grain shape, reef maturity, sulphides as well as any alteration that could be cross-referenced with results from the other methodologies undertaken (Chapter 2.2 to 2.7).

Table 2.2: An example of core logging undertaken for all 49 boreholes. Sample 34 is used below.

Hangingwall	*Reef-Hangingwall Contact*	*Carbon Leader Reef*	*Reef-Footwall Contact*	*Footwall*
Hangingwall is siliceous and clean. Medium to fine-grained with very fine dark grey banding present. Pyrite is also present in foresets alongside the dark grey bands.	Gradual	The No. 1 Facies is dominantly matrix-supported with well-rounded clasts approximately 5 mm to 10 mm in diameter. Disseminated pyrite can be seen in the reef in the uppermost portion, and cubic and disseminated pyrite can be seen in the bottom portion.	Gradual	The footwall appears to be cleaner than usual, with a lighter khaki colour as well. The footwall is medium to fine-grained with small (<5 mm) floating chert clasts. Angular chert clasts (10 mm) are also noted. Well-developed footwall pebble band is seen further away from the No. 1 Facies package and displays a dark green-grey matrix.
				

Of the boreholes that were logged, a total of 15 boreholes had a good quality reef intersection that could be sampled for further analyses (petrological studies, geochemical analyses and gold assaying). The logging and sampling of the boreholes was carried out independently at the AngloGold Ashanti Geoscience Technical Offices based in Carletonville for the purpose of this study. Photographs of the boreholes were taken during the logging process using a Kodak EasyShare M340 Camera to help document finer details of the core. These photos are referred to and used within Chapter 3.1. In-house professional photographs of the boreholes were taken prior to the commencement of this study and prior to an in-house sampling process. The in-house photographs are accredited to Mr. G.C. José and were used to supplement geological

logging of the boreholes (Table 2.2; Appendix 2: Macroscopic Observations) as only ½ and ¼ core was available for the purpose of this research. The professional photographs were used to inform sample description and sample selection while logging.

The 19 tombstones used were previously sampled from underground exposures at TauTona Mine. Photographs and geological descriptions were taken underground by Ms. N. Buqa of the areas where the tombstones were collected from. The tombstones were re-photographed at surface once they had been properly cleaned. The samples, once handed over to SGS South Africa, were again photographed prior to cutting (for geochemical and petrological analyses) and post-cutting. All of the aforementioned photographs of the tombstones as well as the underground geological observations (in the form of underground geological mappings) were made available by AngloGold Ashanti to facilitate the creation of detailed sedimentological descriptions of the sample collection sites, similar to what was done for the boreholes (Table 2.3; Appendix 2: Macroscopic Observations).

Table 2.3: An example of the sedimentological descriptions made for 19 tombstones. Sample 19 is used below.

Hangingwall	*Reef-Hangingwall Contact*	*Carbon Leader Reef*	*Reef-Footwall Contact*	*Footwall*	*Sample before cutting*
Underground observation and hand specimen: Medium to coarse-grained, medium to dark grey quartzite. Several pyrite foresets are present. An 8 mm wide, white, vertical quartz vein is seen cutting the hangingwall, passing though the reef and terminating in the footwall.	Sharp	Approximately 170 mm thick, mostly clast-supported conglomerate. Clasts are between 4-20 mm in size, subangular to well-rounded, and consist of milky to smoky quartz. Pyrite is abundant and occurs mainly in foresets. Small amounts of fly-speck carbon observed in the reef.	Sharp, marked by thin pyrite stringers.	Light grey, medium-grained quartzite, cut by several pyrite stringers. At the base of the stringers is a pebble band ±30 mm thick with subangular to well-rounded clasts of milky and smoky quartz. Chert and pyrite grains are also observed. Below the pebble band is a khaki green coarse to gritty-grained argillaceous quartzite.	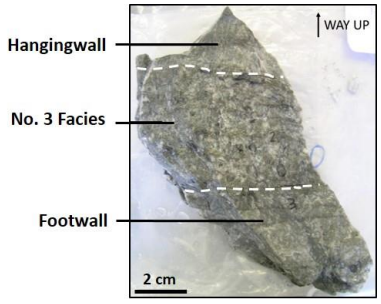

2.2 PETROLOGY

Polished thin sections for the tombstone samples were cut by SGS South Africa prior to the commencement of this research. A total of 84 polished thin sections (23 footwall, 38 Carbon Leader Reef and 23 hangingwall polished thin sections) for the 19 tombstone samples were made available by AngloGold Ashanti to undertake detailed petrographic studies (Appendix 3: Microscopic Observations).

On commencement of this research, 15 boreholes out of the total 49 were made available by AngloGold Ashanti to use for the cutting of polished thin sections and geochemical analyses (refer to Chapter 2.3 and 2.4). Only 15 boreholes were made available due to legal restrictions in place with regards to the usage of stored gold-bearing exploration boreholes by AngloGold Ashanti. Localities of preferred polished thin sections were marked out during the sampling of the boreholes and sent to SGS South Africa for cutting. A total of 15 polished thin sections (15 reef samples) were made available by AngloGold Ashanti for the purpose of this research (Appendix 3: Microscopic Observations).

Detailed petrographic studies were undertaken on a total of 99 polished thin sections to further investigate mineralogy, sedimentary features, metamorphism and alteration patterns of the samples. Both transmitted and reflected light microscopy was used to analyse the polished thin sections that were cut from the tombstones and the boreholes. The microscopic analyses were carried out to compare observations with the findings of the other methodologies used for this research.

2.3 GEOCHEMICAL ANALYSES

Geochemical analyses (XRF, XRD, ICP-OES, LECO analysis and atomic absorption spectroscopy) were carried out by SGS South Africa on 19 tombstones (for the footwall, Carbon Leader Reef and hangingwall) prior to the commencement of this research. A total of 61 samples were analysed and the geochemical results were made available by AngloGold Ashanti (Appendix 4: Geochemical Analyses and Gold Assay). Of the 61 samples: 20 were footwall samples (including a footwall pebble band for Sample 4); 22 were Carbon Leader Reef samples (including 2 reef

bands and Pale Pebbly Quartzite for Sample 2, and internal quartzite for Sample 15); and 19 were hangingwall samples.

Samples selected from the 15 boreholes that were made available by AngloGold Ashanti for this research were sent for geochemical analyses at SGS South Africa on commencement of this project. XRF analyses were carried out on a total of 45 samples (footwall, Carbon Leader Reef and hangingwall portions for each borehole). XRD, ICP-OES, LECO analysis and atomic absorption spectroscopy were only carried out on the reef portions (15 reef samples). The geochemical analyses could not be carried out for the footwall and hangingwall portions of the boreholes due to a shortage of sample material to use (refer to Chapter 2.2 with regard to the restrictions in the storage of gold-bearing exploration boreholes by AngloGold Ashanti). All the geochemical results for the boreholes were made available by AngloGold Ashanti (Appendix 4: Geochemical Analyses and Gold Assay).

Geochemical analyses were necessary to identify geochemical trends within the footwall, Carbon Leader Reef as well as the hangingwall, to compare with the findings in the other methodologies used for this research.

2.4 GOLD ASSAY

Gold assaying was carried out by SGS South Africa for a total of 61 tombstone samples (20 footwall samples, 22 Carbon Leader Reef samples and 19 hangingwall samples). The gold assaying results were made available by AngloGold Ashanti to use for this research (Appendix 4: Geochemical Analyses and Gold Assays).

For the boreholes only 15 Carbon Leader Reef samples were assayed. The assaying results for the boreholes were made available by AngloGold Ashanti (Appendix 4: Geochemical Analyses and Gold Assays).

The gold assaying method currently used at SGS South Africa for AngloGold Ashanti's samples is a (screen) fire assay. Screen fire assay involves pulverising a 1 kg fraction to 75-microns by passing each fraction through a 100-micron nylon screen (In-house Report, 2004b). All screened fractions were weighed, the assay data was combined, and the weighted assay value

was reported (In-house Report, 2004b). Cyanide leach assaying was used to check the screen assay technique and to determine gold content for 1 kg of sample (In-house Report, 2004b).

2.5 SPECTRAL SCANNING AND PROCESSING OF BOREHOLES AND TOMBSTONES

A total of 36 boreholes and 18 tombstones were scanned by AngloGold Ashanti for spectral analysis prior to the commencement of this study. The spectral scanning for the boreholes and tombstones was carried out at the AngloGold Ashanti Geoscience Technical Offices in Carletonville and was supervised by Mr. P. Linton. The boreholes were spectrally scanned using a hyperspectral core imager (Specim's sisuROCK®; Figure 2.1 (a); Appendix 7: Borehole Spectral Profiles and Appendix 8: Borehole Spectral Images) and the tombstones were spectrally scanned with a hand-held spectrometer (the TerraSpec®; Figure 2.1 (b); Appendix 5: Tombstone Spectral Profiles and Appendix 6: Tombstone Spectral Images).

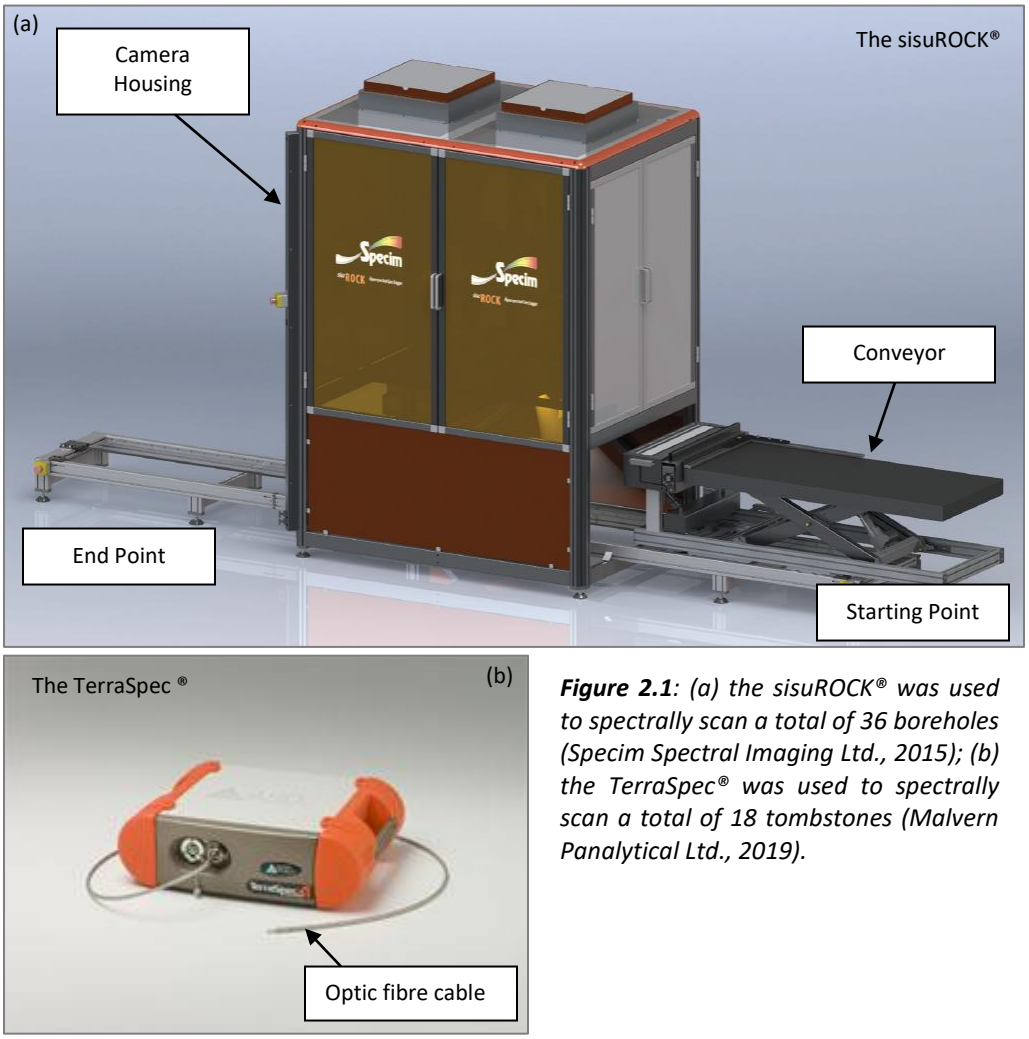

***Figure 2.1**: (a) the sisuROCK® was used to spectrally scan a total of 36 boreholes (Specim Spectral Imaging Ltd., 2015); (b) the TerraSpec® was used to spectrally scan a total of 18 tombstones (Malvern Panalytical Ltd., 2019).*

The default camera on the sisuROCK® is a short-wave infrared camera and is coupled with a Red-Green-Blue camera that offers high resolution colour imagery if textural information about samples is needed (Specim Spectral Imaging Ltd., 2015). The TerraSpec® spectrometer also uses a short-wave infrared technique to determine alteration minerals however, instead of being in a fixed position like the sisuROCK®, it is hand held (Hauff, 2001, p.1). Table 2.4 provides the performance specifications for the camera(s) on both the sisuROCK® and TerraSpec®.

Table 2.4: Performance specifications for the short-wave infrared and Red-Green-Blue cameras on the sisuROCK® (Specim Spectral Imaging Ltd., 2013) and for the short-wave infrared camera on the TerraSpec® spectrometer (ASD Inc., 2008, p.3; Malvern Panalytical Ltd., 2019).

	sisuROCK®		*TerraSpec®*
Camera Type	Short-wave infrared	Red-Green-Blue	Short-wave infrared
Spectral Range	970 to 2 500 nm	N/A	350 to 2 500 nm
Spectral Bands	256	3	Not provided
Spectral Resolution	10 nm	N/A	6 nm at 1 400/2 100 nm
Scanning Time	200 mm/s (full core tray)	200 mm/s (full core tray)	100 milliseconds

The sisuROCK® hyperspectral core imager short-wave infrared camera collects 256 bands of spectral data between the range of 970 to 2 500 nm at a resolution of 10 nm (Specim Spectral Imaging Ltd., 2013). The sisuROCK® uses high speed pushbroom hyperspectral imaging which allows recording of a perpendicular cross-section of any target along the track direction i.e. in perpendicular slices along the length of the core tray (Sigernes *et* al., 2018; Specim Spectral Imaging Ltd., 2013). The measurements are made by feeding a core tray on the conveyor into the camera housing, which is then automatically translated under the spectral camera to build a spectral image using built-in calibration measurements – this takes approximately 45 seconds to scan an entire core tray (Specim Spectral Imaging Ltd., 2013).

Prior to the feeding of each core tray a standard material (Spectralon) is imaged to make a dark current measurement to calculate noise inherent within the system (Specim Spectral Imaging Ltd., 2015; Tappert and Tappert, 2018). The dark current measurement(s) are then used to convert the data to reflectance measurements used for spectral interpretation (Specim Spectral Imaging Ltd., 2015; Tappert and Tappert, 2018).

Spectral data pre-processing requires the removal of all extraneous material from the image by means of masking, following which spectral indices, i.e. the depths, wavelengths and ratios of

absorption features, are calculated (Specim Spectral Imaging Ltd., 2015). From this, a mineral assemblage classification image can be prepared (Specim Spectral Imaging Ltd., 2015). The results are produced in the form of visual images as well as average values of spectral indices per image line (in this instance every 0.45 mm) (Specim Spectral Imaging Ltd., 2015). The spectral indices can be related back to phyllosilicate mineralogy (Specim Spectral Imaging Ltd., 2013).

The TerraSpec® spectrometer is simpler to use than the sisuROCK® and has the ability to collect spectral bands between the range of 350 to 2 500 nm at a resolution of 6 nm (ASD Inc., 2008, p.3; Malvern Panalytical Ltd., 2019). Specially formulated low OH-composition optical fibres are used to collect the optical energy from the surface of the sample (ASD Inc., 2008, p.6). The optic fibre cable is placed directly onto the surface of the sample and delivers the collected optical energy into the instrument, where it is then projected onto a concave holographic diffraction grating (ASD Inc., 2008, p.6). The grating serves to separate and reflect wavelength components for independent measurement by a thermo-electrically cooled Indium Gallium Arsenide detector (ASD Inc., 2008, p.7). The gratings are placed onto an oscillating shaft that moves back and forth through a 15-degree swing and as the grating moves, it exposes the detector to different wavelengths of optical energy (ASD Inc., 2008, p.7). The spectral data is digitised by means of an analogue-to-digital convertor and is transmitted to the instrument controller for further processing as well as analysis, by the controlling software (ASD Inc., 2008, p.7).

Varying processing methods can be used to obtain information from raw spectral image data - dependent on the dataset and processing parameters, different results are provided (Harris, 2006b, p.10). The Red-Green-Blue camera generates a natural colour image of the core (Figure 2.2 (a); Harris, 2006b, p.11). There are three main spectral processing output types for spectrometer systems, including enhanced infrared images, spectral facies (alternatively classification (class) images) and spectral indices (alternatively feature images) (Harris, 2006b, p.12). Figure 2.2 depicts the varying output type(s) generated for the Red-Green-Blue camera and spectrometer data.

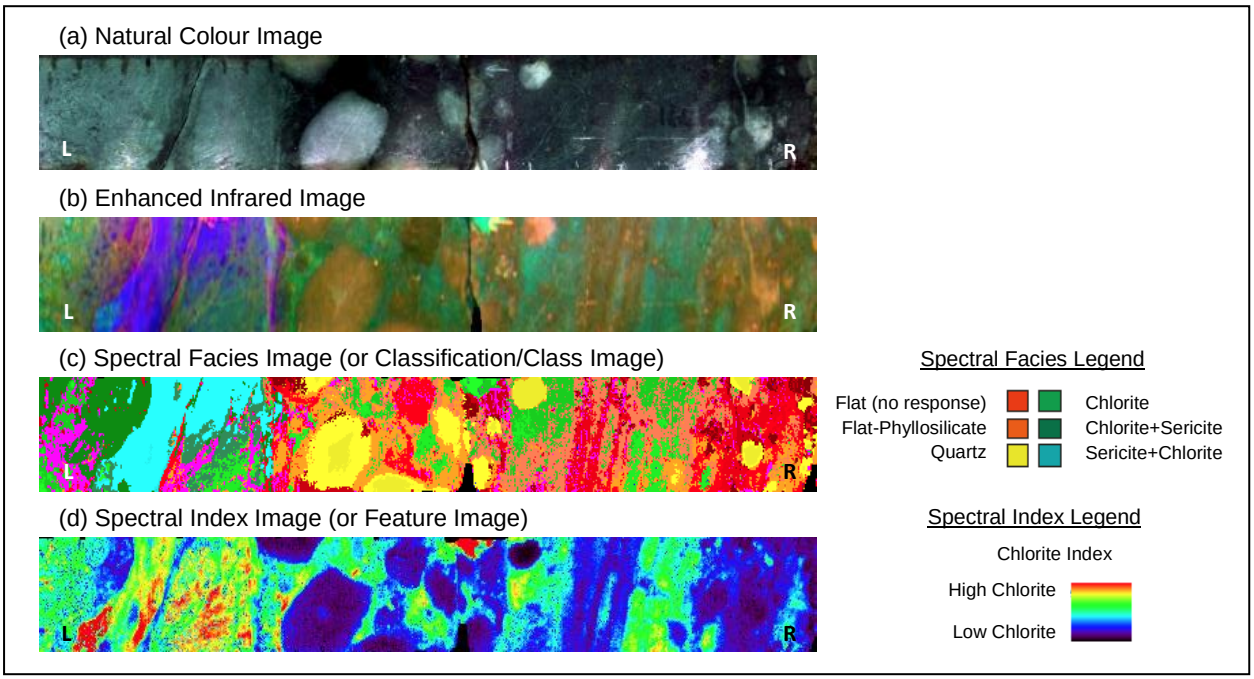

***Figure 2.2**: Examples of image outputs (from a left (L) to right (R) direction) generated for the Red-Green-Blue camera and spectral data: (a) Natural colour image; (b) Enhanced infrared image; (c) Spectral facies image; (d) Spectral index image (Adapted from Harris, 2006b, p.158)*

A natural colour image (Figure 2.2 (a)) is generated by a Red-Green-Blue camera system and produces a true or natural colour image of the sample (Harris, 2006b, p.159). For an accurate natural colour image, the sample should be cleaned and wet prior to spectral scanning (Harris, 2006b, p.159). The purpose of the natural colour image is to generate a continuous core/sample image segment (Harris, 2006b, p.11).

The enhanced infrared image (Figure 2.2 (b)) is created by the application of decorrelation stretch or a selected false-colour composite to the spectral data within the spectrometer system to enhance the colour output in the image (Harris, 2006b, p.11). Decorrelation stretching removes the high correlation commonly found in multispectral data sets (Harris Geospatial Solutions, 2018a). Typically, highly correlated data sets produce dull colour images and applying a decorrelation stretch technique helps to produce a more colourful image (Harris Geospatial Solutions, 2018a; The MathWorks Inc., 2005). Decorrelation stretching ideally needs three bands (for example red, green and blue) for input however it can be applied regardless of the number of colour bands (Harris Geospatial Solutions, 2018a; The MathWorks Inc., 2005). Applying a decorrelation stretch allows for the mapping of the original colour values of the

image to a new set of colour values but with a wider range, thus improving the overall colour of the image (Harris Geospatial Solutions, 2018a; The MathWorks Inc., 2005). The enhanced infrared image serves to discriminate between minerals (Harris, 2006b, p.12).

Figure 2.2 (c) shows a spectral facies image i.e. a classification image that uses the spectral information to define classes within the spectral data (Harris, 2006b, p.12). A multicoloured classification map is generated by plotting regions within the sample that define the presence of a mineral, spectral feature or a mineral assemblage (Harris, 2006b, p.159). Two classification methods can be used to carry out this technique: supervised and unsupervised classification (Amelio and Amelio, 2018; Harris, 2006b, p.12). The supervised classification method is a directed approach which allows for a better means of correlation between datasets that have been individually processed (Amelio and Amelio, 2018; Harris, 2006b, p.99). The unsupervised classification method is a data-driven approach which is dependent on the input data (Amelio and Amelio, 2018; Harris, 2006b, p.99). The unsupervised method reviews what is in the data in comparison to the supervised classification method that aims to determine if a specific response or feature is in the data or not (Harris, 2006b, p.99).

Referring to Figure 2.2 (c), the spectral facies image can be used for immediate mineral identification. The assigned colours in the legend are representative of the mineralogy present. A “flat” response is used to describe a non-response to the classification method i.e. the class has spectra that contain very little or no characteristic absorption features (Harris, 2006b, p.130). A single assignment to one colour such as “chlorite” indicates that the class is spectrally dominated by chlorite (Harris, 2006b, p.130). A dual assignment such as “chlorite + sericite” indicates that the class is characterised by variable amounts of both chlorite and sericite (Harris, 2006b, p.130).

A spectral index image (Figure 2.2 (d)) identifies specific minerals or features within the spectral data and can define variability of these minerals or features (Harris, 2006b, p.12). This image is produced by means of applying a rule-based feature extraction or matching specific spectral information to known mineralogical information (Harris, 2006b, p.96; Harris Geospatial Solutions, 2018a). Application of a feature extraction technique requires a reduction in

dimensionality that can efficiently represent interesting parts of an image, such as absorption feature depths, intensity of features and wavelength of features, as a compact feature vector (Harris, 2006b, p.160; The MathWorks Inc., 2005). This allows for quicker image matching and retrieval (The MathWorks Inc., 2005).

The spectral index image shows the prevalence of certain mineralogy which mostly responds to the results of the feature extraction(s). With regards to the chlorite feature extraction in Figure 2.2 (d), the cooler colours (shades of dark purple and blue) indicate a low response to the feature extraction i.e. low abundance of chlorite. Warmer colours (shades of green, orange and red) indicate a moderate to high response to the feature extraction i.e. moderate to high abundance of chlorite. Table 2.5 summarises the image types, descriptions, the source of the image, processing technique as well as the purpose of the spectral image.

Table 2.5: A summary of the main image outputs from the Red-Green-Blue camera and spectral data (Harris, 2006b).

Image Type	Description	Source of Image	Processing Technique(s)	Purpose
Natural Colour Image	Generated by a Red-Green-Blue camera that produces a true or natural colour image of the core	Camera system	Red-Green-Blue image of the three-band frame camera	Used to generate a continuous core image segment
Enhanced Infrared Image	Created by the application of a technique to the spectral data to enhance the colour output in the image	Spectrometer system	Decorrelation stretch or a selected false-colour composite	Used for the discrimination of minerals, not to identify minerals
Spectral Facies Image (Classification Image)	Spectral facies images use spectral information to define classes within the data	Spectrometer system	Multi-coloured class map generated from a combination of a supervised or unsupervised classification method	Used to define the presence of a mineral, spectral feature or mineral assemblage
Spectral Index Image (Feature Image)	Spectral index images define variability of specific spectral features or a set of features within the data	Spectrometer system	Feature extraction or spectral mapping	Specific minerals or features are targeted in these images

For the purpose of this research both spectral facies and spectral index images were used to identify minerals present within the tombstone and borehole samples, as well as to target spectral features of specific minerals (pyrophyllite, sericite, chlorite and chloritoid) by making use of the respective feature extractions. Collectively the interpretations of both images should

align and complement one another. In Figure 2.2 (c), chlorite was the dominant mineralogy in the left-most portion of the borehole in the spectral facies image, and this was confirmed by the higher response to the chlorite feature extraction in the spectral index image (Figure 2.2 (d)). The presence of chlorite was noted in the right-most portion in between grains of pyrophyllite in the spectral facies image (Figure 2.2 (c)), this was confirmed by the moderate response to the chlorite feature extraction in the spectral index image (Figure 2.2 (d)).

If the interpretations of the spectral facies and spectral index images do not align 100% it is very likely due to mineral mixtures within the spectral index images (Harris, 2006b, p.101; Hauff, 2001, p.2). The mineral mixtures within a sample can affect the measurement method for extraction of composition and crystallinity information, creating inaccurate variations in the measurements (Harris, 2006b, p.101). Additionally, mineral mixtures can change the spectral response including suppressing the contrast, which subsequently changes the depth characteristics of the spectra and ultimately alters the spectral abundance representation i.e. the spectral profile(s) (Harris, 2006b, p.101; Hauff, 2001, p.2). Other features that can influence the spectral facies image and create spectral variation include the presence of water (the sample needs to be dried after a natural colour image has been taken), particle size effects, organic material, material orientation as well as sample texture (Harris, 2006b, p.100; Hauff, 2001, p.2).

For the purpose of this research, AngloGold Ashanti made the already processed data for the tombstones as well as the raw spectral data for the boreholes available. The spectral data for each borehole included a small portion of footwall, hangingwall and the entire Carbon Leader Reef portion. The tombstone spectral images extended from the footwall to the Carbon Leader Reef, through to the hangingwall. Although the initial stages of spectral scanning had already been completed, the raw spectral data for the boreholes had not yet been processed nor interpreted. Processing of the raw spectral data for the boreholes was carried out by TerraCore Geospectral Imaging by means of in-house spectral processing software to produce visual image displays as well as digital data files. The processed data for the tombstones, including the visual image displays and digital data files, were readily available and provided by AngloGold Ashanti for interpretation. Interpretation of the processed spectral data (visual image displays

and digital data files) for both the tombstones and the boreholes was carried out independently, with input from Mr. K. Mushiana from TerraCore Geospectral Imaging. An example of the spectral image outcomes and interpretation of the tombstones is seen in Table 2.6. The remainder of the tombstone spectral images can be referred to in Appendix 6: Tombstone Spectral Images.

Table 2.6: A spectral facies image as well as spectral responses to the pyrophyllite, sericite, chlorite and chloritoid feature extractions (i.e. the spectral index images) in a tombstone, scanned with a TerraSpec® spectrometer. Sample 1 is used below, where the spectral image outcomes for the hangingwall (HW), No. 1 Facies and footwall (FW) are seen. Cooler colours (shades of dark purple and blue) indicate a low response to the feature extraction, and warmer colours (shades of green, orange and red) indicate a moderate to high response to the feature extraction.

Spectral Facies Image	Pyrophyllite (λ = 2 165 nm)	Sericite (λ = 2 200 nm)	Chlorite (λ = 2 250 nm)	Chloritoid (λ = 2 390 nm)
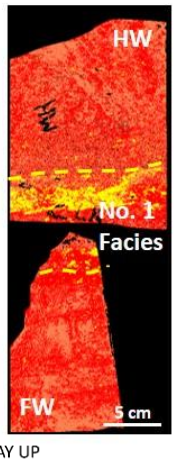	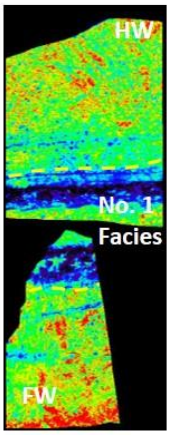	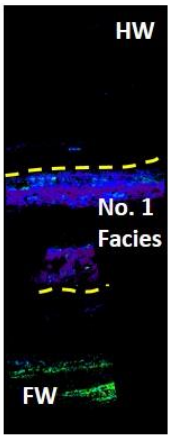	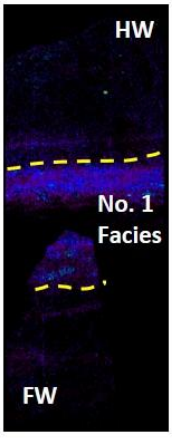	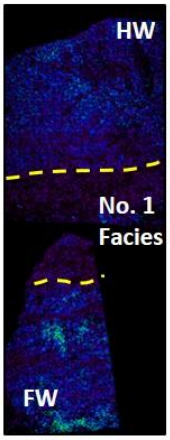
Pyrophyllite + chloritoid and pyrophyllite + chlorite combination present. Flat spectra indicative of silica/pyrophyllite/ chloritoid/chlorite/white mica within sample (no clear indication with the feature extractions).	Pyrophyllite is present within the reef band however not in large amounts such as those seen in the hangingwall and footwall.	The sericite feature extraction indicates a small amount of sericite is present within the reef band.	Chlorite is present in the reef band however in minimal amounts.	Very little response from the chloritoid feature extraction - suggesting that very little chloritoid is present in the reef band. A better response to the feature extraction is seen in the hangingwall and footwall quartzite.
Legend for Spectral Facies Image Flat spectra (+pyrophyllite/ chloritoid/silica/chlorite/white mica) Silica	*Pyrophyllite dominant* Pyrophyllite Pyrophyllite + chloritoid Pyrophyllite + chlorite Pyrophyllite + sericite	*Chloritoid dominant* Chloritoid Chloritoid + pyrophyllite Chloritoid + sericite	*Sericite dominant* Sericite Sericite + chloritoid Sericite + chlorite	*Chlorite dominant* Chlorite Chlorite + sericite

The spectral facies image for the tombstone above indicated high amounts of pyrophyllite in the hangingwall and footwall quartzite combined with chloritoid and chlorite. The No. 1 Facies was pyrophyllite-dominant with flat spectra, which could be interpreted as silica, pyrophyllite, chloritoid, chlorite or white mica within the sample. By referring to the spectral index images

the probable flat spectra could be identified. Comparing the spectral facies image with the spectral index images confirms the presence of pyrophyllite throughout the hangingwall and footwall quartzite with the highest response to the pyrophyllite feature extraction seen above and below the reef, as well as in the centre of the Carbon Leader Reef, suggesting a higher abundance of pyrophyllite. The lower response to the pyrophyllite feature extraction was seen on the outer edges of the Carbon Leader Reef, closer to the contacts with the hangingwall and footwall quartzite. The response to the sericite feature extraction suggests a small amount of sericite was present within the reef - slightly more in comparison to the overlying hangingwall and underlying footwall quartzite. The chlorite feature extraction reveals a low amount of chlorite was present within the reef and the chloritoid feature extraction revealed a better response within the hangingwall and footwall quartzite in comparison to the Carbon Leader Reef. This suggested higher amounts of chloritoid within the hangingwall and footwall. Following the pyrophyllite spectral index image the next greatest response to a feature extraction was the sericite feature extraction. By comparing the locality of the flat spectra within the spectral facies image the higher response to the sericite feature extraction was seen in a similar location in the tombstone, suggesting the flat spectra are indicative of the presence of sericite and chlorite within the No. 1 Facies, hosted within a pyrophyllite-rich matrix.

An example of the spectral image outcomes and interpretation of the boreholes is seen in Table 2.7. The remainder of the borehole spectral images can be referred to in Appendix 8: Borehole Spectral Images. As with the tombstones, the boreholes could be interpreted as follows: both the No. 2A and No. 2B Facies reef bands are sericite-dominant with lesser amounts of chlorite. This was confirmed by the high response to the sericite feature extraction and a moderate response to the chlorite feature extraction in both reef bands. High responses to the sericite and chloritoid feature extractions were seen in the Brown-Orange Argillaceous Zone overlying the No. 2B Facies. This correlated well with the sericite-dominant and chloritoid + sericite combinations noted within the spectral facies image. The highest response to a feature extraction for the Pale Pebbly Quartzite was the pyrophyllite feature extraction, with a moderate response to the sericite and chloritoid feature extractions - which was similarly noted within the spectral facies image.

Table 2.7: A spectral facies image as well as spectral responses to the pyrophyllite, sericite, chlorite and chloritoid feature extractions (i.e. the spectral index images) in a borehole, scanned with sisuROCK® spectrometer. Sample 22 is used below, where the spectral image outcomes for the Brown-Orange Argillaceous Zone (BOAZ), No. 2A and No. 2B Facies, Pale Pebbly Quartzite (PPQ) and footwall (FW) are seen. Cooler colours (shades of dark purple and blue) indicate a low response to the feature extraction, and warmer colours (shades of green, orange and red) indicate a moderate to high response to the feature extraction.

Spectral Facies Image	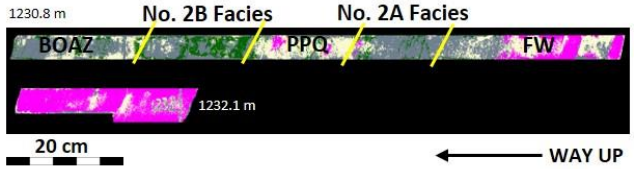	Both the upper (No. 2B Facies) and lower (No. 2A Facies) reef bands are sericite-dominant with lesser amounts of chlorite + sericite combinations. The overlying Brown-Orange Argillaceous Zone is sericite-dominant with smaller occurrences of chloritoid + sericite combinations. The Pale Pebbly Quartzite is pyrophyllite and chloritoid + sericite-rich, and the footwall quartzite is chloritoid and chloritoid + pyrophyllite-dominant with traces of sericite.
Pyrophyllite (λ = 2 165 nm)	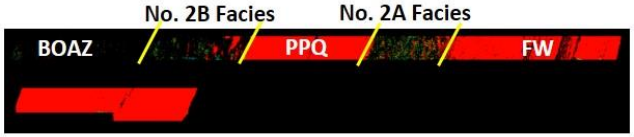	Pyrophyllite is moderately responsive at the bottom contacts for both the upper and lower reef bands, suggesting a concentration of pyrophyllite nearer to the bottom contacts. The Pale Pebbly Quartzite and footwall quartzite are highly responsive, suggesting high amounts of pyrophyllite within these units.
Sericite (λ = 2 200 nm)	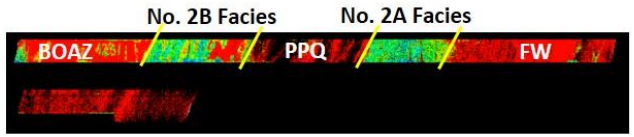	The sericite feature extraction shows sericite is highly responsive in the upper reef band and moderately responsive in the lower reef band, suggesting higher concentrations of sericite in the upper reef band. The units surrounding both reef units are highly responsive to the sericite feature extraction.
Chlorite (λ = 2 250 nm)	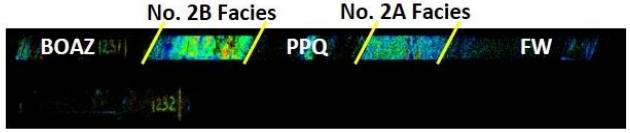	The upper reef band is moderately responsive in comparison to the lower reef band, indicating higher amounts of chlorite are present in the upper reef band. The units surrounding the No. 2A and No. 2B Facies have very little to no response to the chlorite feature extraction.
Chloritoid (λ = 2 390 nm)	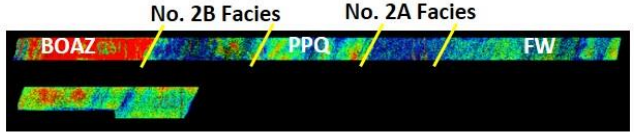	Chloritoid is low to moderately responsive, with the highest response at the base of the upper reef band. The highest response to the chloritoid feature extraction is from the Brown-Orange Argillaceous Zone overlying the No. 2B Facies, followed by the Pale Pebbly Quartzite between the two reef bands.

Legend for Spectral Facies Image

- Flat spectra (+pyrophyllite/ chloritoid/silica/chlorite/white mica)
- Silica

Pyrophyllite dominant
- Pyrophyllite
- Pyrophyllite + chloritoid
- Pyrophyllite + chlorite
- Pyrophyllite + sericite

Chloritoid dominant
- Chloritoid
- Chloritoid + pyrophyllite
- Chloritoid + sericite

Sericite dominant
- Sericite
- Sericite + chloritoid
- Sericite + chlorite

Chlorite dominant
- Chlorite
- Chlorite + sericite

The footwall was chloritoid and chloritoid + pyrophyllite-dominant with traces of sericite. This compared well with the responses to the pyrophyllite, sericite and chloritoid feature extractions. Additional to the spectral image outputs from the spectrometers the digital (spectral) data files that are compiled during spectral scanning could be used to create spectral profiles. Spectral profiles display the mean depth of the mineral and suggest the relative abundance of the mineral within the sample i.e. higher mean depth indicates a higher abundance of a mineral (Murphy *et al*., 2015). The spectral profiles for the tombstones (Appendix 5: Tombstone Spectral Profiles) are different to the boreholes (Appendix 7: Borehole Spectral Profiles) in that the TerraSpec® allowed for only one reading per sedimentological unit i.e. footwall, Carbon Leader Reef and hangingwall in comparison to the tens to hundreds of readings per sedimentological unit carried out by the sisuROCK®. This limits the detail to create entire spectral profiles for the tombstones however the readings per sedimentological unit can be compared with each other to note the variations in mineralogy. The spectral profile data for the tombstones were made available by AngloGold Ashanti for the purpose of this study. The spectral profile data was processed prior to the commencement of this research.

An example of the mean depths for each feature extraction for the tombstones can be seen in Table 2.8. The mean depths could be used to supplement the interpretations of the spectral image outputs.

Table 2.8: Spectral mean depths against the pyrophyllite, sericite, chlorite and chloritoid feature extractions for a tombstone sample, scanned with a TerraSpec® spectrometer. Sample 1 is used below.

Unit	Mean Depth			
	Pyrophyllite (λ = 2 165 nm)	Sericite (λ = 2 200 nm)	Chlorite (λ = 2 250 nm)	Chloritoid (λ = 2 390 nm)
Hangingwall	32.547	0.114	0.758	2.992
Carbon Leader Reef	11.652	5.772	2.767	1.478
Footwall	35.479	0.788	0.253	3.374

When comparing the spectral image outputs in Table 2.6 with the spectral mean depths in Table 2.8 the findings were the same. Both the hangingwall and footwall quartzites have a higher response to the pyrophyllite feature extraction, with the highest response recorded in the footwall suggesting higher amounts of pyrophyllite in the footwall. The reef had a moderate response to the sericite feature extraction and a lower response to the chlorite feature extraction. The responses to these feature extractions were greater than that of the hangingwall and footwall units, suggesting higher amounts of sericite and chlorite could be found in the Carbon Leader Reef in comparison to the overlying hangingwall and underlying

footwall unit. The footwall had a higher response to the chloritoid feature extraction than the hangingwall, and the Carbon Leader Reef had the least response to the chloritoid feature extraction. This suggested higher amounts of chloritoid in the hangingwall and footwall unit in comparison to the Carbon Leader Reef.

The mean depth spectral profiles for the same (borehole) sample used in Table 2.7 can be seen in Figure 2.3.

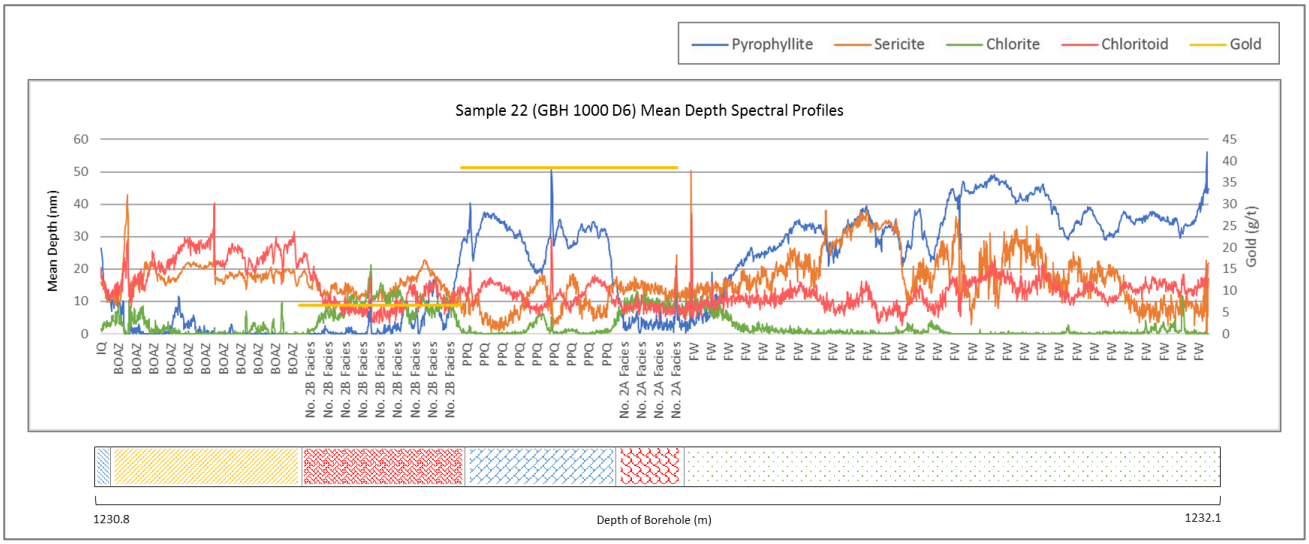

***Figure 2.3**: Mean depth spectral profiles against the pyrophyllite, sericite, chlorite and chloritoid feature extractions. Sample 22 is used above, where the spectral profiles for the Brown-Orange Argillaceous Zone (BOAZ), No. 2A and No. 2B Facies, Pale Pebbly Quartzite (PPQ) and footwall (FW) are seen. A borehole log to show the relative depth of the borehole and the sedimentological unit(s) underlies the spectral profiles.*

The spectral profiles correlated well with the spectral images of Sample 22. A high response to the sericite feature extraction and a moderate response to the chlorite feature extraction in both the No. 2A and No. 2B Facies were seen. High responses were seen to the sericite and chloritoid feature extractions within the Brown-Orange Argillaceous Zone. The highest response recorded within the Pale Pebbly Quartzite was to the pyrophyllite feature extraction, with a moderate response to the sericite and chloritoid feature extractions. The spectral profile for the footwall unit suggested the highest response was to the pyrophyllite feature extraction whereas previously the footwall was classified as chloritoid dominant with chloritoid + pyrophyllite combinations, with traces of sericite.

As with discrepancies between spectral facies images and spectral index images, discrepancies may be encountered between the visual images and the spectral profiles and may influence overall interpretations slightly, however the accuracy of the spectral profile is greater than the

visual images. The spectral profile is based on readings taken of the average values of spectral indices per image line (Specim Spectral Imaging Ltd., 2015). The detail in a spectral profile is singled out per spectral index and the various responses in relation to location can almost be pin-pointed, whereas the visual images are created by grouping similar features, wavelengths, mean depths etc., and the detail of the spectral data is then sometimes lost (Harris, 2006b, p.101; The MathWorks Inc., 2005).

2.6 GEOLOGICAL MODELLING

Using the outcomes from the aforementioned methodologies, a geological model was created to highlight different alteration 'zones', that group areas with characteristically similar alteration styles, across the West Wits Line. This was done using Datamine's StudioRM® software (currently licenced for use at AngloGold Ashanti).

A structure model (used by AngloGold Ashanti) of the West Wits Line was used in the modelling of the alteration zones to get a broader perspective of alteration that has occurred and to note how alteration is influenced by structural controls such as faulting and intrusions. The structure model uses borehole logging and underground mapping of intrusions/faults, and aids mine planning processes that are undertaken at the mine.

The different alteration zones were also cross-correlated with the AngloGold Ashanti Carbon Leader Reef facies model and Carbon Leader Reef estimation domains (refer to Chapter 1.5) to investigate possible correlations (where possible) and to indicate any variances between the different models.

3 RESULTS

3.1 MACROSCOPIC OBSERVATIONS

Hangingwall, footwall as well as Carbon Leader Reef macroscopic descriptions were made for all (19) tombstone samples and (49) boreholes used for this project. The current research focused on the reef intersections as the project was designed to investigate alteration of the Carbon Leader Reef and the possible association between alteration and gold grades. Less emphasis was placed on alteration of the hangingwall and footwall units as

preliminary/previous investigations on the tombstone samples indicated that these do not host significant quantities of gold.

Refer to Appendix 2: Macroscopic Observations for detailed descriptions of all samples (refer to Appendix 1: Sample Locality Map) that were used throughout the proceeding methodology.

3.1.1 Hangingwall Descriptions

The easternmost portion of TauTona Mine characteristically has a fine to medium-grained light grey to dark grey siliceous quartzite as the hangingwall. Pyrite along foresets were common within the area, as were rounded disseminated pyrite grains. Occasionally there is discolouration of the quartzite immediately surrounding the pyrite stringers as well as around small fractures. Disseminated cubic pyrite (1 to 4 mm diameter) was also seen randomly distributed throughout the hangingwall quartzite as isolate crystals and as crystal clusters (Figure 3.1).

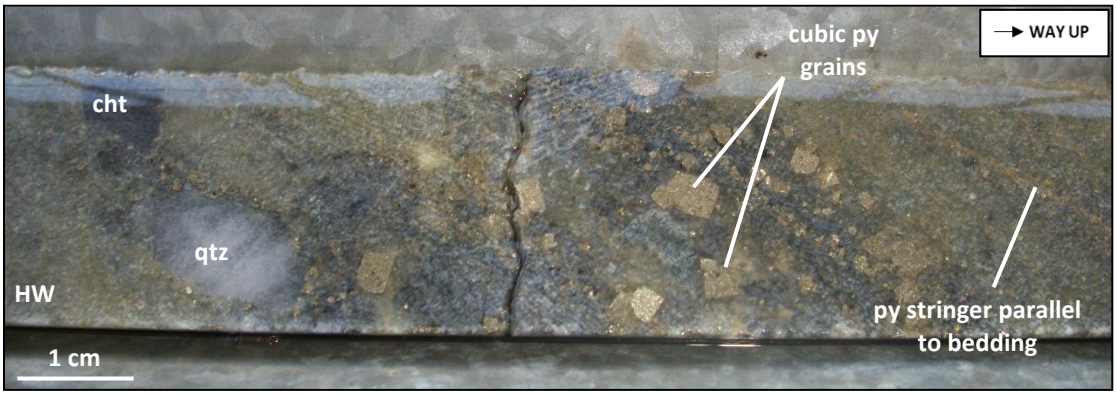

***Figure 3.1**: Close-up of the cubic pyrite (py) grains and pyrite stringers seen in the easternmost areas at TauTona Mine within the hangingwall (HW) quartzite. Floating clasts of chert (cht) and quartz (qtz) were also noted within the hangingwall quartzite – Sample 20.*

In some instances, there is a greenish discolouration (possibly due to chloritisation) of the hangingwall closer to the upper reef contact (Figure 3.2).



***Figure 3.2**: Greenish discolouration (area of possible chloritisation) of the hangingwall (HW) quartzite closer to the No. 1 Facies-hangingwall contact. Pyrite (py) on foresets was seen in between bedding-parallel bluish-grey bands in the hangingwall quartzite – Sample 28.*

Dark bluish-grey bands were also noted within the hangingwall and were aligned parallel to bedding. The bands ranged in thickness from <10 to 50 mm. Pyrite on foresets were noted in between the bluish-grey bands. Quartz veining was common in the hangingwall unit (Figure 3.3 (a)) and on some occasions a poorly developed pebble lag of smoky quartz clasts, averaging 15 mm in diameter, could be seen just above the reef (Figure 3.3 (b)).

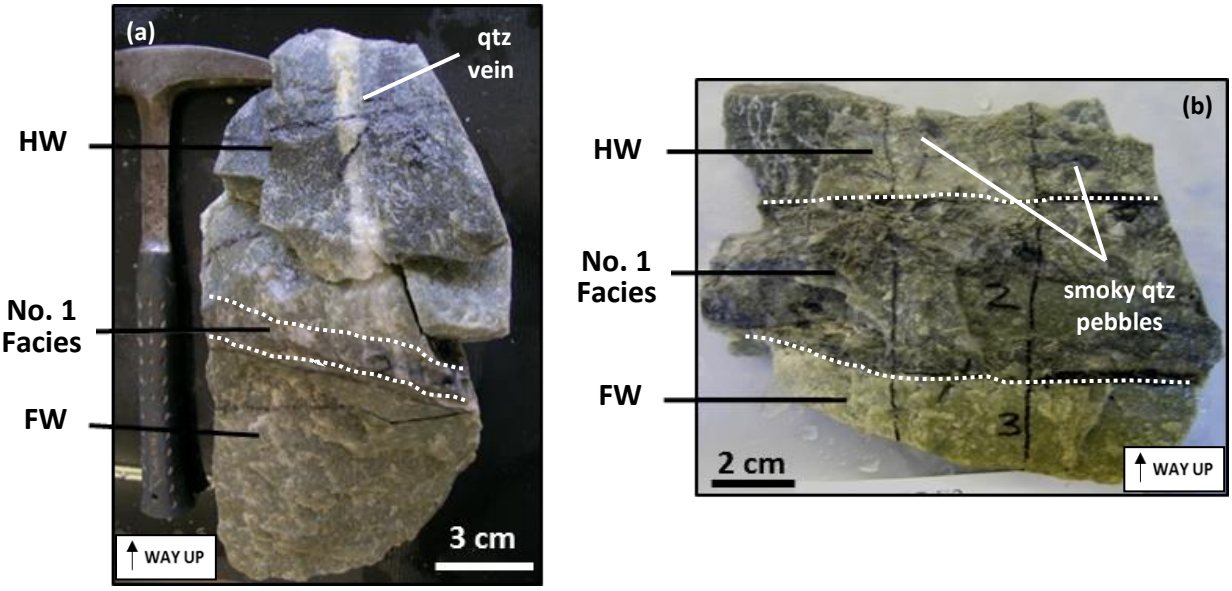

***Figure 3.3**: (a) A 14 mm thick quartz (qtz) vein cutting the hangingwall (HW) quartzite. The vein was truncated at the No. 1 Facies upper contact with the hangingwall quartzite and did not extend to the footwall (FW) quartzite – Sample 5; (b) Scattered clasts (poor pebble lag) in the hangingwall quartzite proximal to the No. 1 Facies contact – Sample 14.*

The southernmost portion of TauTona, as well as within the Mponeng boundary, had similar features to the hangingwall of the easternmost portion however the pebble lag was more defined with rounded to sub-rounded milky and smoky quartz clasts (4 to 10 mm in size). The westernmost portion of TauTona, as well as within the Savuka boundary, showed a similar hangingwall to the easternmost portion with a poorly developed pebble lag above the reef (Figure 3.4).

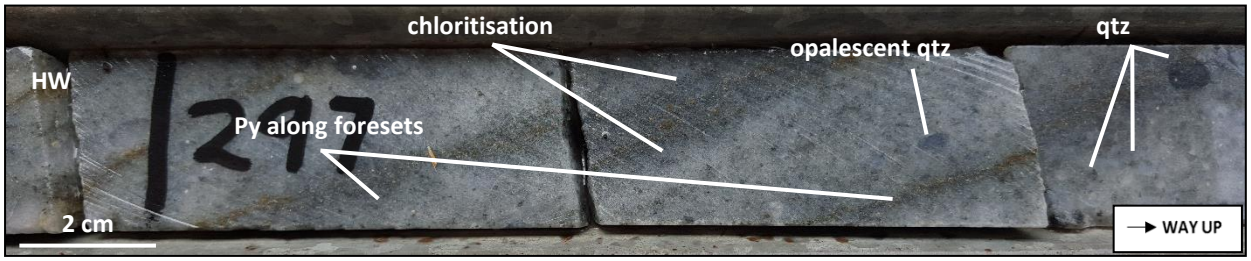

***Figure 3.4**: An under-developed pebble lag comprising various quartz (qtz) clasts above the No. 2B Facies contact within the hangingwall (HW) quartzite. Pyrite (py) along foresets was visible, as are small areas of possible chloritisation within the hangingwall quartzite – Sample 23.*

Typically, the clasts were aligned parallel to bedding, were predominantly smoky and milky quartz, and ranged from <5 to 10 mm in diameter. It was also common to find pyrite stringers aligned parallel to bedding within the hangingwall unit. The stringers were often accompanied by a greenish discolouration (possibly chloritisation) of the host quartzite. Disseminated rounded pyrite was visible in the semi-siliceous to siliceous hangingwall quartzite unit.

3.1.2 Footwall Descriptions

The footwall quartzite in the easternmost portion of TauTona varied in grain size from medium to coarse-grained and was typically semi-argillaceous to argillaceous. The colour varied from a greenish-grey to dark grey and hosted both floating smoky and milky quartz clasts as well as footwall pebble bands. The footwall pebble bands (Figure 3.5 (a)) were moderately developed pebble lags, ranging in thickness from 10 to 50 mm, with smoky and milky quartz clasts as well as a few chert clasts. The floating clasts and clasts within the footwall pebble bands were subrounded to subangular, and ranged in size from 2 to 10 mm in diameter.

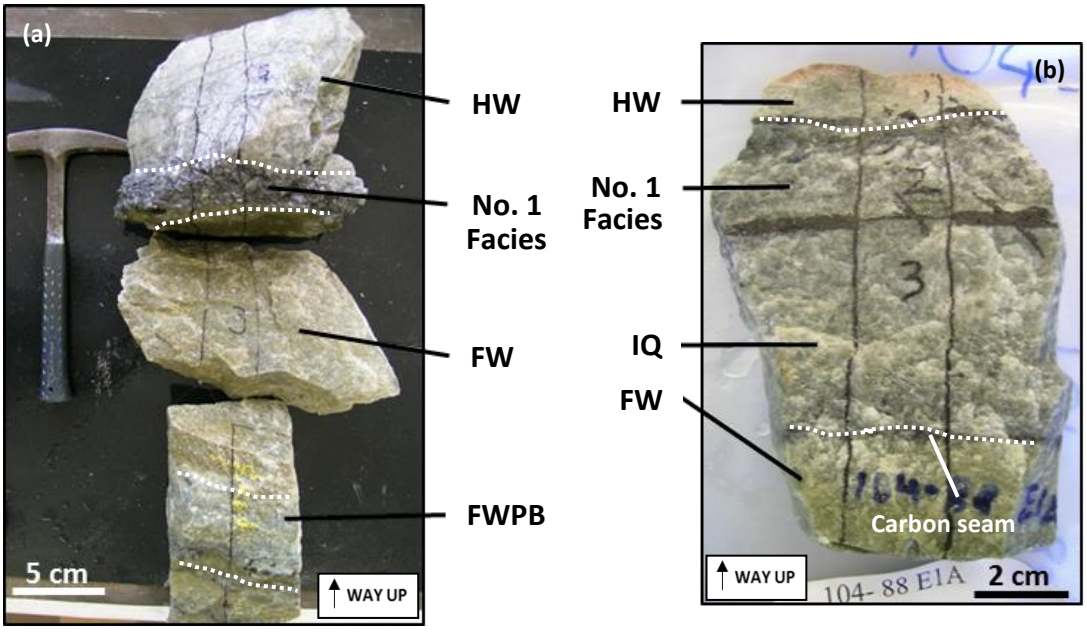

***Figure 3.5**: (a) A poorly developed footwall pebble band (FWPB) in the footwall (FW) quartzite unit underlying the No. 1 Facies and hangingwall (HW) quartzite units – Sample 4; (b) A thin carbon seam separates the footwall quartzite and internal quartzite (IQ) units – Sample 12.*

Very fine-grained rounded disseminated pyrite grains were seen within the quartzite and in the footwall pebble bands. Fine pyrite stringers were present and were often aligned along fractures within the quartzite or were sub-parallel to the bedding of the quartzite. Figure 3.5 (b) shows a thin carbon seam approximately 100 mm below the base of the reef and underlying

internal quartzite that could be initially mistaken as footwall quartzite. The quartzite between the base of the reef and the carbon seam was light grey, medium to coarse-grained and semi-siliceous, with a pebble lag of milky and smoky quartz clasts up to 7 mm in diameter. Below the carbon seam the footwall was a coarse-grained to gritty, greenish-brown argillaceous quartzite.

Another example of a footwall pebble band can be seen in Figure 3.6. Smoky and milky quartz clasts were visible alongside chert clasts and were set within a gritty-textured matrix that was greenish-grey in colour. The pebbles were subrounded to subangular.

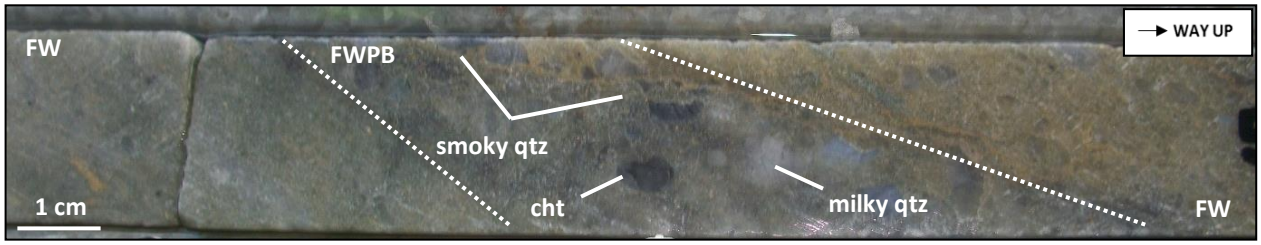

***Figure 3.6**: A poorly developed footwall pebble band (FWPB) hosting milky and smoky quartz (qtz) clasts alongside chert (cht) pebbles in the footwall (FW) quartzite unit. There was a noted colour variation in the footwall quartzite above and below the footwall pebble band – Sample 20.*

There was a definite colour variation in the footwall quartzite above and below the footwall pebble band. The overlying footwall quartzite above the footwall pebble band had a darker khaki-brown colour when compared to the underlying footwall quartzite. Fault-fill veining was noted within the overlying footwall quartzite, suggesting the sample was proximal to a fault or a fault zone. Fluid migration along the fault (or fault zone) may explain why there was a colour variation between the overlying and underlying footwall quartzite units. Rounded disseminated pyrite was seen scattered amongst the clasts. In the same sample there were unusual, apparently chlorite-rich clasts set within a well-developed footwall pebble band (Figure 3.7). The milky quartz clasts had undergone alteration, possibly chloritisation, allowing for a greenish discolouration.



***Figure 3.7**: Footwall pebble band (FWPB) with possible chloritisation of some milky quartz (qtz) clasts. Smoky quartz clasts as well as interstitial pyrite (py) was also noted within the footwall pebble band – Sample 20.*

Within the Mponeng boundary (and south of TauTona and Savuka), the footwall was light greenish-grey to dark khaki-green argillaceous quartzite and was gritty to coarse-grained. The footwall pebble bands were better developed (however, on average are thinner) than within the easternmost portion of TauTona, with rounded to subrounded clasts of milky and smoky quartz as well as chert. The clasts ranged from <5 to 15 mm. Fine-grained and rounded grains of disseminated pyrite was seen to occur interstitially between the clasts and set within a dark greenish-grey coarse-grained matrix (Figure 3.8). Within the footwall quartzite itself subrounded to angular clasts of smoky and milky quartz were observed.

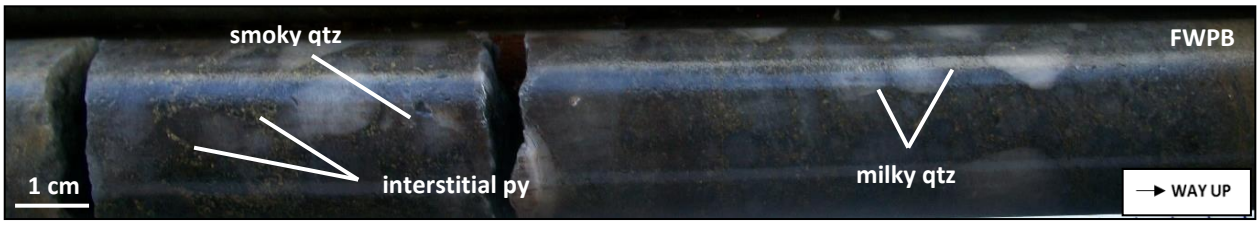

***Figure 3.8**: A well-developed footwall pebble band (FWPB) with predominantly smoky and milky quartz (qtz) clasts set within a dark greenish-grey matrix. Interstitial pyrite (py) occured between the clasts – Sample 34.*

In Sample 34 (Figure 3.9) angular chert clasts were found to be floating within the footwall quartzite unit. Very thin pyrite grains along foresets (comprising very fine-grained rounded pyrite grains) were seen in the footwall quartzite, as well as thin rounded pyrite in stringers along bedding-parallel fractures. Discolouration of the quartzite was seen on the outer edges of the pyrite stringers. Very fine-grained rounded disseminated pyrite was seen in the footwall quartzite however the amount of pyrite was considerably less than in the easternmost region of the TauTona Mine.

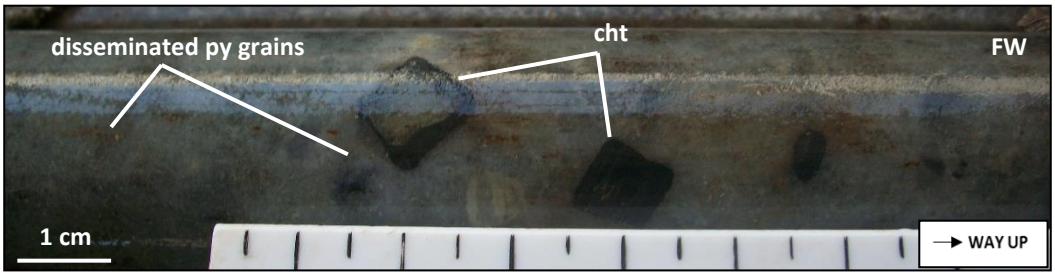

***Figure 3.9**: Angular chert (cht) clasts floating within a coarse-grained greenish-grey footwall (FW) quartzite. Very fine-grained rounded disseminated pyrite (py) grains were visible within the footwall quartzite – Sample 34.*

In the westernmost area of TauTona and within the Savuka boundary the footwall quartzite was similar to the aforementioned area nearer to the Mponeng boundary. The colour variations were similar, ranging from a light greenish-grey to a khaki-green and the unit was gritty to coarse-grained (Figure 3.10). The footwall pebble bands were on average similar

across the West Wits Line however they were better developed with more compacted and rounded clasts ranging from 5 to 10 mm in diameter.



***Figure 3.10**: Greenish-grey argillaceous footwall (FW) quartzite with small floating clasts of rounded smoky quartz (qtz) and elongated to angular chert (cht) – Sample 23.*

In Sample 44 (Figure 3.11) there was discolouration of the footwall unit nearer to the No. 2A Facies, becoming a darker khaki-green with closer proximity to the reef. Floating elongated clasts of smoky and milky quartz (up to 10 mm on the long axis) could be seen aligned parallel to bedding. Fine-grained rounded disseminated pyrite was also seen within the footwall unit.



***Figure 3.11**: Discolouration (darkening) of the footwall (FW) quartzite closer to the No. 2A Facies. Floating clasts of smoky quartz (qtz) are also noted within the footwall quartzite – Sample 44.*

Very small subrounded to rounded floating 2 to 5 mm clasts (possibly a poorly developed footwall pebble band) can be seen in Figure 3.12. The quartzite had a grittier texture compared to that observed in Figure 3.11 and had very small smoky and milky quartz clasts giving the footwall an almost pebbly texture. The chert clasts seen within the borehole were smaller than the quartz clasts and were less frequent than what was typically seen in a footwall pebble band, suggesting the occurrence of these clasts was due to a pebble lag.



***Figure 3.12**: Floating chert (cht), smoky and milky quartz (qtz) clasts scattered across a gritty-textured footwall (FW) quartzite – Sample 48.*

3.1.3 Carbon Leader Reef Descriptions

As previously mentioned in Chapter 1.5, there are three facies types of the Carbon Leader Reef: (i) Carbon Leader Reef with a (basal) carbon seam (No. 1 Facies), (ii) Carbon Leader Reef with

multiple conglomerates (No. 2 Facies) and (iii) Carbon Leader Reef single conglomerate with fly-speck carbon (No. 3 Facies).

(i) *Carbon Leader Reef No. 1 Facies*

The Carbon Leader Reef No. 1 Facies was found in samples from the eastern and south to south-eastern area of TauTona. Table 3.1 summarises the boreholes and tombstones identified to be No. 1 Facies.

Table 3.1: A summary of the borehole and tombstone samples that are representative of the Carbon Leader Reef No. 1 Facies (21 samples in total).

Sample No.	Sample ID	Sample Type	Sample No.	Sample ID	Sample Type
1	94-94 E1	Tombstone	24	GBH 3763	Borehole
3	104-88 W6	Tombstone	27	GBH 4003	Borehole
4	105-86 E2	Tombstone	28	GBH 6000	Borehole
5	112-83 W3	Tombstone	30	GBH 6003	Borehole
6	112-83 W4	Tombstone	32	GBH 6014	Borehole
7	114-78 E1	Tombstone	33	GBH 6028	Borehole
10	96-94 E2	Tombstone	34	GBH 6036	Borehole
12	104-88 E1A	Tombstone	45	GBH 6008	Borehole
13	104-88 W7	Tombstone	65	UD 36 D4	Borehole
14	109-87 E2	Tombstone	66	UD 36 D7	Borehole
15	112-84 Rse	Tombstone			

In the easternmost portion of TauTona the No. 1 Facies was predominantly matrix-supported with a dark to light grey, fine to medium-grained matrix (Figure 3.13).

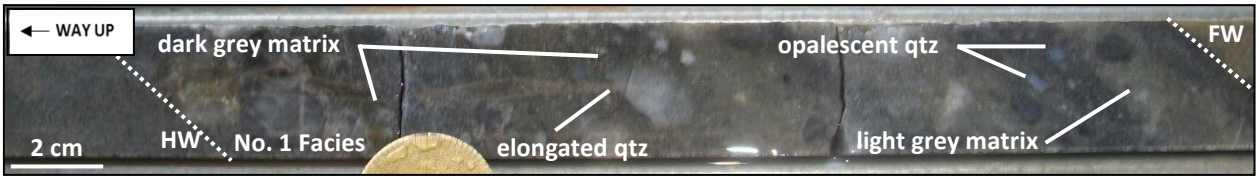

Figure 3.13*: Matrix-supported No. 1 Facies overlying the footwall (FW) quartzite and underlying the hangingwall (HW) quartzite unit. The No. 1 Facies had an alternating dark grey and light grey matrix with varying sizes and types of quartz (qtz) clasts – Sample 24.*

Very fine to fine-grained disseminated rounded and euhedral pyrite grains were visible within the matrix, as well as concentrated around the edges of clasts. The clasts were predominantly smoky and milky quartz, subrounded to rounded, and ranging from 2 to 25 mm in diameter. Elongated clasts of smoky and milky quartz are frequent and are aligned parallel to bedding. Dark grey to black subrounded chert clasts up to 10 mm in diameter could be seen occasionally in the reef as well as small (<5 mm) blue opalescent quartz clasts. The thicknesses of the No. 1 Facies varied from 40 to 95 mm.

A carbon seam could be seen in some of the samples, such as in Samples 4, 7, 12, 15, 17, 32 and 64. Where there was a lack of a carbon seam in the boreholes, in most cases it was assumed to have been washed away during drilling as it is very soft and easily dispersed, particularly in the drilling process where water is used while drilling the core. Very fine-grained fly-speck carbon was seen in several samples, together with euhedral pyrite. A few samples deviate from the light to dark grey matrix and display a light greenish-grey to dark greenish-grey colour, particularly nearer to the footwall-reef contact, including Samples 1, 10, 13, 14 and 15.

Samples in the south to south-east area of TauTona had frequent occurrences of internal quartzite as a part of the reef package (both within the reef or between a carbon seam overlying the footwall and the reef) and on average were not as thick as the reef samples seen in the eastern area. The reef was matrix-supported, with a fine to medium-grained dark grey matrix. Disseminated pyrite was visible in the matrix and around subrounded to rounded clasts of milky and smoky quartz. The clasts ranged from <5 to 15 mm in diameter. Chert clasts were rarely seen however when present were very small (<5 mm) in size. The internal quartzite was light grey, medium-grained and siliceous. Floating clasts of milky and smoky quartz were seen within the internal quartzite. A carbon seam was seen at the base of the reef package, separating the No. 1 Facies from the footwall quartzite as illustrated in Figure 3.14. In the absence of a carbon seam in some of the samples there was black, fine-grained fly-speck carbon that could be identified within the dark grey matrix.



***Figure 3.14**: Matrix-supported No. 1 Facies with a siliceous internal quartzite (IQ) and an underlying carbon seam, separating the reef package from the footwall (FW) quartzite. A 5 mm thick quartz vein (QV) was seen cutting the hangingwall (HW) quartzite overlying the reef package – Sample 32.*

The reef intersection in Sample 33 shows the No. 1 Facies at an apparent thickness of 35 mm (Figure 3.15). For approximately 5 mm at the top of the reef is a small amount of light greenish-grey and medium-grained silica base of the hangingwall draping over the underlying clasts. The reef was seen to be matrix-supported, with a fine-grained light greenish grey matrix. The

discolouration of the matrix is possibly due to chloritisation. Very fine to fine-grained rounded and euhedral disseminated pyrite grains could be seen within the matrix as well as interstitially between clasts of milky, smoky and opalescent quartz.

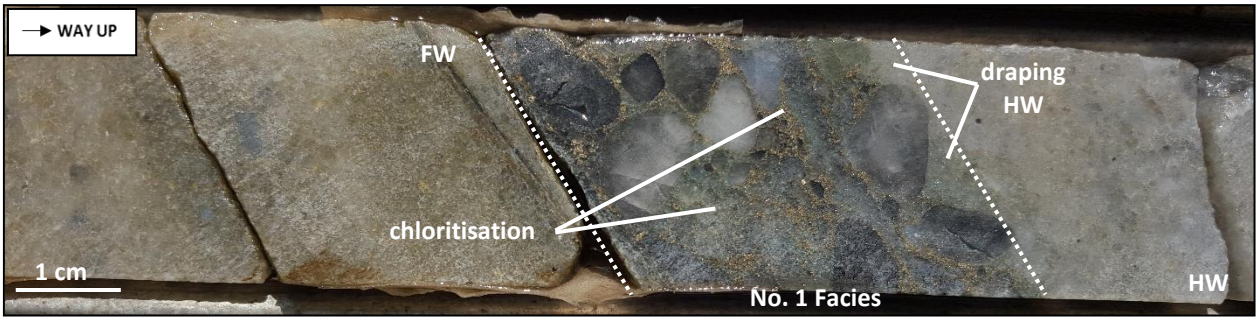

***Figure 3.15**: Matrix-supported No. 1 Facies with possible chloritisation overlying the footwall (FW) quartzite unit. The hangingwall (HW) was seen draping over the underlying clasts of the reef package – Sample 33.*

(ii) *Carbon Leader Reef No. 2 Facies*

The Carbon Leader Reef No. 2 Facies was found in samples from the east to south-eastern area of TauTona, the eastern area of Mponeng and within the south-western portion of Savuka. A few surface boreholes from the Driefontein Mine (east of TauTona) and Elandsrand Mine (west of Savuka) lease areas were also used. Table 3.2 summarises the boreholes and tombstones identified to be No. 2 Facies.

Table 3.2: A summary of the borehole and tombstone samples that are representative of the Carbon Leader Reef No. 2 Facies (30 samples in total).

Sample No.	Sample ID	Sample Type	Sample No.	Sample ID	Sample Type
2	99-94 E2	Tombstone	44	GBH 1000 D11	Borehole
11	100-92 Wze	Tombstone	48	LVBI D2	Borehole
20	DPH 3883	Borehole	49	LVBI D5	Borehole
22	GBH 1000 D6	Borehole	50	LVBI D7	Borehole
23	GBH 2788	Borehole	51	LVBI D10	Borehole
31	GBH 6004	Borehole	52	LVBK D3	Borehole
35	GBH 1000 D0	Borehole	53	LVBL D2	Borehole
36	GBH 1000 D1	Borehole	57	UD 2 D0	Borehole
37	GBH 1000 D2	Borehole	58	UD 2 D2	Borehole
38	GBH 1000 D4	Borehole	59	UD 5 D0	Borehole
39	GBH 1000 D5	Borehole	61	UD 15 D1	Borehole
40	GBH 1000 D7	Borehole	62	UD 25 D11	Borehole
41	GBH 1000 D8	Borehole	63	UD 32 D8	Borehole
42	GBH 1000 D9	Borehole	67	UD 37 D1	Borehole
43	GBH 1000 D10	Borehole	68	UD 37 D2	Borehole

Of the samples that were collected in the east to south-eastern area of TauTona, all but one of the samples had both the No. 2A and 2B Facies (refer to Figure 3.16 (a)). A single sample, Sample 11, displayed only the No. 2A Facies (Figure 3.16 (b)). Both reef bands varied in thickness, stages of development, clast support and mineralisation features. The majority of

the samples had matrix-supported conglomerates for both the No. 2A and 2B Facies. The quartz-rich matrix was dark grey, medium to coarse-grained and hosted milky and smoky quartz clasts, as well as chert clasts. The clasts were typically rounded to subrounded and ranged from 3 to 30 mm in diameter size.

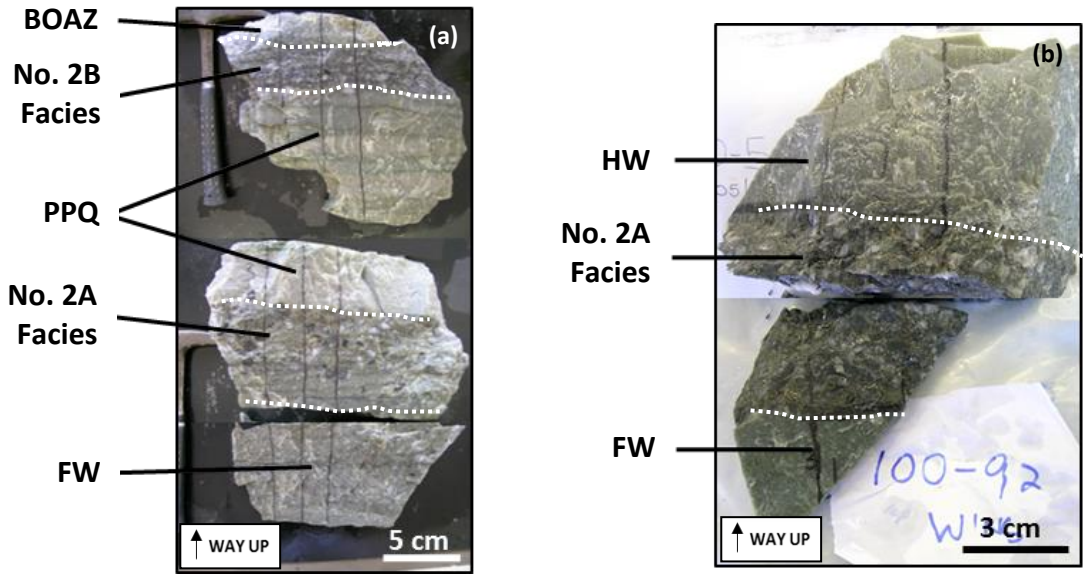

***Figure 3.16**: (a) Carbon Leader Reef No. 2 Facies overlying the footwall (FW) quartzite with distinct No. 2A and No. 2B Facies flanking either side of the Pale Pebbly Quartzite (PPQ). Overlying the No. 2B Facies was a Brown-Orange Argillaceous Zone (BOAZ) – Sample 2; (b) No. 2A Facies intersection with overlying hangingwall (HW) quartzite – Sample 11.*

Very fine to fine-grained rounded to euhedral disseminated pyrite grains were seen in the matrix, as well as concentrated around the clasts set within the matrix. The reef bands were separated by a fine to medium-grained, semi-siliceous to siliceous, pale grey quartzite referred to as Pale Pebbly Quartzite. Clasts were not frequent in the Pale Pebbly Quartzite however in some samples floating clasts of smoky and milky quartz could be seen. Rounded grains of disseminated pyrite as well as fine-grained pyrite along foresets were seen in the Pale Pebbly Quartzite. Overlying the No. 2B Facies was a Brown-Orange Argillaceous Zone of medium-grained quartzite with small (<5 mm) floating clasts of milky and smoky quartz.

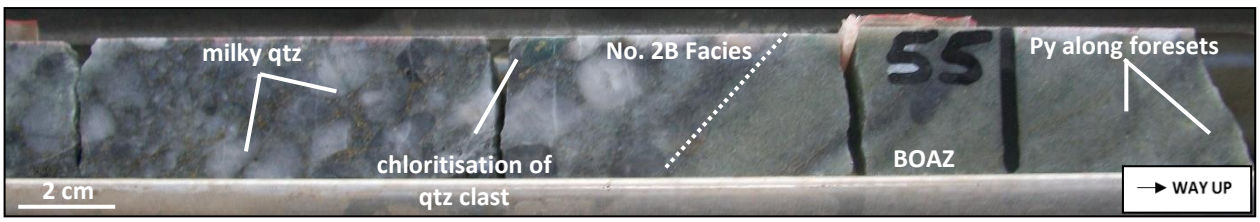

***Figure 3.17**: No. 2B Facies with milky quartz (qtz) clasts and possibly a quartz clast that has undergone chloritisation, overlain by a Brown-Orange Argillaceous Zone (BOAZ) with pyrite (py) along foresets – Sample 31.*

Discolouration of the reef band(s) was not common, however in Sample 31 both the No. 2A and 2B Facies had a greenish discolouration in the matrix and in some of the milky quartz clasts, suggesting chloritisation has taken place (Figure 3.18).

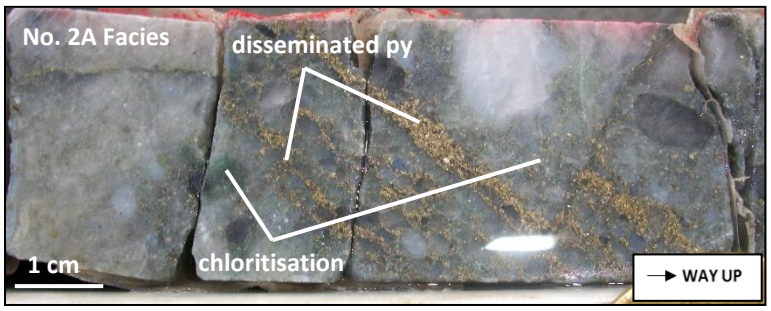

***Figure 3.18**: Greenish discolouration of the No. 2A Facies with possible chloritisation of some of the quartz (qtz) clasts. Rounded disseminated pyrite (py) grains occur interstitially between the quartz clasts – Sample 31.*

The combination of the No. 2A and 2B Facies, Pale Pebbly Quartzite and the Brown-Orange Argillaceous Zone make up the No. 2 Facies package. The entire No. 2 Facies package was generally over 0.5 m in thickness and this was consistently seen throughout the No. 2 Facies samples collected for this project, regardless of the locality. In the westernmost region of Savuka, all but three of the boreholes had both reef bands present.

Sample 36 had missing core and only the No. 2B Facies was retrieved. Samples 57 and 58 had intersected the No. 2A Facies only, however it should be noted that the condition of the core was broken and fragmented for both the samples (boreholes). This is very likely due to drilling through ground that has been fractured and faulted, possibly through a fault zone. This would also explain the lack of the Pale Pebbly Quartzite, No. 2B Facies and Brown-Orange Argillaceous Zone that typically overlie the No. 2A Facies in these samples.

The No. 2A and No. 2B Facies in the western area were predominantly matrix-supported, with clasts of milky and smoky quartz set within a light grey to dark grey fine to medium-grained matrix. The clasts ranged in size from 2 to 15 mm and were rounded to subrounded. Chert clasts, not greater than 5 mm, were also seen within the reef bands. Very fine to fine-grained rounded and euhedral disseminated pyrite was seen within the matrix as well as on the outer edges of the clasts. The disseminated pyrite also formed very fine pyrite stringers along foresets, usually seen in the No. 2B Facies more frequently than in the No. 2A Facies. Fly-speck carbon was occasionally seen in the lighter grey matrix however it was not a common feature.

Pale Pebbly Quartzite overlies the No. 2A Facies and was a light bluish-grey, fine-grained, siliceous quartzite (Figure 3.19). Fine-grained rounded pyrite grains along foresets were seen within the Pale Pebbly Quartzite.



***Figure 3.19**: Matrix-supported No. 2A Facies with interstitial disseminated pyrite (py) between milky and smoky quartz (qtz) clasts. The No. 2A Facies was overlain by a Pale Pebbly Quartzite (PPQ) with floating quartz clasts – Sample 22.*

Separating the No. 2A and No. 2B Facies was a fine to medium-grained, light grey to pale greenish-grey, semi-siliceous Pale Pebbly Quartzite (Figure 3.20). Bedding was visible within the Pale Pebbly Quartzite, as was dark grey banding in some of the samples - such as in Samples 23, 35 and 48. Floating clasts of small (<5 mm) angular to subrounded smoky and milky quartz were seen occasionally in the Pale Pebbly Quartzite as well as fine rounded pyrite grains along foresets.



***Figure 3.20**: Pale Pebbly Quartzite (PPQ) intersection within the No. 2 Facies. The Pale Pebbly Quartzite had rounded disseminated grains of pyrite (py) as well as pyrite along foresets – Sample 35.*

In Samples 49 and 50 the Pale Pebbly Quartzite had a coarser-grained portion with several floating clasts set within a dark grey matrix, creating a poorly developed conglomerate band. In Sample 23, a greenish discolouration of the Pale Pebbly Quartzite was seen along the outer edges of a pyrite lag (Figure 3.21).

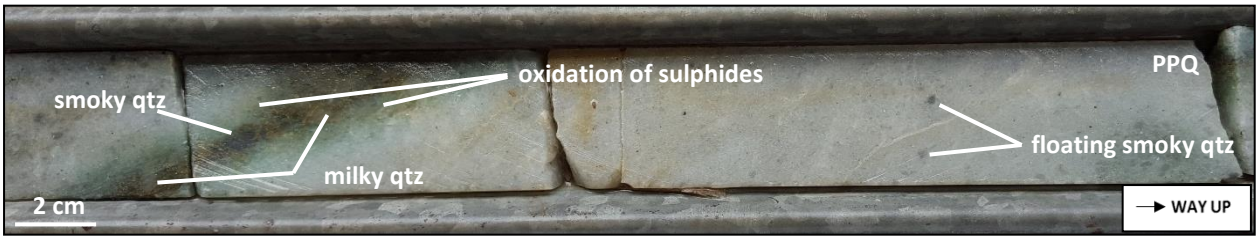

***Figure 3.21**: Alteration of the Pale Pebbly Quartzite (PPQ) within the No. 2 Facies package may be due to oxidation of sulphides. Occasional clasts of smoky and milky quartz (qtz) were seen within a pyrite lag – Sample 23.*

The pyrite lag, with fine-grained rounded pyrite grains, was seen within the quartzite unit with occasional (subrounded) smoky and (rounded) milky quartz clasts. The greenish discolouration of the quartzite may be due to oxidation of the sulphides or due to chloritisation however with the large concentration of pyrite it may likely be the former. It may also be a combination of chloritisation and oxidation.

Overlying the Pale Pebbly Quartzite is the Carbon Leader Reef No. 2B Facies. Typically, the No. 2B Facies was better developed than the No. 2A Facies, with rounded clasts and better sorting and packing of clasts. In some instances, the No. 2B Facies was clast-supported (Figure 3.22) whereas the No. 2A Facies was almost always matrix-supported throughout the area.



Figure 3.22*: Clast-supported No. 2B Facies flanked by a Pale Pebbly Quartzite (PPQ) and a Brown-Orange Argillaceous Zone (BOAZ) of quartzite. The discolouration within the No. 2B Facies may be due to oxidation of the sulphides within the core – Sample 23.*

In Sample 53 a greenish discolouration of the No. 2B Facies was seen. The No. 2B Facies appeared to be poorly developed, hosting very few clasts within a dark greenish grey, medium-grained quartz matrix with rounded and euhedral disseminated pyrite. A greenish discolouration of the matrix was also noted in the No. 2B Facies in Sample 61. The Brown-Orange Argillaceous Zone that overlies the No. 2B Facies had similar features to those observed in the other areas of the mines. Two exceptions noted were in Sample 35, where the Brown-Orange Argillaceous Zone was pale grey in comparison to the brownish-grey to brownish-orange colour typically seen (Figure 3.23), and Sample 53 where there was a greenish alteration of the Brown-Orange Argillaceous Zone.



Figure 3.23*: A Brown-Orange Argillaceous Zone (BOAZ) intersection of the No. 2 Facies package showing the variations in colour. Rounded disseminated pyrite (py) grains were seen within the quartzite – Sample 35.*

The greenish discolouration became darker and more prominent with closer proximity to the fine pyrite stringers seen within the unit (similar to what was observed in the Pale Pebbly Quartzite unit in Figure 3.21).

(iii) *Carbon Leader Reef No. 3 Facies*

The Carbon Leader Reef No. 3 Facies was found in samples from the south-eastern, to south, to southwestern area of TauTona, and the northern to central area of Mponeng. Table 3.3 summarises the boreholes and tombstones identified to be No. 3 Facies.

Table 3.3: A summary of the borehole and tombstone samples that are representative of the Carbon Leader Reef No. 3 Facies (17 samples in total).

Sample No.	Sample ID	Sample Type	Sample No.	Sample ID	Sample Type
8	120-55 W4	Tombstone	29	GBH 6001	Borehole
9	120-77 S1	Tombstone	46	LIB 120 SW1 D0	Borehole
16	120-55 NE7	Tombstone	47	LVB 18 D0	Borehole
17	120-55 W5	Tombstone	54	MPO LIB 2 D2	Borehole
18	120-55 W7	Tombstone	55	MPO LIB 3 D2	Borehole
19	120-70 W1	Tombstone	56	MPO LIB 3 D3	Borehole
21	DPH 4057	Borehole	60	UD 13 D0	Borehole
25	GBH 3844	Borehole	64	UD 33 D15	Borehole
26	GBH 3845	Borehole			

In the south-east of TauTona, the No. 3 Facies was poorly developed and exhibited poor sorting. Minimal disseminated pyrite and clasts were found within the reef (Figure 3.24).

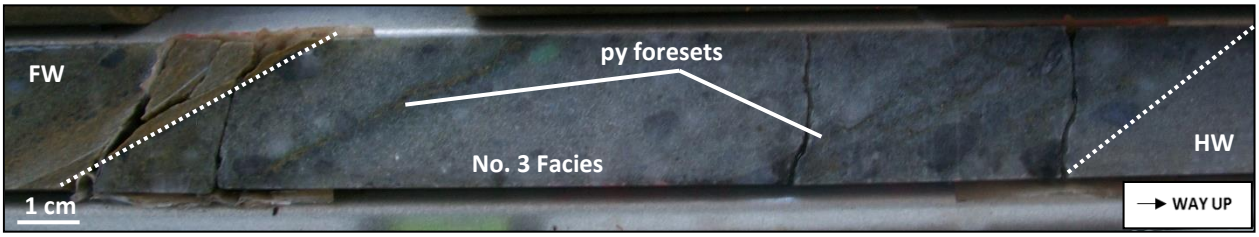

***Figure 3.24**: A poorly developed intersection of the No. 3 Facies overlying the footwall (FW) quartzite. The No. 3 Facies had very fine-grained rounded pyrite along foresets. A slight discolouration was noted on the outer edges of the pyrite along foresets. The No. 3 Facies was overlain by the hangingwall (HW) quartzite – Sample 21.*

Pyrite occurred more frequently along foresets than as scattered rounded disseminated pyrite grains. Clasts that were seen in the No. 3 Facies were subrounded to angular milky and smoky quartz as well as black chert, less than 15 mm in diameter. Overlying the No. 3 Facies was a light grey, fine-grained and siliceous hangingwall quartzite. Additionally, in Sample 21 the footwall-reef contact was sheared and displayed brittle phyllonite that separated the argillaceous footwall quartzite and siliceous reef band (Figure 3.25).

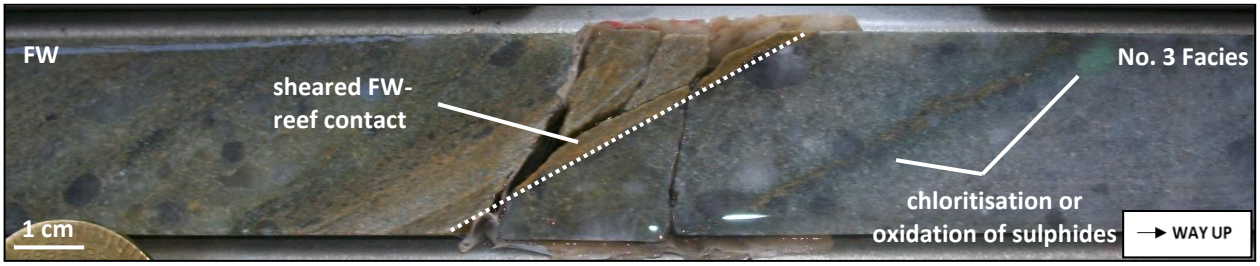

***Figure 3.25**: A close-up of the footwall (FW)-reef contact of the No. 3 Facies. Discolouration was noted on the edges of pyrite along foresets and may be due to oxidation of sulphides or chloritisation within the core – Sample 21.*

Within the No. 3 Facies the rounded pyrite grains were concentrated around clast edges and there was a greenish discolouration of the immediate quartzite on the outer edges of the pyrite along foresets. This discolouration may be as a result of oxidation of the sulphides present within the core. One of the milky quartz clasts in Sample 21 had been discoloured to a minty-green colour - this discolouration may be due to chloritisation.

In the southern portions of TauTona and the northern/central regions of Mponeng, the No. 3 Facies had a thickness of up to 170 mm in the tombstone samples. The reef band varied from matrix to clast-supported, with a predominantly fine-grained, light to dark grey matrix. Clasts seen included smoky and milky quartz (4 to 20 mm), as well as black chert (<5 mm) and occasional opalescent quartz, ranging from 2 to 5 mm in diameter. The clasts were subangular to subrounded to well rounded, with a few clasts being elongated. The elongated clasts were seen to be aligned parallel to bedding. Rounded and anhedral to euhedral grains of disseminated pyrite was seen within the matrix, as well as along foresets. Fly-speck carbon was seen within several samples and occurred independently of a carbon seam in most of the samples. Sample 25 was one example that had a thin carbon seam at the base of the reef package (Figure 3.26).

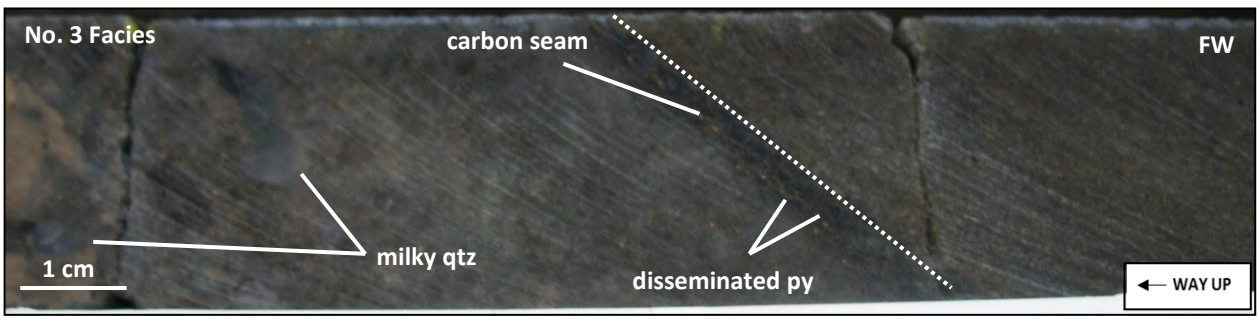

***Figure 3.26**: A close-up of a thin carbon seam at the base of the No. 3 Facies, separating the footwall (FW) quartzite and the reef band. Fine grains of rounded disseminated pyrite (py) occurred within the carbon seam. Milky quartz (qtz) clasts were visible within the No. 3 Facies – Sample 25.*

Discolouration of clasts and the surrounding matrix was not common for the No. 3 Facies however Sample 25 showed a discolouration of the dark grey matrix to a dark greenish-grey. There was also discolouration of milky quartz clasts set within the dark greenish-grey matrix (Figure 3.27). The discolouration seen may be as a result of chloritisation. A concentration of disseminated rounded pyrite grains was seen nearer to the base of the No. 3 Facies.



***Figure 3.27**: Greenish discolouration of the matrix within the No. 3 Facies. Possible chloritisation of a milky quartz (qtz) clast was noted within the reef, as well as a concentration of disseminated rounded pyrite grains nearer to the base of the No. 3 Facies – Sample 25.*

Overlying the No. 3 Facies was a light grey, fine-grained and siliceous hangingwall quartzite. Floating clasts (<10 mm diameter) were occasionally seen within the hangingwall quartzite, as were disseminated pyrite grains, pyrite stringers and pyrite along foresets. These identifying features were seen in Samples 25, 29, 47, 55, 60 and 64. In a few of the samples the hangingwall quartzite had a bluish-grey to dark grey colour – this is seen in Samples 26, 46 and 54.

Figure 3.28 shows subrounded to elongated floating clasts of milky and smoky quartz, up to 15 mm in length, within the hangingwall quartzite (overlying the No. 3 Facies). A concentration of disseminated rounded and anhedral to euhedral pyrite grains occurred interstitially between the floating clasts.

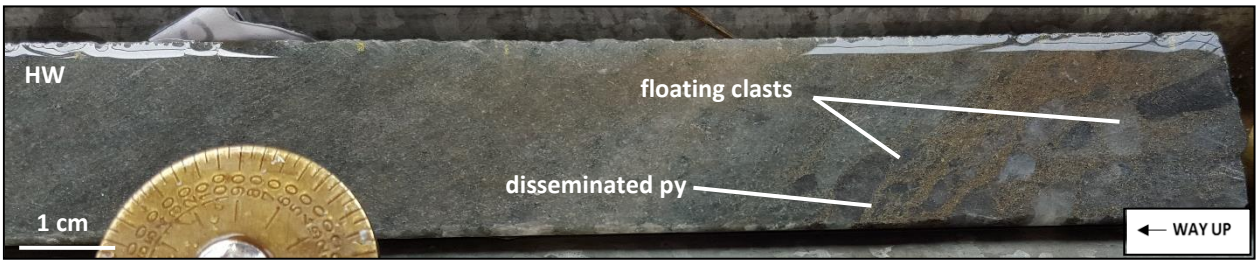

***Figure 3.28**: Floating clasts of milky and smoky quartz, hosted within an area dense with disseminated pyrite (py) grains within the overlying hangingwall (HW) quartzite – Sample 26.*

In the southwestern area of TauTona the No 3. Facies was up to 115 mm thick. The reef varied from a clast-supported conglomerate to a matrix-supported conglomerate (Figure 3.29 (a)). The

matrix was light to medium grey and medium-grained. Clasts within the reef included subrounded smoky and milky quartz and infrequent chert, ranging from 3 to 20 mm in diameter. Disseminated rounded pyrite was seen within the matrix as well as concentrated around the clast edges. Pyrite stringers were also seen in some of the samples and extended into the overlying hangingwall unit. Fly-speck carbon was noted within the matrix of the reef band.

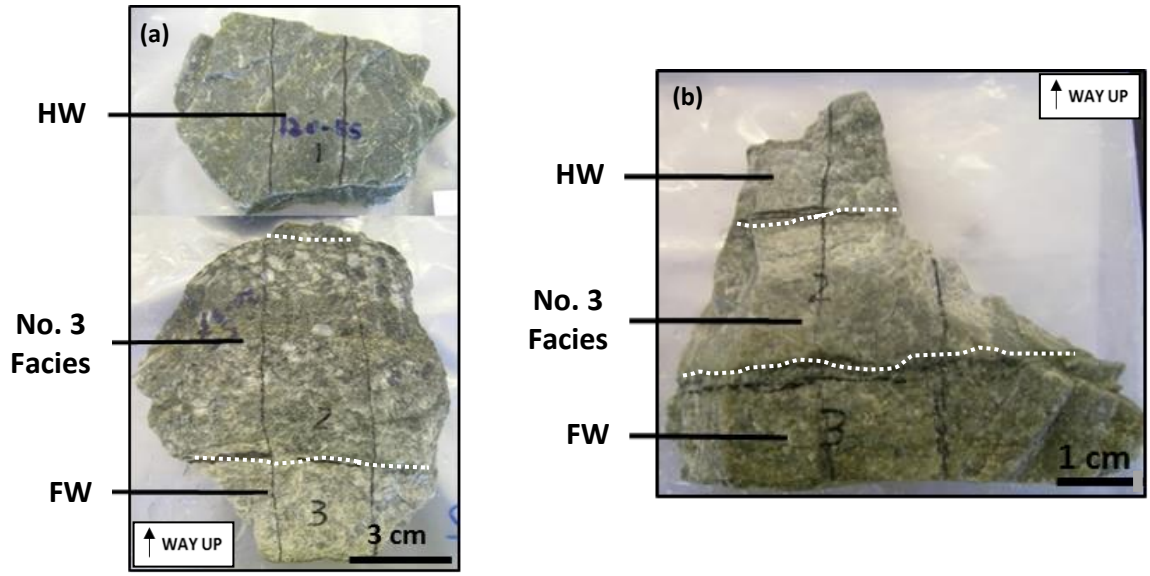

***Figure 3.29**: (a) Alternating matrix-supported and clast-supported bands within the No. 3 Facies, underlying a siliceous hangingwall (HW) quartzite and overlying a coarse-grained argillaceous footwall (FW) quartzite – Sample 16; (b) Clasts were absent from the No. 3 Facies in Sample 17 however there was a very thin carbon seam separating the reef from the footwall quartzite – Sample 17.*

In Sample 17 the No. 3 Facies, with the absence of clasts, was distinguishable by colour, a lower carbon seam, an upper pyrite stringer as well as fly-speck carbon (Figure 3.29 (b)). A greenish discolouration of the matrix within the No. 3 Facies was noted in Sample 8 as well as Sample 18.

3.1.4 Discussion

The hangingwall quartzite across the mines did not vary greatly and was consistently fine to medium-grained, light to dark grey in colour, siliceous, with rounded grains of disseminated pyrite, thin pyrite stringers as well as pyrite along foresets present. Alteration was occasionally noted in the hangingwall quartzite with increasing proximity to the (upper) reef contact. The hangingwall exhibited some variation in colour from a light grey to a darker grey colour, and a light green to darker green in other areas. It is not uncommon to see discolouration near the

contact between the hangingwall and the reef where there is a transition from one (sedimentary) unit into the next, where the contact between adjacent sedimentary packages has acted as a conduit for post-depositional fluid flow (Tucker *et al*., 2016). A more distinct discolouration was noted on the outer edges of pyrite along foresets, pyrite lags as well as along fractures. This is likely as a result of chloritisation, sericitic alteration or oxidation of sulphides. Chloritisation occurs when (hydrothermal) fluid reacts with wall rock, altering the mineral assemblage of the wall rock and subsequently the fluid composition (Robb, 2005). Where chloritisation is noted, it is likely to indicate the potential conduit(s) for fluid flow (Robb, 2005). The origin of the fluid flow may be from post-depositional processes such as faulting or dyke intrusions (Drennan and Robb, 2006; Jolley *et al*., 2004). The oxidation of sulphides as well as sericitic alteration may, similarly to chloritisation processes, have occurred with the interaction of (hydrothermal) fluid and wall rock.

The footwall quartzite across the West Wits Line was medium-grained to coarse-grained and semi-argillaceous to argillaceous with a greenish-grey to dark grey colour. The footwall pebble bands ranged from a pebble lag of smoky and milky quartz clasts, to a moderately developed pebble band. The footwall pebble bands varied from 10 to 50 mm in thickness. The matrix had a gritty-texture and was dark greenish-grey in colour, hosting subrounded to subangular chert, smoky and milky quartz clasts. Rounded disseminated pyrite, pyrite along foresets and pyrite stringers were seen in the footwall quartzite and within the footwall pebble bands. Alteration was noted in several samples. Milky quartz clasts had a greenish discolouration and displayed a minty-green to dark green colour. The clasts were hosted in a dark greenish-grey matrix within a footwall pebble band. This discolouration is very likely as a result of chloritisation. Discolouration of the footwall quartzite was noted with increasing proximity to the reef contact, becoming a dark khaki-green colour towards the contact. This was similar to what was noted in the hangingwall unit nearer to the reef contact, where the contact has acted as a conduit for post-depositional fluid flow.

The three variations of the Carbon Leader Reef revealed noticeable differences across the West Wits Line with some similarities seen, particularly in the alteration of the reef packages. The Carbon Leader Reef No. 1 Facies was predominantly matrix-supported with a fine-grained to medium-grained matrix. The matrix was light to dark grey in the easternmost area of TauTona and was dark grey in the south-east to southern areas. Very fine to fine-grained rounded and

euhedral to anhedral disseminated pyrite grains were seen within the matrix and concentrated around the outer edges of chert and smoky/milky quartz clasts. The clasts ranged from 2 to 25 mm in diameter in the easternmost area and 5 to 15 mm in the south-east to southern areas. Chert clasts were infrequent in the south-east to southernmost areas and were very small, with a maximum diameter of 5 mm. Very fine-grained fly-speck carbon was seen within the matrix in some samples, however a thin carbon seam was frequently noted at the base of the conglomerate. The reef was 40 to 95 mm thick in the easternmost area of TauTona, becoming thinner heading south-east to south. Internal quartzite was seen frequently in the south-east to southernmost areas and was seen both within the conglomerate as well as between the reef and a carbon seam, separating the reef package from the footwall quartzite. The internal quartzite was light grey, medium-grained and siliceous. Floating clasts of milky and smoky quartz were on occasion seen within the internal quartzite. Alteration noted within the No. 1 Facies included discolouration of the internal quartzite to a greenish-grey colour near the contact with the footwall, as well as discolouration of the matrix to a light greenish-grey. The discolouration at the contacts is common and is likely due to the contact acting as a conduit for post-depositional fluid flow. The discolouration of the matrix is likely to be as a result of chloritisation or sericitic alteration.

The Carbon Leader Reef No. 2 Facies in the east to south-east of TauTona had dark grey, medium to coarse-grained, matrix-supported No. 2A and No. 2B Facies. Rounded to subrounded chert and milky to smoky quartz clasts hosted within the matrix ranged in size from 3 to 30 mm. Very fine to fine-grained rounded and euhedral disseminated pyrite grains were visible within the matrix. In the westernmost areas the No. 2B Facies was better developed than the No. 2A Facies, with rounded to well-rounded clasts and better sorting. The matrix was lighter in colour and the clasts ranged from 2 to 15 mm in diameter. Pyrite along foresets was seen, predominantly in the No. 2B Facies. Infrequent fly-speck carbon was observed in the lighter matrix of the No. 2 Facies. The Pale Pebbly Quartzite between the two reef bands was fine to medium-grained, semi-siliceous to siliceous and pale grey in the east to south-east area of TauTona. The Pale Pebbly Quartzite in the west was light grey to pale greenish-grey and was predominantly semi-siliceous. Dark grey banding was seen within the Pale Pebbly Quartzite across the mines, as were floating clasts of angular to subrounded milky

and smoky quartz. Rounded disseminated pyrite as well as pyrite along foresets were also seen across the area.

The remaining units between the No. 2B Facies and the hangingwall quartzite unit were consistently similar throughout the area. Overlying the No. 2B Facies the Brown-Orange Argillaceous Zone was medium-grained, argillaceous and displayed a brownish-orange colour. The hangingwall overlying the Brown-Orange Argillaceous Zone was fine-grained, light grey in colour with infrequent floating milky and smoky quartz clasts. Alteration noted within the No. 2 Facies included a greenish discolouration along the outer edges of pyrite lags within both the Pale Pebbly Quartzite and Brown-Orange Argillaceous Zone, as well as a greenish discolouration of the reef matrix and milky quartz clasts hosted within the matrix of the reef. The discolouration is likely to be as a result of chloritisation or due to oxidation of sulphides as a result of interaction with post-depositional fluids.

South-east of TauTona the Carbon Leader Reef No. 3 Facies was poorly developed, poorly sorted with minimal disseminated pyrite and clasts, however a thin carbon seam was noted within most of the samples. Pyrite along foresets was frequently seen in comparison to rounded disseminated pyrite grains. Clasts seen included subrounded to angular milky and smoky quartz (<15 mm) as well as chert, typically 5 to 10 mm in size. Hangingwall quartzite overlies the conglomerate band and was light grey in colour, fine-grained and siliceous. In the southernmost area of TauTona, and within the northern/central areas of Mponeng the No. 3 Facies reached up to 170 mm in thickness and was matrix to clast-supported. The matrix was fine-grained and light to dark grey in colour, hosting black chert as well as opalescent, milky and smoky quartz clasts. The clasts were subangular to subrounded to well-rounded and range from 4 to 20 mm in size. Fly-speck carbon occurred within the matrix. The hangingwall quartzite overlying the reef was light grey, fine-grained, siliceous and was seen hosting floating quartz clasts less than 10 mm in diameter. Pyrite in the form of rounded to anhedral disseminated grains, along foresets and in stringers were seen within the hangingwall quartzite.

In the south-west to westernmost areas of the West Wits Line the No. 3 Facies reached 115 mm in thickness and varied from clast to matrix-supported. The matrix was medium-grained and light to medium grey in colour, hosting subrounded chert, milky and smoky quartz clasts (3 to 20 mm diameter). Rounded and anhedral to euhedral disseminated pyrite grains were seen within the matrix as were pyrite along foresets. The pyrite stringers were seen

extending into the hangingwall quartzite in the form of a cross-cutting micro vein. Fine-grained fly-speck carbon was also seen within the matrix. Alteration noted within the No. 3 Facies included a greenish discolouration on the outer edges of pyrite stringers, milky quartz clasts, as well as discolouration of the matrix. The discolouration of these samples is likely due to chloritisation. Table 3.4 summarises the noted alteration and unusual observations that were noted in the samples. This information was cross-correlated with the results from the other methodologies to investigate possible overlapping or complementary observations.

Table 3.4: A summary of the noted alteration styles and unusual observations in some samples. Samples not included in the table below did not have notable alteration or unusual macroscopic observations however, the macroscopic observations can be referred to in Appendix 2: Macroscopic Observations. A red-yellow-green colour scale highlights the varying gold grades (red = high gold grade; yellow = intermediate gold grade; green = low gold grade). N/D: not determined.

Sample	Sample ID	Unit	Noted Macroscopic Observations	Gold grade (g/t)
1	94-94 E1	Hangingwall	Greenish discolouration of quartzite on outer edges of pyrite along foresets	0.2
		No. 1 Facies	Greenish discolouration of matrix with increasing proximity from the footwall	10.3
		Footwall	Pyrite along fractures	0.2
3	104-88 W6	No. 1 Facies	Greenish discolouration of matrix	172.0
4	105-85 E2	No. 1 Facies	Thin carbon seam at the base of the reef	227.0
5	112-83 W3	Hangingwall	Rounded disseminated pyrite grains along fractures and thick quartz vein cutting hangingwall	0.6
7	114-78 E1	No. 1 Facies	Thin carbon seam at the base of the reef	21.1
8	120-55 W4	Hangingwall	Disseminated rounded pyrite along fractures and foresets; discolouration of quartzite surrounding foresets and fractures	0.2
		No. 3 Facies	Upper half of the reef has a greenish discolouration	311.0
10	96-94 E2	Hangingwall	Darkening of the quartzite on outer edges of pyrite stringers	2.7
		No. 1 Facies	The reef is carbon (fly-speck) and pyrite enriched; where there is an absence of fly-speck carbon and pyrite the matrix is dark green	284.0
12	104-88 E1A	No. 1 Facies	Thin carbon seam and pyrite stringer mark the base of the reef	83.9
13	104-88 W7	No. 1 Facies	Dark green to dark grey matrix	130.0
15	112-84 Rse	No. 1 Facies	Thin carbon seam with rounded disseminated pyrite grains mark the base of the reef below an internal quartzite unit	79.5
16	120-55 NE7	No. 3 Facies	Two pyrite stringers mark the base of the reef; fly-speck carbon occurs together with the pyrite stringers	36.0
17	120-55 W5	No. 3 Facies	Thin carbon seam with abundant pyrite marks the base of the reef	15.4
		Footwall	Greenish discolouration of quartzite on outer edges of fault/shear at the contact with the reef	0.9
18	120-55 W7	No. 3 Facies	Upper reef has a greenish discolouration of matrix; pyrite stringer together with fly-speck carbon marks the base of the reef	173.0
19	120-70 W1	Hangingwall	Quartz vein cutting hangingwall, reef and terminating at the footwall-reef contact	8.0
		No. 3 Facies	Thin pyrite stringers mark the base of the reef	141.0
20	DPH 3883	Hangingwall	Greenish discolouration of quartzite on outer edges of pyrite along foresets	N/D
		Footwall	Greenish discolouration of several milky quartz clasts in a footwall pebble band; fault-fill veining	N/D
21	DPH 4057	No. 3 Facies	Sheared contact with the footwall quartzite; discolouration of a single milky quartz clast to minty-green	64.3
22	GBH 1000 D6	Hangingwall	Greenish-grey hangingwall with quartz veining present	N/D
		Footwall	Darkening of the footwall quartzite with increasing proximity to the reef	N/D
23	GBH 2788	PPQ	Greenish discolouration of the Pebble Pale Quartzite (PPQ), particularly around a pyrite lag	N/D
		No. 2B Facies	Discolouration of sulphides - possibly due to oxidation	9.3
25	GBH 3844	No. 3 Facies	Greenish discolouration of matrix as well as discolouration of milky quartz clasts; thin carbon seam at the base of the reef	31.4
26	GBH 3845	Hangingwall	Quartz veining present in the hangingwall quartzite	N/D
28	GBH 6000	Hangingwall	Greenish discolouration of hangingwall quartzite with increasing proximity to the reef	N/D
		Footwall	Greenish discolouration at footwall pebble band contacts	N/D
31	GBH 6004	No. 2A Facies	Greenish discolouration with possible chloritisation of some of the quartz clasts	12.8
32	GBH 6014	No. 1 Facies	Thin carbon seam marks the base of the reef	67.5
33	GBH 6028	No. 1 Facies	Greenish discolouration of matrix	0.6
51	LVBI D10	BOAZ	Brown-Orange Argillaceous Zone (BOAZ) is grey-orange in colour	N/D
53	LVBL D2	Hangingwall	Greenish discolouration of hangingwall quartzite surrounding pyrite along foresets	N/D
		No. 2B Facies	Matrix has a greenish discolouration	4.9
		BOAZ	Greenish discolouration of Brown-Orange Argillaceous Zone (BOAZ) on outer edges of pyrite along foresets	N/D
57	UD 2 D0	No. 2A Facies	Broken core - potentially due to a fault zone	N/D
58	UD 2 D2	Hangingwall	Greenish discolouration of the hangingwall quartzite; broken core - potentially due to a fault zone	N/D
59	UD 5 D0	No. 2B Facies	Matrix has a greenish discolouration	1.7
61	UD 15 D1	Hangingwall	Darkening of the hangingwall quartzite with increasing proximity to the reef	N/D
		No. 2B Facies	Quartz vein cutting reef and Brown-Orange Argillaceous Zone (BOAZ)	N/D
62	UD 25 D11	No. 2A Facies	Greenish discolouration of the matrix and several milky quartz clasts	7.0
63	UD 32 D8	BOAZ	Greenish discolouration of the Brown-Orange Argillaceous Zone (BOAZ) on outer edges of pyrite along foresets	N/D
64	UD 33 D15	Hangingwall	Very fine quartz veining in hangingwall quartzite	N/D
		No. 3 Facies	Thin carbon seam marks the base of the reef	8.2

3.2 PETROGRAPHIC OBSERVATIONS

Petrographic observations were undertaken on all 19 tombstone samples. From these 19 samples a total of 23 thin sections representing hangingwall, 23 representing footwall and 38 representing Carbon Leader Reef were investigated. An additional 15 polished thin sections of Carbon Leader Reef were made from reef intersections in 15 boreholes. The microscopic analyses were undertaken at the University of the Witwatersrand in the Geosciences Petrology Lab, using an Olympus BX41 Microscope. Microphotographs were taken of representative sample material using reflected and transmitted light microscopy. This research focused on the reef polished thin sections as the project was designed to investigate alteration of the Carbon Leader Reef and the possible association between alteration and gold grades. Less emphasis was placed on alteration of the hangingwall and footwall units as preliminary investigations on the tombstone samples indicated that these do not host significant quantities of gold. Refer to Appendix 3: Microscopic Observations for petrological descriptions of all the Carbon Leader Reef samples (as illustrated in Appendix 1: Sample Locality Map) that were used for the microscopic observations.

Although XRD analysis is a geochemical technique it was included within this sub-chapter to supplement the microscopic findings within the polished thin sections, particularly where there are very small traces of minerals (for example, chromite) within samples that are not visibly apparent within the polished thin section, as the thin section was cut from a portion of the sample that was not sent for geochemical analyses. XRD analyses were carried out on a total of 61 samples for the tombstones, of which 19 were hangingwall samples, 20 were footwall samples (inclusive of 2 footwall pebble bands) and 22 were Carbon Leader Reef samples (including internal quartzite samples). XRD analyses were also carried out for 15 Carbon Leader Reef samples for the boreholes. The XRD results were used in conjunction with the modal abundances determined through microscopic observations in this sub-chapter.

3.2.1 Hangingwall Descriptions

The dominant mineral assemblage seen throughout the (23) hangingwall samples comprises quartz (consistently >75%), with pyrophyllite, sericitic muscovite, chlorite, chloritoid and sulphides making up the remaining modal content. Figure 3.30 (a) and (b) are

microphotographs of hangingwall samples and show the typical mineral make-up of the hangingwall quartzite.

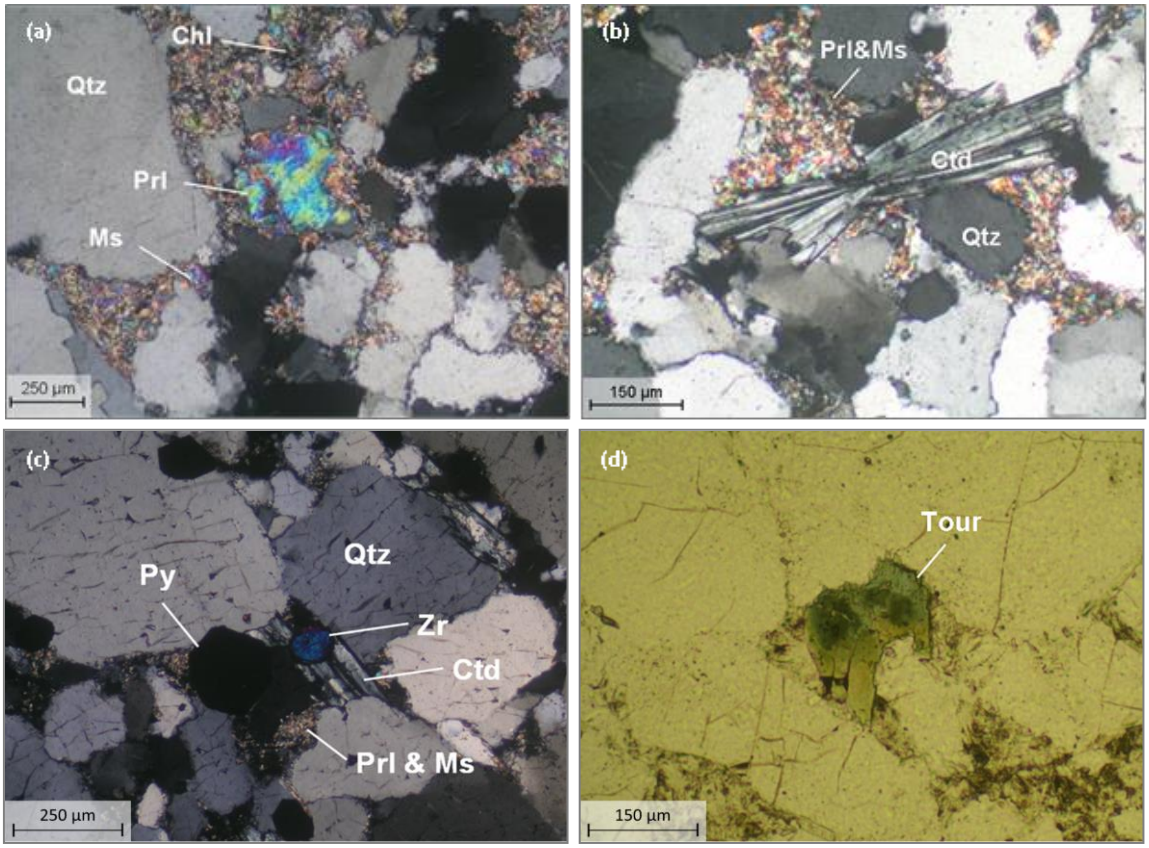

***Figure 3.30**: (a) Typical mineral assemblage of the hangingwall unit overlying the Carbon Leader Reef comprising quartz (Qtz), pyrophyllite (Prl), muscovite (Ms) and chlorite (Chl) – Sample 1, viewed in cross-polarised transmitted light. The major mineral assemblage seen in (a) was noted across all the hangingwall samples, regardless of facies type, with the exception of Sample 4 overlying the No. 1 Facies where there was an absence of chlorite; (b) Chloritoid (Ctd) was also seen throughout all of the hangingwall samples (across all facies types) – Sample 11, viewed in cross-polarised transmitted light; (c) A single detrital zircon (Zr) grain enclosed within a chloritoid (Ctd) lath alongside a rounded detrital pyrite (Py) grain, hosted between quartz (Qtz) clasts and within a pyrophyllite (Prl)-muscovite (Ms) matrix – Sample 5, viewed in cross-polarised transmitted light. Zircon was noted within hangingwall samples that were overlying the No. 1 and the No. 3 Facies; (d) A euhedral columnar grain of tourmaline (Tour) between quartz (Qtz) clasts within the hangingwall quartzite - Sample 10, viewed in plane-polarised transmitted light.*

The quartz clasts were angular to rounded and were predominantly monocrystalline with fewer subangular to rounded polycrystalline clasts. The interstitial matrix between the larger quartz clasts (0.01 to 1.6 mm in size) had a mixture of very fine sericitic muscovite, pyrophyllite and chlorite grains. In most of the samples the pyrophyllite was not easily distinguishable from the muscovite, however the pyrophyllite grains were typically slightly coarser than the muscovite. Pyrophyllite and muscovite abundance, on average, for samples overlying the No. 3 Facies was lower than samples overlying the No. 1 and No. 2 Facies.

Chlorite (found in all the hangingwall samples, with the exception of Sample 4 that overlies the No. 1 Facies) made up a small amount (<5%) within the matrix and it was very fine-grained. Samples overlying the No. 1 and No. 3 Facies were noted to have (on average) a greater abundance of chlorite and chloritoid. Chloritoid grains (Figure 3.30 (b)) were frequent within the hangingwall samples (overlying all the facies types) and were typically in the form of elongated/columnar laths. They were seen cutting into quartz and pyrite clasts as well as enclosing rounded zircon grains (Figure 3.30 (c)). Zircon was noted within hangingwall samples overlying the No. 1 and No. 3 Facies. Tourmaline was seen in a few of the hangingwall samples and typically had anhedral (Samples 7 and 14, both overlying the No. 1 Facies) to euhedral columnar grains (Samples 10, 12 and 13 overlying the No. 1 Facies, as well as Sample 16 overlying the No. 3 Facies), as seen in Figure 3.30 (d). Tourmaline was not noted within any of the samples overlying the No. 2 Facies.

A variation of rounded pyrite as well as anhedral to euhedral pyrite grains were observed in the hangingwall quartzite typically occurring along foresets however, disseminated cubic pyrite grains were seen in the hangingwall quartzite itself, as well as in fractures. The highest abundance of pyrite was noted in Sample 6 at 4%, overlying the No. 1 Facies. Chromite was detected in some of the samples by XRD and was only noted in thin section for Samples 7 and 14 (overlying the No. 1 Facies) and Sample 8 (overlying the No. 3 Facies). A rounded detrital grain (approximately 0.2 mm in diameter) was observed in Sample 14 (Figure 3.31 (a)).

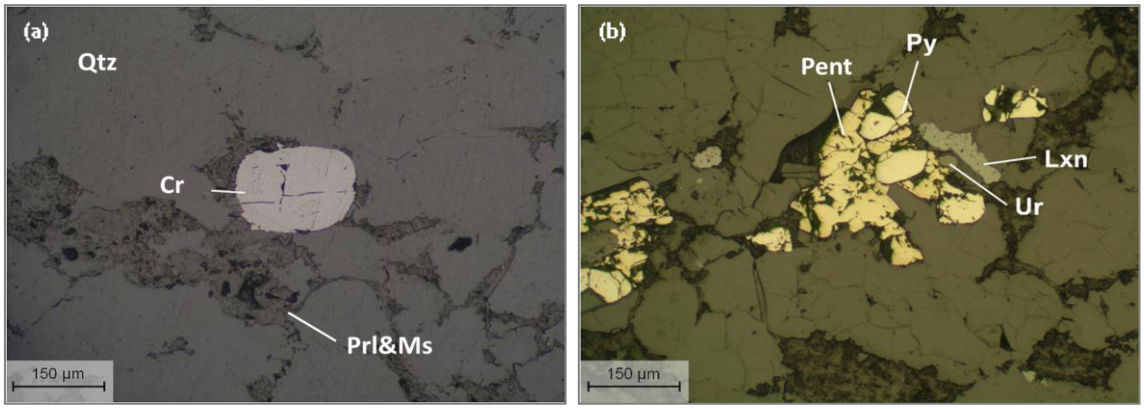

Figure 3.31*: (a) A rounded grain of chromite (Cr) in the hangingwall quartzite. The grain occurs interstitially between quartz (Qtz) clasts and within a pyrophyllite (Prl) and muscovite (Ms) matrix – Sample 14, viewed in reflected light; (b) A rounded grain of uraninite (Ur) observed to be in association with detrital pyrite (Py), pentlandite (Pent) and leucoxene (Lxn) – Sample 4, viewed in reflected light.*

Rounded grains of chalcopyrite were seen in the samples and occurred independently of other sulphides as well as inclusions in pyrite and pyrrhotite. Chalcopyrite was noted within

hangingwall samples overlying all the facies types. Pyrrhotite was seen in the form of rounded to angular grains as well as in the form of veinlets in pyrite. Pyrrhotite was noted in thin section for hangingwall samples overlying the No. 1 and No. 3 Facies. Rounded uraninite was only observed in one polished thin section (0.03 mm diameter) and was seen to be associated with detrital pyrite, pentlandite as well as leucoxene in Sample 4 (Figure 3.31 (b)).

Carbon was identified in thin section as fly-speck carbon in Samples 1, 2 and 15 (Figure 3.32 (a)). In Figure 3.32 (a) it appears that rounded pyrite has been overgrown by secondary pyrite and occurs along a foreset. Samples 1 and 15 were overlying the No. 1 Facies, and Sample 2 was overlying the No. 2 Facies.

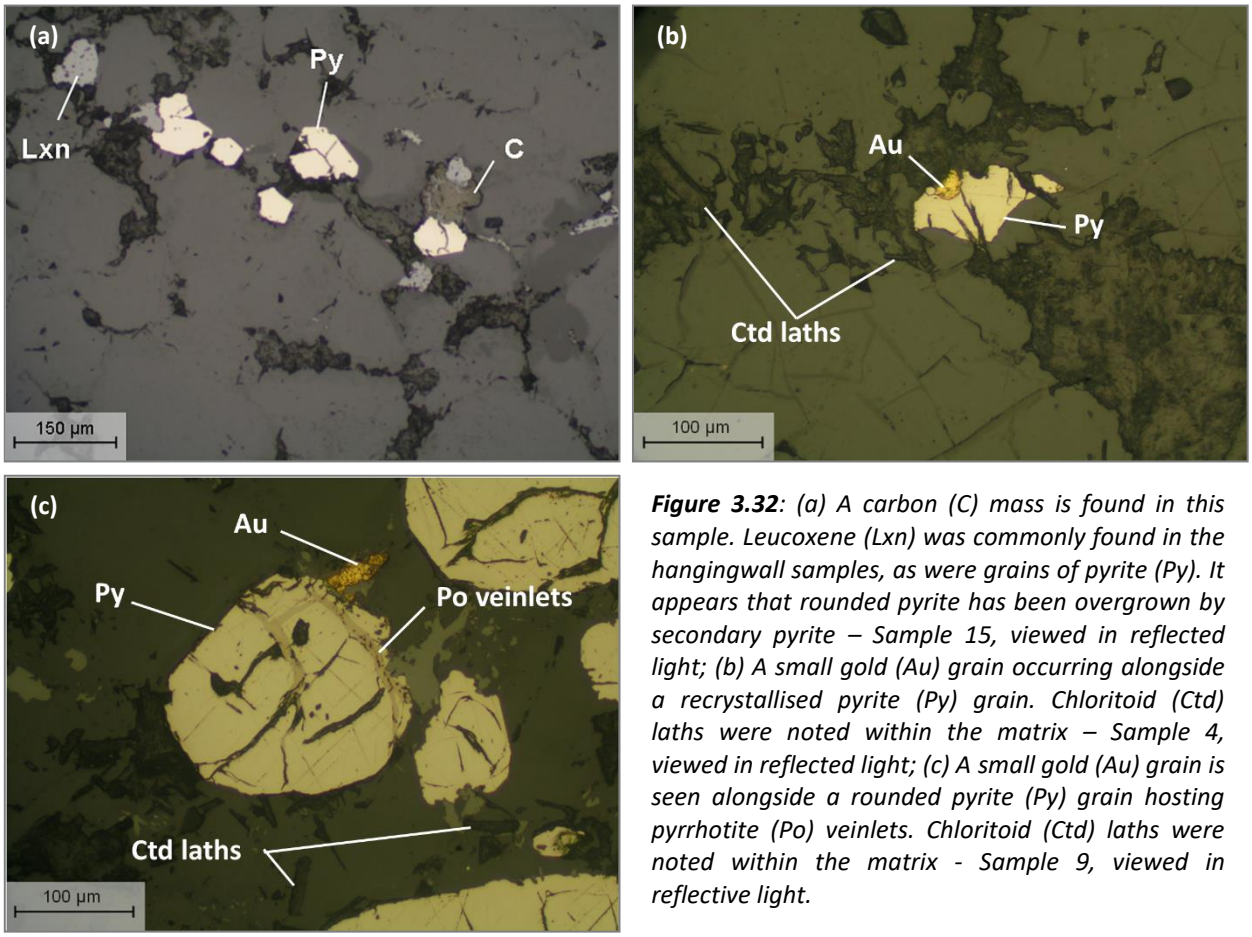

***Figure 3.32**: (a) A carbon (C) mass is found in this sample. Leucoxene (Lxn) was commonly found in the hangingwall samples, as were grains of pyrite (Py). It appears that rounded pyrite has been overgrown by secondary pyrite – Sample 15, viewed in reflected light; (b) A small gold (Au) grain occurring alongside a recrystallised pyrite (Py) grain. Chloritoid (Ctd) laths were noted within the matrix – Sample 4, viewed in reflected light; (c) A small gold (Au) grain is seen alongside a rounded pyrite (Py) grain hosting pyrrhotite (Po) veinlets. Chloritoid (Ctd) laths were noted within the matrix - Sample 9, viewed in reflective light.*

Leucoxene was present in all of the samples and was seen to be associated with rounded to subrounded, as well as anhedral grains of rutile (0.025 to 0.15 mm). Gold was observed in thin section in two of the hangingwall samples – Sample 4 (Figure 3.32 (b)) and Sample 9 (Figure 3.32 (c)). In Figure 3.32 (b) the small gold grain occurs alongside a recrystallised pyrite grain. In Figure 3.32 (c) the gold grain is seen alongside a rounded pyrite grain hosting pyrrhotite

veinlets. Hangingwall samples noted to have a gold grade greater than 1 g/t include Sample 4, 10, 14 and 15 (overlying the No. 1 Facies) as well as Samples 9, 16, 18 and 19 (overlying the No. 3 Facies).

Sample 4 was the only hangingwall sample that had pentlandite and uraninite noted in thin section and it overlies a very high-grade No. 1 Facies (227.0 g/t). Sample 10 overlies a very high-grade No. 1 Facies (284.0 g/t), with Samples 14 and 15 overlying high-grade No. 1 Facies (132.0 g/t and 79.5 g/t respectively). Samples 9 and 16 overlie a high grade No. 3 Facies (80.7 g/t and 36.0 g/t respectively). Samples 18 and 19 overlie a very high grade No. 3 Facies (173.0 g/t and 141.0 g/t respectively). It should be noted that higher gold grades within the hangingwall samples were accompanied by higher gold grades within the Carbon Leader Reef. This suggests that gold has been remobilised from the reef unit into the overlying hangingwall unit.

Comparing the petrology of the hangingwall samples with the macroscopic observations (noted in Chapter 3.1, Table 3.4), Sample 5 was noted to have rounded disseminated pyrite grains along fractures with a 1 cm thick quartz vein cutting the hangingwall. The pyrite abundance was notably high (4%) in comparison to the other hangingwall samples in thin section, as was the pyrophyllite abundance (13%). This suggests that pyrophyllitic alteration may have taken place in the hangingwall portion of Sample 5. An elevated abundance of pyrophyllite was also noted in Sample 1 (overlying the No. 1 Facies), Sample 8 (overlying the No. 3 Facies) and Sample 10 (overlying the No. 1 Facies), suggesting the discolouration of the host rock (hangingwall quartzite) may be as a result of pyrophyllitic alteration in those samples. In Sample 19 a quartz vein less than 1 cm thick was noted to be cutting the hangingwall. In thin section it was noted that chlorite and chloritoid (combined) had a greater abundance than pyrophyllite and sericitic muscovite, suggesting chloritisation has occurred within the hangingwall.

Refer to Table 3.5 for the modal abundance and the gold grades of all the hangingwall samples, combined with XRD analyses results.

Table 3.5: The modal abundance of 19 hangingwall (tombstone) samples. The modal abundance comprises % content (where applicable) for: quartz (Qtz), pyrophyllite (Prl), muscovite (Ms), chlorite (Chl), chromite (Cr), pyrite (Py), rutile (Rut) and leucoxene (Lxn), chloritoid (Ctd), zircon (Zr), pyrrhotite (Po), carbon (C), gersdorffite (Gdf), chalcopyrite (Cpy), tourmaline (Tour), pentlandite (Pent) and uraninite (Ur). *Gold (Au) appears as a trace element in most of the samples – the gold grade (g/t) determined by fire assay has been included. Samples 4, 9, 10, 14, 15, 16, 18 and 19 were noted to have a gold grade greater than 1 g/t. Minerals noted to have a trace amount are denoted by Tr. Where no detail is included this indicates the mineral was not present within the polished thin section and/or XRD analysis. [(a)] Determined by means of XRD analysis as they were not seen within the polished thin section.

Hangingwall Samples: Modal Abundance (%)																		
	Sample ID.	*Underlying Reef Unit*	*Qtz*	*Prl*	*Ms*	*Chl*	*Cr*	*Py*	*Rut/ Lxn*	*Ctd*	*Zr*	*Po*	*C*	*Gdf*	*Cpy*	*Tour*	*Pent*	*Ur*	*Au**
1	94-94 E1	No. 1 Facies	86	9	2	2	Tr[(a)]	1	Tr	Tr	Tr	Tr	Tr						0.2
2	99-94 E2	No. 2B Facies	85	10	2	2	Tr[(a)]	1	Tr	Tr			Tr		Tr				0.7
3	104-88 W6	No. 1 Facies	84	11	1	3	Tr[(a)]	1	Tr	Tr	Tr				Tr				0.1
4	105-86 E2	No. 1 Facies	89	7	3		Tr[(a)]	1	Tr	Tr	Tr						Tr	Tr	1.4
5	112-83 W3	No. 1 Facies	77	13	4	2		4	Tr	Tr	Tr				Tr				0.6
6	112-83 W4	No. 1 Facies	86	7	2	4		1	Tr	Tr	Tr	Tr			Tr				0.3
7	114-78 E1	No. 1 Facies	88	4	1	5	1	1	Tr	Tr		Tr			Tr	Tr			0.6
8	120-55 W4	No. 3 Facies	85	7	3	3	1	1	Tr	Tr		Tr		Tr					0.2
9	120-77 S1	No. 3 Facies	88	7	2	3	Tr[(a)]	1	Tr	Tr	Tr	Tr							3.9
10	96-94 E2	No. 1 Facies	84	8	4	3		1	Tr	Tr					Tr	Tr			2.7
11	100-92 Wze	No. 2A Facies	88	4	3	1		1	1	2									0.6
12	104-88 E1A	No. 1 Facies	88	6	4	1		1	Tr	Tr	Tr				Tr	Tr			0.4
13	104-88 W7	No. 1 Facies	84	7	5	3		1	Tr	Tr	Tr					Tr			0.8
14	109-87 E2	No. 1 Facies	87	4	4	2	Tr	1	Tr	2						Tr			2.5
15	112-84 Rse	No. 1 Facies	87	4	4	2		1	Tr	2			Tr						1.2
16	120-55 NE7	No. 3 Facies	93	1	1	5		2	Tr	Tr	Tr	Tr				Tr			1.2
17	120-55 W5	No. 3 Facies	89	1	3	3		1	Tr	3	Tr								0.1
18	120-55 W7	No. 3 Facies	89	1	2	4		2	Tr	2	Tr	Tr			Tr				1.1
19	120-70 W1	No. 3 Facies	93	1	2	1		2	Tr	2	Tr	Tr							8.0

3.2.2 Footwall Descriptions

The dominant mineral assemblage seen throughout the (23) footwall quartzite samples comprises quartz (>63%), with pyrophyllite, sericitic muscovite, chlorite, chloritoid (with the exception of Sample 1 that was noted to have an absence of chloritoid) and sulphides making up the remaining modal content. Figure 3.33 (a) and (b) show the typical mineral composition of the footwall quartzite. Angular to subrounded quartz clasts ranging from 0.01 mm up to 2 mm in diameter were seen in thin section. The majority of the quartz clasts were monocrystalline with a few smaller polycrystalline grains (Figure 3.33 (a)).

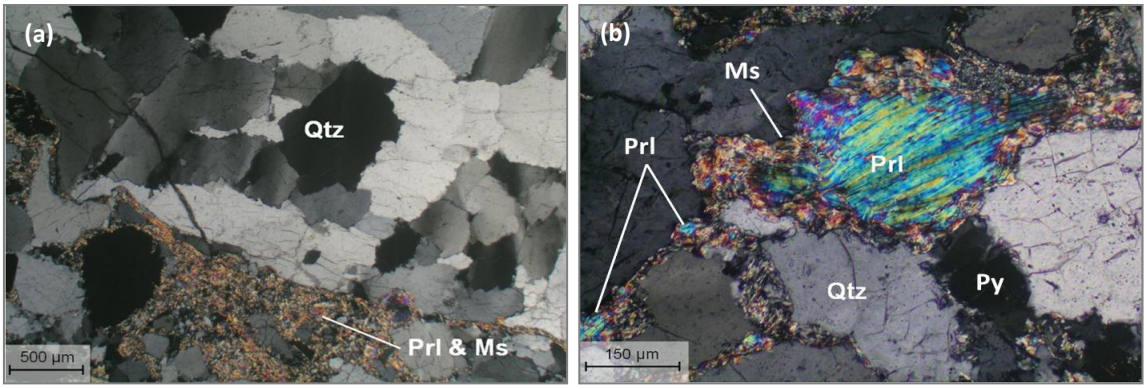

***Figure 3.33**: (a) Monocrystalline quartz (Qtz) clasts constitute the bulk mineralogy within the footwall quartzite. Pyrophyllite (Prl) and muscovite (Ms) occur interstitially between the quartz (Qtz) clasts – Sample 2, viewed in cross-polarised transmitted light; (b) A large pyrophyllite (Prl) grain surrounded by a very fine sericitic muscovite (Ms) and chlorite matrix, occurring interstitially between clasts of quartz (Qtz). Muscovite appears to be replacing pyrophyllite. Grains of pyrite (Py) were noted within the polished thin section – Sample 14, viewed in cross-polarised transmitted light.*

Quartz abundance was on average the lowest in footwall samples underlying the No. 1 Facies and is the highest in footwall samples underlying the No. 2 Facies. This suggests that footwall samples underlying the No. 1 and No. 3 Facies are less siliceous than footwall samples underlying the No. 2 Facies. Occurring interstitially between the quartz clasts was a matrix of very fine material comprising pyrophyllite, sericitic muscovite as well as chlorite grains. Although the pyrophyllite and muscovite grains were difficult to differentiate within the matrix, a few pyrophyllite grains were coarser (up to 1.1 mm) (Figure 3.33 (b)). In Sample 14 it appears that muscovite is replacing the pyrophyllite. Pyrophyllite was the second most abundant mineral in the footwall after quartz and occupied between 1% and 21% of the total modal abundance. The pyrophyllite abundance of footwall samples underlying the No. 1 Facies was greater than within the No. 3 Facies. Footwall samples underlying the No. 2 Facies had the lowest abundance of pyrophyllite. The modal abundance of the footwall samples exhibit

elevated pyrophyllite abundances compared to the amount recorded for the hangingwall samples, but show lesser chloritoid abundances.

Chloritoid laths were noted to occur within the pyrophyllite-muscovite-chlorite matrix between quartz clasts (Figure 3.34 (a)). A few of the chloritoid laths occurred in radiating masses, and ranged in size from 0.1 to 1 mm in length. Chloritoid was noted in all the footwall samples, with the exception of Sample 1.

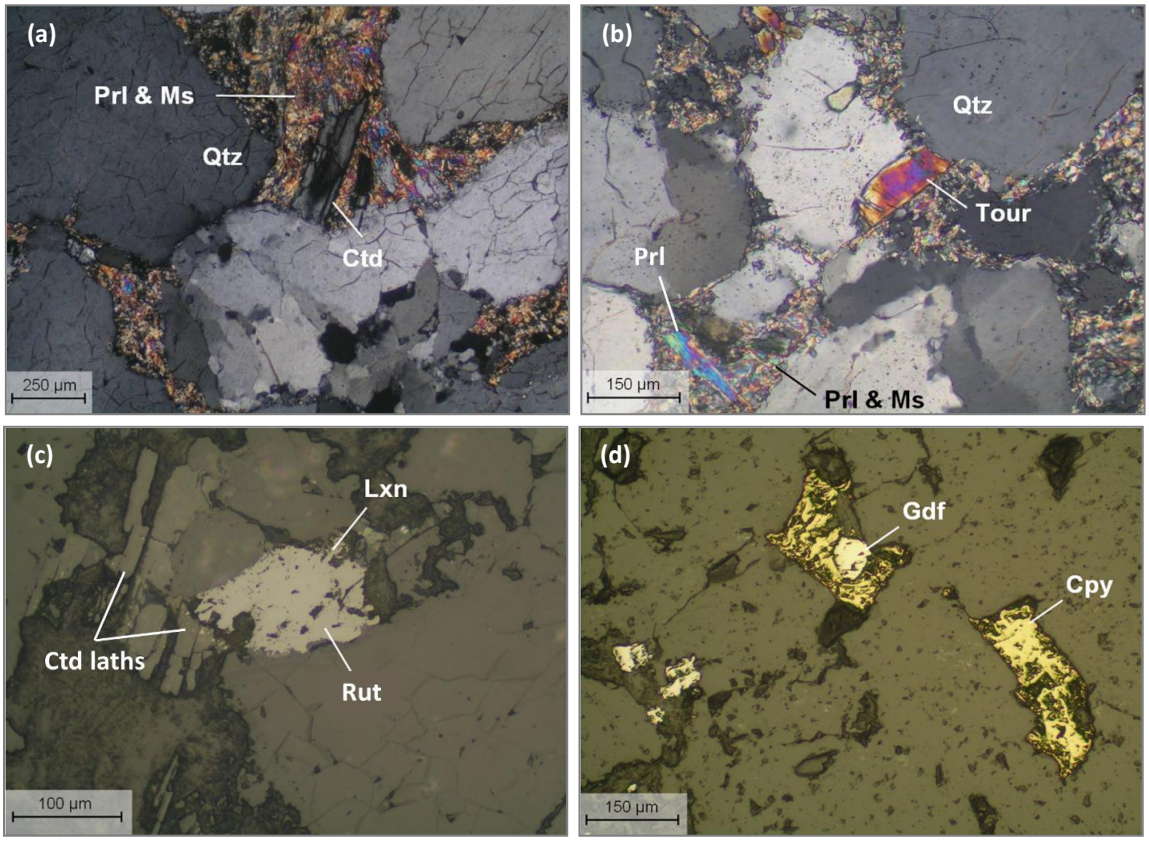

***Figure 3.34**: (a) Pyrophyllite (Prl) and muscovite (Ms) both occurred as very fine matrix material and were not easily distinguishable from one another however a few pyrophyllite (Prl) grains were noted to be coarser. Chloritoid (Ctd) laths were also seen within the fine-grained matrix occurring interstitially between quartz (Qtz) clasts – Sample 6, viewed in cross-polarised transmitted light; (b) Angular to columnar tourmaline (Tour) grains were seen in some of the footwall samples, occurring between quartz (Qtz) clasts and within a pyrophyllite (Prl) and muscovite (Ms) matrix – Sample 2, viewed in cross-polarised transmitted light; (c) Rutile (Rut) was seen to be associated with leucoxene (Lxn) in all of the footwall samples. Chloritoid (Ctd) laths were noted within the matrix – Sample 9, viewed in reflected light; (d) A grain of gersdorffite (Gdf) occurring within a footwall sample. In this microphotograph it is seen with a chalcopyrite (Cpy) overgrowth – Sample 4$^{(b)}$, viewed in reflected light.*

Euhedral columnar grains of tourmaline were seen in 4 of the footwall samples: Samples 1, 3 and 13 (underlying the No. 1 Facies) and Sample 19 (underlying the No. 3 Facies) and were seen wedged between the quartz clasts and/or occurring within the fine-grained matrix (Figure 3.34 (b)). Leucoxene was associated with rutile in all the samples observed (Figure 3.34 (c)) as well

as occurring as fine-grained material in fractures. Rutile was also observed in the footwall samples alongside leucoxene. The rutile grains were typically subrounded, and ranged in size from 0.005 mm up to 0.6 mm.

Subrounded gersdorffite grains were seen in thin section in Samples 1 and $4^{(b)}$ (underlying the No. 1 Facies) as well as Samples $9^{(b)}$ and 18 (underlying the No. 3 Facies). In Sample $4^{(b)}$, the gersdorffite grain was seen with a chalcopyrite overgrowth (Figure 3.34 (d)). Chalcopyrite typically occurred as rounded inclusions (0.01 to 0.07 mm) within pyrite and pyrrhotite. Chalcopyrite also occurred as euhedral grains (0.02 to 0.15 mm) when not associated with other sulphides. It was also noted that chalcopyrite occurred within footwall samples underlying all the facies types. Veinlets of pyrrhotite were seen infilling fractures within pyrite grains and as anhedral grains (up to 0.25 mm) when not associated with other sulphides. Pyrrhotite was noted more frequently within footwall samples underlying the No. 3 Facies.

Euhedral as well as rounded pyrite grains were seen along foresets, in fractures as well as disseminated within the footwall quartzite, and ranged from 0.01 to 0.9 mm in diameter. Higher abundances of pyrite were noted in footwall samples underlying the No. 1 and No. 3 Facies. The highest pyrite abundance was noted in Sample $4^{(b)}$ (underlying the No. 1 Facies) which may be as a result of the sample representing a footwall pebble band, allowing for the concentration of sulphides between quartz clasts within a pyrophyllite-rich matrix.

XRD analyses detected chromite within 10 of the samples, with only Samples 4, $4^{(b)}$ and 7 (underlying the No. 1 Facies) and Sample 18 (underlying the No. 3 Facies) having visible rounded chromite grains in thin section.

For the modal abundance of all the footwall samples, refer to Table 3.6. The modal abundances are combined with XRD analyses results.

Table 3.6: The modal abundance of 20 hangingwall (tombstone) samples. The modal abundance comprises % content (where applicable) for: quartz (Qtz), pyrophyllite (Prl), muscovite (Ms), chlorite (Chl), chromite (Cr), pyrite (Py), rutile (Rut) and leucoxene (Lxn), chloritoid (Ctd), zircon (Zr), pyrrhotite (Po), carbon (C), gersdorffite (Gdf), chalcopyrite (Cpy), tourmaline (Tour), uraninite (Ur) and gold (Au). *Gold (Au) appears as a trace element in all the samples – the gold grade (g/t) determined by fire assay has been included. Samples 9[(b)], 10, 11, 12, 15, 18 and 19 were noted to have a gold grade greater than 1 g/t. Minerals noted to have a trace amount are denoted by Tr. Where no detail is included this indicates the mineral was not present within the polished thin section and/or XRD analysis. [(a)] Determined by means of XRD analysis as they were not seen within the polished thin section. [(b)] Footwall pebble band samples.

			Footwall Samples: Modal Abundance (%)															
	Sample ID.	*Overlying Reef Unit*	*Qtz*	*Prl*	*Ms*	*Chl*	*Cr*	*Py*	*Rut/ Lxn*	*Ctd*	*Zr*	*Po*	*C*	*Gdf*	*Cpy*	*Tour*	*Ur*	*Au**
1	94-94 E1	No. 1 Facies	77	7	13	2	Tr[(a)]	1	Tr		Tr	Tr		Tr	Tr	Tr		0.1
2	99-94 E2	No. 2A Facies	88	6	3	2		1	Tr	Tr	Tr	Tr			Tr			0.2
3	104-88 W6	No. 1 Facies	80	13	3	2	Tr[(a)]	1	1	Tr						Tr		0.9
4	105-86 E2	No. 1 Facies	75	17	3	3	1	1	Tr	Tr	Tr							0.2
4[(b)]	105-86 E2	No. 1 Facies	83	9	1	3	1	3	Tr	Tr	Tr			Tr	Tr			0.5
6	112-83 W4	No. 1 Facies	86	9	1	3	Tr[(a)]	1	Tr	Tr	Tr				Tr			0.4
7	114-78 E1	No. 1 Facies	77	13	4	4	1	1	Tr	Tr	Tr							0.9
8	120-55 W4	No. 3 Facies	83	12	2	2	Tr[(a)]	1	Tr	Tr		Tr			Tr			0.5
9	120-77 S1	No. 3 Facies	66	21	8	4	Tr[(a)]	1	Tr	Tr	Tr							0.5
9[(b)]	120-77 S1	No. 3 Facies	82	12	3	3	Tr[(a)]	1	Tr	Tr	Tr	Tr		Tr	Tr			2.8
10	96-94 E2	No. 1 Facies	63	17	12	7		1	Tr	Tr								1.3
11	100-92 Wze	No. 2A Facies	93	1	1	4		1	Tr	Tr					Tr			1.1
12	104-88 E1A	No. 1 Facies	87	6	3	3		1	Tr	Tr		Tr						3.8
13	104-88 W7	No. 1 Facies	93	2	4	1		Tr	Tr	Tr						Tr		0.5
14	109-87 E2	No. 1 Facies	87	8	4	1		Tr	Tr	Tr								0.6
15	112-84 Rse	No. 1 Facies	87	3	6	2		2	Tr	Tr								2.1
16	120-55 NE7	No. 3 Facies	89	1	7	2		1	Tr	Tr								0.1
17	120-55 W5	No. 3 Facies	87	3	7	2		1	Tr	Tr		Tr						0.9
18	120-55 W7	No. 3 Facies	84	4	6	3	1	2	Tr	Tr	Tr	Tr	Tr	Tr	Tr		Tr	135.0
19	120-70 W1	No. 3 Facies	91	3	3	1		2	Tr	Tr	Tr		Tr			Tr	Tr	26.8

Several footwall samples were noted to have a gold grade greater than 1 g/t including Samples 10, 12 and 15 (underlying the No. 1 Facies), Sample 11 (underlying the No. 2 Facies), as well as Samples 9(b), 18 and 19 (underlying the No. 3 Facies). For all the footwall samples that carried a gold grade greater than 1 g/t, the overlying reef unit was noted to have a high to very high gold grade.

Gold was observed in two footwall polished thin sections – Samples 18 and 19 (Figure 3.35 (a) and (b) respectively – both underlying the No. 3 Facies). Rounded to anhedral masses of fly-speck carbon were seen occurring with disseminated pyrite in Sample 18, and carbon was seen to fill fractures in uraninite grains in Sample 19. Uraninite grains were seen as inclusions within the carbon masses in Sample 18. Uraninite and carbon content was only noted in the two samples (Samples 18 and 19) occurring together with gold and carrying high gold grades.

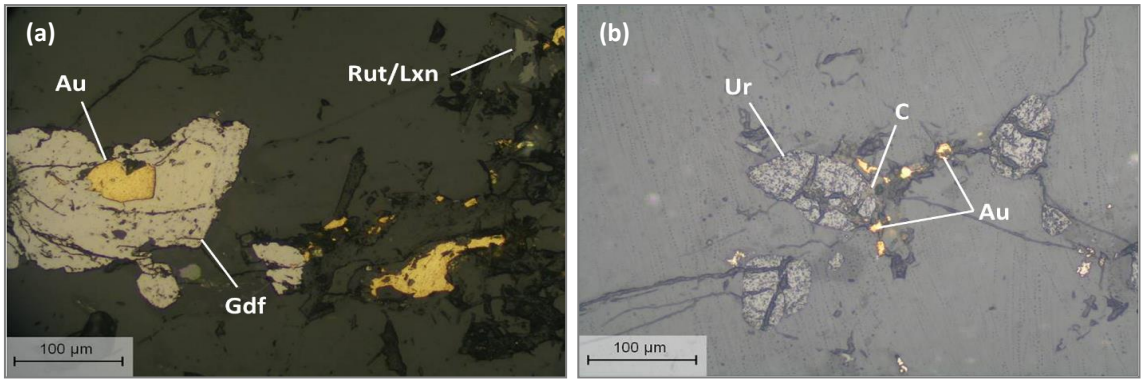

***Figure 3.35**: (a) A grain of gold (Au) enclosed by gersdorffite (Gdf). Rutile (Rut) and/or leucoxene (Lxn) was also seen proximal to a gold grain in the uppermost right corner of the microphotograph. An anhedral gold grain is seen in the bottom left portion of the microphotograph – Sample 18, viewed in reflected light; (b) Gold (Au) associated with carbon (C) and uraninite (Ur) in the footwall sample – Sample 19, viewed in reflected light.*

Sample 18 had a significantly high gold grade for a footwall sample (135.0 g/t) and may have been misidentified as footwall rather than reef. The gold grade for the overlying No. 3 Facies was 173.0 g/t and the likelihood of the remobilisation of such a significant amount of gold from the reef unit is unlikely. The sample may also be anomalously mineralised. Sample 19 had a gold grade of 26.8 g/t and is overlain by a high-grade No. 3 Facies (141.0 g/t). The gold grade within Sample 19, as well as the other samples with trace amounts of gold grade, may be due to the remobilisation of gold from the overlying reef unit.

Comparing the petrology and the macroscopic observations of the footwall samples, Sample 1 was noted to have pyrite along fractures in hand specimen and in thin section it was noted to have an elevated abundance of sericitic muscovite with rounded pyrite grains occurring within

the sericite-rich matrix. This suggests sericitic alteration may have taken place and the pyrite grains may have been remobilised into the fractures.

Sample 17 was noted to have a greenish discolouration of the footwall quartzite on the outer edge of the fault/shear located at the contact between the reef and the footwall. In thin section Sample 17 was noted to have an elevated abundance of sericitic muscovite, suggesting the discolouration of the footwall quartzite is due to sericitic alteration.

3.2.3 Carbon Leader Reef Descriptions

A total of 53 polished thin sections, of which 38 were tombstone samples and 15 were borehole samples, were investigated in order to characterise the Carbon Leader Reef. When comparing the various facies types of the Carbon Leader Reef in thin section a few obvious differences become apparent. One such difference was the variation between facies types in modal abundance of quartz, sericitic muscovite and chloritoid within the reef.

Samples from the No. 3 Facies had the highest occurrence of pyrophyllite (after quartz), sericitic muscovite, chlorite and chloritoid of all the reef samples (Figure 3.36 (a)). Samples from the No. 1 Facies exhibited a similar modal abundance to the No.3 Facies of pyrophyllite, sericitic muscovite, chlorite and chloritoid (Figure 3.36 (b)), followed by samples representing the No. 2 Facies (Figure 3.36 (c)).

The quartz clasts were similar across the facies types, in that they were angular to subrounded in shape and were mainly monocrystalline. The average occurrence of quartz in thin section for the No. 1 Facies and the No. 2 Facies was 87%, with an average of 84% determined for the No. 3 Facies. The lower average for the No. 3 Facies was affected by Sample 8 that has a higher amount of alteration minerals, particularly pyrophyllite, in comparison to the other samples from the No. 3 Facies. Removing Sample 8 from the average for the No. 3 Facies increased the modal abundance of quartz to 85%, suggesting samples from the No. 1 and No. 2 Facies have less alteration minerals in comparison to samples from the No. 3 Facies. This further suggests that samples from the No. 3 Facies have undergone more alteration than samples from the No. 1 and No. 2 Facies.

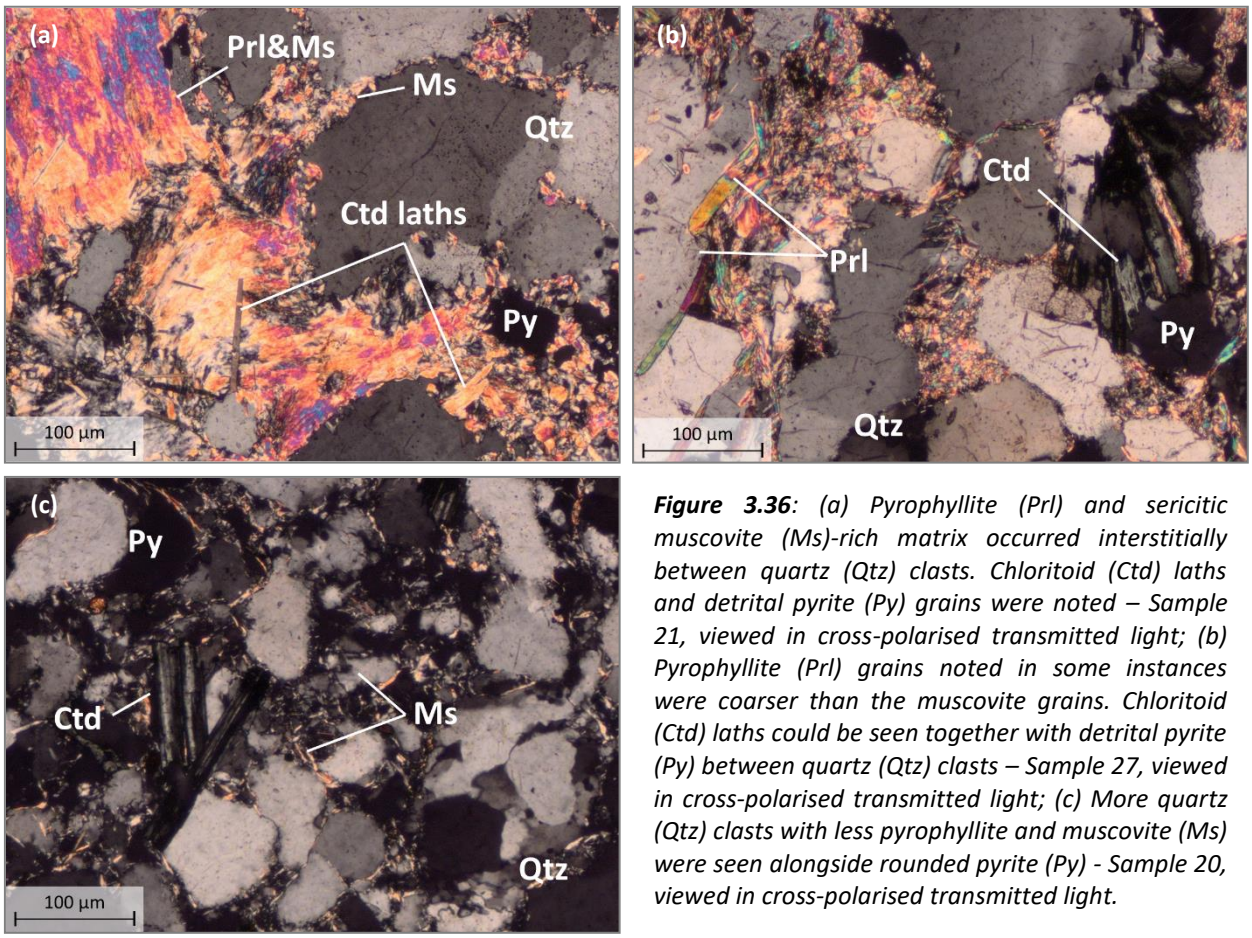

***Figure 3.36**: (a) Pyrophyllite (Prl) and sericitic muscovite (Ms)-rich matrix occurred interstitially between quartz (Qtz) clasts. Chloritoid (Ctd) laths and detrital pyrite (Py) grains were noted – Sample 21, viewed in cross-polarised transmitted light; (b) Pyrophyllite (Prl) grains noted in some instances were coarser than the muscovite grains. Chloritoid (Ctd) laths could be seen together with detrital pyrite (Py) between quartz (Qtz) clasts – Sample 27, viewed in cross-polarised transmitted light; (c) More quartz (Qtz) clasts with less pyrophyllite and muscovite (Ms) were seen alongside rounded pyrite (Py) - Sample 20, viewed in cross-polarised transmitted light.*

Occurring interstitially between the quartz clasts was a very fine to fine-grained matrix of pyrophyllite, sericitic muscovite and chlorite. The pyrophyllite grains were differentiated from the muscovite by their slightly coarser grain size. The modal abundance of pyrophyllite across all the facies types, on average, was 5%. By removing Sample 8 from the No. 3 Facies the average pyrophyllite abundance was decreased to 4%. Overall, it appeared that samples from the No. 1 and No. 2 Facies were slightly more pyrophyllite-rich than samples within the No. 3 Facies, suggesting less pyrophyllitic alteration has occurred within the No. 3 Facies (with the exception of Sample 8).

The modal abundance of all the Carbon Leader Reef polished thin section samples can be found in Table 3.7.

Table 3.7: The modal abundance of 37 Carbon Leader Reef (tombstone and borehole) samples. The modal abundance comprises % content (where applicable) for: quartz (Qtz), pyrophyllite (Prl), muscovite (Ms), chlorite (Chl), chromite (Cr), pyrite (Py), rutile (Rut) and leucoxene (Lxn), chloritoid (Ctd), zircon (Zr), pyrrhotite (Po), carbon (C), gersdorffite (Gdf), chalcopyrite (Cpy), tourmaline (Tour), uraninite (Ur), bornite (Bor), hematite (Hem) and gold (Au). *Gold (Au) appears in all the reef samples – the gold grade (g/t) determined by fire assay has been included. Minerals noted to have a trace amount are denoted by Tr. Where no detail is included this indicates the mineral was not present within the polished thin section and/or XRD analysis. [(a)] Determined by means of XRD analysis as they were not seen within the polished thin section. [(b)] Pale Pebbly Quartzite (PPQ) unit for Sample 2. [(c)] No. 2A Facies for Sample 2. [(d)] Internal Quartzite (IQ) for Sample 15.

Carbon Leader Reef Samples: Modal Abundance (%)																			
	Sample ID	*Unit*	*Qtz*	*Prl*	*Ms*	*Chl*	*Ctd*	*Tour*	*Py*	*Cr*	*Rut/Lxn*	*Zr*	*Po*	*C*	*Gdf*	*Cpy*	*Ur*	*Bor*	*Hem*	*Au**
1	94-94 E1	No. 1 Facies	88	5	2	3	1		1	Tr	Tr	Tr	Tr	Tr	Tr	Tr				10.3
2	99-94 E2	No. 2B Facies	83	9	3	2	1		2	Tr[(a)]	Tr	Tr	Tr	Tr	Tr	Tr	Tr			41.2
2[(b)]	99-94 E2	PPQ	83	8	3	2	1	1	2	Tr	Tr	Tr	Tr			Tr				0.5
2[(c)]	99-94 E2	No. 2A Facies	86	7	2	1	1	1	2		Tr	Tr	Tr	Tr	Tr	Tr				40.1
3	104-88 W6	No. 1 Facies	85	8	3		1		3	Tr	Tr	Tr	Tr	Tr		Tr				172.0
4	105-86 E2	No. 1 Facies	82	9	3	2	1		3	Tr[(a)]	Tr	Tr	Tr	Tr	Tr	Tr	Tr			227.0
5	112-83 W3	No. 1 Facies	85	6	2	4	1	1	1		Tr	Tr	Tr			Tr				73.6
6	112-83 W4	No. 1 Facies	87	6	2	3	1		1	Tr	Tr	Tr	Tr		Tr	Tr	Tr			119.0
7	114-78 E1	No. 1 Facies	89	4	2	3	1		1	Tr[(a)]	Tr	Tr	Tr	Tr	Tr	Tr				21.1
8	120-55 W4	No. 3 Facies	72	15	5	5	1		2	Tr	Tr	Tr	Tr	Tr		Tr	Tr			311.0
9	120-77 S1	No. 3 Facies	86	5	2	3	1		3	Tr	Tr	Tr	Tr	Tr	Tr	Tr	Tr			80.7
10	96-94 E2	No. 1 Facies	86	5	5		2	1	1	Tr	Tr	Tr		Tr	Tr		Tr			284.0
11	100-92 Wze	No. 2A Facies	92	3	1	2	1		1			Tr		Tr		Tr	Tr			128.0
12	104-88 E1A	No. 1 Facies	88	3	4		2		3	Tr	Tr	Tr			Tr	Tr	Tr			83.9
13	104-88 W7	No. 1 Facies	88	3	5		3		1	Tr	Tr	Tr	Tr	Tr	Tr	Tr	Tr			130.0
14	109-87 E2	No. 1 Facies	88	4	4		2	1	1	Tr	Tr	Tr	Tr		Tr	Tr	Tr			132.0
15	112-84 Rse	No. 1 Facies	88	4	3	2	2		1		Tr	Tr	Tr	Tr		Tr	Tr			79.5
15[(d)]	112-84 Rse	IQ	88	3	5		2		2		Tr	Tr				Tr				41.1
16	120-55 NE7	No. 3 Facies	85	2	5	3	2	1	2	Tr	Tr	Tr		Tr		Tr	Tr			36.0
17	120-55 W5	No. 3 Facies	83	4	5	2	3	1	2		Tr	Tr	Tr	Tr	Tr					15.4

Table 3.7 - continued: The modal abundance of 37 Carbon Leader Reef (tombstone and borehole) samples. The modal abundance comprises % content (where applicable) for: quartz (Qtz), pyrophyllite (Prl), muscovite (Ms), chlorite (Chl), chromite (Cr), pyrite (Py), rutile (Rut) and leucoxene (Lxn), chloritoid (Ctd), zircon (Zr), pyrrhotite (Po), carbon (C), gersdorffite (Gdf), chalcopyrite (Cpy), tourmaline (Tour), uraninite (Ur), bornite (Bor), hematite (Hem) and gold (Au). *Gold (Au) appears in all the reef samples – the gold grade (g/t) determined by fire assay has been included. Minerals noted to have a trace amount are denoted by Tr. Where no detail is included this indicates the mineral was not present within the polished thin section and/or XRD analysis. [(a)] Determined by means of XRD analysis as they were not seen within the polished thin section.

	Carbon Leader Reef Samples: Modal Abundance (%)																		
	Sample ID	*Unit*	*Qtz*	*Prl*	*Ms*	*Chl*	*Ctd*	*Tour*	*Py*	*Cr*	*Rut/Lxn*	*Zr*	*Po*	*C*	*Gdf*	*Cpy*	*Ur*	*Bor*	*Hem*	*Au**
18	120-55 W7	No. 3 Facies	89	2	2	2	1		4	Tr	Tr	Tr	Tr	Tr	Tr	Tr				173.0
19	120-70 W1	No. 3 Facies	90		3	2	2		3	Tr	Tr	Tr	Tr	Tr	Tr	Tr	Tr			141.0
20	DPH 3883	No. 2A Facies	90	3	3		2		2		Tr	Tr	Tr	Tr		Tr	Tr			89.7
21	DPH 4057	No. 3 Facies	81	8	5		3		3			Tr	Tr	Tr		Tr	Tr	Tr		64.3
22	GBH 1000 D6	No. 2A Facies	84	3	5	2	2		4		Tr	Tr	Tr	Tr		Tr				4.5
23	GBH 2788	No. 2B Facies	87	2	5	2	1		3		Tr[(a)]		Tr	Tr		Tr			Tr	9.3
24	GBH 3763	No. 1 Facies	88	5	3	1	2		1		Tr		Tr	Tr		Tr	Tr			41.0
25	GBH 3844	No. 3 Facies	87	3	4	1	2	1	2		Tr	Tr	Tr			Tr	Tr		Tr	31.4
26	GBH 3845	No. 3 Facies	84	7	3	1	3		2		Tr		Tr	Tr		Tr	Tr			1.6
27	GBH 4003	No. 1 Facies	86	4	3	2	3		2		Tr[(a)]		Tr	Tr		Tr	Tr			86.8
28	GBH 6000	No. 1 Facies	86	3	6	1	2		2			Tr	Tr	Tr		Tr	Tr			80.8
29	GBH 6001	No. 3 Facies	82	3	7	3	3		2		Tr			Tr		Tr	Tr			36.4
30	GBH 6003	No. 1 Facies	88	3	3	1	3		2		Tr		Tr	Tr		Tr	Tr			6.4
31	GBH 6004	No. 2B Facies	89	3	2	1	2		3		Tr		Tr	Tr		Tr				12.8
32	GBH 6014	No. 1 Facies	86	3	6	3	1		1		Tr[(a)]	Tr		Tr		Tr	Tr			67.5
33	GBH 6028	No. 1 Facies	84	7	4	1	3		1		Tr	Tr		Tr	Tr	Tr	Tr			0.6
34	GBH 6036	No. 1 Facies	85	5	4	3	2		1		Tr[(a)]	Tr		Tr		Tr	Tr			29.6

Chlorite grains were noted to occur within the matrix and were seen more frequently in samples within the No. 2 and the No. 3 Facies. Higher chlorite abundances were noted in samples within the No. 1 and the No. 3 Facies, suggesting the samples from the No. 1 and the No. 3 Facies were chlorite-rich. Chloritoid was seen in the form of laths as well as in radiating masses (0.05 to 1 mm in size) within the matrix across all the facies types. Samples within the No. 1 and the No. 3 Facies have, on average, a higher chloritoid abundance in comparison to samples from the No. 2 Facies. Combining the observations of chlorite and chloritoid across the facies types, samples from both the No. 1 and the No. 3 Facies are more likely to have undergone chloritisation than samples from the No. 2 Facies.

Grains of tourmaline were seen across the facies types in a subset of samples and typically occurred as anhedral to euhedral columnar grains (0.05 to 0.3 mm). Samples 5, 10 and 14 from the No. 1 Facies had gold grades of 73.6 g/t, 284.0 g/t and 132.0 g/t respectively. Sample $2^{(b)}$ from the No. 2 Facies had a gold grade of 0.5 g/t which is expected from the Pale Pebbly Quartzite unit, and Sample $2^{(c)}$ had a gold grade of 40.1 g/t. Samples 16, 17 and 25 from the No. 3 Facies had gold grades of 36.0 g/t, 15.4 g/t and 31.4 g/t respectively. As with hangingwall and footwall samples, tourmaline was associated with the presence of gold grade. Tourmaline was also noted to occur more frequently in reef samples from the No. 1 and the No. 3 Facies.

Rounded grains of pyrite were seen within the matrix (0.01 to 1 mm in size). Recrystallisation of pyrite was noted within the matrix as there were overgrowths of pyrite on rounded pyrite grains. Microcrystalline pyrite was also observed along fractures cross-cutting quartz clasts. Secondary colloform pyrite was noted in Sample 2 (No. 2 Facies) and Sample 18 (No. 3 Facies). A higher abundance of pyrite, on average, was noted in samples from the No. 3 Facies. Samples from the No. 1 Facies and the No. 2 Facies had an average of 2% pyrite whereas samples from the No. 3 Facies had an average of 3% pyrite.

Rounded grains of zircon were visible in most of the samples across the facies types, as were secondary anhedral grains of chalcopyrite and pyrrhotite. Chalcopyrite occurred as inclusions within recrystallised pyrite grains as well as rounded grains within the matrix. Pyrrhotite was seen mostly in the form of veinlets within pyrite.

In the majority of the samples anhedral masses of leucoxene (Figure 3.37 (a)) associated with rutile were seen (Figure 3.37 (b)) as part of the matrix material. Rutile and leucoxene seemed

to have an association with pyrite and in some samples, with gold (Samples 12 and 15 from the No. 1 Facies as well as Sample 17 from the No. 3 Facies). Leucoxene was also seen infilling fractures in quartz clasts. The presence of leucoxene/rutile was confirmed by XRD analyses for Sample 23 (No. 2 Facies) as well as Samples 27, 32 and 34 (all from the No. 1 Facies).

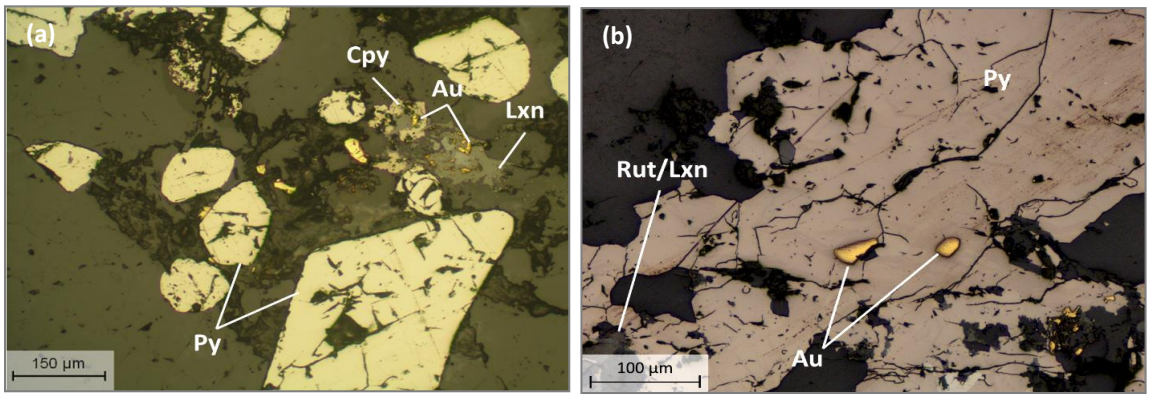

***Figure 3.37**: (a) A mass of secondary leucoxene (Lxn) surrounded by euhedral to rounded (detritral) pyrite (Py) grains. Gold (Au) occurs with rounded pyrite (Py) grains within the matrix as well as with leucoxene (Lxn) – Sample 2, viewed in reflected light; (b) Rutile (Rut) and leucoxene (Lxn) occurred together within the sample. Gold (Au) occurred as inclusions within the anhedral pyrite (Py) grain as well as within the matrix – Sample 23, viewed in reflected light.*

Anhedral to euhedral grains of gersdorffite (0.05 to 0.2 mm in size) occurred within the reef samples predominantly from the No. 1 and the No. 3 Facies. Gold was observed associated with gersdorffite in Samples 1, 10 and 13 (all from the No. 1 Facies) as well as Sample 2 (both reef bands, from the No. 2 Facies). Gold was occasionally contained within the gersdorffite as an inclusion (Figure 3.38 (a)). Gersdorffite was also seen to occur in fractures alongside pyrite, chalcopyrite, rutile and leucoxene. Chromite, bornite and hematite were seen inconsistently within the reef samples with rounded grains of chromite being most frequent in samples from the No. 1 and the No. 3 Facies. The presence of chromite was confirmed by means of the XRD analyses for Sample 2 (No. 2 Facies) as well as Samples 4 and 7 (both from the No. 1 Facies). Bornite was noted to occur only in Sample 21 (No. 3 Facies) and hematite was noted in Sample 23 (No. 2 Facies) and Sample 25 (No. 3 Facies).

Subrounded to rounded grains of uraninite (up to 0.2 mm in size) were seen in Samples 4, 6, 12, 14, 15, 24, 28 and 33 (No. 1 Facies), Samples 22 and 23 (No. 2 Facies) as well as Samples 9, 25 and 26 (No. 3 Facies), occurring together with carbon masses (fly-speck carbon). Gold occurred along the edges of the carbon-uraninite masses as infilling fractures in rounded pyrite in Sample 4 (Figure 3.38 (b)). Fractured grains of uraninite were common, with carbon observed infilling the fractures (Samples 10 and 13 from the No. 1 Facies, Sample 11 from the

No. 2 Facies and Samples 16 and 18 from the No. 3 Facies). Carbon occurred as large masses (up to 0.4 mm in size) and was associated with both uraninite and gold, and occasionally with leucoxene. In Figure 3.38 (c) the gold is hosted within the carbon-uraninite mass, whereas in Figure 3.38 (d) the gold occurs as micro-nuggets within the matrix, in close proximity to leucoxene. The gold micro-nuggets varied in size from 0.001 to 0.14 mm and were rounded.

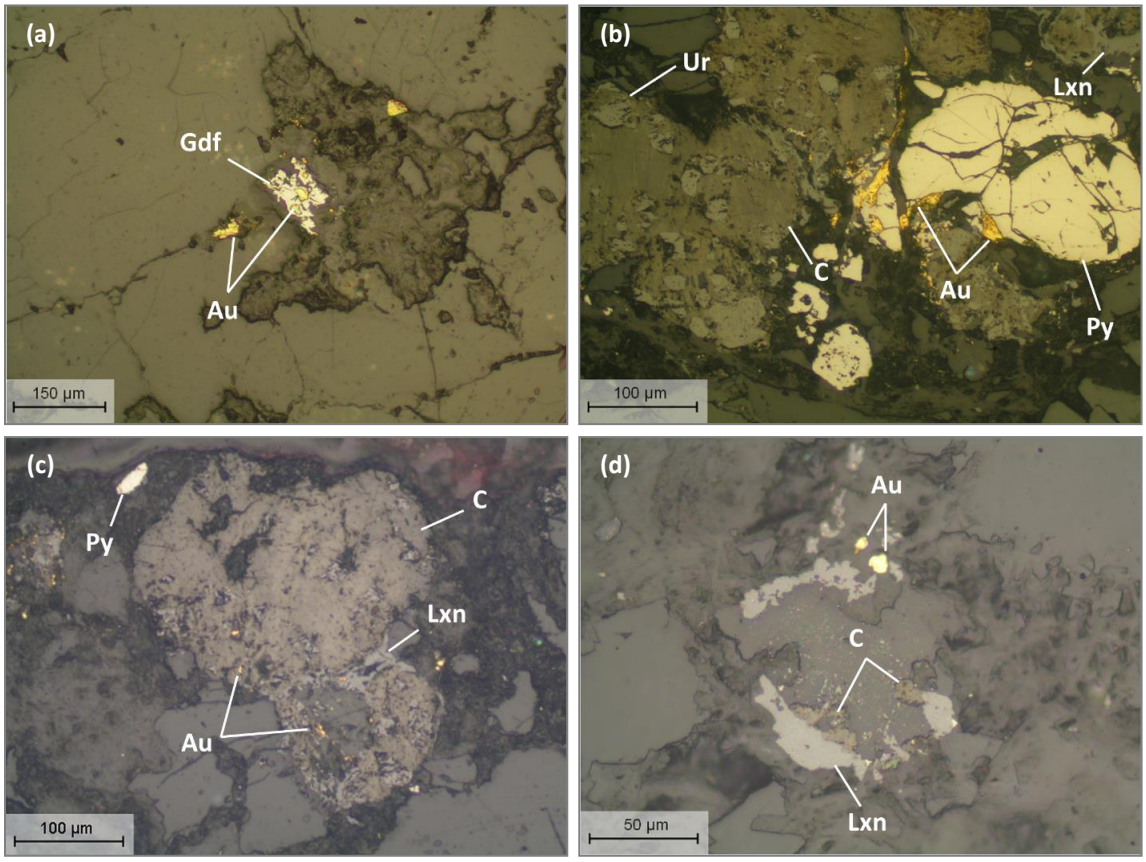

***Figure 3.38**: (a) Anhedral gersdorffite (Gdf) with gold (Au) inclusions and gold micro-nuggets within the matrix of the reef – Sample 2, viewed in reflected light; (b) Uraninite (Ur) grains with carbon (C) masses, with gold (Au) rimming the carbon masses and occurring in infilling fractures in rounded rounded pyrite. Leucoxene (Lxn) is noted within the uppermost right corner adjacent to (fly-speck) carbon nodules – Sample 4, viewed in reflected light; (c) A carbon (C) nodule (fly-speck carbon) associated with leucoxene (Lxn) and gold (Au). A pyrite (Py) grain was noted within the matrix of the reef – Sample 10, viewed in reflected light; (d) Leucoxene (Lxn) occurring together with carbon (C) and gold (Au). The gold occurs as micro-nuggets within the matrix of the reef – Sample 8, viewed in reflected light.*

Gold seen occurring in fractures alongside uraninite and leucoxene, suggests remobilisation of gold has taken place. When gold is observed with alteration minerals (for example leucoxene) it occurs as anhedral grains or within veins/along fractures.

Comparing the petrology and the macroscopic observations of the reef samples, Sample 1 (No. 1 Facies, TauTona estimation domain) was noted to have a greenish discolouration of the reef matrix with increasing proximity to the footwall. In thin section, the dominant alteration

mineral was pyrophyllite. The overlying hangingwall was also noted to have an elevated abundance of pyrophyllite in thin section. This suggests that pyrophyllitic alteration has taken place in the reef and the hangingwall units. The footwall portion of Sample 1 however, had an elevated abundance of sericitic muscovite, suggesting sericitic alteration has taken place in the footwall unit. The discolouration of the reef matrix with increasing proximity to the footwall may be as a result of a combination of sericitic alteration and pyrophyllitic alteration. The gold grade of Sample 1 was 10.3 g/t, which is considerably low for a No. 1 Facies and TauTona estimation domain sample.

Sample 3 (No. 1 Facies, TauTona estimation domain) was noted to have a greenish discolouration of the matrix. In thin section, the reef sample was pyrophyllite-dominant and had no chlorite present. The overlying hangingwall and underlying footwall were noted to have an elevated abundance of pyrophyllite. This suggests that pyrophyllitic alteration has taken place in the hangingwall, reef and footwall units. Sample 3 aligned with the alteration mineral characteristics of a sample within the No. 1 Facies and the TauTona estimation domain, and had a gold grade of 172.0 g/t.

Samples 8 and 18, both from the No. 3 Facies and Peggy estimation domain, were noted to have a greenish discolouration of the reef matrix with increasing proximity to the hangingwall quartzite. Sample 8 was noted to have an elevated pyrophyllite abundance (the highest pyrophyllite abundance of all the reef samples across the various facies types) whereas Sample 18 was noted to have a low abundance of phyllosilicate minerals. The overlying hangingwall unit of Sample 8 was noted to have an elevated abundance of pyrophyllite, suggesting pyrophyllitic alteration may have taken place in the upper portion of the reef and hangingwall unit. The hangingwall unit of Sample 18 was noted to have an elevated abundance of chlorite, suggesting that chloritisation may have taken place in the upper portion of the reef and the hangingwall unit. Sample 8, with a gold grade of 311.0 g/t, did not align with the intermediate gold grades for samples typically found within the Peggy estimation domain however it did fit within the facies model. Sample 18 (173.0 g/t) fits within the facies model as well as within the Peggy estimation domain.

Samples 10 and 13, both from the No. 1 Facies and the TauTona estimation domain, were noted to have a dark green matrix in the reef. Both samples were also noted to have an absence of chlorite in thin section, with elevated abundances of pyrophyllite and sericitic

muscovite in Sample 10 and an elevated abundance of sericitic muscovite in Sample 13. This suggests a combination of pyrophyllitic and sericitic alteration has taken place in Sample 10, with predominantly sericitic alteration in Sample 13. The alteration minerals present within both samples contradict the findings of Burnett *et al*. (2015) in that samples found within the north-east area of the TauTona estimation domain are pyrophyllite-dominant. In terms of the facies model, Sample 10 (284.0 g/t) and Sample 13 (130.0 g/t) were both aligned in terms of gold grade and locality within the No. 1 Facies.

A quartz vein was noted in hand specimen in Sample 19 (No. 3 Facies, TauTona estimation domain), cutting through the hangingwall unit, reef unit and terminating at the footwall-reef contact. In thin section, the reef sample had an absence of pyrophyllite and an elevated abundance of sericitic muscovite. The overlying hangingwall unit had a low phyllosilicate abundance overall, with the sericitic muscovite abundance higher than the other alteration minerals. The underlying footwall unit had both sericitic muscovite and pyrophyllite with a greater abundance than chlorite. Chloritoid was absent in both the hangingwall and footwall units of Sample 19 however it was present alongside chlorite in the reef unit. The elevated presence of sericitic muscovite in the hangingwall, reef and footwall units suggests that sericitic alteration may have occurred. Sample 19 (141.0 g/t) aligns with the facies model however it did not agree with the characteristics of samples found within the south-west area of the TauTona estimation domain. The samples are typically chloritoid-rich but in Sample 19 the greatest abundance of an alteration mineral was noted for sericitic muscovite, followed by chlorite and chloritoid.

Footwall and hangingwall thin sections were not made for Samples 20 through to 34 which limits the overall interpretation for alteration of the reef however the remaining methodologies could be used to supplement the findings within this chapter.

Sample 21 (No. 3 Facies, TauTona estimation domain) was noted to have a sheared contact with the underlying footwall quartzite and the discolouration of a single milky quartz clast to a minty-green colour. In thin section, the reef was noted to have an absence of chlorite with an elevated abundance of pyrophyllite. This suggests pyrophyllitic alteration has taken place in the reef. Sample 21 aligned with the TauTona estimation domain in terms of pyrophyllite being the dominant alteration mineral in the north-east portion of the estimation domain. The sample also aligned with the facies model and had a gold grade of 64.3 g/t. It was also noted that

bornite was found in thin section. Bornite may alter to chalcopyrite should it undergo alteration (Nesse, 2001, p.392). Chalcopyrite was noted in Sample 21 and may further confirm that some form of alteration has taken place.

Sample 23 (No. 2 Facies, Savuka estimation domain) was noted to have a discolouration of the sulphides in the matrix of the reef. In thin section there was an elevated abundance of sericitic muscovite, a 3% modal abundance for pyrite and more importantly, trace anhedral grains of hematite present. Hematite, an iron oxide, is formed as a result of the weathering or hydrothermal alteration of iron-bearing minerals (Nesse, 2001, p.365). With only a single reef sample having hematite present, it is possible that the discolouration of the sulphides within the matrix of the reef may have been due to oxidation of the sulphides, allowing for hematite to form. Sample 23 was aligned to the Savuka estimation domain as it had an elevated sericitic muscovite abundance. Sample 23 was also aligned to the facies model and had a low gold grade of 9.3 g/t, which is expected for a No. 2 Facies sample.

Macroscopically Sample 25 (No. 3 Facies, TauTona estimation domain) was noted to have a greenish discolouration of the reef matrix. With reference to its petrology, Sample 25 had an elevated abundance of sericitic muscovite, suggesting sericitic alteration may have taken place. The reef sample was also noted to have a chloritoid abundance of 2% however this does not agree with the typical findings of a sample in the south-west area of the TauTona estimation domain. Samples in the south-west area are usually chloritoid-dominant and this was not the case for Sample 25. The gold grade for Sample 25 was 31.4 g/t which is another contributing factor to the sample not aligning to the estimation domain model or the No. 3 Facies type as the gold grades are typically a lot higher.

In Sample 31 (No. 2 Facies, Driefontein estimation domain) the reef was noted to have a greenish discolouration of the matrix with possible chloritisation of some of the quartz clasts. By referring to the thin section of the reef, the sample was pyrophyllite dominant, with a slightly lower abundance of sericitic muscovite and chloritoid. It is likely that chloritisation has taken place within the sample, however it may also be a combination of sericitic alteration or pyrophyllitic alteration, or all three collectively. The gold grade of Sample 31 was 12.8 g/t, which did not align to the typical findings of a sample within the Driefontein estimation domain as they hold erratic medium to high gold grades. The gold grade however did align with the No. 2 Facies type, where lower gold grades are expected.

Sample 33 (No. 1 Facies, TauTona estimation domain) was also noted to have a greenish discolouration of the reef matrix. The sample had an abundance of pyrophyllite, which aligns with samples found in the north-east portion of the TauTona estimation domain. The elevated abundance of pyrophyllite suggests that possible pyrophyllitic alteration has taken place. The gold grade of Sample 33 (0.6 g/t) was considerably low for a sample that lies within the TauTona estimation domain as well as within the No. 1 Facies.

Overall, it appears that samples from the No. 1 and the No. 3 Facies have undergone a greater amount of alteration (noticeable in both hand specimen and in petrological analyses) than samples from the No. 2 Facies.

In thin section, carbon was noted in several samples across the facies types and was not restricted to samples that held higher gold grades. Carbon was however found to be strongly associated with rounded grains of uraninite (across all the facies types) in most of the samples, as well as with rounded grains of chromite predominantly in the No. 1 and the No. 3 Facies samples. Samples noted to have an absence of uraninite were also noted to have a lower gold grade than 50 g/t, with the exception of Samples 3 and 5 (both from the No. 1 Facies with gold grades of 172.0 g/t and 73.6 g/t respectively) as well as Sample 18 (No. 3 Facies with a gold grade of 173.0 g/t).

3.2.4 Discussion

The modal abundance percentages for the hangingwall, footwall and Carbon Leader Reef samples were used to create ternary plots to determine any similarities between the samples in terms of phyllosilicate material. The plots of pyrophyllite against chlorite and muscovite (Figure 3.39 (a) and (b)) as well as the plots of the sum of pyrophyllite and muscovite against chlorite and chloritoid (Figure 3.39 (c) and (d)) indicate variations in the alteration assemblages.

Figure 3.39 (a) shows variable amounts of muscovite and pyrophyllite with higher amounts of chlorite in the hangingwall samples (Samples 6 and 7, both overlying the No. 1 Facies as well as Samples 17 and 18, both overlying the No. 3 Facies, have greater than 30% chlorite).

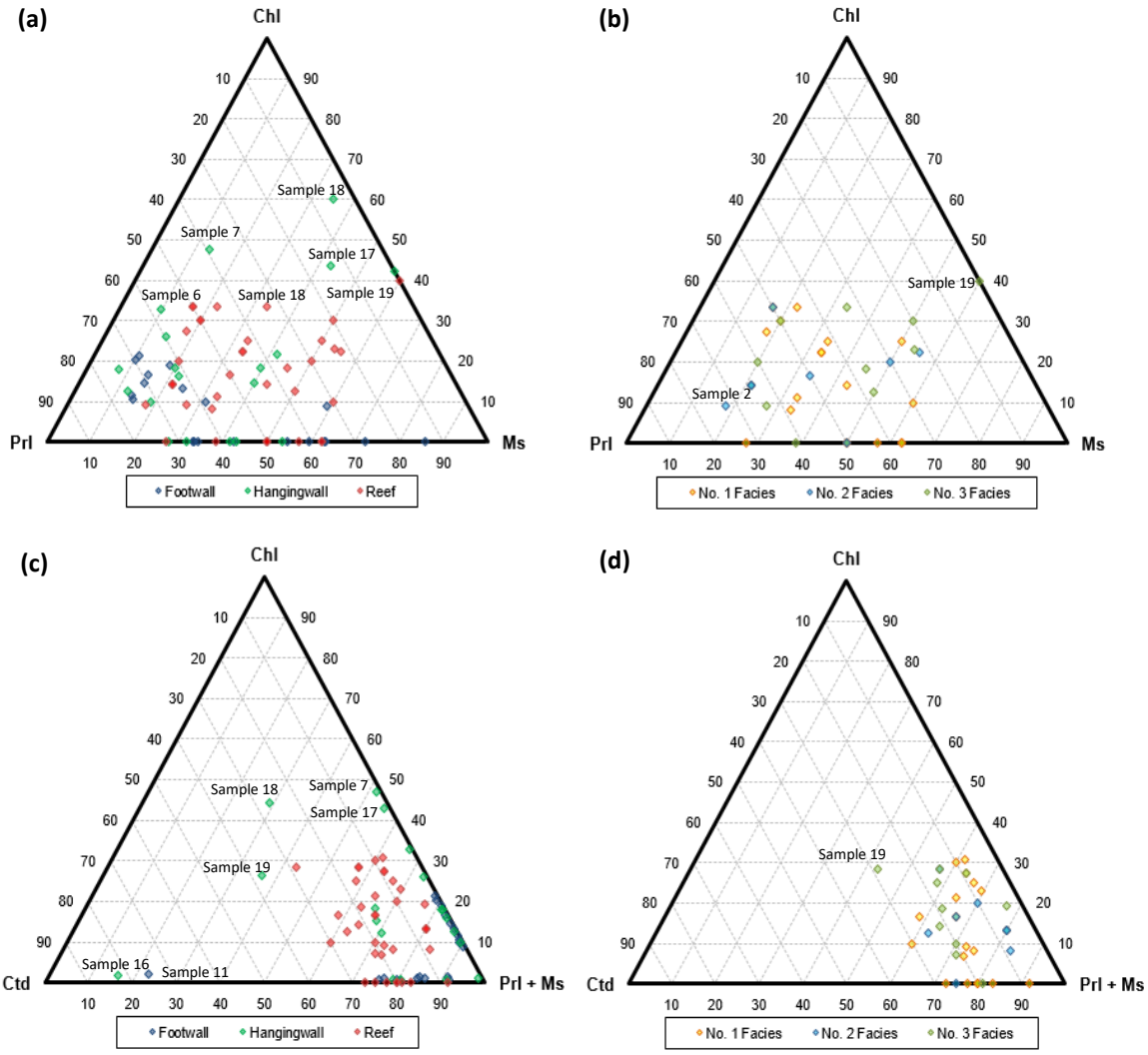

***Figure 3.39**: Ternary diagrams comparing the phyllosilicate concentrations of the hangingwall (HW), footwall (FW) and reef samples: (a) Pyrophyllite (Prl), chlorite (Chl) and muscovite (Ms) plot showing higher amounts of chlorite within the hangingwall samples. The footwall samples have lower muscovite content with higher pyrophyllite. The reef samples have variable muscovite content with lower chlorite; (b) Carbon Leader Reef facies comparison for pyrophyllite (Prl), chlorite (Chl) and muscovite (Ms) with the No. 1 and No. 3 Facies having higher chlorite and muscovite content than in the No. 2 Facies; (c) The sum of pyrophyllite (Prl) and muscovite (Ms), chlorite (Chl) and chloritoid (Ctd) plot indicating lower chloritoid content and higher amounts of chlorite within the hangingwall samples in comparison to the footwall sample; (d) Carbon Leader Reef facies comparison for the sum of pyrophyllite (Prl) and muscovite (Ms), chlorite (Chl) and chloritoid (Ctd) with the chloritoid content variable for all facies types (Ternary plot template used for all diagrams: Warnsloh, 2015).*

In thin section, samples overlying the No. 3 Facies were found to have lower pyrophyllite and muscovite abundances than samples overlying the No. 1 and the No. 2 Facies. Chlorite was noted to occur in thin section in all the hangingwall samples with the exception of Sample 4, overlying the No. 1 Facies. The underlying No. 1 Facies portion of Sample 4 was noted to have chlorite, suggesting the positioning of the thin section in the hangingwall portion of Sample 4 may have not included a portion of the sample with chlorite present.

The footwall samples typically had lower muscovite content with higher pyrophyllite. The chlorite in the footwall samples varied from 0% to 20%. The footwall samples underlying the No. 1 and the No. 3 Facies were notably less siliceous than the samples underlying the No. 2 Facies. This suggests that there are more alteration minerals present in the footwall underlying the No. 1 and the No. 3 Facies, with the footwall underlying the No. 2 Facies having undergone a lesser amount of alteration. Referring to the pyrophyllite content, the footwall samples underlying the No. 1 and the No. 3 Facies had a greater abundance of pyrophyllite in comparison to the footwall samples underlying the No. 2 Facies. The footwall samples underlying the No. 1 Facies, on average, had the highest pyrophyllite abundance.

The reef samples had variable muscovite content and lower chlorite, with pyrophyllite ranging from 20% to 75%. When comparing the different facies types (Figure 3.39 (b)) the No. 1 and No. 2 Facies both had similar modal abundances for phyllosilicate minerals, with the No. 3 Facies having a slightly lower abundance of phyllosilicate minerals.

From Figure 3.39 (c) it is apparent that the hangingwall samples had variable amounts of pyrophyllite and muscovite, with the majority of the samples having greater than 50% pyrophyllite and muscovite. Samples below 50% pyrophyllite and muscovite include Samples 16, 18 and 19 (all overlying the No. 3 Facies). In thin section, hangingwall samples overlying the No. 1 and the No. 3 Facies were noted to have a greater abundance of chlorite and chloritoid than samples overlying the No. 2 Facies. Lower chloritoid content and higher amounts of chlorite were seen in the hangingwall samples compared to the footwall and reef samples.

The footwall samples had low amounts of chloritoid and chlorite, with higher pyrophyllite and muscovite content in comparison to the hangingwall samples. All the footwall samples, with the exception of Sample 1 (underlying the No. 1 Facies), had noted chloritoid in thin section. The majority of the reef samples had greater than 55% pyrophyllite and muscovite combined, with similar amounts of chloritoid and chlorite. Overall, a higher amount of phyllosilicate material was seen in the footwall samples with lower amounts in both the reef and hangingwall samples.

Figure 3.39 (d) shows a comparison of the Carbon Leader Reef facies types. The No. 1 Facies had less than 20% chloritoid with higher amounts of chlorite. The No. 1 and No. 3 Facies types

had a higher abundance of chloritoid compared to the No. 2 Facies, and the chlorite content is variable.

The petrological observations for the hangingwall, reef and footwall samples revealed mineralogical similarities for all the units across the facies types. Rutile and leucoxene grains were observed in all the hangingwall samples. Grains of zircon (rounded), tourmaline (anhedral to euhedral columnar), pyrrhotite (rounded to angular as well as veinlets in pyrite) and chromite (rounded) were only observed in hangingwall samples overlying the No. 1 and the No. 3 Facies. The highest abundance of pyrite within the hangingwall samples was noted in Sample 4 (overlying the No. 1 Facies). Sample 4 was also noted to be the only hangingwall sample with uraninite and pentlandite present in thin section. Only 2 hangingwall samples, Sample 4 and Sample 9 (overlying the No. 3 Facies), had gold visible in thin section. Hangingwall samples that had a gold grade greater than 1 g/t were noted to overlie the No. 1 or the No. 3 Facies. The gold grades of the underlying reef were also notably high, suggesting there was remobilisation of gold from the reef unit to the hangingwall unit. Fly-speck carbon masses were noted in thin section for 3 hangingwall samples: Samples 1 and 15 (both overlying the No. 1 Facies) and Sample 2 (overlying the No. 2 Facies). Large masses of carbon were also noted in thin section for the reef portions of Samples 1, 2 and 15, suggesting possible remobilisation of carbon from the reef unit to the hangingwall unit.

In all the footwall samples, both leucoxene and rutile occurring together as well as chalcopyrite were noted in thin section. Tourmaline grains, anhedral to euhedral columnar in shape, were noted in Samples 1, 3 and 12 (all underlying the No. 1 Facies) as well as Sample 19 (underlying the No. 3 Facies). Gersdorffite was noted in Samples 1 and $4^{(b)}$ (underlying the No. 1 Facies) and Samples $9^{(b)}$ and 18 (underlying the No. 3 Facies). Pyrrhotite was noted to occur more frequently in footwall samples underlying the No. 3 Facies. The abundance of pyrite in thin section was noted to be on average higher within samples underlying the No. 1 and the No. 3 Facies. Rounded chromite grains were only noted in thin section in Samples 4, $4^{(b)}$ and 7 (all underlying the No. 1 Facies) as well as Sample 18 (underlying the No. 3 Facies). Only 2 footwall samples, Samples 18 and 19 – both underlying a high grade No. 3 Facies, were noted to have gold visible in thin section. Sample 18 was noted to have fly-speck carbon and Sample 19 was noted to have carbon infilling fractures in uraninite. Carbon occurred together with the gold noted in these samples, and the gold grades of the samples were high. Referring to the gold

grades of the footwall samples, it was noted that most of the samples that carried a gold grade of greater than 1 g/t were underlying the No. 1 or the No. 3 Facies, with the exception of Sample 11 that underlies the No. 2 Facies.

Within the majority of the reef samples, across all facies types, rounded grains of zircon, subrounded grains of chalcopyrite, masses of rutile and leucoxene, as well as rounded to angular grains of pyrrhotite were noted in thin section. Columnar tourmaline grains were noted in samples across the facies types however they were noted more in samples from the No. 1 and the No. 3 Facies. Pyrite abundance was noted to be higher on average in samples from the No. 3 Facies. Anhedral to euhedral grains of gersdorffite in the reef samples were noted predominantly in samples from the No. 1 and the No. 3 Facies. Gold was associated with gersdorffite in 3 samples from the No. 1 Facies, and 1 sample from the No. 2 Facies. Gold was occasionally contained within the gersdorffite as an inclusion. Gersdorffite was also noted to occur in fractures alongside pyrite, chalcopyrite, rutile and leucoxene. Rounded chromite grains were noted more frequently in thin section for reef samples from the No. 1 and the No. 3 Facies. Bornite was only noted in Sample 21 (No. 3 Facies) and hematite was noted in Sample 23 (No. 2 Facies) and Sample 25 (No. 3 Facies). Uraninite grains (rounded) occurring with carbon were noted in predominantly samples from the No. 1 and the No. 3 Facies. Fractured uraninite grains and carbon infilling the fractures were also predominantly noted within samples from the No. 1 and No. 3 Facies.

By comparing the gold grade of the samples with the microscopic observations, the greatest gold grades were noted within reef samples with higher pyrophyllite (in comparison to muscovite, chlorite and chloritoid) content – refer to Table 3.8. When noting the various mineral compositions as well as the gold grades for the reef samples, there were a few misalignments in terms of the findings of this research versus the findings of Muller (1991), Fletcher (2009) and Burnett *et al*. (2015). For example, the reef sample with the highest pyrophyllite content was noted to have the highest gold grade (Sample 8 at 311.0 g/t, No. 3 Facies, Peggy estimation domain). The high gold grade of Sample 8 did not align with the intermediate gold grades that are typically found within the Peggy estimation domain however it does align with the facies model.

Table 3.8: Microscopic observations for all reef samples. A red-yellow-green colour scale highlights the varying gold grades (red = high gold grade; yellow = intermediate gold grade; green = low gold grade).

Sample	Sample ID	Unit	Noted Microscopic Observations	Gold grade (g/t)
1	94-94 E1	No. 1 Facies	Pyrophyllite is the dominant alteration mineral, followed by chlorite. Detrital chromite and pyrite grains present. Anhedral to euhedral hydrothermal pyrite grains observed. Carbon nodules present with leucoxene. Rounded grains of zircon within the matrix. Possible pyrophyllitic or sericitic alteration. Gold grade is not aligned to facies model or to TauTona estimation domain.	10.3
2	99-94 E2	No. 2B Facies	Pyrophyllite is the dominant alteration mineral, followed by muscovite. Chromite detected by XRD analysis. Anhedral rutile observed with leucoxene and carbon. Rounded grains of zircon noted within the matrix. Gold grade is not aligned to the TauTona estimation domain. Occurence of carbon is not aligned to the facies model.	41.2
		PPQ	Pyrophyllite is the dominant alteration mineral, followed by muscovite. Anhedral rutile associated with leucoxene. Leucoxene seen along fractures. Euhedral grains of tourmaline noted.	0.5
		No. 2A Facies	Pyrophyllite is the dominant alteration mineral, followed by muscovite. Rounded and anhedral rutile occurring with leucoxene. Carbon occurring in fractures with leucoxene along their periphery. Euhedral grains of tourmaline and rounded grains of zircon noted within the reef. Gold grade is not aligned to the TauTona estimation domain. Occurrence of carbon is not aligned to the facies model.	40.1
3	104-88 W6	No. 1 Facies	Pyrophyllite is the dominant alteration mineral, followed by muscovite. No chlorite present within the sample. Rounded and anhedral rutile occurring with leucoxene. Carbon occurring in fractures with leucoxene. Possible pyrophyllitic alteration.	172.0
4	105-86 E2	No. 1 Facies	Pyrophyllite is the dominant alteration mineral, followed by muscovite. Chromite was detected by XRD. Detrital uraninite. Anhedral rutile occurring with leucoxene. Carbon occurring in fractures.	227.0
5	112-83 W3	No. 1 Facies	Pyrophyllite is the dominant alteration mineral, followed by chlorite. Anhedral rutile occuring with leucoxene. Tourmaline grains noted in the reef. The gold grade is slightly low for a sample from the No. 1 Facies and TauTona estimation domain.	73.6
6	112-83 W4	No. 1 Facies	Pyrophyllite is the dominant alteration mineral, followed by chlorite. Rounded detrital chromite and uraninite. Anhedral rutile occurring together with leucoxene. Leucoxene is mobilised along fractures.	119.0
7	114-78 E1	No. 1 Facies	Pyrophyllite is the dominant alteration mineral, followed by chlorite. Anhedral grains of rutile. Leucoxene and carbon in fractures. Chromite detected by XRD. Low gold grade for a sample from the No. 1 Facies and TauTona estimation domain.	21.1
8	120-55 W4	No. 3 Facies	Pyrophyllite is the dominant alteration mineral, followed by muscovite and chlorite. Highest pyrophyllite in reef samples. Anhedral rutile occurring with leucoxene. Detrital chromite observed. Carbon associated with gold and leucoxene. Possible pyrophyllitic alteration. Very high gold grade for a sample within the No. 3 Facies and the Peggy estimation domain.	311.0
9	120-77 S1	No. 3 Facies	Pyrophyllite is the dominant alteration mineral, followed by chlorite. Anhedral rutile grains and leucoxene observed in fractures, together with carbon. Detrital chromite grains observed. Lower gold grade than expected within the TauTona estimation domain.	80.7
10	96-94 E2	No. 1 Facies	Pyrophyllite and muscovite are the dominant alteration minerals. Detrital uraninite and pyrite grains. Carbon occurring with uraninite and gold along fractures. Tourmaline grains present. Possible pyrophyllitic or sericitic alteration.	284.0
11	100-92 Wze	No. 2A Facies	Low phyllosilicate content. Pyrophyllite is the dominant alteration mineral, followed by chlorite. Rounded detrital uraninite and chromite. Carbon occurring with uraninite and along fractures. Occurrence of carbon and high gold grade is not aligned to the facies model. The mineralogy does not align to the estimation domain model.	128.0
12	104-88 E1A	No. 1 Facies	Muscovite is the dominant alteration mineral, followed by pyrophyllite. No chlorite present. Detrital grains of chromite and uraninite. Anhedral rutile and leucoxene. Mineralogy and gold grade does not align to the TauTona estimation domain. The gold grade also does not align with the typical higher grades noted within the No. 1 Facies.	83.9
13	104-88 W7	No. 1 Facies	Muscovite is the dominant alteration mineral, followed by pyrophyllite and chloritoid. No chlorite present. Detrital grains of chromite and uraninite. Anhedral rutile and leucoxene. Infilling carbon in fractures of uraninite. Possible sericitic alteration. Mineralogy is not aligned to the TauTona estimation domain.	130.0
14	109-87 E2	No. 1 Facies	Muscovite and pyrophyllite are the dominant alteration mineral, followed by chloritoid. No chlorite present. Detrital grains of chromite and uraninite. Anhedral rutile and leucoxene. Tourmaline present. Mineralogy is not aligned to the TauTona estimation domain.	132.0
15	112-84 Rse	IQ	Muscovite is the dominant alteration mineral, followed by pyrophyllite. No chlorite present. Anhedral rutile and leucoxene.	41.1
		No. 1 Facies	Pyrophyllite is the dominant alteration mineral, followed by muscovite. Anhedral rutile grains and leucoxene observed in fractures. Detrital uraninite grains observed. Infilling carbon in veinlets in uraninite. Gold grade does not align to facies or estimation domain model.	79.5
16	120-55 NE7	No. 3 Facies	Muscovite is the dominant alteration mineral, followed by chlorite. Anhedral rutile grains and leucoxene observed in fractures. Detrital uraninite and chromite grains observed. Carbon strongly associated with uraninite. Tourmaline grains present. Lower gold grade than typically noted within the Peggy estimation domain and the No. 3 Facies.	36.0
17	120-55 W5	No. 3 Facies	Muscovite is the dominant alteration mineral, followed by pyrophyllite. Anhedral rutile and leucoxene occurring along a pyrite foreset. Carbon associated with leucoxene. Tourmaline grains present. Lower gold grade than typically noted within the No. 3 Facies and the Peggy estimation domain.	15.4
18	120-55 W7	No. 3 Facies	Low phyllosilicate content. Detrital uraninite and chromite. Anhedral rutile occurring with leucoxene. Possible chloritisation.	173.0
19	120-70 W1	No. 3 Facies	No pyrophyllite in sample. Muscovite is the dominant alteration mineral. Detrital uraninite and chromite. Anhedral rutile occurring with leucoxene. Infilling carbon in uraninite grains. Possible sericitic alteration. Mineralogy is not aligned to the TauTona estimation domain.	141.0
20	DPH 3883	No. 2A Facies	Pyrophyllite and muscovite are the dominant alteration minerals. No chlorite present within sample. Detrital uraninte. Anhedral rutile occurring with leucoxene. Mineralogy does not align with the estimation domain model.	89.7
21	DPH 4057	No. 3 Facies	Pyrophyllite is the dominant alteration mineral, followed by muscovite. No chlorite present. Detrital uraninite. Possible pyrophyllitic alteration.	64.3
22	GBH 1000 D6	No. 2A Facies	Muscovite is the dominant alteration mineral, followed by pyrophyllite. Anhedral grains of rutile occurring with leucoxene.	4.5
23	GBH 2788	No. 2B Facies	Muscovite is the dominant alteration mineral, followed by pyrophyllite and chlorite. Anhedral grains of rutile and leucoxene. Possible sericitic alteration or oxidation.	9.3
24	GBH 3763	No. 1 Facies	Pyrophyllite is the dominant alteration mineral, followed by muscovite.Anhedral grains of rutile and leucoxene. Detrital uraninite. Lower than typical gold grade within the No. 1 Facies and the TauTona estimation domain.	41.0
25	GBH 3844	No. 3 Facies	Muscovite content greater than pyrophyllite content, followed by chloritoid. Anhedral grains of rutile and leucoxene. Detrital uraninite. Grains of tourmaline present. Possible sericitic alteration. Mineralogy and gold grade do not align to the TauTona estimation domain and No. 3 Facies.	31.4
26	GBH 3845	No. 3 Facies	Pyrophyllite content greater than muscovite content., followed by chloritoid. Anhedral grains of rutile and leucoxene. Detrital uraninite. Mineralogy and gold grade do not align to the TauTona estimation domain and No. 3 Facies.	1.6
27	GBH 4003	No. 1 Facies	Pyrophyllite is the dominant alteration mineral, followed by muscovite. Anhedral grains of rutile and leucoxene. Detrital uraninite.	86.8
28	GBH 6000	No. 1 Facies	Muscovite content greater than pyrophyllite content. Detrital uraninite. Mineralogy does not align to the TauTona estimation domain.	80.8
29	GBH 6001	No. 3 Facies	Muscovite content greater than pyrophyllite content. Anhedral grains of rutile and leucoxene. Detrital uraninite. Mineralogy and gold grade do not align to the TauTona estimation domain and the No. 3 Facies.	36.4
30	GBH 6003	No. 1 Facies	Low pyrophyllite content. Anhedral rutile and leucoxene. Detrital uraninite. Sample does not align to the Driefontein estimation domain or the No. 1 Facies.	6.4
31	GBH 6004	No. 2B Facies	Low pyrophyllite content. Anhedral grains of rutile and leucoxene. Possible sericitic, pyrophyllitic or chloritic alteration. Mineralogy does not align with the estimation domain model.	12.8
32	GBH 6014	No. 1 Facies	Muscovite content greater than pyrophyllite content, followed by pyrophyllite and chloritoid. Anhedral grains of rutile and leucoxene. Detrital uraninite. Mineralogy does not align to the TauTona estimation domain. The gold grade is also low for a No. 1 Facies sample.	67.5
33	GBH 6028	No. 1 Facies	Pyrophyllite is the dominant alteration mineral, followed by muscovite. Anhedral grains of rutile and leucoxene. Detrital uraninite. Possible pyrophyllitic alteration. Gold grade does not align to the No. 1 Facies or to the TauTona estimation domain.	0.6
34	GBH 6036	No. 1 Facies	Pyrophyllite is the dominant alteration mineral, followed by muscovite. Anhedral grains of rutile and leucoxene. Detrital uraninite. Gold grade does not align to the No. 1 Facies or to the TauTona estimation domain.	29.6

In another example, Sample 25 (at 31.4 g/t, No. 3 Facies, TauTona estimation domain) had an elevated abundance of sericitic muscovite which does not align to the typical findings of a sample in the south-west area of the TauTona estimation domain. The samples are typically chloritoid-dominant however this was not the case for Sample 25. The gold grade was also lower than the gold grades expected from both the TauTona estimation domain and the No. 3 Facies. Reef samples from the No. 2 Facies were noted to have carbon present in hand specimen and thin section which challenges the facies model. The No. 2 Facies typically has very little carbon however carbon was frequently noted in thin section and in hand specimen. On average it was noted that reef samples from the No. 3 Facies were higher than the reef samples from the No. 1 Facies, which also disagrees with the facies model as the higher gold values are usually noted within samples from the No. 1 Facies. The No. 3 Facies samples were also noted to have a thin carbon seam in hand specimen, further disagreeing with the facies model as fly-speck carbon is more characteristic of the No. 3 Facies. These findings suggest that the estimation domain model as well as the facies model may need to be revised.

The pyrite grains seen in thin section varied in shape. The rounded grains of pyrite as well as uraninite, zircon and chromite are typically associated with detrital origin (Guy *et al*., 2010; Guy *et al*., 2014; Tucker *et al*., 2016). In the instance where the grains are anhedral to euhedral, this is representative of a hydrothermal origin (Guy *et al*., 2010; Guy *et al*., 2014). Throughout the hangingwall, footwall and reef samples the shapes of the grains differ, and it was noted that gold grains are mostly rounded (detrital) unless they are associated with alteration minerals or within veins/along fractures where they appear to be anhedral. In samples from the No. 3 Facies the recrystallisation of pyrite was noted within the matrix as there were overgrowths of pyrite on detrital pyrite grains. Microcrystalline pyrite was observed along fractures cross-cutting quartz clasts (all facies types). Secondary colloform pyrite was noted in Sample 2 from the No. 2 Facies and Sample 18 from the No. 3 Facies.

Rutile and leucoxene were seen occurring together in almost all of the samples (hangingwall, reef and footwall) in thin section. Leucoxene forms as a result of the alteration of rutile (Nesse, 2000, p.368; Tucker *et al*., 2016). Both rutile and leucoxene occurred as anhedral masses in the majority of the samples, suggesting hydrothermal alteration has taken place. Uraninite is commonly seen in the reef samples and is formed as a result of oxidation of iron-bearing minerals (Nesse, 2000, p.370; Tucker *et al*., 2016). The uraninite grains were mostly detrital

which suggests that the oxidation of the iron-bearing minerals possibly took place in the source area and the resultant mineral (i.e. uraninite) was then transported into the Basin.

By comparing the findings from the hangingwall, reef and footwall samples a definite trend can be noted. There are many similarities in the mineralogy of the reef samples from both the No. 1 and the No. 3 Facies and the similarities, particularly with regards to the sulphides, are further noted in the overlying hangingwall samples and the underlying footwall samples. The similarities noted in the hangingwall and footwall samples are most likely due to the contact between the adjacent reef acting as a conduit for post-depositional fluid flow. The post-depositional fluid flow along the contact(s) would allow for the remobilisation of sulphides (and gold) from the reef unit to the overlying hangingwall and underlying footwall units. The alteration assemblages nearer to the contacts would also differ slightly from the mineralogy noted further away from the contacts.

According to Fletcher (2009) and an In-house Report (2004a), the No. 2 and the No. 3 Facies are precursors to the No. 1 Facies. This would imply that there should be similarities for all the facies types however the findings of this research (thus far) suggest that the No. 1 and the No. 3 Facies are more similar in terms of mineralogy and gold grade. The No. 2 Facies was not dissimilar to the No. 1 and the No. 3 Facies however the correlation was not as strong as between the No. 1 and the No. 3 Facies. The presence of a thin basal seam of carbon for the No. 1 and the No. 3 Facies was another similarity that was noted in the samples used for this research, in contradiction to the findings of Depiné *et al.* (2013), Fletcher (2009), Janisch (1986) and Phillips and Law (2000) who all noted the No. 3 Facies to have fly-speck carbon rather than an actual seam.

The mineralogical similarities noted between the No. 1 and the No. 3 Facies samples suggest a similar origin and depositional environment in comparison to the No. 2 Facies. The similarities further suggest that both the No. 1 and the No. 3 Facies have undergone similar alteration due to hydrothermal fluid flow. The alteration similarities were noted in both hand specimen and/or in thin section. Alteration was noted more frequently in samples from the No. 1 and the No. 3 Facies however, it does not necessarily mean that the No. 2 Facies was not altered or exposed to similar post-depositional alteration (i.e. hydrothermal fluid flow).

3.3 GEOCHEMICAL & GOLD ASSAY ANALYSES

Geochemical analyses and gold assaying were necessary to identify geochemical as well as mineralisation trends within the hangingwall, Carbon Leader Reef and footwall, to compare with the findings in the other methodologies used for this research. It should be noted that the borehole and tombstone samples were split vertically in two parts (for geochemical analyses and thin section cutting) and as a result what is noted in one methodology/analysis may not necessarily be observed in the other.

Prior to the commencement of this research, geochemical analyses (including XRF, XRD, ICP-OES, LECO analysis and AAS) as well as gold assaying were carried out by SGS South Africa on 19 tombstones. A total of 61 samples were analysed and the geochemical results as well as the gold assays were made available by AngloGold Ashanti (Appendix 4: Geochemical Analyses and Gold Assay). Of the 61 samples: 20 were footwall samples (including a footwall pebble band for Sample 4); 22 were Carbon Leader Reef samples (including two reef bands and Pale Pebbly Quartzite for Sample 2, and internal quartzite for Sample 15); and 19 were hangingwall samples.

The 15 boreholes that were made available by AngloGold Ashanti for sampling were sent for geochemical analyses at SGS South Africa on commencement of this research. XRF analyses were carried out on a total of 45 samples (footwall, Carbon Leader Reef and hangingwall portions for each borehole). XRD, ICP-OES, LECO analysis, AAS and gold assay were only carried out on the reef portions (15 reef samples). The geochemical analyses could not be carried out for the footwall and hangingwall portions of the boreholes due to a shortage of material to use (refer to Chapter 2.2 with regard to the restrictions in the storage of gold-bearing exploration holes by AngloGold Ashanti). All the geochemical results and gold assays were made available by AngloGold Ashanti (Appendix 4: Geochemical Analyses and Gold Assay). The XRD results are referred to in Chapter 3.2, where they were used to supplement the microscopic findings (and modal abundances) within the polished thin sections.

3.3.1 Geochemical & Gold Assay Results (Hangingwall & Footwall samples)

The gold grades of the hangingwall samples were on average, below 1.4 g/t. Five samples had a higher gold grade than the average: Sample 4 (1.4 g/t) overlying a very high-grade (227.0 g/t)

No. 1 Facies; Sample 9 (3.9 g/t) overlying a high-grade (80.7 g/t) No. 3 Facies; Sample 10 (2.7 g/t) overlying a very high-grade (284.0 g/t) No. 1 Facies; Sample 14 (2.5 g/t) overlying a high-grade (132.0 g/t) No. 1 Facies and Sample 19 (8.0 g/t) overlying a high-grade (141.0 g/t) No. 3 Facies.

There was a strong correlation between gold grade and U_3O_8 (R^2=0.5913), gold grade and U (R^2=0.5896) as well as gold grade and Pb (R^2= 0.4273) within the hangingwall samples (Figure 3.40).

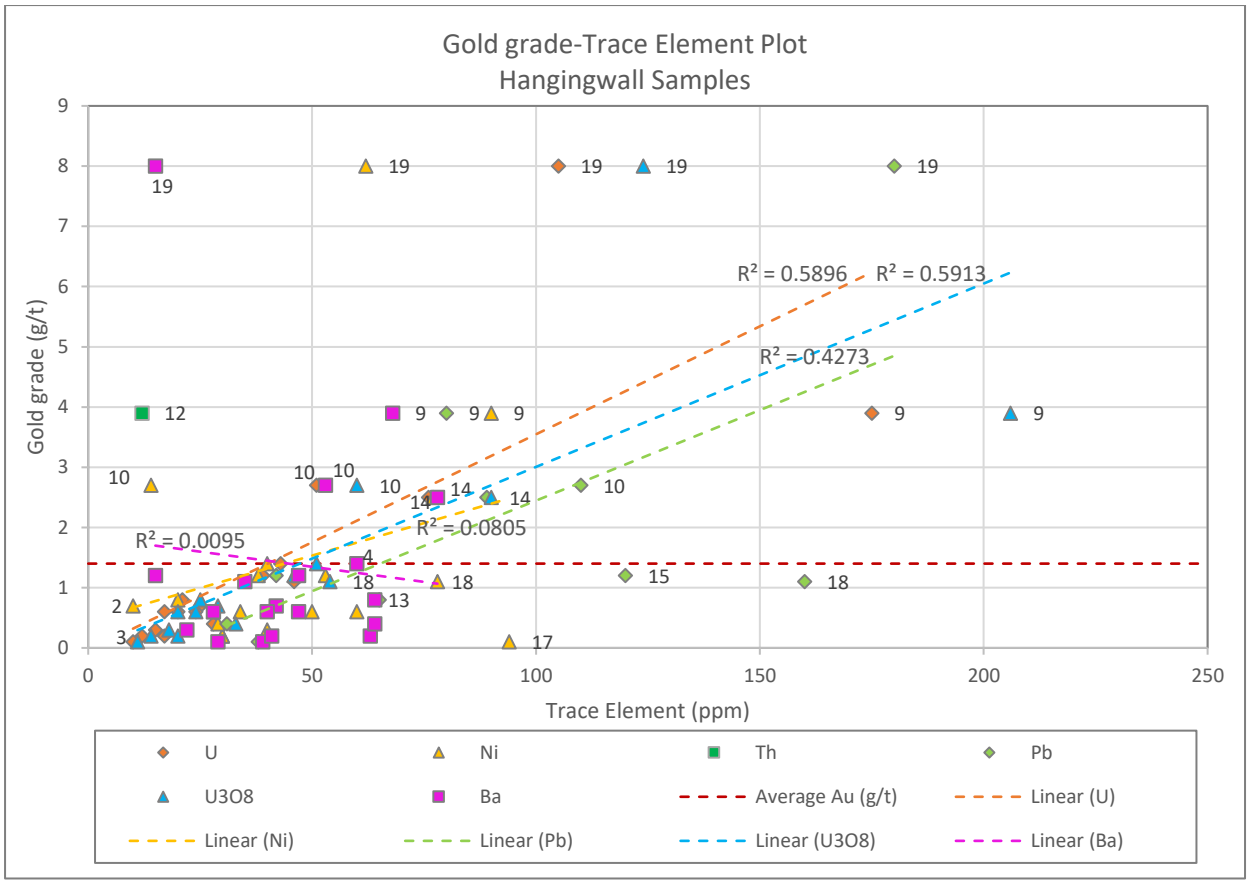

***Figure 3.40**: Gold grade-trace element plot of the hangingwall samples. The strongest correlation noted within in the hangingwall samples was gold grade against U_3O_8, followed by gold grade against U and gold grade against Pb. Hangingwall Samples 1 to 19 are plotted above. The markers are annotated by sample number.*

A small gold grain was seen occurring alongside a detrital pyrite grain hosting pyrrhotite veinlets in (polished) thin section for Sample 9. Samples 10, 14 and 19 had no gold noted in thin section, however it was noted that a detrital gold grain occurred on the rim of a recrystallised pyrite grain in Sample 4. Although a definite trend could not be identified, in most instances the higher gold-grade hangingwall samples were seen to be overlying high to very high-grade Carbon Leader Reef samples, particularly the No. 1 and No. 3 Facies.

A positive correlation occurred between gold grade and Ni concentration (R^2=0.0805). This is likely due to the presence of pyrite (Tucker *et al*., 2016). The concentration for Ba, also associated with the presence of pyrite (Nesse, 2000, p.346) was erratic, with no definite trend when plotted against gold grade (R^2=0.0095). A lower detection limit of 10 ppm was applied for Th and as a result no trend could be identified as the majority of the samples were below the detection limit of 10 ppm. The geochemical and gold assay results used in Figure 3.40 (tombstone hangingwall samples) are listed in Table 3.9.

Table 3.9: The geochemical analyses and gold assay results of hangingwall Samples 1 to 19. The trace elements (ppm) include: U, Ni, Th, Pb, U_3O_8 and Ba. The major oxides (%) include: Fe_2O_3, K_2O, MgO, TiO_2, Al_2O_3, Na_2O. The remaining trace elements and major oxides have been included in Appendix 4: Geochemical Analyses and Gold Assay. The oxides, U, Th and U_3O_8 were determined by XRF. Ni, Pb and Ba were determined by ICP-OES. Gold grade (g/t) was determined by fire assay. Five hangingwall samples were noted to have a higher than average (1.4 g/t) gold grade: Sample 4 (1.4 g/t), Sample 9 (3.9 g/t), 10 (2.7 g/t), 14 (2.5 g/t) and 19 (8.0 g/t). Gold was seen occurring alongside detrital pyrite in thin section for Sample 9. Samples 10, 14 and 19 had no gold noted in thin section, however it was noted that gold occurred alongside a recrystallised pyrite grain in Sample 4. *Below the lower detection limit.

Hangingwall Samples: Geochemical Analyses and Gold Assay														
Sample ID		ppm						%						g/t
		U	*Ni*	*Th*	*Pb*	*U_3O_8*	*Ba*	*Fe_2O_3*	*K_2O*	*MgO*	*TiO_2*	*Al_2O_3*	*Na_2O*	*Au*
Lower Detection Limit		*10*	*10*	*10*	*30*	*10*	*2*	*0.01*	*0.01*	*0.05*	*0.01*	*0.05*	*0.05*	*0.02*
1	94-94 E1	12	30	*	*	14	63	0.74	0.35	0.12	0.13	4.94	0.06	0.7
2	99-94 E2	25	10	*	*	29	42	0.91	0.21	0.15	0.09	5.42	*	0.7
3	104-88 W6	10	*	*	*	11	39	0.86	0.20	0.08	0.08	5.27	*	0.1
4	105-86 E2	43	40	*	*	51	60	0.98	0.35	0.09	0.09	4.80	0.14	1.4
5	112-83 W3	24	60	*	*	28	28	3.22	0.11	0.35	0.06	3.06	*	0.6
6	112-83 W4	15	40	*	*	18	22	2.45	0.09	0.53	0.10	4.78	*	0.3
7	114-78 E1	17	50	*	*	20	47	2.03	0.24	0.35	0.07	5.15	0.08	0.6
8	120-55 W4	17	30	*	*	20	41	1.98	0.22	0.17	0.14	5.20	0.05	0.2
9	120-77 S1	175	90	12	80	206	68	2.68	0.34	0.10	0.15	5.26	0.07	3.9
10	96-94 E2	51	14	*	110	60	53	0.72	0.24	0.05	0.11	5.83	0.07	2.7
11	100-92 Wze	20	34	*	*	24	40	1.25	0.19	0.27	0.08	4.00	*	0.6
12	104-88 E1A	28	29	*	31	33	64	1.90	0.28	0.06	0.07	4.96	0.08	0.4
13	104-88 W7	21	20	*	65	25	64	0.82	0.28	0.05	0.12	5.83	0.11	0.8
14	109-87 E2	76	77	*	89	90	78	1.53	0.36	0.28	0.13	5.41	0.11	2.5
15	112-84 Rse	39	38	*	120	46	47	1.66	0.26	0.46	0.10	4.90	0.14	1.2
16	120-55 NE7	*	53	*	42	*	15	3.96	0.02	0.35	0.15	4.74	*	1.2
17	120-55 W5	*	94	*	38	*	29	2.32	0.12	1.03	0.11	3.94	*	0.1
18	120-55 W7	46	78	*	160	54	35	4.20	0.08	0.98	0.12	4.64	*	1.1
19	120-70 W1	105	62	*	180	124	15	2.61	0.03	0.25	0.08	1.92	*	8.0

The gold grade-oxide plot for the hangingwall samples can be seen in Figure 3.41. The majority of the tombstone hangingwall Fe_2O_3 ranges from 0.72 to 4.20%, with gold grades greater than 1.4 g/t correlating with lower percentages (less than 2%) of Fe_2O_3. Fe_2O_3 indicates the presence of iron-rich minerals, such as magnetite and hematite, which were not seen in thin section for the hangingwall samples however this does not necessarily mean there are not traces of iron-rich minerals within the samples as there were noted pyrite grains.

The borehole hangingwall samples had a higher Fe_2O_3 range from 1.02 to 5.55% (refer to Appendix 4) however could not be compared to gold grade as the gold grade was only determined for the reef samples of the boreholes. The percentage Al_2O_3 ranges from 1.92 to 5.83% for the tombstone hangingwall samples, with higher gold grades correlating with percentages greater than 4.5 g/t. Al_2O_3 is associated with the presence of muscovite (Nesse, 2000, p.366) and pyrophyllite (Nesse, 2000, p.243). Muscovite is present within thin section - it was noted to be sericitic (%K_2O) and occurring in the matrix with very fine grains of pyrophyllite between larger quartz clasts. MgO had no definite correlation when plotted against gold grade (R^2=0.0247). MgO is present in both chlorite (Nesse, 2000, p.251) and chloritoid (Nesse, 2000, p.321), however only chlorite was noted to occur within thin section and macroscopically (possible chloritisation). TiO_2 and Na_2O also had no correlations with gold grade (R^2=0.0027 and R^2=0.0052 respectively). TiO_2 is associated with the presence of rutile and/or leucoxene (Nesse, 2000, p.367). Rounded to subrounded grains of leucoxene and anhedral grains of rutile were noted to occur within all the hangingwall sample thin sections as trace minerals.

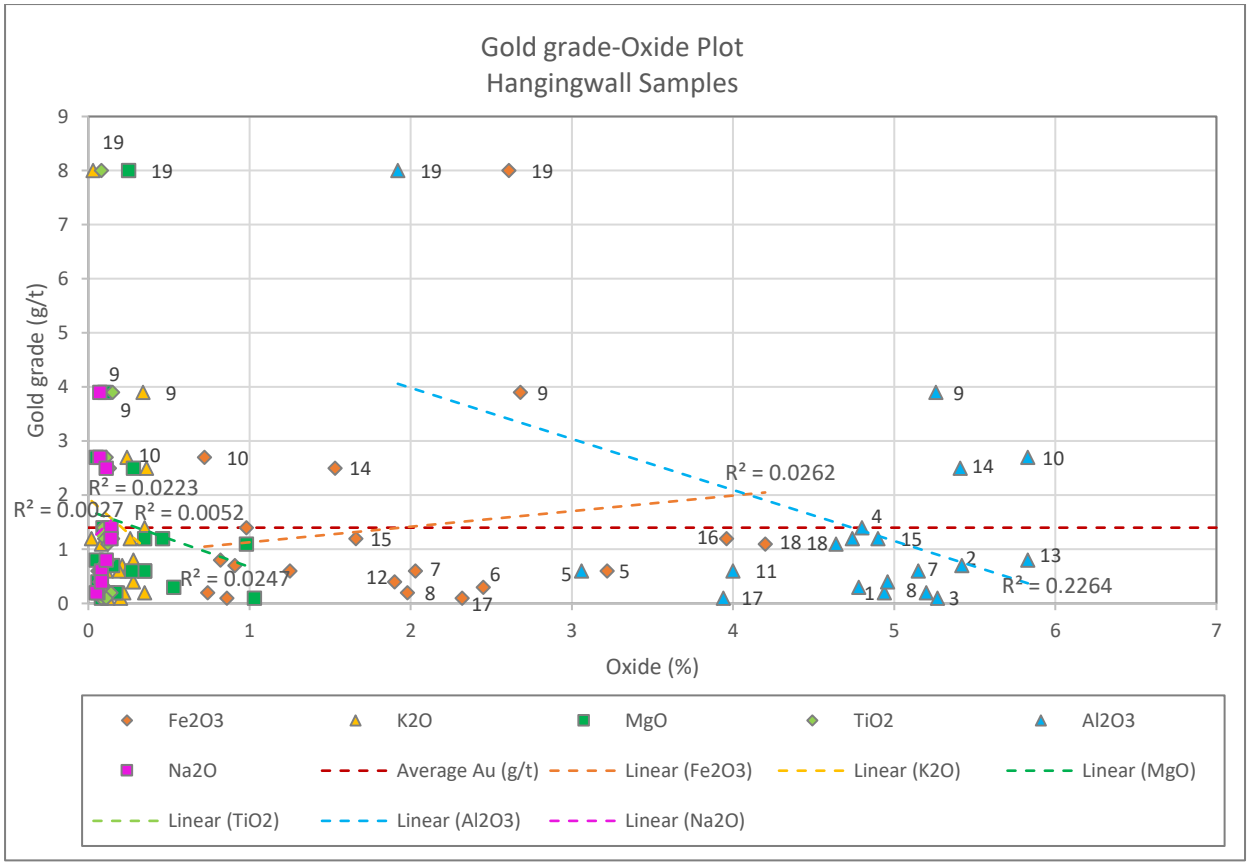

***Figure 3.41**: Gold grade-oxide plot of the hangingwall samples. Hangingwall Samples 1 to 19 are plotted above. The markers are annotated by sample number.*

Gold grades across the footwall samples ranged from 0.1 g/t to 125.0 g/t (or ppm). The gold grades for the footwall were typically less than 3.8 g/t, with the exception of Sample 18 (135.0 g/t) and Sample 19 (26.8 g/t). Samples 18 and 19 were overlain by a very high-grade No. 3 Facies, 173.0 g/t and 141.0 g/t, respectively. Gold was observed in thin section for both Samples 18 and 19.

A detrital grain of gold was seen to be enclosed by gersdorffite in Sample 18. Rutile and leucoxene were seen proximal to secondary gold grains within the same sample. In Sample 19, detrital grains of gold were associated with both carbon masses (fly-speck carbon) and uraninite within the sample thin section. Higher concentrations of U, Pb and U_3O_8 were noted for both these samples in Table 3.10. This was also noted for a footwall pebble band sample occurring within the footwall quartzite, where gold grade was 2.8 g/t (Sample 9) and the surrounding footwall quartzite had a gold grade of 0.5 g/t. The geochemical and gold assay results (tombstone footwall samples) are listed in Table 3.10.

Table 3.10: The geochemical analyses and gold assay results of footwall Samples 1 to 19. The trace elements (ppm) include: U, Ni, Th, Pb, U_3O_8 and Ba. The major oxides (%) include: Fe_2O_3, K_2O, MgO, TiO_2, Al_2O_3, Na_2O. The oxides, U, Th and U_3O_8 were determined by means of XRF. Ni, Pb and Ba were determined by means of ICP-OES. Gold grade (g/t) was determined by fire assay. The remaining trace elements and major oxides have been included in Appendix 4: Geochemical Analyses and Gold Assay. Two footwall samples were noted to have a high-grade gold: Sample 18 (135.0 g/t) and Sample 19 (26.8 g/t). A grain of gold was seen enclosed by gersdorffite in Sample 18 and gold was seen to be associated with both carbon and uraninite in Sample 19. [(a)] Footwall pebble band samples; *Below the lower detection limit.

Footwall Samples: Geochemical Analyses and Gold Assay

Sample ID		ppm						%						g/t
		U	*Ni*	*Th*	*Pb*	*U_3O_8*	*Ba*	*Fe_2O_3*	*K_2O*	*MgO*	*TiO_2*	*Al_2O_3*	*Na_2O*	*Au*
Lower Detection Limit		*10*	*10*	*10*	*30*	*10*	*2*	*0.01*	*0.01*	*0.05*	*0.01*	*0.05*	*0.05*	*0.02*
1	94-94 E1	10	30	*	30	12	127	0.71	0.73	0.08	0.23	8.11	0.14	0.1
2	99-94 E2	14	30	*	30	16	37	0.59	0.19	0.05	0.12	5.67	0.06	0.2
3	104-88 W6	33	40	*	30	39	62	2.30	0.36	0.15	0.24	7.42	*	0.9
4	105-86 E2	10	*	*	30	*	70	0.97	0.40	0.11	0.25	9.46	0.15	0.2
4[(a)]	105-86 E2	47	140	14	30	55	39	3.65	0.13	0.09	0.22	5.41	*	0.5
6	112-83 W4	*	30	*	30	*	48	0.98	0.23	0.1	0.1	5.18	*	0.4
7	114-78 E1	*	50	*	30	10	105	2.43	0.52	0.11	0.21	9.61	0.14	0.9
8	120-55 W4	*	30	*	30	*	32	1.94	0.16	0.18	0.15	5.98	*	0.5
9	120-77 S1	*	60	*	30	*	114	3.45	0.52	0.22	0.4	10.7	0.12	0.5
9[(a)]	120-77 S1	222	110	35	110	262	109	4.54	0.44	0.17	0.4	8.47	*	2.8
10	96-94 E2	12	20	*	43	14	150	1.82	0.64	0.14	0.36	15.8	0.15	1.3
11	100-92 Wze	19	89	*	43	22	56	3.94	0.02	0.37	0.08	4.61	*	1.1
12	104-88 E1A	100	26	*	83	118	49	0.72	0.21	0.07	0.09	4.77	*	3.8
13	104-88 W7	13	29	*	68	15	76	0.94	0.33	0.09	0.18	6.46	0.05	0.5
14	109-87 E2	*	13	*	30	*	95	1.00	0.36	0.10	0.13	6.98	0.08	0.6
15	112-84 Rse	27	31	*	76	32	69	1.27	0.34	0.07	0.11	4.16	0.08	2.1
16	120-55 NE7	*	22	*	97	*	96	1.10	0.52	0.16	0.10	5.63	0.14	0.1
17	120-55 W5	14	17	*	120	17	95	1.95	0.53	0.18	0.16	8.02	0.09	0.9
18	120-55 W7	133	49	13	140	157	95	1.32	0.49	0.09	0.18	5.77	0.06	135
19	120-70 W1	254	54	16	200	300	69	1.32	0.38	0.06	0.07	2.65	0.06	26.8

Both Sample 18 and Sample 19 plot significantly higher than the other footwall samples (Figure 3.42). To determine the correlation between the trace elements and gold grade it was necessary to remove the extreme outliers (i.e. Samples 18 and 19) to prevent the skewing of the data (Figure 3.43).

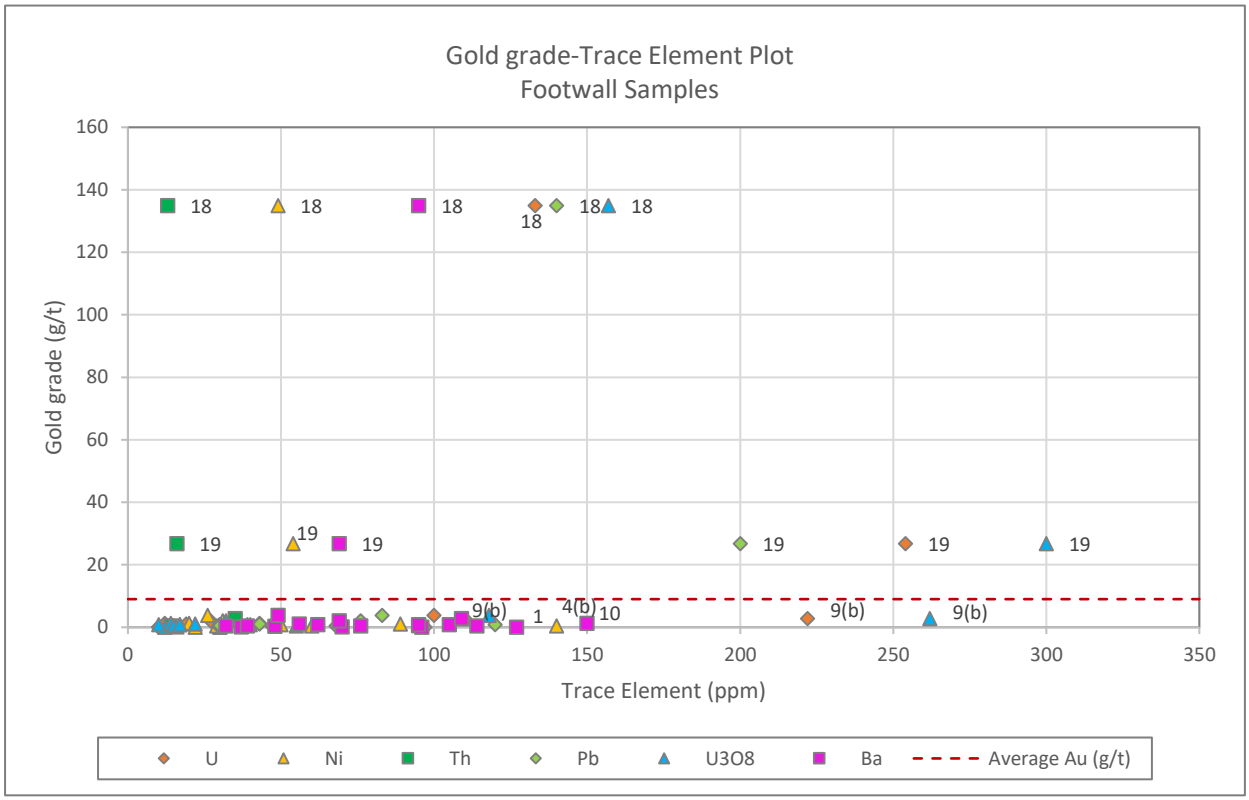

***Figure 3.42**: Gold grade-trace element plot of the footwall samples, inclusive of the extreme outlying gold grades for Samples 18 and 19. The markers are annotated by sample number.*

From the removal of the outliers, a very strong correlation was noted between Th and gold grade (R^2=1). A strong correlation between gold grade and U_3O_8 (R^2=0.4837) as well as gold grade and U (R^2=0.4924) was also noted, even with the exclusion of the only two samples with gold grains seen in thin section. Less of a correlation was noted for gold grade and Pb (R^2=0.2641), which may indicate the presence of galena however there were no grains found within the footwall samples. Gold grade and Ni had no correlation (R^2=0.018), which corresponds to the fewer observations of pyrite and a presence of subrounded gersdorffite grains in the footwall samples (in comparison to the reef samples).

No correlation was noted between gold grade and Ba (R^2=0.00002), typically associated with galena and pyrite (Nesse, 2000, p.346). As there were no microscopic observations of galena

and fewer observations of pyrite in the footwall samples (in comparison to the reef samples), it was expected that the Ba concentration was lower.

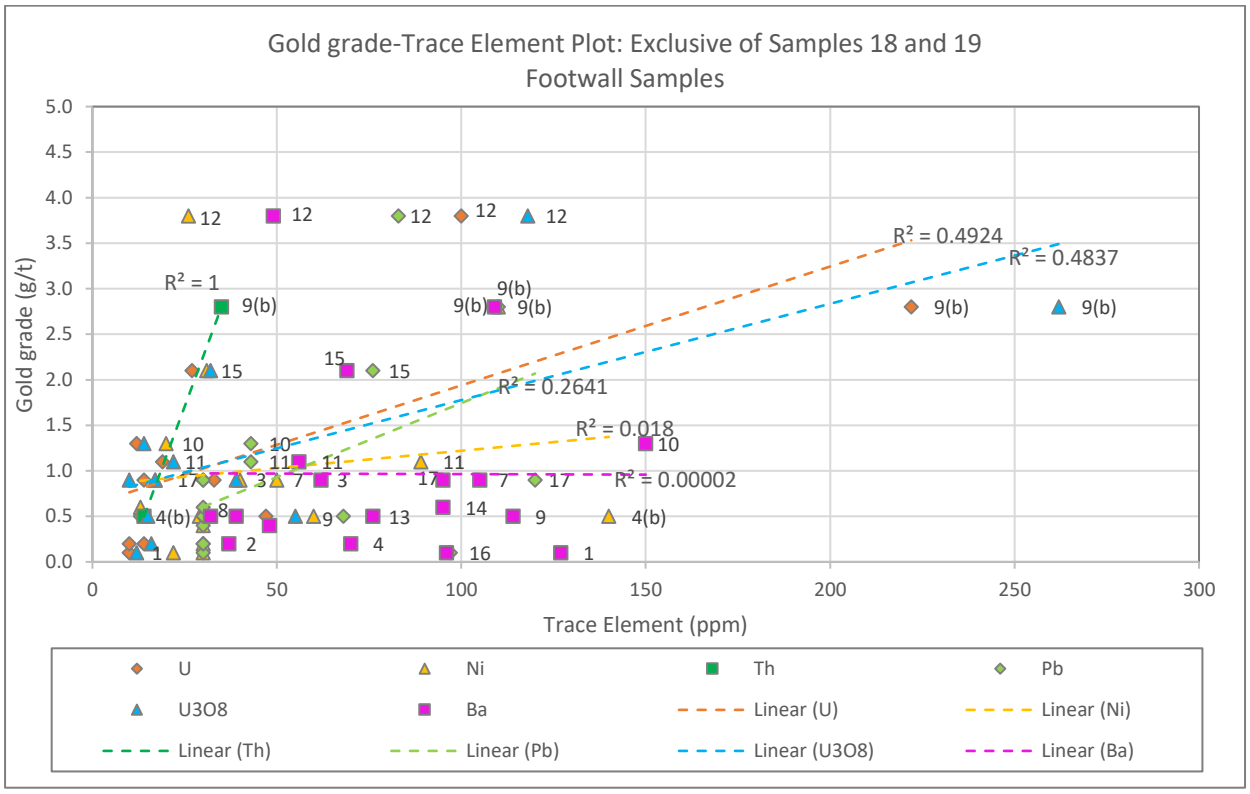

***Figure 3.43**: Gold grade-trace element plot, exclusive of the extreme outlying gold grades. The strongest correlation noted within in the footwall samples is gold grade against Th, followed by gold grade against U and gold grade against U_3O_8. Footwall Samples 1 to 19 are plotted above. The markers are annotated by sample number.*

When comparing the hangingwall and footwall samples, the strongest correlations were noted between gold grade and U_3O_8 (hangingwall), and gold grade and Th (footwall), followed by gold grade and U for both the hangingwall and footwall. This suggests that higher radioactive element concentrations may be accompanied by higher gold grade in both the hangingwall and footwall quartzites.

Figure 3.44 (a) shows a gold grade-oxide plot of the footwall samples, inclusive of the extreme outlying gold grades for Samples 18 and 19. Figure 3.44 (b) excludes the outliers of the footwall samples. For $\%Al_2O_3$ the majority of the footwall samples (exclusive of Samples 18 and 19) lie within the range of 4.16 to 10.70%, with lower gold grades (less than 1 g/t). Sample 18 had an Al_2O_3 percentage of 5.77% and Sample 19 had an Al_2O_3 percentage of 2.65%. Sample 10 had a noticeably higher Al_2O_3 at 15.80%, with a low gold grade of 1.3 g/t. This is depicted more clearly in Figure 3.44 (b).

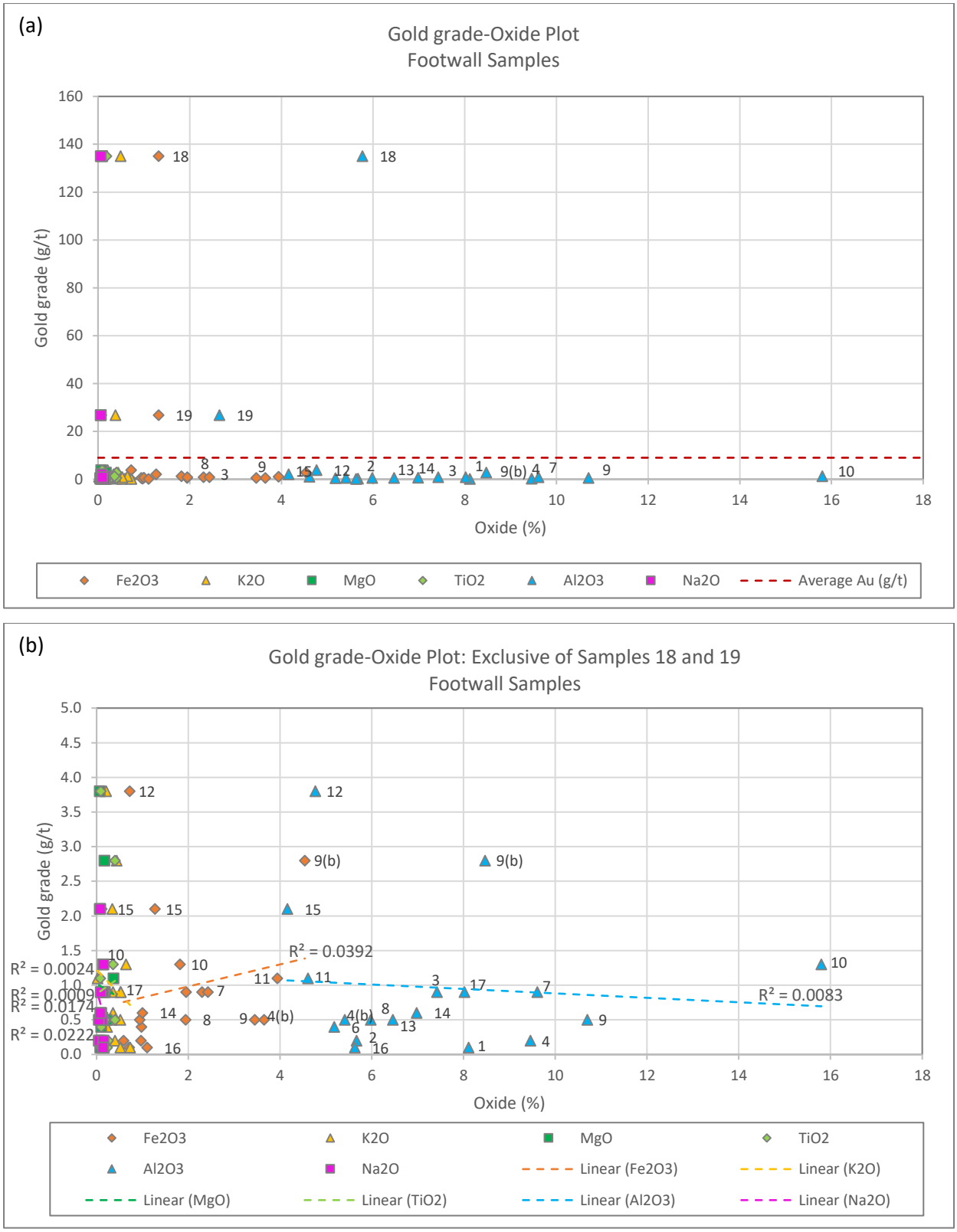

***Figure 3.44**: (a) Gold grade-oxide plot of the footwall samples. Correlations are not immediately noted between gold grade and the major oxides as the very high-grade Samples 18 and 19 are skewing the data; (b) Gold grade-oxide plot of the footwall samples, exclusive of the extreme outlying gold grades. Footwall Samples 1 to 17 are plotted above. The markers are annotated by sample number.*

It should be noted that the samples with higher Al_2O_3 concentration were overlain by predominantly the No. 1 Facies, followed samples overlain by the No. 3 Facies. The correlation of Al_2O_3 with gold grade within the footwall (exclusive of Samples 18 and 19) was non-existent at R^2=0.0083. Inclusive of the outlying samples, R^2=0.0302, which remains as no correlation between Al_2O_3 and gold grade. A large concentration of pyrophyllite and sericitic muscovite was noted in thin section, and this was confirmed by the geochemical data.

The MgO within most of the footwall samples was seen to fall between 0.05 and 0.37%, with no relationship to the gold grade (R^2=0.009). No chloritoid was seen within thin section for the footwall samples, however chlorite grains were noted to occur microscopically. For TiO_2 the footwall samples lie within the range 0.08 to 0.4%, with no relationship to the gold grade (R^2=0.0024). Rutile and leucoxene were found to occur as trace elements in thin section and were seen to be associated with detrital gold grains in Samples 18 and 19. Although a slightly better correlation was noted with K_2O (sericitic muscovite) and gold grade (R^2=0.0174) in comparison to MgO and TiO_2, the relationship between these oxides and gold grade is non-existent.

The "strongest" correlation seen between the oxides and gold grade within the footwall samples was seen between Fe_2O_3 and gold grade, where R^2=0.0392 (exclusive of Samples 18 and 19). This is likely due to the presence of iron-rich sulphides within the footwall samples, such as pyrite, that have undergone oxidation. The correlation between Fe_2O_3 and gold grade decreases to R^2=0.0139 with the inclusion of Samples 18 and 19, suggesting lower amounts of iron-rich sulphides are present within the samples with higher gold grade. Euhedral and detrital pyrite grains were noted to occur along foresets and in fractures within the footwall, as well as disseminated throughout the sample. Pyrite occurred in greater abundances than the other sulphides in thin section, suggesting the %Fe_2O_3 may be representative of the pyrite within the footwall samples.

3.3.2 Geochemical & Gold Assay Results (Carbon Leader Reef samples)

A total of 22 Carbon Leader Reef tombstone samples (including two reef bands and Pale Pebbly Quartzite for Sample 2, and internal quartzite for Sample 15) as well as 15 Carbon Leader Reef borehole samples were geochemically analysed (XRF, XRD, ICP-OES, LECO analysis and AAS) and

assayed for gold grade. As previously mentioned, the XRD results are referred to in Chapter 3.2. The XRD results have been included in the overall discussion (Chapter 3.3.3) for this chapter.

The reef samples have been separated by facies type however all of the samples have very similar outcomes in terms of their geochemical composition. Higher overall gold grades were observed in the No. 3 Facies, with medium to high gold grades observed in the No. 1 Facies, and medium to low gold grades seen in the No. 2 Facies (Figure 3.45). The highest gold grade was noted to occur within Sample 8 (311.0 g/t) and lies within the No. 3 Facies. The highest concentration of U was noted within Sample 13 (5746 ppm) and lies within the No. 1 Facies.

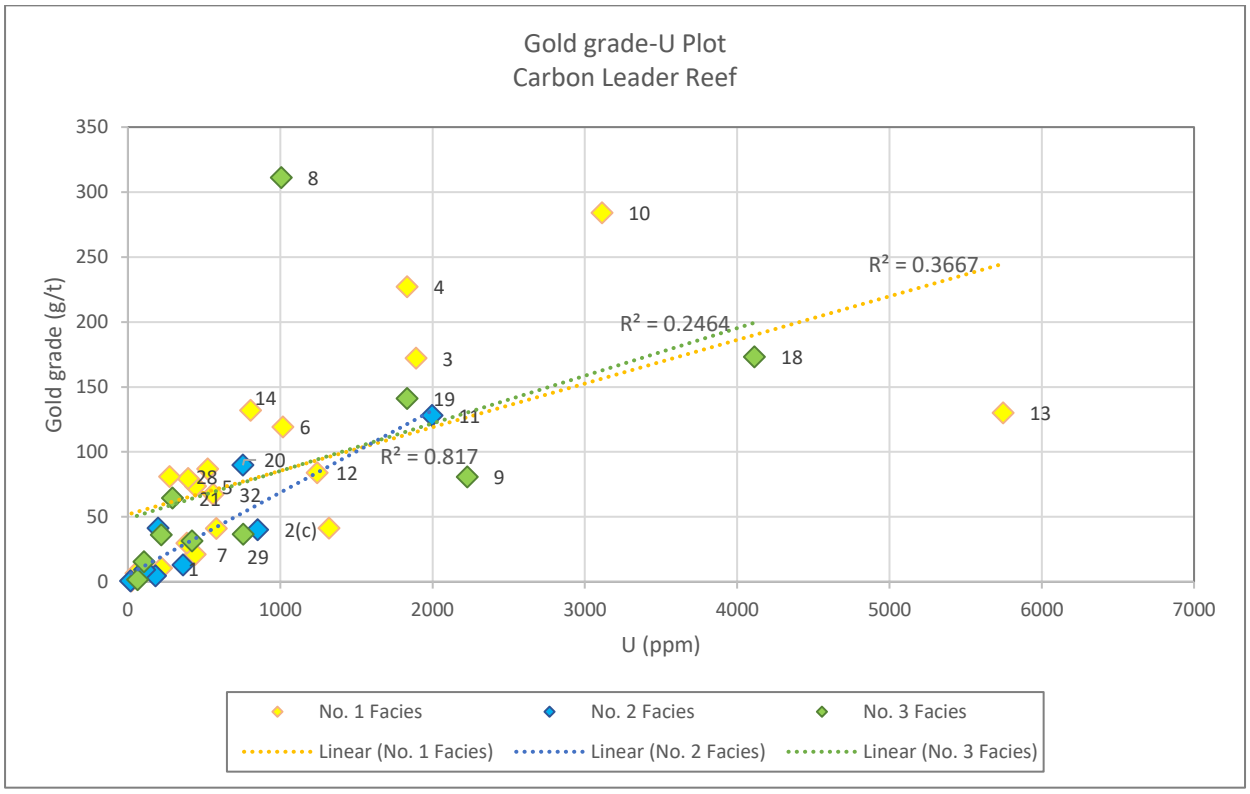

***Figure 3.45**: Gold grade-U plot of the Carbon Leader Reef (tombstone and borehole) samples. The highest gold grade was noted to occur within Sample 8 (311.0 g/t) and lies within the No. 3 Facies. The highest concentration of uranium was noted within Sample 13 (5746 ppm) and lies within the No. 1 Facies. The markers are annotated by sample number.*

The No. 2 Facies was noted to have the strongest correlation between gold grade and U (R^2=0.8170). The No. 1 Facies had the second strongest correlation between gold grade and U (R^2=0.3667), followed by the No. 3 Facies (R^2=0.2462).

The geochemical analyses of the trace elements and gold assay results for all the Carbon Leader Reef (tombstone and borehole) samples are listed in Table 3.11.

Table 3.11: The geochemical analyses for trace elements and gold assay results of all the Carbon Leader Reef (tombstone and borehole) samples. Ag was determined by means of AAS. Total Sulphur and Carbon were determined by LECO Carbon and Sulphur Analysis. U, U_3O_8 and Th were determined by means of XRF and the remaining trace elements As, Ba, Co, Cu, Ni, Pb and Zn were determined by ICP-OES. Gold grade (g/t) was determined by fire assay. [a] Total Sulphur/Carbon; [b] Pale Pebbly Quartzite (PPQ) for Sample 2; [c] No. 2B Facies for Sample 2; [d] Internal Quartzite (IQ) for Sample 15; [e] 0.01% for Samples 1 to 19; 0.05% for Samples 20 to 34; [f] 10 ppm for Samples 1 to 19; 8 ppm for Samples 20 to 34; [g] 50 ppm for Samples 1 to 19; 30 ppm for Samples 20 to 34; [h] 2 ppm for Samples 1 to 19; 10 ppm for Samples 20 to 24; [i] 30 ppm for Samples 1 to 19; 20 ppm for Samples 20 to 34; I/S: Insufficient Sample; N/D: Not Determined; *Below the lower detection limit.

Carbon Leader Reef Samples: Geochemical Analyses and Gold Assay

Sample ID		Unit	%		ppm											g/t
			S[a]	*C[a]*	*Ag*	*U*	*U_3O_8*	*Th*	*As*	*Ba*	*Co*	*Cu*	*Ni*	*Pb*	*Zn*	*Au*
Lower Detection Limit			*0.01*	*0.01[e]*	*1*	*10[f]*	*10*	*10*	*50[g]*	*2[h]*	*10*	*10*	*10*	*30[i]*	*10*	*0.02*
1	94-94 E1	No. 1 Facies	3.16	*	2	220	259	22	270	79	90	20	140	70	20	10.3
2	99-94 E2	No. 2A Facies	2.78	*	7	198	234	21	180	41	70	40	90	70	20	41.2
2[b]	99-94 E2	PPQ	1.30	*	*	18	21	*	50	44	30	10	40	*	20	0.5
2[c]	99-94 E2	No. 2B Facies	0.70	*	9	852	1005	55	50	58	20	*	40	230	20	40.1
3	104-88 W6	No. 1 Facies	1.82	0.03	36	1891	2230	127	80	105	60	10	130	720	20	172.0
4	105-86 E2	No. 1 Facies	0.94	0.15	19	1833	2162	125	470	114	90	*	280	780	20	227.0
5	112-83 W3	No. 1 Facies	0.30	*	11	444	523	29	*	69	20	*	50	150	*	73.6
6	112-83 W4	No. 1 Facies	0.93	*	15	1018	1201	71	60	60	30	10	80	460	20	119.0
7	114-78 E1	No. 1 Facies	0.64	*	2	441	520	30	*	60	20	10	70	110	10	21.1
8	120-55 W4	No. 3 Facies	3.62	*	49	1007	1188	72	220	173	90	20	130	410	20	311.0
9	120-77 S1	No. 3 Facies	1.41	0.01	9	2228	2627	155	140	124	70	20	210	860	*	80.7
10	96-94 E2	No. 1 Facies	3.61	0.11	37	3113	3671	221	*	150	260	17	730	1400	28	284.0
11	100-92 Wze	No. 2A Facies	2.10	0.04	18	1997	2355	137	*	47	120	100	240	850	26	128.0
12	104-88 E1A	No. 1 Facies	1.16	*	11	1242	1465	83	*	85	54	16	150	530	12	83.9
13	104-88 W7	No. 1 Facies	4.70	0.21	59	5746	6776	387	*	150	210	30	570	2200	43	130.0
14	109-87 E2	No. 1 Facies	1.11	0.04	15	806	950	51	*	87	30	11	36	300	16	132.0
15	112-84 Rse	No. 1 Facies	0.60	0.02	12	1320	1557	87	*	65	31	24	43	430	18	79.5
15[d]	112-84 Rse	IQ	1.14	0.04	5	396	467	26	*	86	44	10	46	200	60	41.1
16	120-55 NE7	No. 3 Facies	2.09	0.02	5	219	258	22	*	52	73	12	120	170	24	36.0
17	120-55 W5	No. 3 Facies	0.29	*	3	106	125	*	*	57	31	*	40	96	22	15.4
18	120-55 W7	No. 3 Facies	4.31	0.10	37	4114	4851	282	*	52	180	230	130	1700	42	173.0
19	120-70 W1	No. 3 Facies	2.35	0.03	23	1832	2160	128	*	30	93	33	160	970	18	141.0

Table 3.11 - continued: The geochemical analyses for trace elements and gold assay results of all the Carbon Leader Reef (tombstone and borehole) samples. Ag was determined by means of AAS. Total Sulphur and Carbon were determined by LECO Carbon and Sulphur Analysis. U, U_3O_8 and Th were determined by means of XRF and the remaining trace elements As, Ba, Co, Cu, Ni, Pb and Zn were determined by ICP-OES. Gold grade (g/t) was determined by fire assay. [(a)] Total Sulphur/Carbon; [(b)] Pale Pebbly Quartzite (PPQ) for Sample 2; [(c)] No. 2B Facies for Sample 2; [(d)] Internal Quartzite (IQ) for Sample 15; [(e)] 0.01% for Samples 1 to 19; 0.05% for Samples 20 to 34; [(f)] 10 ppm for Samples 1 to 19; 8 ppm for Samples 20 to 34; [(g)] 50 ppm for Samples 1 to 19; 30 ppm for Samples 20 to 34; [(h)] 2 ppm for Samples 1 to 19; 10 ppm for Samples 20 to 24; [(i)] 30 ppm for Samples 1 to 19; 20 ppm for Samples 20 to 34; I/S: Insufficient Sample; N/D: Not Determined; *Below the lower detection limit.

Carbon Leader Reef Samples: Geochemical Analyses and Gold Assay

Sample ID		Unit	%		ppm											g/t
			S[(a)]	*C[(a)]*	*Ag*	*U*	*U_3O_8*	*Th*	*As*	*Ba*	*Co*	*Cu*	*Ni*	*Pb*	*Zn*	*Au*
Lower Detection Limit			*0.01*	*0.01[(e)]*	*1*	*10[(f)]*	*10*	*10*	*50[(g)]*	*2[(h)]*	*10*	*10*	*10*	*30[(i)]*	*10*	*0.02*
20	DPH 3883	No. 2A Facies	0.40	*	I/S	755	N/D	N/D	60	50	30	140	370	290	I/S	89.7
21	DPH 4057	No. 3 Facies	0.93	*	7	293	N/D	N/D	100	80	40	40	90	220	*	64.3
22	GBH 1000 D6	No. 2A Facies	1.23	*	*	180	N/D	N/D	60	50	40	50	60	110	*	4.5
23	GBH 2788	No. 2B Facies	0.97	*	*	109	N/D	N/D	210	70	40	50	40	100	10	9.3
24	GBH 3763	No. 1 Facies	0.18	*	5	581	N/D	N/D	70	70	20	60	380	310	20	41.0
25	GBH 3844	No. 3 Facies	1.73	*	3	421	N/D	N/D	40	30	60	40	70	230	20	31.4
26	GBH 3845	No. 3 Facies	0.86	*	*	63	N/D	N/D	60	30	20	50	30	90	20	1.6
27	GBH 4003	No. 1 Facies	0.64	*	8	524	N/D	N/D	110	70	40	50	70	260	*	86.8
28	GBH 6000	No. 1 Facies	0.77	*	I/S	273	N/D	N/D	*	60	20	40	20	110	I/S	80.8
29	GBH 6001	No. 3 Facies	1.52	*	4	756	N/D	N/D	*	80	20	120	130	340	20	36.4
30	GBH 6003	No. 1 Facies	0.58	*	*	53	N/D	N/D	50	40	10	130	70	50	20	6.4
31	GBH 6004	No. 2B Facies	1.66	*	2	361	N/D	N/D	50	40	40	70	80	190	*	12.8
32	GBH 6014	No.1 Facies	0.45	*	I/S	559	N/D	N/D	*	60	10	30	40	240	*	67.5
33	GBH 6028	No. 1 Facies	0.30	0.11	I/S	23	N/D	N/D	90	50	20	40	40	50	I/S	0.6
34	GBH 6036	No. 1 Facies	1.56	*	4	386	N/D	N/D	150	30	60	80	90	220	10	29.6

In terms of relationships between gold grade and trace element concentration it was noted, as with the hangingwall and footwall samples, that gold grade and radioactive elements correlate well, particularly gold grade and U (Figure 3.45 and Figure 3.46). The higher gold grades correspond to higher U concentrations, with favourable gold grades observed mostly in the No. 1 and No. 3 Facies.

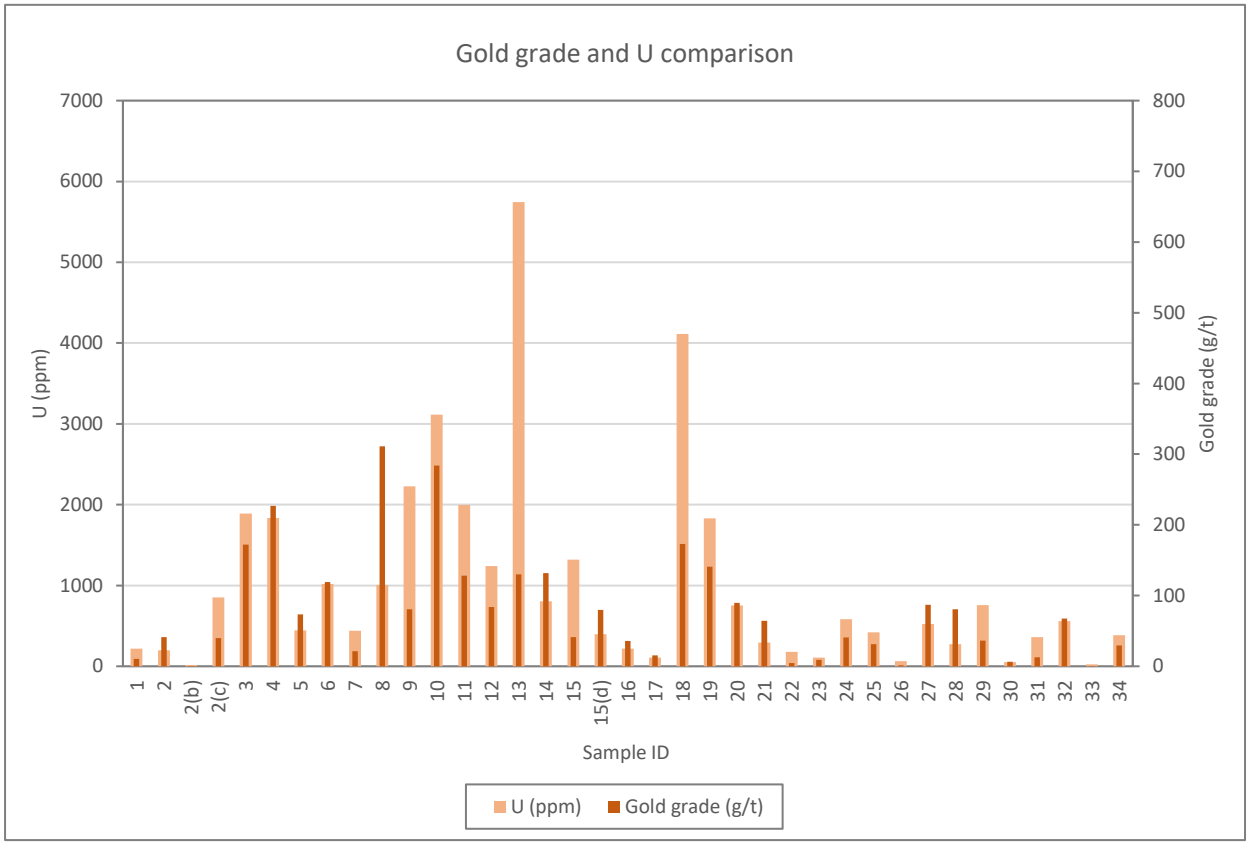

***Figure 3.46**: Gold grade (g/t) and U (ppm) comparison for all the Carbon Leader Reef tombstone and boreholes samples. The higher gold grades correspond to higher U concentrations, with favourable gold grades seen predominantly in the No. 1 and No. 3 Facies.*

From the geochemical data the highest average concentration of U was seen in the No. 3 Facies (average of 1104 ppm), followed by the No. 1 Facies (average of 1098 ppm). Although the No. 2 Facies had a higher correlation between gold grade and U, the lowest average concentration of U was seen (average of 559 ppm). This was similarly noted when plotting gold grade against U + Th, and against uraninite (U_3O_8) in Figure 3.47 (a) and (b), respectively. The No. 2 Facies was noted to have the strongest correlation between gold grade and U + Th (R^2=0.9038), followed by the No. 1 Facies (R^2=0.2622) and the No. 3 Facies (R^2=0.1126). The highest average concentration of U + Th was seen in the No. 3 Facies (average of 1694 ppm), followed by the No. 1 Facies (average of 1644 ppm).

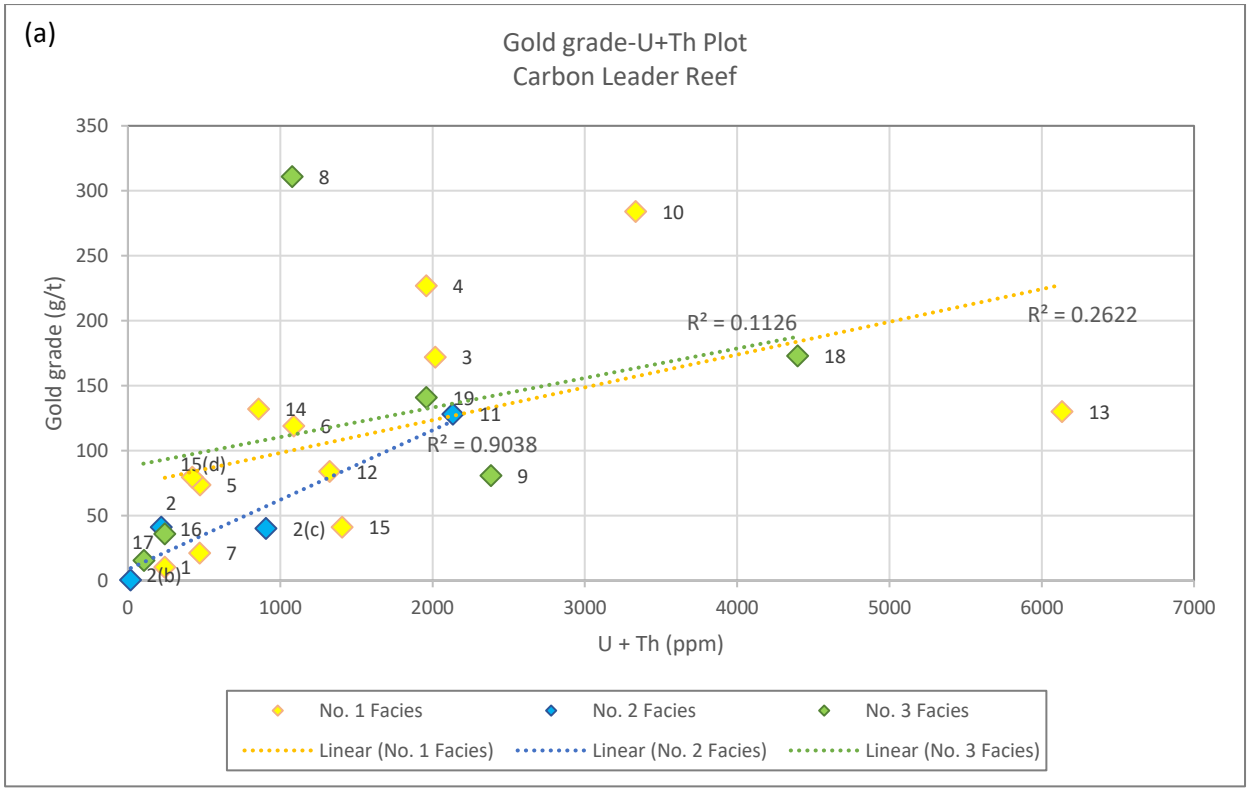

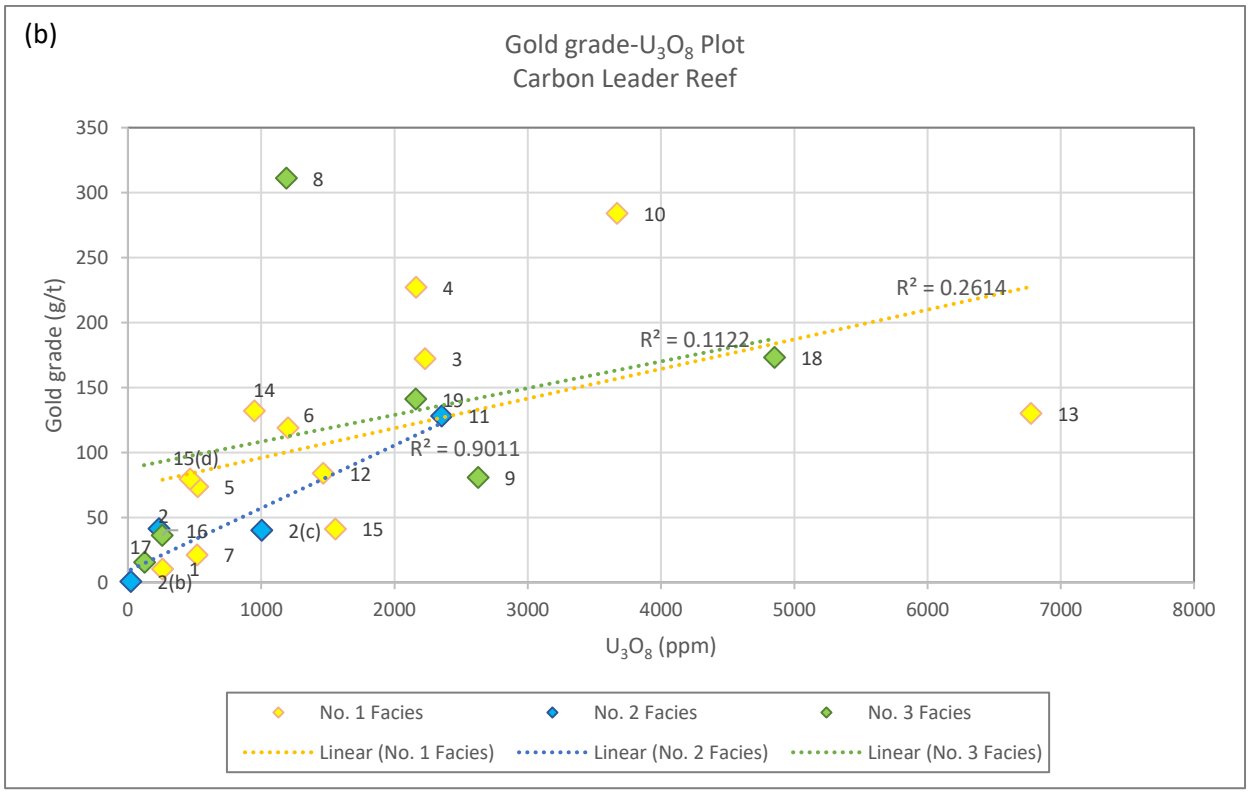

***Figure 3.47**: (a) Gold grade (g/t) and U + Th (ppm) plot of the Carbon Leader Reef (tombstone) samples. The strongest correlation between gold grade and U + Th was seen in the No. 2 Facies (R^2=0.9038); (b) Gold grade (g/t) and U_3O_8 (ppm) plot of the Carbon Leader Reef (tombstone) samples. The strongest correlation between gold grade and U_3O_8 was seen in the No. 2 Facies (R^2= 0.9011). The markers are annotated by sample number.*

The No. 2 Facies had the lowest average concentration of U + Th (average of 820 ppm) despite having the strongest correlation with gold grade. In Figure 3.47 (b), the correlation between gold grade and U_3O_8 was strongest for the No. 2 Facies (R^2=0.9011), with the second strongest correlation seen for the No. 1 Facies (R^2=0.2614) followed by the No. 3 Facies (R^2=0.1122). The highest average concentration of U_3O_8 was noted within the No. 3 Facies (average of 1868 ppm), followed by the No. 1 Facies (average of 1815 ppm) and the No. 2 Facies (average of 904 ppm). This was confirmed in thin section by the presence of detrital uraninite grains associated with gold grains in most of the No. 1 Facies samples, followed by the No. 3 Facies. Uraninite grains were less common in the No. 2 Facies and were noted to occur as detrital grains and associated with detrital gold grains in Samples 2, 11 and 20.

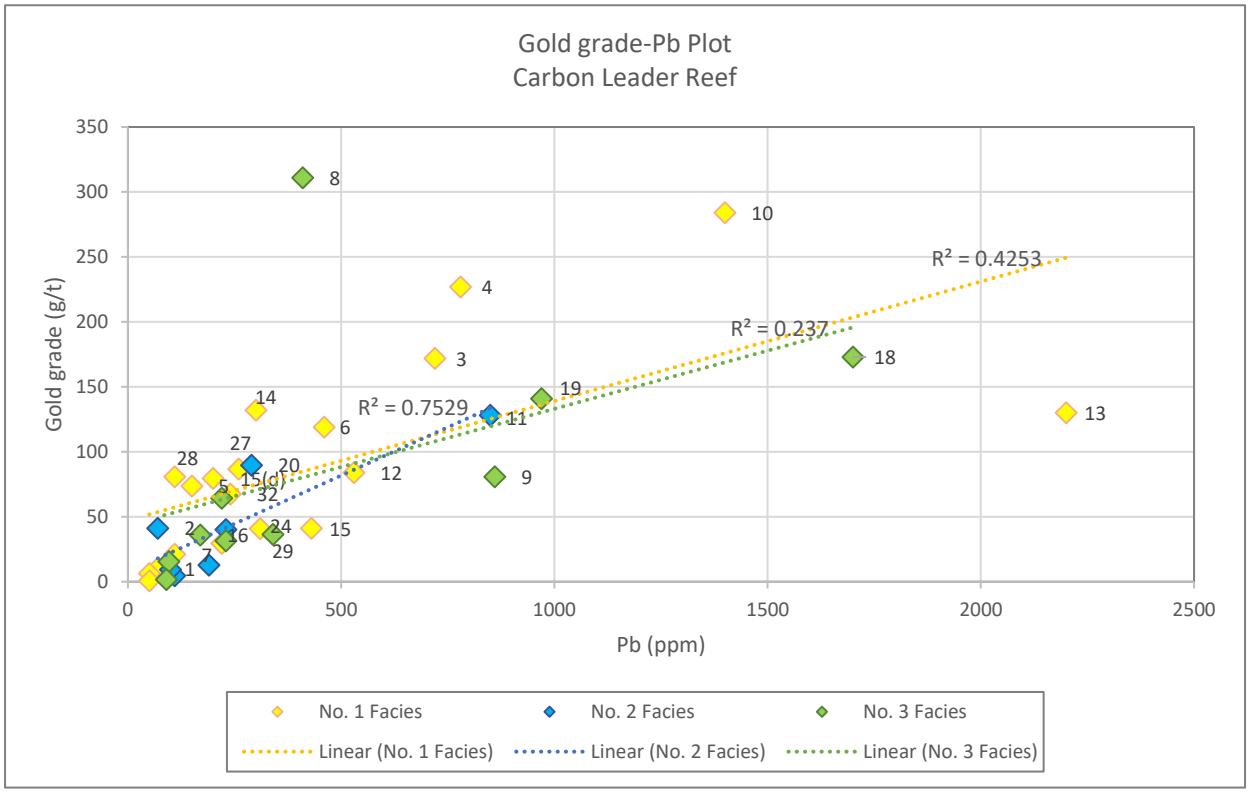

***Figure 3.48**: Gold grade (g/t) and Pb (ppm) plot of the Carbon Leader Reef (tombstone and borehole) samples. The strongest correlation between gold grade and Pb was noted within the No. 2 Facies (R^2=0.7529). The markers are annotated by sample number.*

Figure 3.48 shows a plot of gold grade versus Pb. The No. 2 Facies had the strongest correlation (R^2=0.7529), followed by the No. 1 Facies (R^2=0.4253) and No. 3 Facies (R^2=0.2370). The highest average concentration of Pb was noted within the No. 3 Facies (average of 509 ppm). The No. 1 Facies follows with an average of 452 ppm Pb, and the No. 2 Facies has the lowest average of 263 ppm Pb. Pb is associated with the decay of (radioactive) uranium and is typically present in

thin section as small grains of galena (Tucker *et al*., 2016). No galena was noted in thin section of the reef samples used within this study. As previously mentioned, the borehole and tombstone samples were split vertically in two parts (for geochemical analyses and thin section cutting) and as a result what is noted in one methodology/analysis may not necessarily be observed in the other. This may be the reason as to why Pb was determined geochemically and not microscopically.

The geochemical observations noted for all the radioactive trace elements were similar, with the No. 2 Facies having the strongest correlations against gold grade however the gold grades and concentrations of the radioactive trace elements were the lowest, on average. The No. 3 Facies radioactive trace elements were noted to have the weakest correlation against gold grade however the gold grades and concentrations of the radioactive trace elements were the highest, on average.

The gold grades and the corresponding radioactive trace element concentrations from the geochemical data disagrees to an extent with the Carbon Leader Reef facies model. The facies model proposes the highest gold grades are found within the No. 1 Facies (characterised by a thin hydrocarbon seam at its base), and that the No. 3 Facies (characterised by fly-speck carbon) hosts high and persistent gold grades, but less so than the No. 1 Facies. The geochemical data (in this study) shows the opposite is true, where the No. 3 Facies had the higher gold grades, followed by the No. 1 Facies. The geochemical data, however, does agree that the No. 2 Facies hosts lower grade than the No. 1 and No. 3 Facies. The higher gold grades and U/U_3O_8 concentrations were noted to occur within the reef bands that have carbon present. This is because of a gold-hydrocarbon-uranium relationship commonly recognised within the Witwatersrand Basin (Agangi *et al*., 2015; Depiné *et al.*, 2013; Drennan and Robb, 2006; Phillips and Powell, 2015).

From the geochemical data it can be noted that the strongest correlations between gold grade and the radioactive trace elements occur within the No. 2 Facies, suggesting that the stronger correlations are accompanied by lower gold grades and lower radioactive trace element concentrations. The same can be said about the lower correlations between gold grade and radioactive trace elements, and that the lower correlations were accompanied by higher gold grades and higher radioactive trace element concentrations (as seen in Facies No. 3 and No. 1).

Referring to the total carbon percentage within the reef samples, a higher gold grade and carbon correlation (R^2=0.6044) was noted within the No. 3 Facies, followed by the No. 1 Facies (R^2=0.0777) (Figure 3.49). The gold grade-carbon correlations determined for the reef samples disagree with the Carbon Leader Reef facies model. The facies model proposes that the strongest correlations occur within the No. 1 Facies whereas the observations from the reef samples in the current investigation suggest the strongest correlations are within the No. 3 Facies. A single sample (Sample 11) from the No. 2 Facies is noted to have a carbon concentration above the lower detection limit of 0.01%.

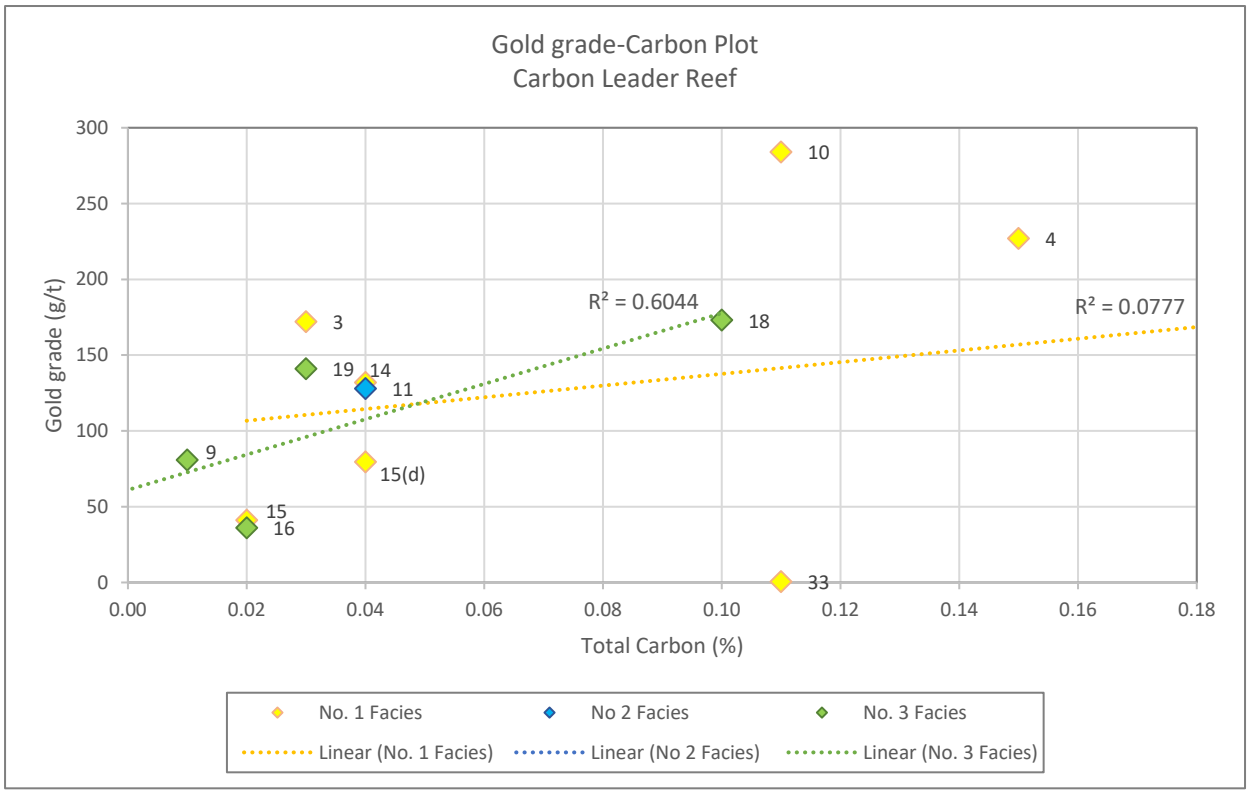

***Figure 3.49**: Gold grade (g/t) and total carbon (%) plot of the Carbon Leader Reef (tombstone and borehole) samples. The strongest correlation between gold grade and carbon was noted for the No. 3 Facies (R^2=0.6044), followed by the No. 1 Facies (R^2=0.0777). Sample 11 was the only sample from the No. 2 Facies with carbon concentration above the lower detection limit of 0.01%. The markers are annotated by sample number.*

Out of a total of 37 samples, 24 samples were below detection for total carbon and could not be plotted. However, in thin section, carbon was frequently noted to occur in masses (fly-speck nodules) and in thin seams alongside detrital uraninite and gold. Although the No. 2 Facies is not typically associated with carbon in comparison to the No. 1 and No. 3 Facies, carbon was noted in thin section in all of the No. 2 Facies samples (albeit very small amounts) with the exception of the Pale Pebbly Quartzite of Sample 2 that did not have any carbon present. Macroscopically, carbon was noted to occur as a thin carbon seam in Sample 4 and Sample 15

(both within the No. 1 Facies). Fly-speck carbon was noted in Sample 10 (No. 1 Facies), Sample 16 (No. 3 Facies) and Sample 18 (No. 3 Facies). Samples that had very fine carbon seams present macroscopically with no carbon detected geochemically include Sample 7 (No. 1 Facies), Sample 12 (No. 1 Facies), Sample 17 (No. 3 Facies), Sample 25 (No. 3 Facies), Sample 32 (No. 1 Facies) and Sample 64 (No. 3 Facies). Although the samples were noted to have carbon present in hand specimen, it is possible that there was sample loss during cleaning and cutting of the hand specimens to be used for the geochemical analyses, resulting in a carbon concentration below the lower detection limit of 0.01% for each of the samples.

Samples from the No. 3 Facies are typically associated with the presence of fly-speck carbon rather than actual seams however they were noted to have thin carbon seams in Samples 17, 25 and 64.

Corresponding high gold grades were noted to occur with the higher carbon content in Sample 4 (No. 1 Facies), Sample 10 (No. 1 Facies) and Sample 18 (No. 3 Facies). Sample 33 (No. 1 Facies) had a higher carbon content in comparison to higher gold grade samples, however the gold grade was very low at 0.6 g/t. Macroscopically this sample was noted to have a greenish discolouration of the matrix. Microscopically it was noted that Sample 33 had a higher concentration of sericitic muscovite than pyrophyllite and chloritoid was noted to have a greater concentration than chlorite. The other No. 1 Facies samples within the same area of the mine (Samples 5, 6 and 7) had a more pyrophyllite-dominant matrix with greater chlorite content than chloritoid. Sample 33 may be different in composition due to its proximity to the No. 1 and No. 3 Facies boundary, however its location does not explain the lack of gold grade that corresponds to the higher carbon content. The remainder of the samples (from the No. 1, No. 2 and No. 3 Facies) were seen to have variable gold grades corresponding with carbon content of less than 0.05%.

Other trace elements that correlated well with the gold grade include Ag as well as Ni and are shown in Figure 3.50 (a) and Figure 3.50 (b) respectively. There was a strong correlation between gold grade and Ag, particularly where samples contained less than 20 ppm Ag (Figure 3.50). Above 20 ppm there is more scatter. The strongest correlation was noted within the No. 3 Facies (R^2=0.9534), followed by the No. 2 Facies (R^2=0.9528) and the No. 1 Facies (R^2=0.4349).

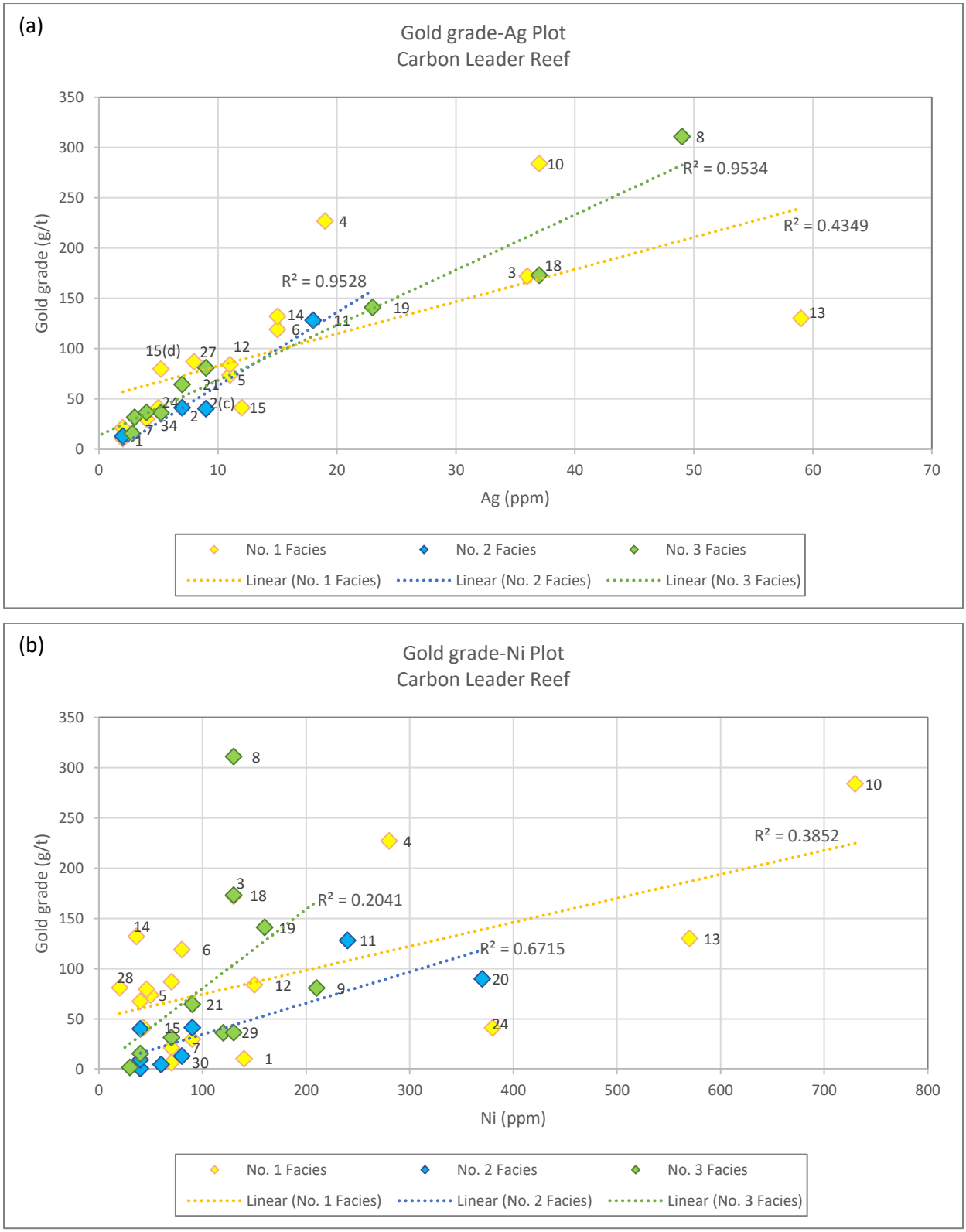

***Figure 3.50**: (a) Gold grade (g/t) and Ag (ppm) plot of the Carbon Leader Reef (tombstone and borehole) samples. The strongest correlation between gold grade and Ag was noted within the No. 3 Facies (R^2=0.9534); (b) Gold grade (g/t) and Ni (ppm) plot of the Carbon Leader Reef (tombstone and borehole) samples. The strongest correlation between gold grade and Ni was noted within the No. 2 Facies (R^2=0.6715). The markers are annotated by sample number.*

Samples from the No. 1 Facies had, on average, the highest Ag abundance (16.1 ppm), followed by the No. 3 Facies (15.6 ppm) and the No. 2 Facies (9 ppm). Ag is a common trace element within the Witwatersrand Basin and is found to have a strong correlation with gold (Depiné *et al*., 2013). Although the geochemical data suggests the presence of Ag, no Ag was identified in thin section for any of the reef samples because Ag typically occurs as an alloy within native gold (Allan and Woodcock, 2001; Jones and Fleischer, 1969; Nesse, 2000, p. 398).

Figure 3.50 (b) shows the gold grades plotted against Ni concentration. The No. 1 Facies had a few higher Ni concentrations, and on average was the highest in Ni with 160 ppm, followed by the No. 2 Facies at 120 ppm. The No. 3 Facies had the lowest average Ni concentration at 111 ppm. The No. 2 Facies had the strongest correlation between Ni concentration and gold grade, where R^2=0.6715. The No. 3 Facies had the lowest correlation at R^2=0.2041. Samples with the highest Ni concentration (greater than 200 ppm) lie within the No. 1 Facies (Samples 4, 10, 13 and 24) and the No. 3 Facies (Samples 11 and 20). Samples within the No. 2 Facies were found to be below 200 ppm, with the exception of Sample 9 (210 ppm). Ni as well as Co (Figure 3.52) is associated with presence of syngenetic, rounded pyrite (Tucker *et al.*¸ 2016). Detrital pyrite and secondary pyrite were noted within all the reef samples. In some of the samples, grains of gersdorffite that were associated with gold grains were noted in mostly the No. 1 and No. 3 Facies samples, with observations in thin section in Sample 2 for both the No. 2A and No. 2B Facies.

The highest Co concentration, on average, was noted within the No. 3 Facies (average of 68 ppm) (Figure 3.51(a)). The No. 2 Facies had an average Co concentration of 49 ppm, and the No. 1 Facies had an average of 59 ppm. The highest Co was noted within Sample 10 (260 ppm) that has a very high gold grade of 284.0 g/t. Sample 13 (210 ppm Co) had a high gold grade of 130 g/t. Both Samples 10 and 13 lie within the No. 1 Facies. Sample 18, from the No. 3 Facies, had a Co concentration of 180 ppm with a high gold grade of 173.0 g/t. Although the No. 2 Facies was noted to have the lowest average Co concentration, it had the strongest correlation with gold grade (R^2=0.4464) in comparison to the No. 1 Facies (R^2=0.4440) and No. 3 Facies (R^2=0.4007). Higher Ni/Co ratios and low gold grade are typically associated with post-sedimentary pyrite i.e. of hydrothermal origin, and lower Ni/Co ratios with high gold grade are seen to be associated with pyrite grains that have a syn-sedimentary origin (Koglin *et al*., 2010).

Comparing the Ni and the Co concentrations (Figure 3.51(b)), it was noted that the highest correlation between the trace elements was for the No. 1 Facies (R^2=0.8002).

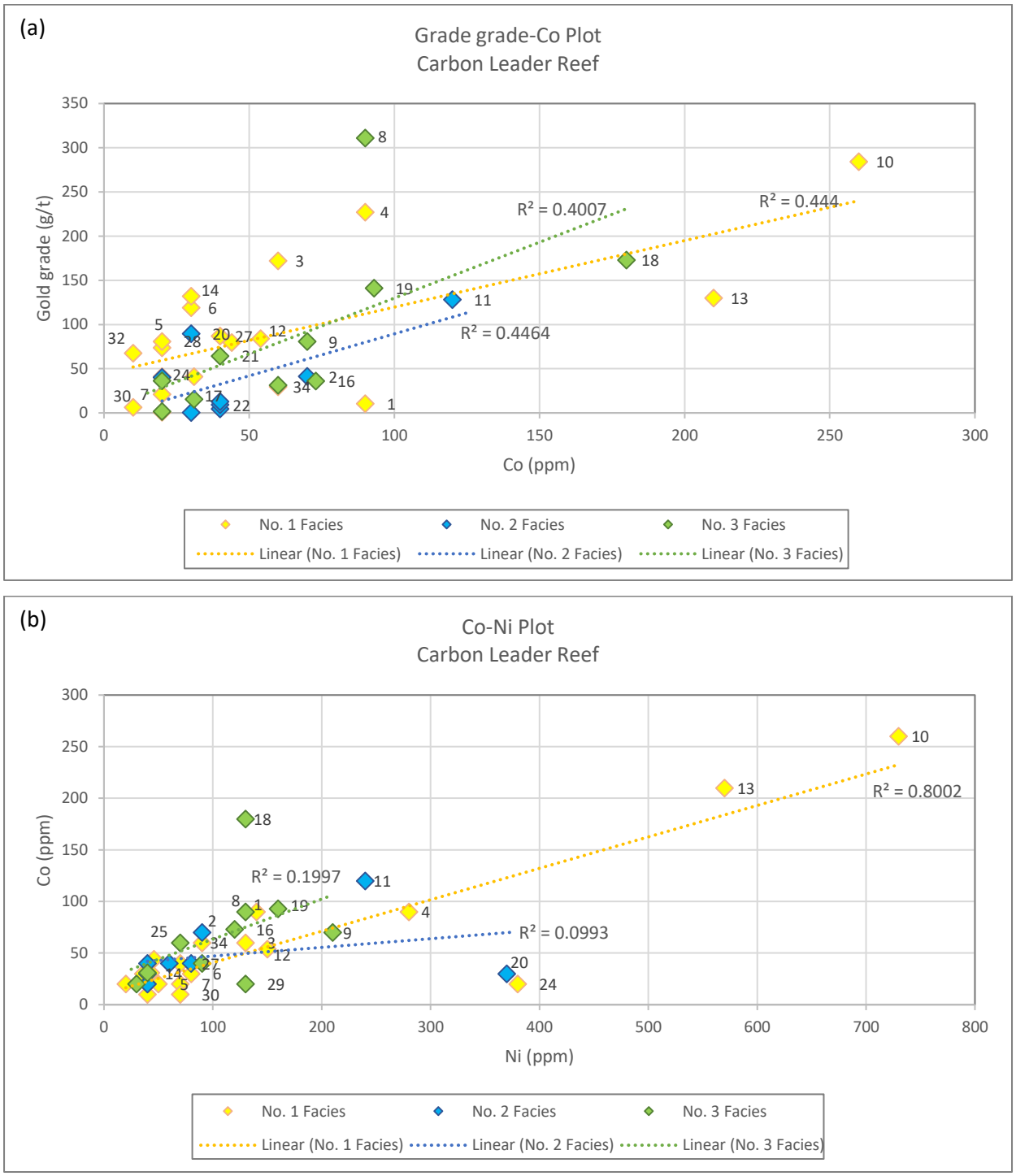

***Figure 3.51**: (a) Gold grade (g/t) and Co (ppm) plot of the Carbon Leader Reef (tombstone and borehole) samples. The correlations were similar across the facies types, with No. 2 Facies having the strongest correlation between gold grade and Co concentration (R^2=0.4464); (b) Co (ppm) and Ni (ppm) plot of the Carbon Leader Reef (tombstone and borehole) samples. The No. 1 Facies was noted to have the strongest correlation between the trace elements, suggestive of a different depositional environment of pyrite and/or different type(s) of pyrite in comparison to the No. 2 and No. 3 Facies of the Carbon Leader Reef. The markers are annotated by sample number.*

The stronger relationship between Co and Ni noted within the No. 1 Facies is suggestive of a different depositional environment of pyrite and/or different type(s) of pyrite in comparison to the No. 2 and No. 3 Facies that have considerably weaker relationships between the trace elements (Koglin *et al.*, 2010). Detrital pyrite as well as anhedral to euhedral pyrite grains were noted to occur within the No. 1 Facies across the West Wits Line, whereas the No. 2 and No. 3 Facies had predominantly detrital pyrite grains accompanied by detrital uraninite and chromite grains.

The No. 1 Facies was noted to have the strongest correlation (R^2=0.6428) between Ba and gold grade (Figure 3.52).

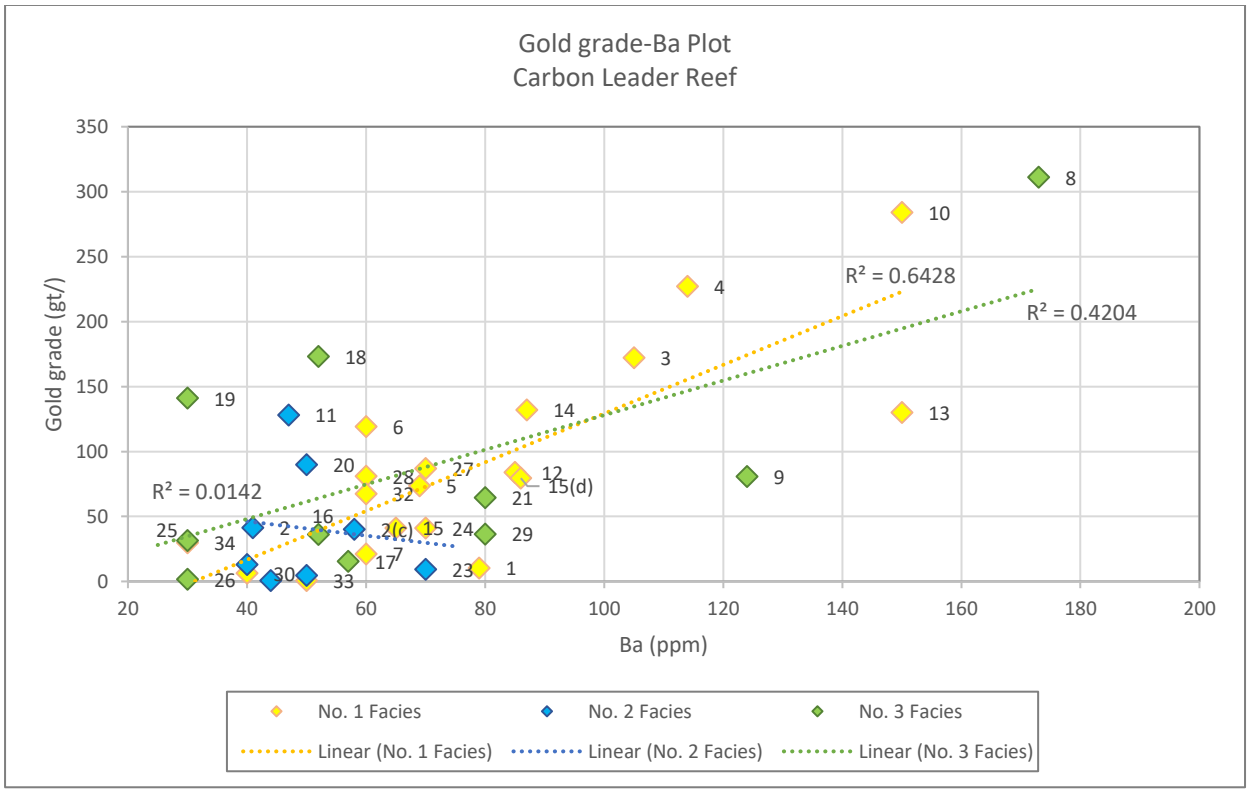

***Figure 3.52**: Gold grade (g/t) and Ba (ppm) plot of the Carbon Leader Reef (tombstone and borehole) samples. The No. 1 Facies was noted to have the strongest correlation (R^2=0.6428) and the No. 2 Facies was noted to have the weakest (non-existent) correlation (R^2=0.0142) between gold grade and Ba concentration. The markers are annotated by sample number.*

The average Ba concentration in the reef samples shows the No. 1 Facies to have higher Ba (average of 78 ppm), followed by the No. 3 Facies (average of 71 ppm) and the No. 2 Facies (50 ppm). Ba is commonly associated with galena, pyrite and carbonates within hydrothermal deposits (Nesse, 2000, p.346). The correlation with gold grade is likely due to the presence of pyrite within the Carbon Leader Reef. Two types of pyrite grains were noted within the No. 1

Facies (detrital and anhedral to euhedral), in comparison to the No. 2 and No. 3 Facies that had predominantly detrital pyrite grains.

A plot of gold grade and Cu concentration is seen in Figure 3.53. Cu is associated with the presence of chalcopyrite within the Carbon Leader Reef. Chalcopyrite is often seen together with galena and pyrite in hydrothermal deposits (Nesse, 2000, p. 387). On average, the No. 2 Facies had the largest Cu concentration (66 ppm) with the strongest correlation against gold grade (R^2=0.5954). The highest Cu concentration was noted within the Facies No. 3 - Sample 18 (230 ppm) with a gold grade of 173.0 g/t. The second highest Cu concentration was noted within the No. 2 Facies – Sample 20 at 140 ppm. Most of the samples from the No. 1 Facies, with the exception of Samples 24, 34 and 30, had a Cu concentration of less than 50 ppm. Similarly, most of the samples from the No. 3 Facies, with the exception of Samples 18 and 20, had a Cu concentration of less than 50 ppm. This suggests chalcopyrite is more frequent within the No. 2 Facies in comparison to the No. 1 and No. 3 Facies. Chalcopyrite was noted in many of the Carbon Leader Reef samples, across all the facies types.

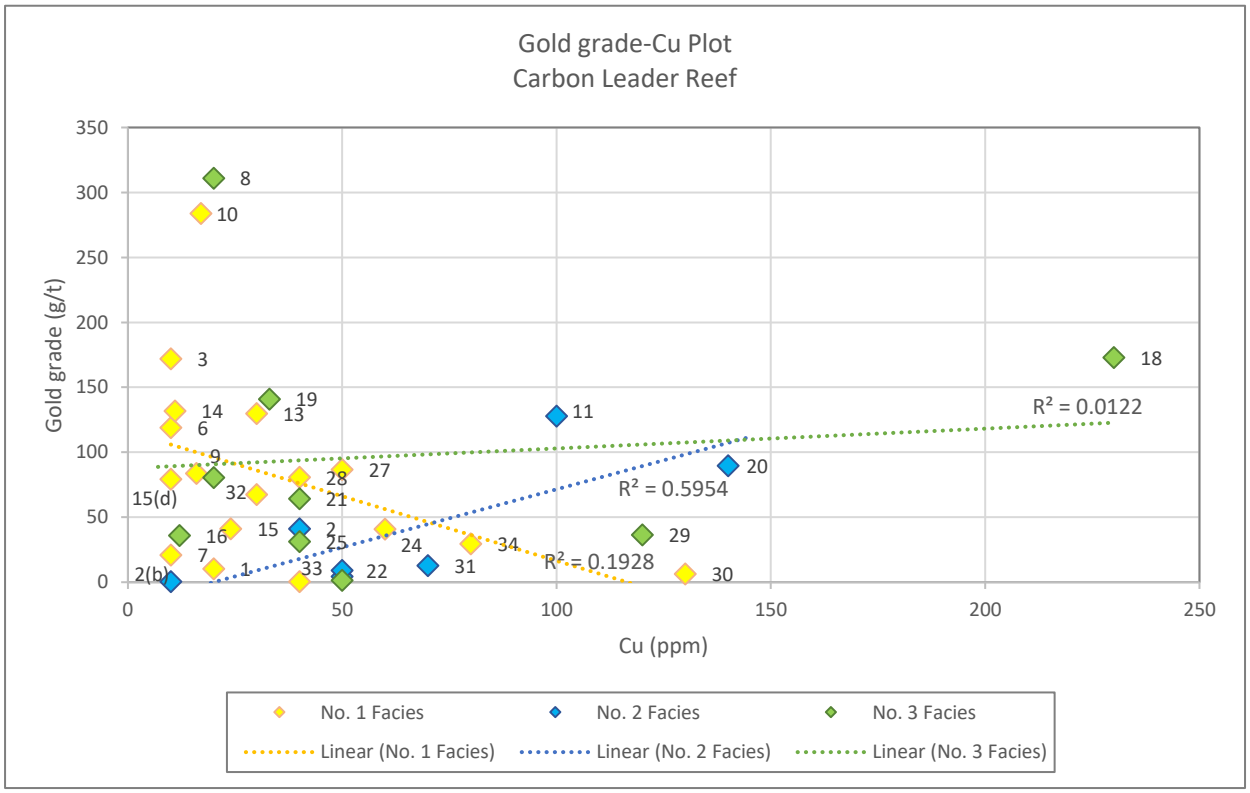

***Figure 3.53**: Gold grade (g/t) and Cu (ppm) plot of the Carbon Leader Reef (tombstone and borehole) samples. The strongest correlation was noted within the No. 2 Facies (R^2=0.5954). The highest Cu concentration was seen in Sample 18 (230 ppm) at a gold grade of 173.0 g/t. The markers are annotated by sample number.*

Chalcopyrite was observed as independent subrounded grains within the Carbon Leader Reef matrix (across all the facies types) in Samples 11, 18, 20, 24, 27, 29, 30, 31 and 34. The samples where chalcopyrite was noted to occur as inclusions in pyrite alongside independent chalcopyrite grains had lower Cu concentration than the samples that only had independent chalcopyrite grains.

Additional to the trace elements, major element oxides were also determined for the Carbon Leader Reef. In comparison to the trace elements, the major oxides show fewer correlations with gold grade. The geochemical analyses of the major oxides and gold assay results for all the Carbon Leader Reef (tombstone and borehole) samples are listed in Table 3.12. In Figure 3.54, a strong correlation was noted between $\%Fe_2O_3$ and gold grade for the No. 3 Facies (R^2=0.7442), followed by the No. 2 Facies (R^2=0.1274), with the No. 1 Facies having the lowest correlation with gold grade (R^2=0.0564) which is considered to be non-existent.

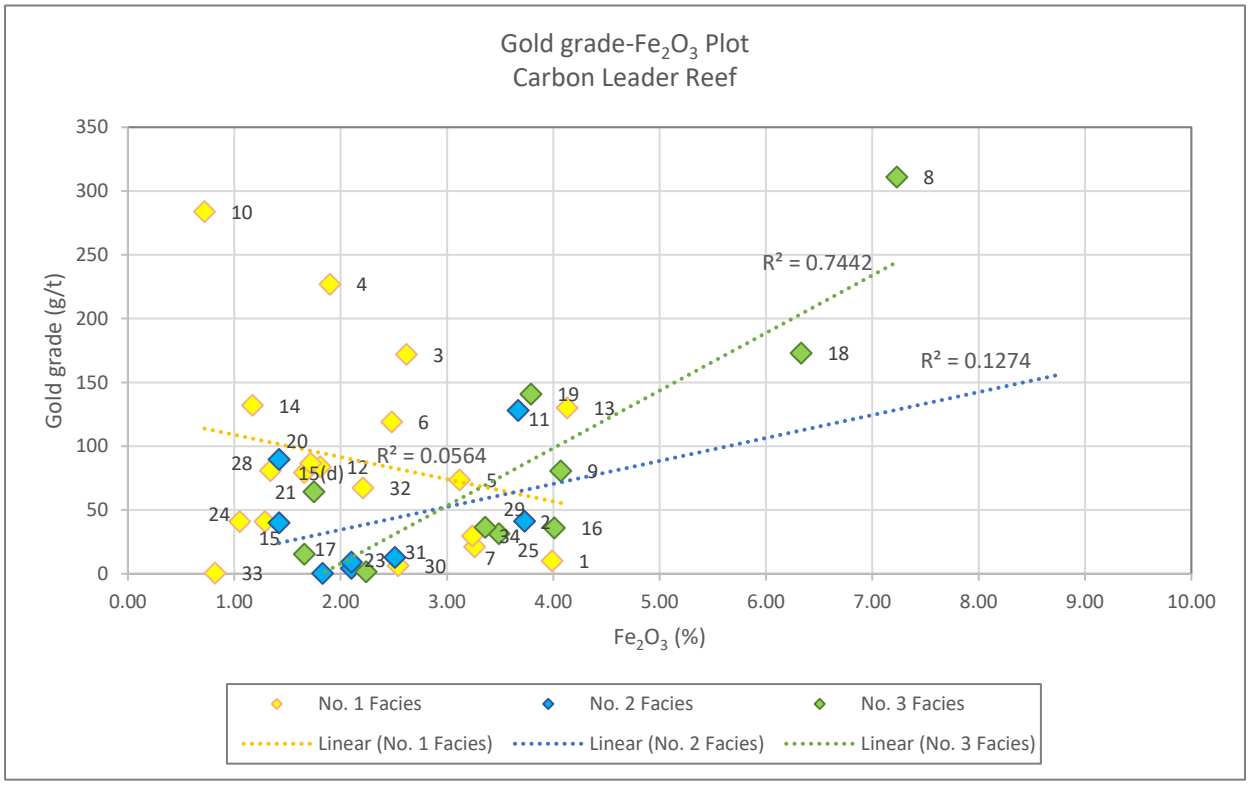

***Figure 3.54**: Gold grade (g/t) and Fe_2O_3 (%) plot of the Carbon Leader Reef (tombstone and borehole) samples. The No. 3 Facies was noted to have the strongest correlation (R^2=0.7442). The markers are annotated by sample number.*

Corresponding to the strong relationship between $\%Fe_2O_3$ and gold grade, the highest average $\%Fe_2O_3$ was noted within the No. 3 Facies (average of 3.79%), followed by the No. 2 Facies (average of 2.35%) and the No. 1 Facies (average of 2.16%).

Table 3.12: The geochemical analyses for major oxides and gold assay results of all the Carbon Leader Reef (tombstone and borehole) samples. All the major oxides were determined by means of XRF. Gold grade (g/t) was determined by fire assay. [(a)] Loss on ignition (LOI); [(b)] Pale Pebbly Quartzite (PPQ) for Sample 2; [(c)] No. 2B Facies for Sample 2; [(d)] Internal Quartzite (IQ) for Sample 15; *Below the lower detection limit.

Carbon Leader Reef Samples: Geochemical Analyses and Gold Assay															
	Sample ID	*Unit*	%												g/t
			SiO_2	*Al_2O_3*	*CaO*	*MgO*	*Fe_2O_3*	*K_2O*	*MnO*	*Na_2O*	*P_2O_5*	*TiO_2*	*Cr_2O_3*	*V_2O_5*	*LOI[(a)]*	*Au*
Lower Detection Limit			*0.05*	*0.05*	*0.01*	*0.05*	*0.01*	*0.01*	*0.01*	*0.05*	*0.01*	*0.01*	*0.01*	*0.01*	*-50*	*0.02*
1	94-94 E1	No. 1 Facies	87.5	3.6	0.01	0.16	3.99	0.39	*	*	*	0.24	0.08	*	2.35	10.3
2	99-94 E2	No. 2A Facies	87.5	5.28	0.01	0.06	3.73	0.22	*	*	0.03	0.19	0.04	*	2.49	41.2
2[(b)]	99-94 E2	PPQ	93.4	3.49	*	0.08	1.83	0.24	*	*	*	0.14	0.06	*	1.21	0.5
2[(c)]	99-94 E2	No. 2B Facies	92.9	4.8	0.01	0.18	1.42	0.27	*	0.08	0.03	0.16	0.03	*	1.27	40.1
3	104-88 W6	No. 1 Facies	90.8	3.64	0.02	0.09	2.62	0.41	*	0.08	0.03	0.27	0.07	*	1.72	172.0
4	105-86 E2	No. 1 Facies	88.4	6.63	0.03	0.14	1.9	0.55	*	0.21	0.04	0.41	0.05	*	1.85	227.0
5	112-83 W3	No. 1 Facies	88.8	4.97	0.02	0.25	3.12	0.33	0.02	0.08	0.03	0.12	0.12	*	0.81	73.6
6	112-83 W4	No. 1 Facies	90	3.8	*	0.38	2.48	0.23	*	*	0.02	0.19	0.06	*	1.16	119.0
7	114-78 E1	No. 1 Facies	91.6	3.62	0.02	0.16	3.26	0.28	0.04	0.10	0.02	0.13	0.13	*	0.63	21.1
8	120-55 W4	No. 3 Facies	77	10.1	0.02	0.29	7.23	0.73	0.02	0.11	0.03	0.55	0.17	*	3.39	311.0
9	120-77 S1	No. 3 Facies	86.9	5.39	*	0.13	4.07	0.59	0.01	0.12	0.03	0.31	0.18	*	1.45	80.7
10	96-94 E2	No. 1 Facies	91.4	5.72	*	0.05	0.72	0.24	*	0.08	0.02	0.1	0.03	*	2.31	284.0
11	100-92 Wze	No. 2A Facies	90.2	2.14	0.05	0.43	3.67	0.14	*	*	0.02	0.22	0.1	*	1.86	128.0
12	104-88 E1A	No. 1 Facies	92.4	3.59	0.02	0.13	1.81	0.37	*	0.05	0.02	0.18	0.07	*	1.22	83.9
13	104-88 W7	No. 1 Facies	84.4	5	0.04	0.09	4.13	0.5	*	0.16	0.05	0.62	0.19	*	2.68	130.0
14	109-87 E2	No. 1 Facies	92.2	4.41	0.02	0.06	1.17	0.37	0.07	0.11	0.01	0.13	0.02	*	0.98	132.0
15	112-84 Rse	No. 1 Facies	93	3.37	0.01	0.23	1.29	0.3	*	*	0.03	0.13	0.03	*	0.92	79.5
15[(d)]	112-84 Rse	IQ	91	4.19	0.02	0.21	1.66	0.44	*	0.08	0.02	0.15	0.04	*	1.21	41.1
16	120-55 NE7	No. 3 Facies	89.1	3.12	0.01	0.59	4.01	0.27	*	*	0.02	0.14	0.05	*	1.91	36.0
17	120-55 W5	No. 3 Facies	91.1	4.74	*	0.34	1.66	0.28	*	0.06	0.01	0.16	0.04	*	1	15.4
18	120-55 W7	No. 3 Facies	85.6	2.28	0.02	0.48	6.33	0.12	*	*	0.04	0.28	0.14	*	3.05	173.0
19	120-70 W1	No. 3 Facies	89.1	1.61	0.02	0.22	3.79	0.11	*	*	0.02	0.09	0.04	*	1.78	141.0
20	DPH 3883	No. 2A Facies	92.8	3.71	0.31	0.12	1.42	0.26	0.02	0.09	0.02	0.13	0.05	*	0.65	89.7
21	DPH 4057	No. 3 Facies	88	6.94	0.24	0.08	1.75	0.45	*	0.09	0.02	0.27	0.04	*	1.6	64.3
22	GBH 1000 D6	No. 2A Facies	91.7	3.08	0.06	0.12	2.1	0.38	*	*	0.01	0.12	0.03	*	0.98	4.5
23	GBH 2788	No. 2B Facies	91.6	2.39	0.17	*	2.1	0.43	0.02	*	0.02	0.13	0.03	*	0.37	9.3
24	GBH 3763	No. 1 Facies	91.8	4.43	0.13	0.07	1.05	0.24	0.01	0.05	0.02	0.12	0.02	*	0.74	41.0
25	GBH 3844	No. 3 Facies	89.7	3.01	0.15	0.08	3.49	0.13	*	*	0.04	0.22	0.022	*	0.95	31.4
26	GBH 3845	No. 3 Facies	89	4.1	0.08	*	2.24	0.14	0.02	*	0.03	0.2	0.19	*	1.34	1.6
27	GBH 4003	No. 1 Facies	91	4.62	0.06	0.24	1.72	0.3	0.01	0.11	0.02	0.15	0.03	*	0.95	86.8
28	GBH 6000	No. 1 Facies	92.6	3.05	0.15	*	1.34	0.55	*	*	0.02	0.12	0.02	*	0.76	80.8
29	GBH 6001	No. 3 Facies	86	4.46	0.26	0.52	3.36	0.59	0.02	0.08	0.02	0.15	0.01	*	1.52	36.4
30	GBH 6003	No. 1 Facies	90	4.11	0.06	0.75	2.54	0.27	0.01	0.12	0.02	0.12	0.03	*	1.1	6.4
31	GBH 6004	No. 2B Facies	90	2.78	0.3	*	2.51	0.21	0.02	*	0.04	0.22	0.04	*	2.28	12.8
32	GBH 6014	No.1 Facies	90.6	4.55	0.09	0.42	2.21	0.38	*	0.07	0.03	0.14	0.1	*	1.03	67.5
33	GBH 6028	No. 1 Facies	90.6	5.74	0.07	*	0.82	0.31	*	0.08	0.02	0.13	0.03	*	1.8	0.6
34	GBH 6036	No. 1 Facies	89.8	2.19	0.06	0.47	3.24	0.15	*	0.11	0.01	0.17	0.07	*	0.78	29.6

The $\%Fe_2O_3$ indicates the presence of iron-rich minerals such as magnetite and hematite. Subrounded grains of hematite were noted to occur as a trace mineral in Sample 23 (No. 2B Facies) and Sample 25 (No. 3 Facies) in polished thin section. The presence of pyrite is also indicated by $\%Fe_2O_3$ (Nesse, 2000, p. 389).

The highest $\%Fe_2O_3$ sample (Sample 8) was from the No. 3 Facies (7.23%) with the highest gold grade of 311.0 g/t. The next highest was Sample 18, also from the No. 3 Facies, with 6.33% Fe_2O_3 and a high gold grade of 173 g/t. The remaining samples for all the facies types were seen to have lower than 5.00% Fe_2O_3, with gold grades lower than 150.0 g/t, with the exception of Samples 3, 4 and 10 having higher than 150.0 g/t of gold grade.

Al_2O_3 is associated with the presence of aluminous minerals such as muscovite and andalusite (Nesse, 2000, p.366) as well as pyrophyllite (Nesse, 2000, p.243). Gold grades versus $\%Al_2O_3$ for the reef samples do not reveal any distinct trend(s) however, the majority of the samples lie between 2.00% and 6.00% Al_2O_3 (Figure 3.55), with the exception of Sample 4 (from the No. 1 Facies) and Samples 8 and 21 (from the No. 3 Facies) that were greater than 6.00% Al_2O_3.

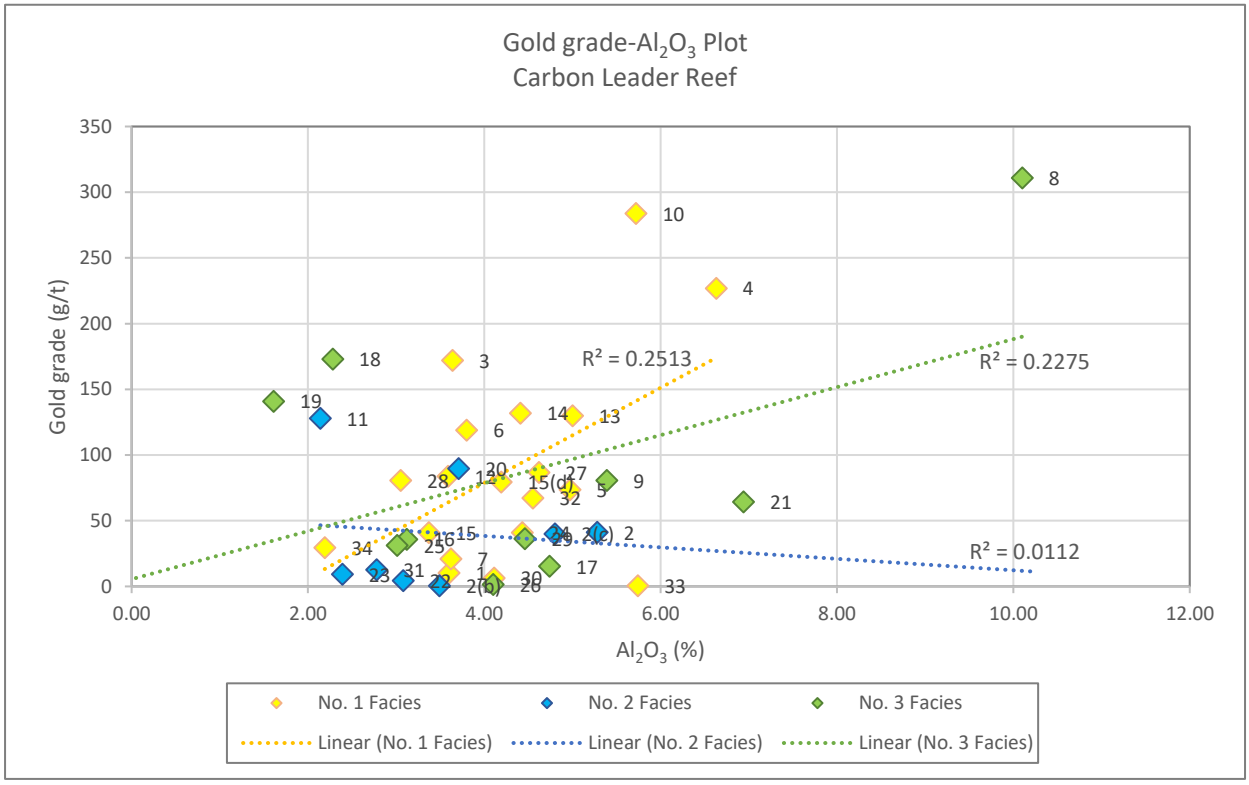

***Figure 3.55**: Gold grade (g/t) and Al_2O_3 (%) plot of the Carbon Leader Reef (tombstone and borehole) samples. The highest $\%Al_2O_3$ was noted within Sample 8 (10.10%) within the No. 3 Facies. The markers are annotated by sample number.*

The strongest correlation was noted within the No. 1 Facies (R^2=0.2513) followed by the No. 3 Facies (R^2=0.2275). The average %Al_2O_3 was highest within the No. 3 Facies (average of 4.58%), followed by the No. 1 Facies (average of 4.28%) and the No. 2 Facies (average of 3.46%). This was similar to the findings in the microscopic observations where greater concentrations of sericitic muscovite and pyrophyllite are noted within the No. 1 and No. 3 Facies in comparison to the No. 2 Facies. Distinguishing between the two minerals (sericitic muscovite and pyrophyllite) was achieved by microscopic observation.

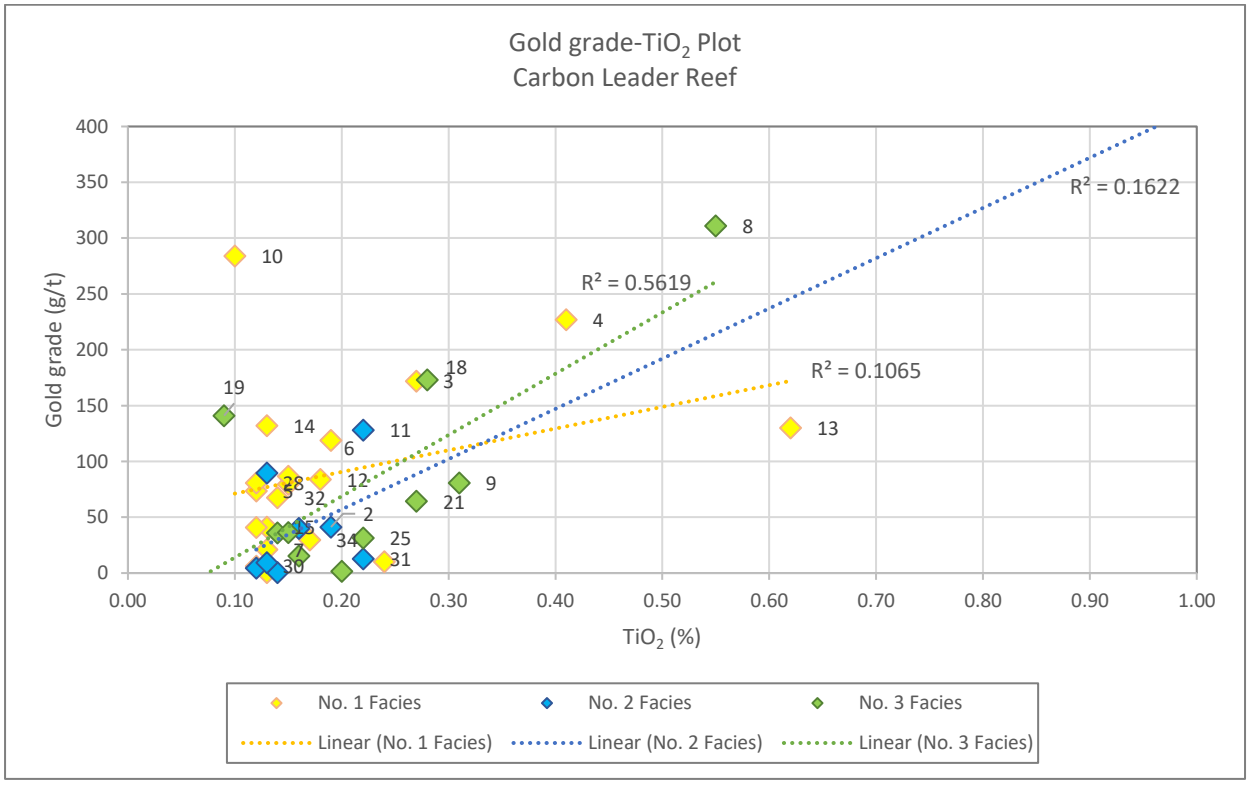

***Figure 3.56**: Gold grade (g/t) and TiO_2 (%) plot of the Carbon Leader Reef (tombstone and borehole) samples. The highest %TiO_2 was noted within Sample 13 (0.62%) within the No. 1 Facies. The markers are annotated by sample number.*

TiO_2 is associated with rutile that can undergo alteration to form leucoxene and is commonly found as a heavy mineral within clastic sediments (Nesse, 2000, p.367). %TiO_2 and gold grade had the highest correlation within the No. 3 Facies (R^2=0.5619), followed by the No. 2 Facies (R^2= 0.1622) and the No. 1 Facies (R^2=0.1065) (Figure 3.56). Rutile and leucoxene were noted to occur as trace minerals (in polished thin section or confirmed by XRD analysis) in all of the Carbon Leader Reef samples, with the exception of Sample 11 (No. 2 Facies), Sample 21 (No. 3 Facies), Sample 28 (No. 1 Facies). On average, the highest %TiO_2 was noted within the No. 3 Facies (average of 0.24%), followed by the No. 1 Facies (average of 0.19%) and the No. 2 Facies

(average of 0.16%). This suggests that higher concentrations of rutile and/or leucoxene are found within the No. 3 Facies and the No. 1 Facies of the Carbon Leader Reef, further suggesting greater amounts of alteration has occurred in the No. 3 and No. 1 Facies.

Figure 3.57 shows that the higher gold grades were associated with less than 0.05% CaO, suggesting that CaO has little to no association with gold grade.

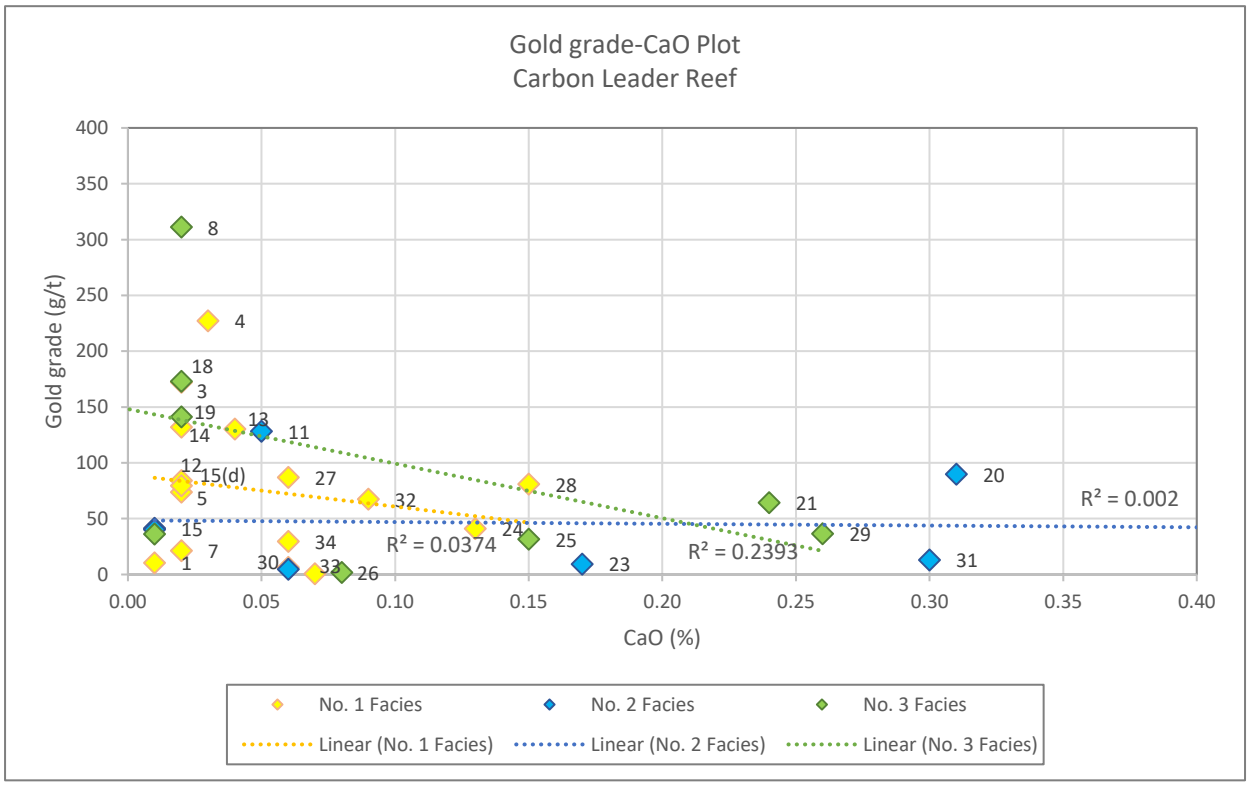

***Figure 3.57**: Gold grade (g/t) and CaO (%) plot of the Carbon Leader Reef (tombstone and borehole) samples. %CaO relative to the gold grade shows there was very little to no association. The markers are annotated by sample number.*

CaO is an oxide in calcite and is commonly found as a gangue mineral in hydrothermal deposits as well as within fracture infill (Nesse, 2000, p.329). Overall, the average %CaO for the No. 2 Facies was highest at 0.13%, followed by the No. 3 Facies at 0.10% and the No. 1 Facies at 0.05%. This suggests that higher CaO amounts are found in the No. 2 and No. 3 Facies in comparison to the No. 1 Facies, however the presence of calcite within polished thin section was not noted in any of the samples as the percentage concentration is very low.

MgO is present in chlorite (Nesse, 2000, p.251) and chloritoid (Nesse, 2000, p.321). Chloritoid that has undergone alteration may alter to chlorite or sericite, and also forms in

hydrothermally altered rocks (Nesse, 2000, p.321). The %MgO in relation to gold grade can be seen in Figure 3.58.

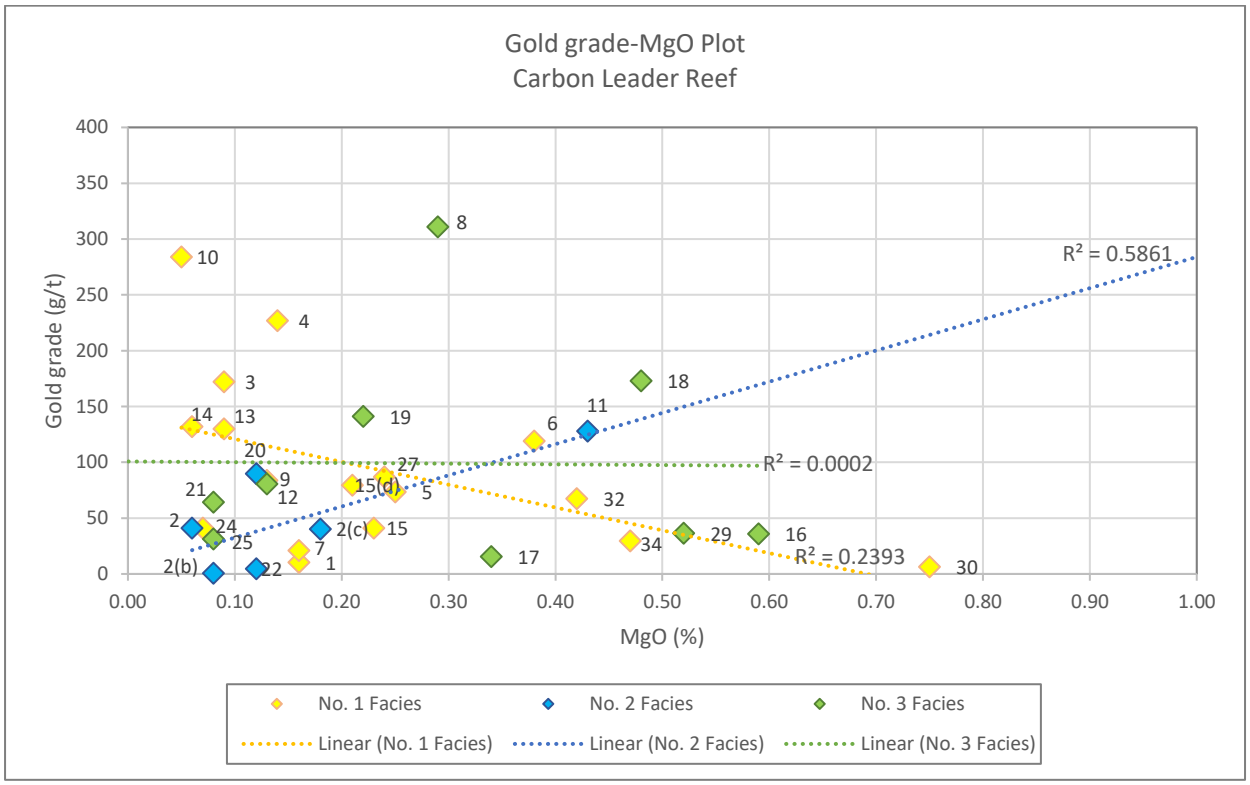

***Figure 3.58**: Gold grade (g/t) and MgO (%) plot of the Carbon Leader Reef (tombstone and borehole) samples. The strongest correlation between gold grade and %MgO was noted within the No. 2 Facies (R^2=0.5861). The No. 3 Facies had the weakest (non-existent) correlation (R^2=0.0002). The markers are annotated by sample number.*

Although the No. 2 Facies was noted to have the strongest correlation between gold grade and %MgO, it was noted to have the lowest average %MgO (average of 0.17 ppm) in comparison to the No. 3 Facies (average of 0.30 ppm) and the No. 1 Facies (average of 0.23 ppm). This suggests that higher %MgO concentrations can be seen in the No. 3 and No. 1 Facies, however they have a weak correlation to gold grade in comparison to the No. 2 Facies. When comparing the geochemical analyses with the microscopic observations, it was noted that the No. 1 and No. 3 Facies had higher occurrences of chlorite and chloritoid, which agrees with the findings in the geochemical data. Distinguishing between the two minerals (chlorite and chloritoid) was achieved by microscopic observation.

Figure 3.59 shows the relationship between $\%K_2O$ and gold grade of the Carbon Leader Reef samples. K_2O is commonly found within sericite and is a product of hydrothermal alteration of feldspars or other K-bearing and Al-bearing minerals (Nesse, 2000, p.245). Although the No. 1 Facies had the poorest correlation between gold grade and $\%K_2O$, on average the $\%K_2O$ is the

highest of the three facies types (average of 0.35%). The No. 3 Facies was the next highest %K_2O with an average of 0.34%.

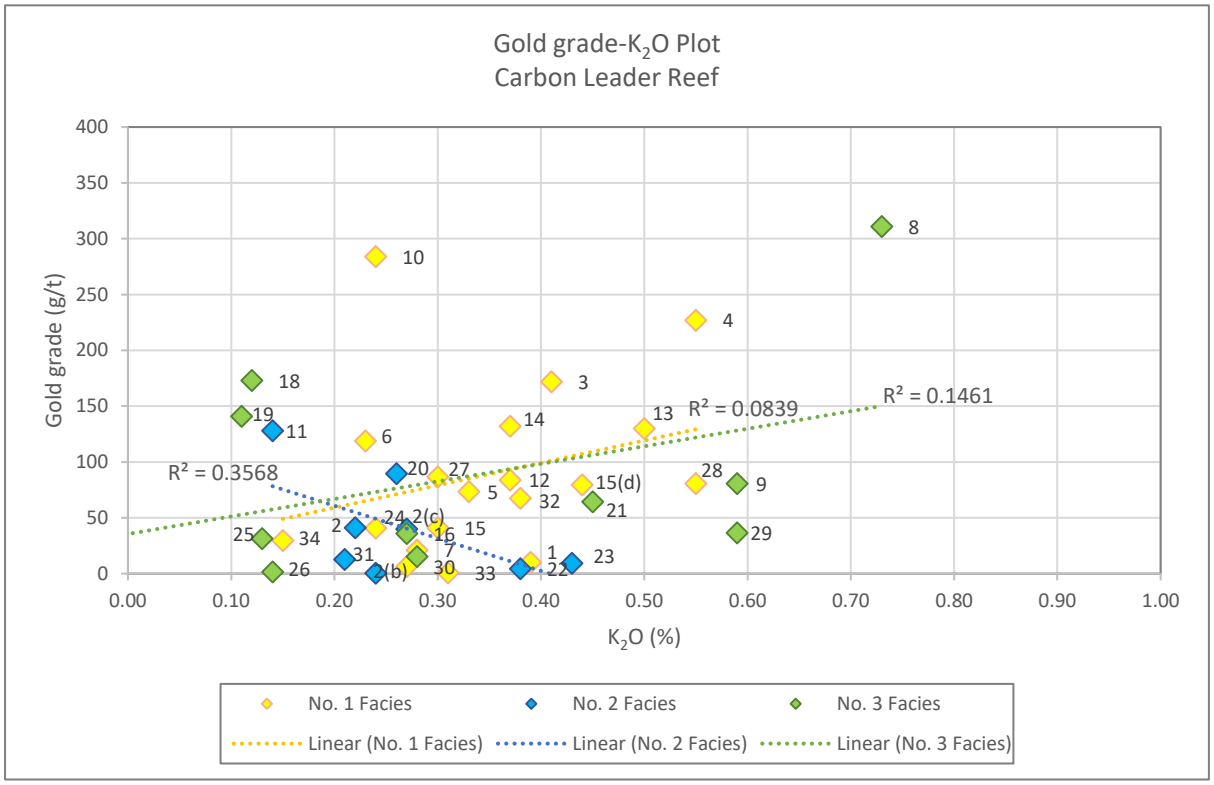

***Figure 3.59**: Gold grade (g/t) and K_2O (%) plot of the Carbon Leader Reef (tombstone and borehole) samples. The poorest (non-existent) correlation between gold grade and %K_2O was noted within the No. 1 Facies (R^2=0.0839).*

The strongest correlation between gold grade and %K_2O was noted within the No. 2 Facies however it yielded the lowest average %K_2O at 0.27%. This suggests that a higher abundance of sericite can be expected within the No. 1 and No. 3 Facies, with a lower abundance within the No. 2 Facies. In comparison to the microscopic observations, the geochemical data agrees that higher sericitic abundances were noted in samples that lie within the No. 1 and No. 3 Facies. The No. 1 Facies had, on average, the greatest sericite abundance in comparison to the No. 2 and No. 3 Facies (refer to Chapter 3.2, Table 3.7).

Cr_2O_3 is often found to be concentrated in detrital sands (Nesse, 2000, p. 361). %Cr_2O_3 was compared to the gold grade of the Carbon Leader Reef samples (Figure 3.60). It was noted that the strongest correlation between gold grade and %Cr_2O_3 was for the No. 2 Facies (R^2=0.5401). The poorest correlation (non-existent) was noted for the No. 1 Facies (R^2=0.0016). Sample 13, from the No. 1 Facies, had a %Cr_2O_3 of 0.19%. Sample 26, from the No. 3 Facies, also had a %Cr_2O_3 of 0.19% but had a lower gold grade (1.6 g/t in comparison to Sample 13 at 130.0 g/t).

On average, the higher %Cr_2O_3 was noted within the No. 3 Facies (average of 0.09%), followed by the No. 1 Facies (average of 0.06%) and the No. 2 Facies (average of 0.05%).

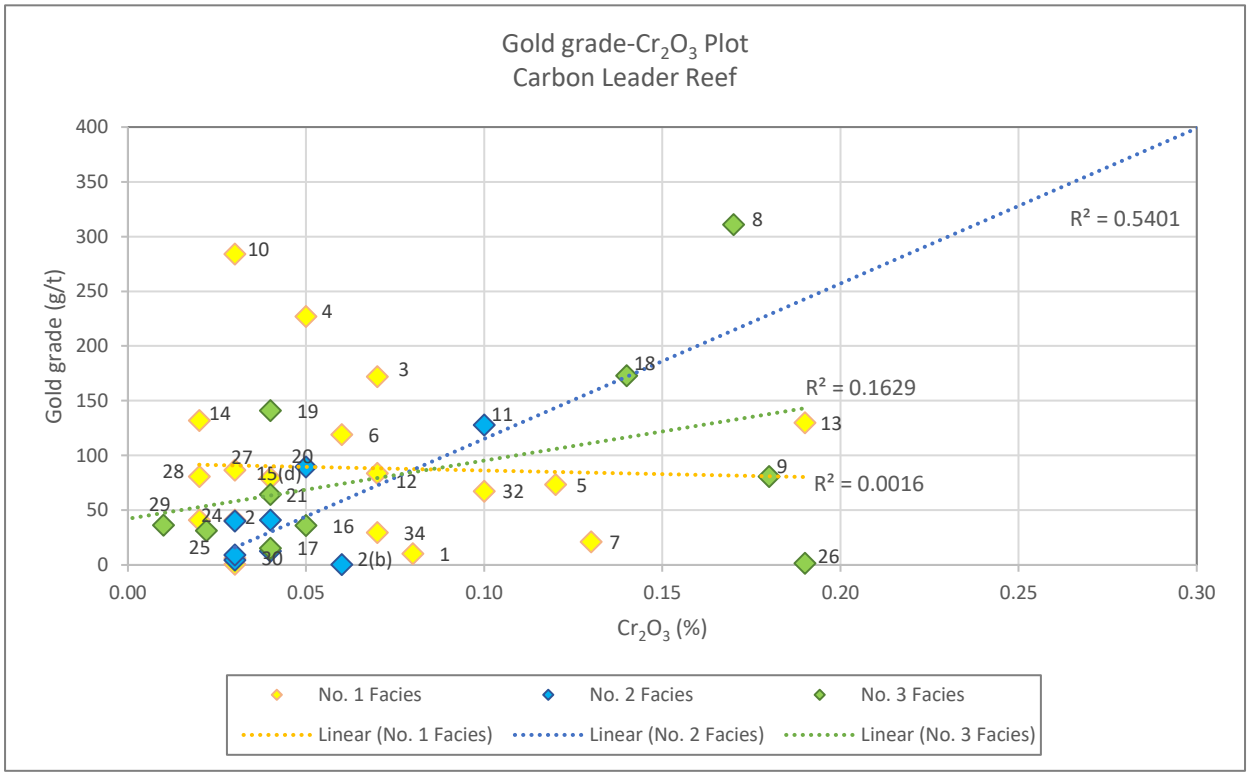

***Figure 3.60**: Gold grade (g/t) and Cr_2O_3 (%) plot of the Carbon Leader Reef (tombstone and borehole) samples. The No. 2 Facies was noted to have the highest correlation between gold grade and %Cr_2O_3 (R^2=0.5401). The No. 1 Facies had the poorest correlation (non-existent) between gold grade and %Cr_2O_3 (R^2=0.0016). The markers are annotated by sample number.*

The geochemical data suggests that a higher abundance of Cr_2O_3 can be expected in the No. 3 Facies (the greatest abundance) followed by the No. 1 Facies. The geochemical data corresponds well to the observations of detrital chromite grains in the reef samples, where most samples with chromite present (either seen in polished thin section or confirmed by means of XRD analysis) were from the No. 1 or No. 3 Facies. One exception noted was for Sample 2 within the No. 2 Facies, where the presence of chromite was determined by XRD analysis.

3.3.3 Discussion

A strong (positive) correlation was noted with gold grade and radioactive trace elements. This was seen throughout the hangingwall, footwall and Carbon Leader Reef samples. This strong correlation stems from the gold grade-hydrocarbon-uranium association noted within the Witwatersrand Basin (Agangi *et al.*, 2015; Depiné *et al.*, 2013; Drennan and Robb, 2006; Phillips

and Powell, 2015; Tucker *et al.*, 2016). The presence of U_3O_8 is due to the oxidation of uraninite (UO_2), which is the main uranium mineral that occurs within the reef bands of the Witwatersrand Basin (Tucker *et al.*, 2016). The decay of radioactive uranium allows for the formation of (radioactive) Pb, which was often represented in polished thin section by grains of galena, however no galena was seen within any of the samples (hangingwall, footwall and Carbon Leader Reef) used in this study. Detrital uraninite grains were noted to be associated with detrital gold grains in mostly the No. 1 Facies samples followed by the No. 3 Facies samples. Uraninite grains were less common in the No. 2 Facies and were noted to occur as detrital grains and were associated with detrital gold grains in Samples 2, 11 and 20.

The gold grades and the corresponding concentrations of the radioactive trace elements disagree with the Carbon Leader Reef facies model, which proposes that the highest gold grades are found in the No. 1 Facies (with the presence of a thin carbon seam) followed by the No. 3 Facies (with the presence of mostly fly-speck carbon in comparison to a carbon seam). The geochemical data shows that the No. 3 Facies had the higher gold grades, followed by the No. 1 Facies. Higher gold grades and U/U_3O_8 concentrations were noted to occur in samples with carbon present, in agreement with the gold-carbon-uranium relationship noted to occur within the Witwatersrand Basin.

The outcome of the LECO analysis carried out on the reef samples showed that several samples had carbon below the lower detection limit but may exhibit gold mineralisation, however all the samples with carbon concentrations above the detection limit also carried gold grade. This suggests that the absence of carbon is not necessarily an indication of poor gold grade, however the presence of carbon is an indication of favourable gold grades. The gold grade-carbon correlations determined for the reef samples also disagree with the Carbon Leader Reef facies model. The facies model proposes that the strongest correlations should be seen within the No. 1 Facies whereas the geochemical data from the reef samples suggest the strongest correlations are noted within the No. 3 Facies. Microscopically and macroscopically carbon was noted in most of the reef samples. The No. 3 Facies is typically associated with a greater amount of fly-speck carbon however it was noted that several samples from the No. 3 Facies were bearing a thin carbon seam at the base of the reef unit (Samples 17, 25 and 64). Microscopically carbon was noted to occur in masses (fly-speck carbon nodules) and in thin basal seams alongside detrital uraninite and gold grains.

Silver typically occurs as an alloy within native gold (Allan and Woodcock, 2001; Jones and Fleischer, 1969; Nesse, 2000). This was confirmed by the strong correlation noted between gold grade and the concentration of Ag within the reef samples. Ni and Co were also noted to have a strong correlation with gold grade, with the strongest correlation between Ni and Co with gold grade noted within the No. 1 Facies, with poorer correlations noted within the No. 3 Facies and the No. 2 Facies. Koglin *et al*. (2010) proposed that Ni/Co ratios and the relative gold grade may indicate a different origin of the associated pyrite grains. It was proposed that higher Ni/Co ratios accompanied by lower gold grades are typically associated with post-sedimentary pyrite (i.e. hydrothermal origin), and lower Ni/Co ratios accompanied by higher gold grades are typically associated with syn-sedimentary origin pyrite (Koglin *et al.*, 2010).

By comparing the Ni/Co ratios of the various facies types of the Carbon Leader Reef, it was noted that the No. 1 Facies had the highest Ni/Co correlation (R^2=0.8002), followed by the No. 3 Facies (R^2=0.1997), with the smallest correlation (non-existent) noted in the No. 2 Facies (R^2=0.0993). This suggests that the varying facies types have different origins according to the principles proposed by Koglin *et al.* (2010). The No. 1 Facies pyrite, with the highest Ni/Co correlation, may be of hydrothermal origin. This is confirmed microscopically by the presence of the both detrital and euhedral to anhedral (hydrothermal) pyrite grains seen within the No. 1 Facies samples. The No. 2 and No. 3 Facies pyrite was noted to be mostly detrital, with fewer euhedral to anhedral pyrite grains, accompanied by detrital uraninite and chromite grains, suggesting some level of hydrothermal activity has taken place but less so than syn-sedimentary processes that dominated the No. 2 and No. 3 Facies.

Ba concentration is also likely due to the presence of pyrite within the Carbon Leader Reef samples and corresponds to the findings of the Ni and Co correlations with gold grade, where the strongest correlation was noted within the No. 1 Facies (R^2=0.6428), followed by the No. 3 Facies (R^2=0.4204), with the poorest (non-existent) correlation with gold grade noted within the No. 2 Facies (R^2=0.0142).

The concentration of Cu in the samples is likely to be due to the presence of chalcopyrite within the Carbon Leader Reef samples. Chalcopyrite was noted in many of the Carbon Leader Reef samples, occurring as inclusions within pyrite or as independent grains within the reef matrix. The samples where chalcopyrite was noted to occur as inclusions in pyrite grains alongside independent chalcopyrite grains within the reef matrix were noted to have a lower Cu

concentration than samples that only had chalcopyrite occurring as independent grains within the reef matrix. No particular trend was noted microscopically across the facies types with regards to the presence of chalcopyrite, however the geochemical data shows the No. 3 Facies to have the poorest (non-existent) gold grade-Cu correlation (R^2=0.0122). The No. 2 Facies was noted to have the strongest gold grade-Cu correlation at R^2=0.5954, followed by the No. 1 Facies at R^2=0.1928. This suggests the presence of higher gold grade (No. 1 and No. 3 Facies) may be accompanied by lower Cu concentrations, with lower gold grade (No. 2 Facies) accompanied by higher Cu concentrations.

The average gold assay and trace element analyses for the hangingwall, footwall, average of all the Carbon Leader Reef facies types combined as well as the average for each facies type (No. 1 Facies, No. 2 Facies and No. 3 Facies) are shown in Figure 3.61.

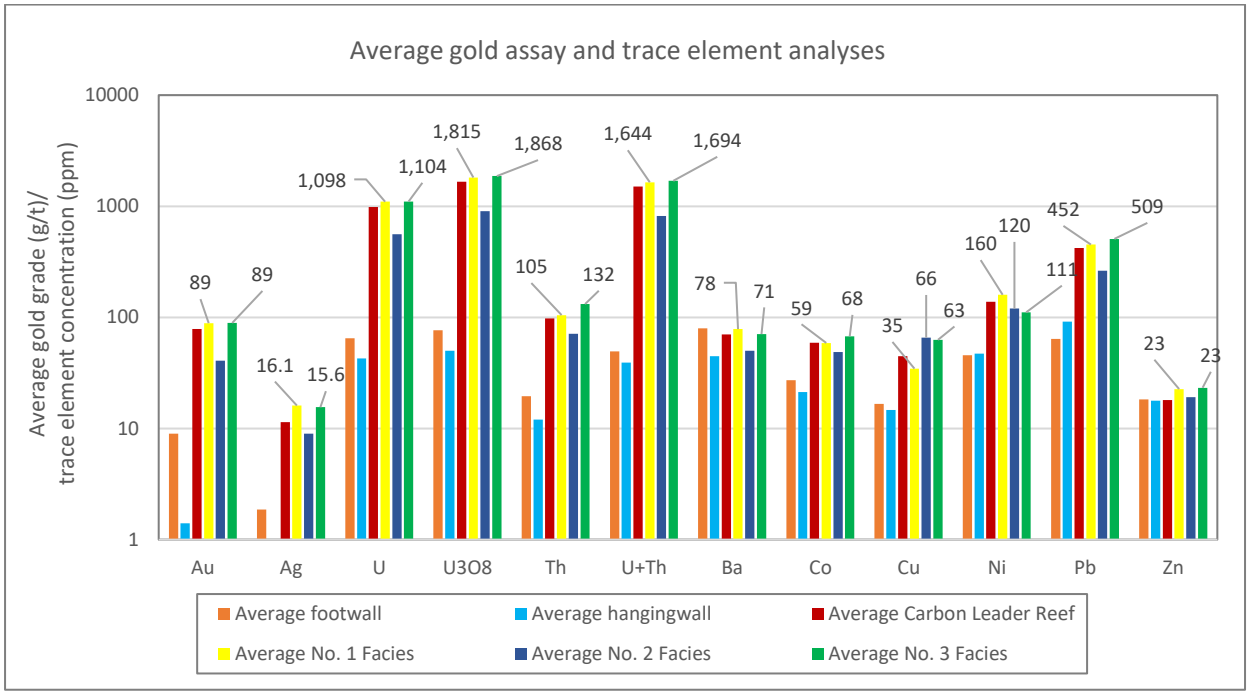

***Figure 3.61**: The average gold assay and trace element analyses for the hangingwall, footwall, Carbon Leader Reef average, No. 1 Facies, No. 2 Facies and No. 3 Facies. The data labels above the plotted bars indicate the highest average concentrations for the Carbon Leader Reef units.*

Comparing the hangingwall and footwall quartzites with the Carbon Leader Reef and the facies types there are distinct differences in the gold grade and the concentration of Ag, U, U_3O_8, Th, U + Th, Co, Cu, Ni and Pb.

Additional to the trace elements, major element oxides were also determined for the Carbon Leader Reef samples. The major oxides (geochemically and microscopically) show fewer

correlations with gold grade in comparison to the trace elements that have visibly stronger correlations with gold grade.

Figure 3.62 below shows the average major element oxide compositions for the hangingwall, footwall and the Carbon Leader Reef (average of all Carbon Leader Reef facies types), No. 1 Facies, No. 2 Facies and No. 3 Facies.

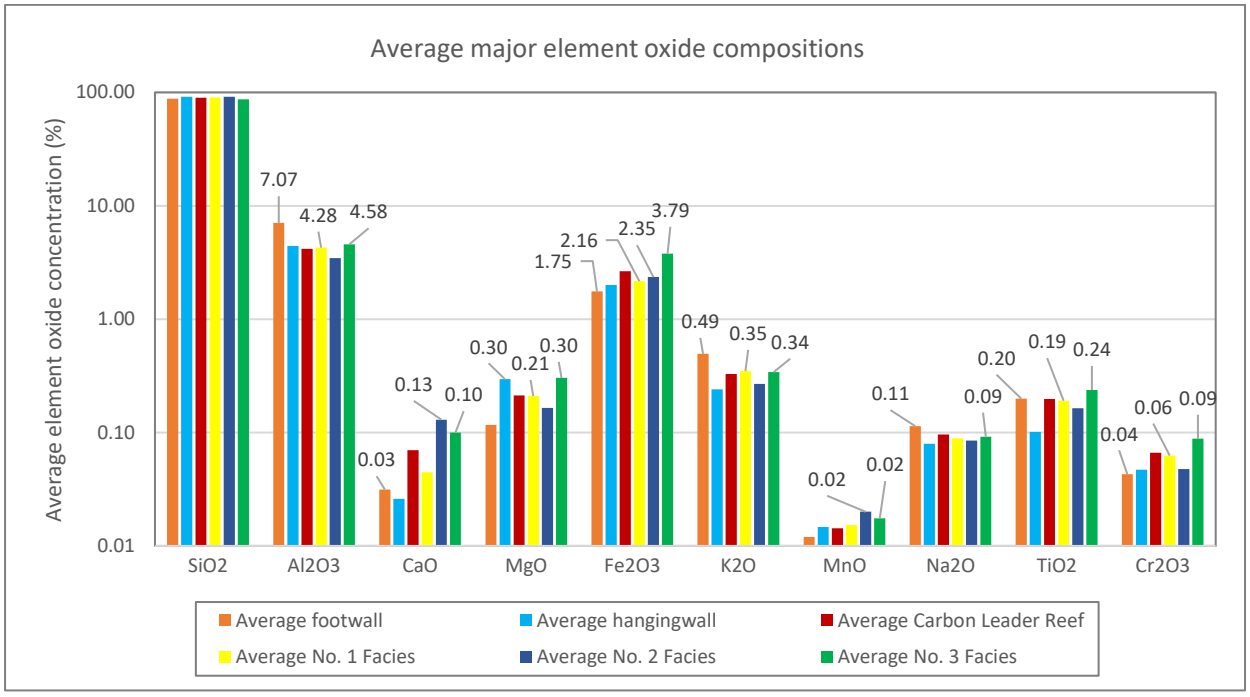

***Figure 3.62**: The average major element compositions for the hangingwall, footwall, Carbon Leader Reef average, No. 1 Facies, No. 2 Facies and No. 3 Facies. The data labels above the plotted bars indicate the highest average element oxide concentrations for the various units.*

Element oxides that show an increase from the footwall to the hangingwall include SiO_2 and Fe_2O_3, indicating that the reef and hangingwall quartzite are enriched in quartz (more siliceous) and iron-rich minerals such as pyrite, hematite and magnetite, relative to the footwall quartzite. This was further supported by macroscopic observations, where the hangingwall quartzite and the quartz clasts within the reef were noticeably more siliceous than the footwall quartzite. Hematite grains were only noted in two reef samples: Sample 23 (No. 2B Facies) and Sample 25 (No. 3 Facies). The geochemical data agrees with the presence of iron-rich minerals such as hematite and pyrite within these representative samples, where the No. 3 Facies and No. 2 Facies averages were higher than the No. 1 Facies.

A decrease in element oxides from the footwall to the hangingwall include Al_2O_3, K_2O and Na_2O abundances. This suggests that the footwall samples contain more hydrous phyllosilicate

minerals such as sericitic muscovite and pyrophyllite in comparison to the hangingwall and reef samples. This corresponds to the macroscopic observations of the samples, where the footwall samples were argillaceous quartzites and the hangingwall samples were orthoquartzites. This was also seen in the microscopic observations, where the presence of pyrophyllite and sericitic muscovite was significantly higher in the footwall quartzite in comparison to the hangingwall quartzite and the Carbon Leader Reef (across all facies types). Pyrophyllitic alteration or sericitic alteration may have taken place in some of the samples however the geochemical data does not differentiate between the two alteration types, making it necessary to refer to microscopic observations to note higher concentrations of the two mineral types (pyrophyllite and sericitic muscovite), and confirm the potential alteration by referring to the spectral scanning results (Chapter 3.4).

TiO_2 concentration was noted to be high within the footwall quartzite, with a decrease in concentration within the hangingwall quartzite. Elevated average concentrations were noted in the No. 1 and No. 3 Facies, suggesting higher concentrations of rutile and leucoxene within the No. 1 and No. 3 Facies. Only three reef samples did not have rutile and leucoxene present in both microscopic observations and geochemical data (confirmed by means of XRD analysis): Sample 11 (No. 2 Facies), Sample 21 (No. 3 Facies) and Sample 28 (No. 1 Facies). This may indicate that these samples did not undergo the same alteration as the other samples that were observed.

There was an increase in MgO concentration from the footwall quartzite to the hangingwall quartzite. The increasing concentration of MgO suggests the amount of chlorite and chloritoid in the reef and hangingwall quartzite was higher in comparison to the footwall quartzite. This corresponds with what was seen in the microscopic observations. Chloritisation may have taken place in some of the samples and may be identifiable by macroscopic observations as well as within thin section, where the modal abundance of chlorite and chloritoid were significantly higher than the presence of sericitic muscovite and pyrophyllite, however spectral scanning can be used to confirm potential alteration that has taken place.

Elevated concentrations of CaO (indicator oxide for calcite) and Cr_2O_3 (indicator oxide for chromite) were noted within the reef samples in comparison to the hangingwall and footwall quartzites, suggestive of higher calcite and chromite concentrations within the reef samples.

The high average concentrations of Cr_2O_3 in the reef samples were consistent with its sedimentological setting (i.e. a heavy mineral trap) (Fuchs *et al*., 2016) and correspond to the observation of detrital chromite grains in the reef thin section samples.

Overall, the correlation between gold grade against radioactive trace elements (U, U_3O_8, U +Th and Pb) was stronger than the correlation between gold grade and the non-radioactive trace elements (Ba, Cu, Co and Ni) and even less so against the major oxide elements. This suggests that radioactivity is a more reliable means of following gold grade than alteration.

3.4 SPECTRAL SCANNING OBSERVATIONS

Prior to the commencement of this research, 18 of the 19 tombstone samples as well as 36 of the 49 boreholes made available by AngloGold Ashanti were scanned for spectral analysis. The tombstones were spectrally scanned by a hand-held spectrometer (the TerraSpec®), and the boreholes were spectrally scanned using a hyperspectral core imager (the sisuROCK®). The spectral scanning of the tombstones and the boreholes was supervised by Mr. P. Linton and was carried out at the AngloGold Ashanti Geoscience Technical Offices based in Carletonville.

The raw spectral data from the spectral analyses for the boreholes, as well as the already processed data for the tombstones, was made available by AngloGold Ashanti for the purpose of this research. The spectral data for each borehole includes a small portion of footwall, hangingwall and the entire Carbon Leader Reef portion, and in some instances extends further into the hangingwall units (Rice Pebble Marker and the Green Bar). The tombstone spectral images extend from the immediate footwall, to the Carbon Leader Reef, through to the immediate hangingwall. The results from the two scanners differ slightly in colour output however the same minerals (using the same wavelengths) were scanned for (including pyrophyllite, sericite, chlorite and chloritoid).

The raw spectral data for the boreholes had not been processed nor interpreted although the initial stages of spectral scanning had been completed prior to the commencement of this study. The processing of the raw spectral data for the boreholes was carried out by TerraCore Geospectral Imaging by means of in-house spectral processing software, to produce visual image displays as well as digital data files (refer to Chapter 2.5 for more detail on the processing of raw spectral data). The processed data for the tombstones, inclusive of the visual

image displays and digital data files, were readily available and provided by AngloGold Ashanti for interpretation. The interpretation of the processed spectral data for the tombstones and the boreholes was carried out independently as part of this research, with input from Mr. K. Mushiana from TerraCore Geospectral Imaging.

Refer to Appendix 5: Tombstone Spectral Profiles as well as Appendix 6: Tombstone Spectral Images for the tombstone samples that were spectrally scanned. For the borehole samples that were spectrally scanned, refer to Appendix 7: Borehole Spectral Profiles and Appendix 8: Borehole Spectral Images. Refer to Appendix 1: Sample Locality Map, to note the location of tombstone and borehole samples that were used throughout the proceeding methodology. As with the previous methodologies used, the Carbon Leader Reef samples were grouped according to facies type.

3.4.1 Spectral Scanning Results (Tombstone samples)

The spectral profiles, using mean depth, for the hangingwall units of the tombstone samples (exclusive of Sample 4 that was not spectrally scanned, and Sample 16 that had no spectral data for the hangingwall unit) are displayed in Figure 3.63 (a). The spectral profiles for the footwall units of the tombstone samples (exclusive of Sample 4 that was not spectrally scanned) are displayed in Figure 3.63 (b). The spectral profiles are ordered by sample location extending from west to east of TauTona Mine. The mean depth of the mineral suggests the relative abundance of the mineral within the sample, i.e. higher mean depth indicates higher abundance of a mineral (Murphy *et al*., 2015). By using the spectral profiles, the abundance of pyrophyllite, sericite, chlorite and chloritoid could be determined.

The hangingwall mean depths were highest for pyrophyllite, particularly the units overlying the No. 1 and No. 2 Facies, and more so for the eastern area of TauTona Mine in comparison to the western area. The noted presence of pyrophyllite in the spectral scanning correlates well to what was seen macroscopically and geochemically for the hangingwall samples, where the highest pyrophyllite content was noted within the hangingwall units overlying the No. 1 Facies with the lowest pyrophyllite content noted within the hangingwall units overlying the No. 3 Facies.

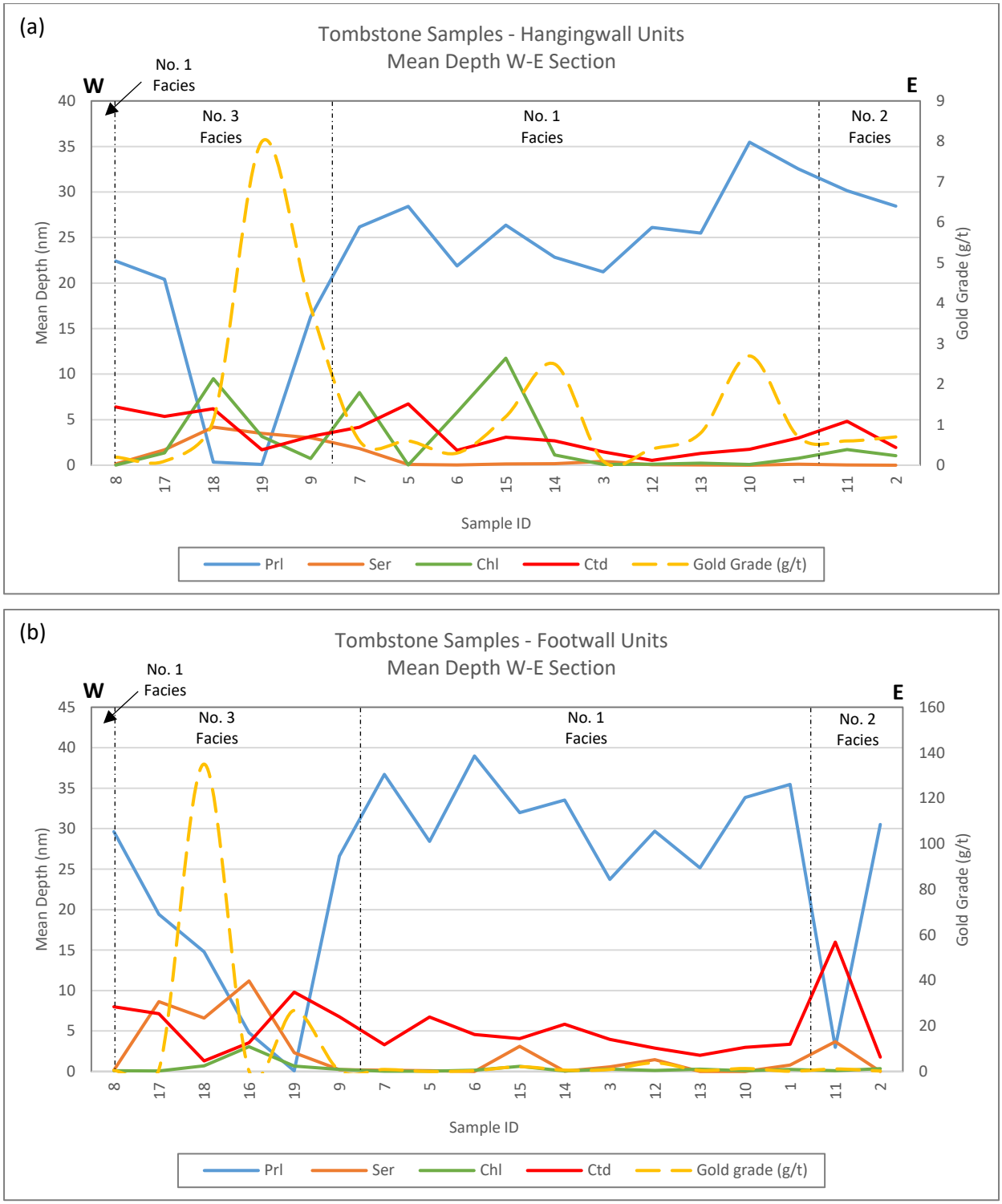

***Figure 3.63**: (a) Spectral mean depths (nm) of pyrophyllite (Prl), sericite (Ser), chlorite (Chl) and chloritoid (Ctd) of the hangingwall units overlying the Carbon Leader Reef in west-east section across TauTona Mine, plotted against gold grade (g/t); (b) Spectral mean depths (nm) of pyrophyllite (Prl), sericite (Ser), chlorite (Chl) and chloritoid (Ctd) of the footwall units underlying the Carbon Leader Reef in west-east section across TauTona Mine, plotted against gold grade (g/t).*

Chlorite was noted to have a low to moderate response to the chlorite feature extraction within the hangingwall samples. The highest responses to the chlorite feature extraction were

noted to occur within the hangingwall units overlying the No. 1 and No. 3 Facies, particularly in the No. 3 Facies. This corresponded well to the findings microscopically and geochemically, where the chlorite concentration was noticeably higher in the hangingwall samples overlying the No. 3 Facies, with lessor chlorite concentration in the samples overlying the No. 1 Facies.

Chloritoid was noted to have a greater response to the chloritoid feature extraction to the western portion of TauTona, suggesting a higher abundance in hangingwall samples from this area of the mine in comparison to the eastern portion of TauTona Mine. Chloritoid was not noted within the microscopic observations of the hangingwall, however geochemically the %MgO may be a combination of the presence of chlorite and chloritoid within the hangingwall units.

Sericite had the lowest mean depths recorded across the mine, with slightly higher responses to the feature extraction noted within the western area of TauTona Mine, particularly within the samples overlying the No. 3 Facies. This suggests the hangingwall samples are more sericitic in the west of TauTona, becoming less sericitic towards the east of TauTona Mine. Geochemically and microscopically there was not a noticeable trend with regards to the presence of sericite (sericitic muscovite) within the hangingwall samples.

As with the hangingwall samples, the footwall samples had the highest spectral response noted for pyrophyllite, particularly for the samples underlying the No. 1 and No. 3 Facies. Microscopically and geochemically, the data agrees with the spectral findings. Sericite had a low response in the samples underlying the No. 1 and No. 2 Facies, with a low to moderate response noted within the samples underlying the No. 3 Facies. This suggests a higher abundance of sericite within the No. 3 Facies, with the western portion of TauTona Mine having favourable sericite abundance in comparison the east of TauTona. Geochemically it was noted for the footwall samples that samples with higher $\%Al_2O_3$ were noted to be overlain by predominantly the No. 1 Facies, followed by the No. 3 Facies. Microscopically the footwall samples showed similar sericitic muscovite abundances in the No. 1 and No. 3 Facies. The discrepancies noted between the spectral scanning data and the geochemical/microscopic observations may be due to the greater intervals the TerraSpec® has for readings, and a clearer perspective may be provided if smaller intervals were used. It is also suggested that the presence of organic material may influence the spectral facies image and create spectral

variation (Harris, 2006b, p.100). The presence of carbon within the No. 1 and No. 3 Facies of the Carbon Leader Reef, and the proximity of the footwall to the basal carbon seam within the No. 1 Facies may affect the spectral responses for the footwall samples.

Chloritoid had a low to moderate response to the chloritoid feature extraction across TauTona Mine. A peak response was noted within the No. 2 Facies for the footwall unit of Sample 11. Microscopically no chloritoid was noted within thin section however geochemically the largest %MgO was noted in Sample 11 (0.37% MgO), suggesting the presence of chloritoid accounts for the %MgO, with lesser amounts of chlorite within the sample. Chlorite had the lowest spectral response overall. This agrees with the geochemical and microscopic observations, where the overlying hangingwall units are chlorite-rich in comparison to the underlying footwall units. No definite trend could be determined between the spectral responses and gold grade for both the hangingwall and footwall (tombstone) samples.

The hangingwall and footwall units had much higher mean depths recorded for pyrophyllite in comparison to the Carbon Leader Reef (Figure 3.64). A peak in the pyrophyllite response was noted within the No. 2 Facies to the east of TauTona Mine. The hangingwall units had much lower mean depths recorded for sericite than within the Carbon Leader Reef units, and the footwall units had the highest mean depths for sericite recorded in the westernmost portion of TauTona Mine. In comparison to the hangingwall units, the Carbon Leader Reef had a lower overall response to the chlorite feature extraction however the response was greater than what was noted within the footwall. This suggests the concentration of chlorite was greatest within the hangingwall units, followed by the Carbon Leader Reef. The greater presence of chlorite within the hangingwall units in comparison to the Carbon Leader Reef and the footwall units, was also confirmed microscopically and geochemically. Similarly to the hangingwall units, the Carbon Leader Reef had a low to moderate response to the chloritoid feature extraction across TauTona Mine. A small increase was noted in the chloritoid response on the western portion of the mine, and this was similarly seen in the overlying hangingwall units and underlying footwall units in the west of TauTona. The higher response to the chloritoid feature extraction in the westernmost area of TauTona may indicate a higher abundance of chloritoid within the area.

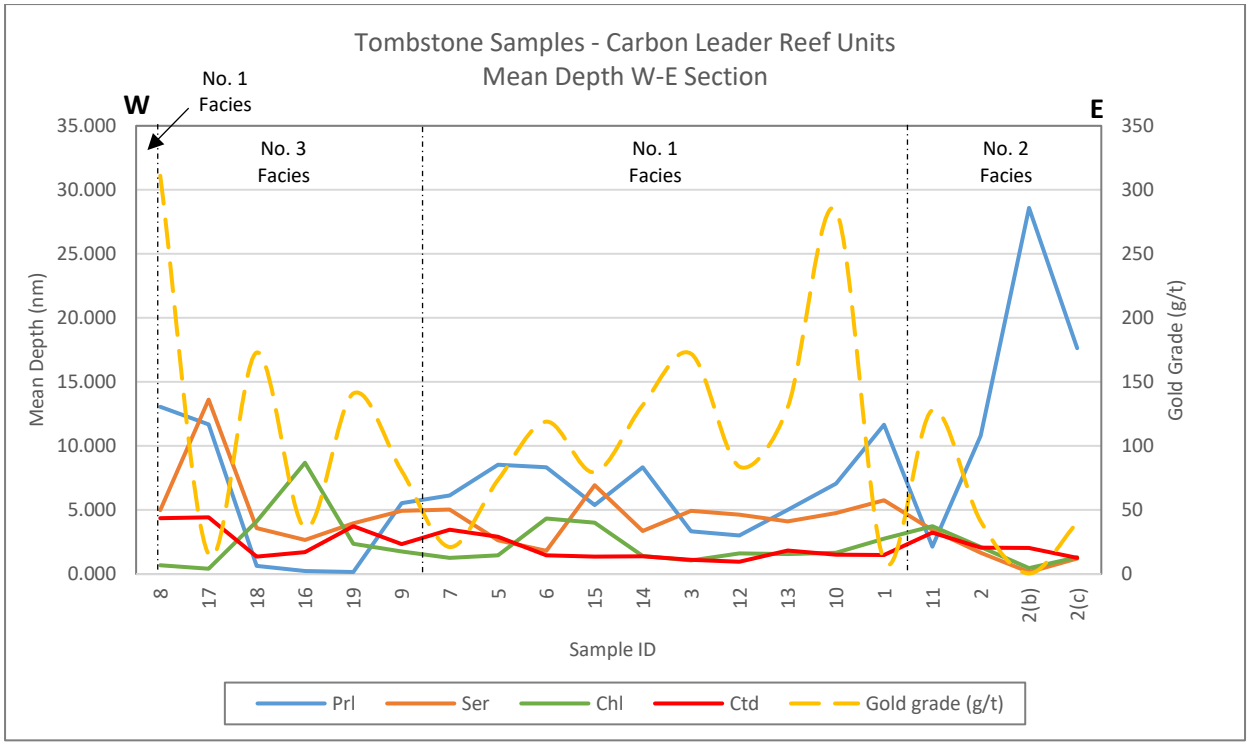

***Figure 3.64**: Spectral mean depths (nm) of pyrophyllite (Prl), sericite (Ser), chlorite (Chl) and chloritoid (Ctd) of the Carbon Leader Reef units in west-east section across TauTona Mine, plotted against gold grade (g/t).*

Focusing on the Carbon Leader Reef units of the tombstones, the mean depth of chlorite and chloritoid was similar across all samples. A few elevated mean depths for chlorite were seen in Samples 6, 11, 15, 16 and 18, with the highest mean depth noted to occur in Sample 16 (No. 3 Facies). On average, the highest responses against the chlorite feature extractions were noted within the No. 3 Facies, with lessor responses in the No. 1 Facies. This was also seen in the microscopic modal abundances of the reef samples, as well as within the geochemical data where the No. 3 Facies had the higher chlorite and %MgO concentrations, followed by the No. 1 Facies.

Elevated mean depths for chloritoid were noted in Samples 5, 7, 8, 11, 17 and 19, with the highest mean depth noted to occur in Sample 17 (No. 3 Facies). Sample 17 had a noticeably greater concentration of chloritoid present in thin section in comparison to the other reef (tombstone) samples and this correlated well with the spectral scanning data. The highest responses against the chloritoid feature extractions were noted within the No. 3 Facies, followed by the No. 2 Facies, suggesting the lowest abundance of chloritoid occurs within the No. 1 Facies. This contradicts the modal abundances noted for the Carbon Leader Reef samples as the No. 2 Facies had lower chloritoid presence within thin section. As previously mentioned,

the presence of organic material may create spectral variation in the spectral outputs. The presence of carbon within the No. 1 and No. 3 Facies may be responsible for the discrepancies between the microscopic, geochemical and spectral data observations.

Higher mean depths of sericite were seen in the No. 1 and No. 3 Facies, with very low mean depths recorded in the No. 2 Facies samples, suggesting lower concentrations of sericite within the No. 2 Facies samples. This is in agreement with the microscopic and geochemical observations for the Carbon Leader Reef (tombstone) samples.

Samples from the No. 3 Facies, on average, had the higher gold grades followed by the No. 1 Facies with moderate to high gold grades, and the No. 2 Facies had the lowest gold grades. As with the hangingwall and footwall units of the tombstone samples, no definite trend could be determined between the spectral responses and gold grade.

To supplement the spectral profiles the spectral images can be referred to (and vice versa). The spectral images for Sample 3 (No. 1 Facies) are seen in Table 3.13.

Table 3.13: A spectral facies image as well as spectral responses to the pyrophyllite, sericite, chlorite and chloritoid feature extractions for Sample 3 – including the hangingwall (HW), footwall (FW) and a footwall pebble band (FWPB). The legend for the spectral facies image has been included below the images. Cooler colours (shades of dark purple and blue) indicate a low response to the feature extraction, and warmer colours (shades of green, orange and red) indicate a moderate to high response to the feature extraction.

Spectral Facies Image	Pyrophyllite (λ = 2 165 nm)	Sericite (λ = 2 200 nm)	Chlorite (λ = 2 250 nm)	Chloritoid (λ = 2 390 nm)
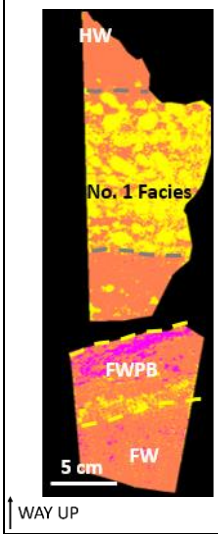	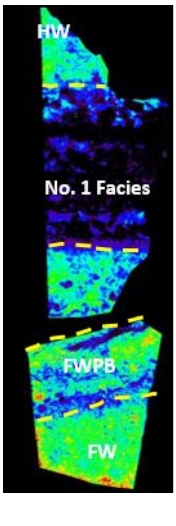	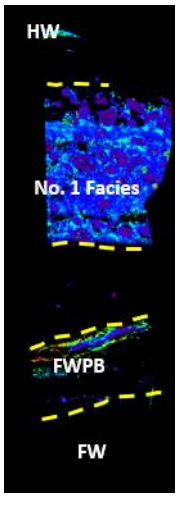	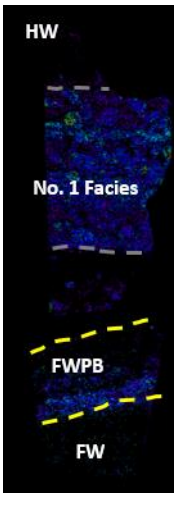	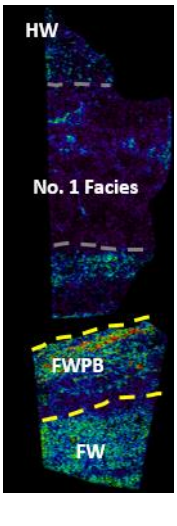

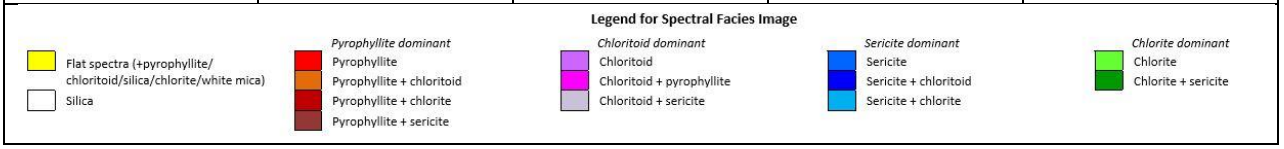

With reference to Table 3.13 (and additional spectral facies imaging tables throughout this Chapter), the cooler colours (dark purple and shades of blue) indicate a low response to the feature extraction i.e. low abundance of that mineral. Warmer colours (green, orange and red) indicate a moderate to high response to the feature extraction i.e. a moderate to high abundance of that mineral.

Referring back to Figure 3.63 (a), Figure 3.63 (b) and Figure 6.64 the spectral profiles for Sample 3 show a low response to the chloritoid and chlorite feature extraction, and a low to moderate response to the sericite and pyrophyllite feature extractions for the reef unit of the tombstone. Very low responses were noted within the hangingwall unit for sericite, chlorite and chloritoid, with a very high response noted against the pyrophyllite feature extraction. Very low responses were noted within the footwall unit for sericite and chlorite, with a low response to the chloritoid feature extraction. The highest response was noted against the pyrophyllite feature extraction.

In comparison to the spectral profiles, the classification image shows a pyrophyllite + chloritoid combination (pyrophyllite dominant) occurring interstitially between silica-rich clasts however, when combining the moderate response to the sericite feature extraction it can be said that the matrix has a moderate amount of sericite alongside pyrophyllite. The hangingwall and footwall units were highly responsive to the pyrophyllite feature extraction, with a much lower response seen from the sericite and chlorite feature extractions. The footwall unit only had a slight response to the chloritoid feature extraction.

The mean depths for each feature extraction correlates well with what was seen in the spectral images (Table 3.14). Although the responses to the feature extractions in this sample for the reef were low to moderate, the gold grade was high (at 172.0 g/t).

Table 3.14: Spectral mean depths (nm) against the pyrophyllite, sericite, chlorite and chloritoid feature extractions as well as gold grade (g/t) for comparison – Sample 3.

Unit	Mean Depth (nm)				Gold grade (g/t)
	Pyrophyllite	Sericite	Chlorite	Chloritoid	
Hangingwall	21.219	0.435	0.083	1.466	0.1
No. 1 Facies	3.332	4.937	1.064	1.117	172.0
Footwall	23.734	0.562	0.295	3.959	0.9

The spectral profiles for Sample 11 (No. 2A Facies) show a very low mean depth for sericite in the hangingwall unit, with a low mean depth in the footwall and Carbon Leader Reef units. Low

responses were also noted within the hangingwall unit for chlorite and chloritoid, chlorite within the footwall unit, as well as for chlorite, chloritoid and pyrophyllite within the Carbon Leader Reef unit. A very high response was noted within the hangingwall unit and on the opposite spectrum, the footwall was noted to have a low response to the pyrophyllite feature extraction, but the footwall's response was slightly greater than that of the reef unit.

The spectral images of Sample 11 can be seen in Table 3.15. The reef is chlorite-rich with a smaller amount of pyrophyllite than sericite and chloritoid within the matrix. The response of the hangingwall unit to the pyrophyllite feature extraction was much higher than the reef and footwall units. There was very little response from the sericite feature extraction in the hangingwall, with moderate responses from the reef and footwall units. A moderate to high response to the chlorite feature extraction was noted within the hangingwall and reef units, with very little response in the footwall. The footwall was highly responsive to the chloritoid feature extraction, suggesting a higher abundance of chloritoid than with the hangingwall and Carbon Leader Reef units.

Table 3.15: A spectral facies image as well as spectral responses to the pyrophyllite, sericite, chlorite and chloritoid feature extractions for Sample 11 – including the hangingwall (HW) and footwall (FW). The legend for the spectral facies image has been included below the images. Cooler colours (shades of dark purple and blue) indicate a low response to the feature extraction, and warmer colours (shades of green, orange and red) indicate a moderate to high response to the feature extraction.

Spectral Facies Image	Pyrophyllite (λ = 2 165 nm)	Sericite (λ = 2 200 nm)	Chlorite (λ = 2 250 nm)	Chloritoid (λ = 2 390 nm)
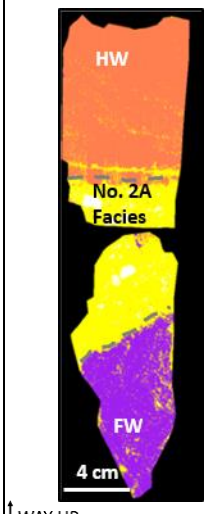	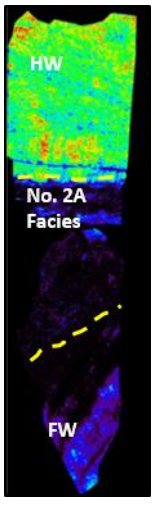	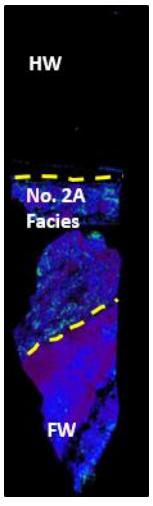	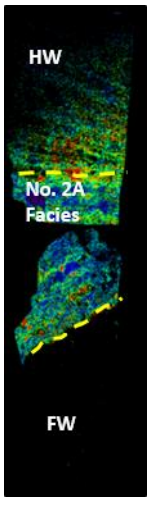	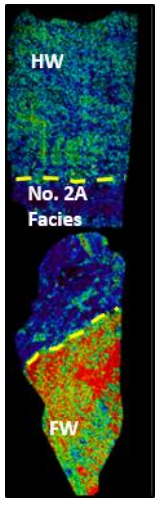

The mean depths for each feature extraction correlates well with what was seen in the spectral images (Table 3.16).

Table 3.16: Spectral mean depths (nm) against the pyrophyllite, sericite, chlorite and chloritoid feature extractions as well as gold grade (g/t) for comparison – Sample 11.

Unit	Mean Depth				Gold grade (g/t)
	Pyrophyllite	Sericite	Chlorite	Chloritoid	
Hangingwall	30.133	0.022	1.710	4.817	0.6
No. 2A Facies	2.129	3.447	3.746	3.233	128.0
Footwall	2.980	3.690	0.107	15.984	1.1

Although the responses of the reef to the feature extractions were relatively low, the gold grade was moderate (128.0 g/t). The No. 3 Facies sample with the highest grade (Sample 8) spectral images can be seen in Table 3.17.

Table 3.17: A spectral facies image as well as spectral responses to the pyrophyllite, sericite, chlorite and chloritoid feature extractions for Sample 8 – including the hangingwall (HW) and the footwall (FW). The legend for the spectral facies image has been included below the images. Cooler colours (shades of dark purple and blue) indicate a low response to the feature extraction, and warmer colours (shades of green, orange and red) indicate a moderate to high response to the feature extraction.

Spectral Facies Image	Pyrophyllite (λ = 2 165 nm)	Sericite (λ = 2 200 nm)	Chlorite (λ = 2 250 nm)	Chloritoid (λ = 2 390 nm)
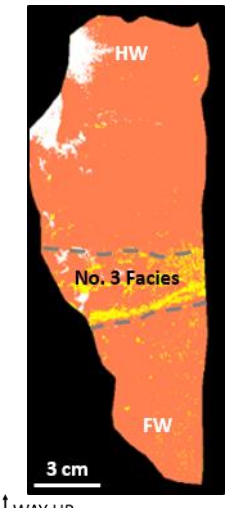	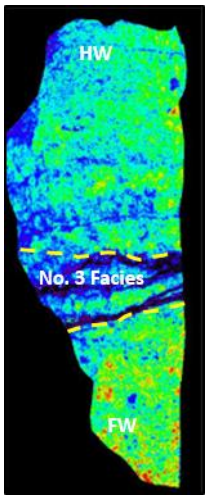	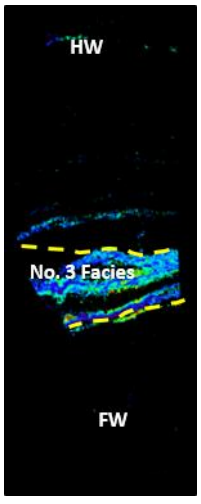	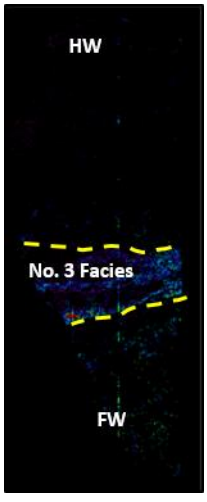	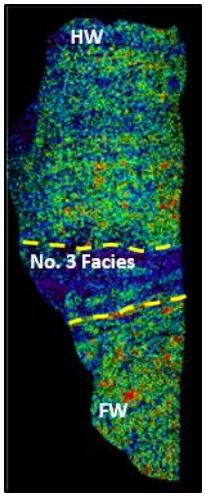

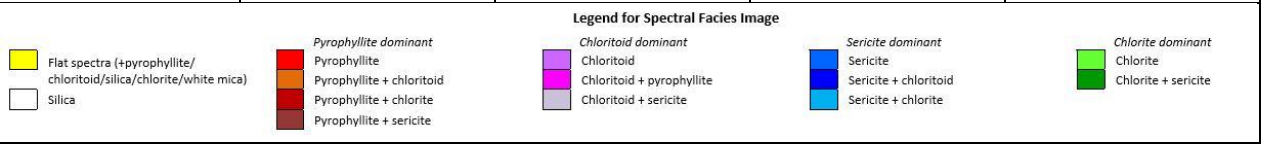

The spectral profiles for Sample 8 show low responses to the chlorite and sericite feature extractions within the hangingwall and footwall units, with a low response to the chloritoid feature extraction and a very high response to the pyrophyllite feature extraction in both units. The Carbon Leader Reef had a low response to the chlorite feature extraction, a low response

to the chloritoid and sericite feature extractions and a moderate response to the pyrophyllite feature extraction.

The spectral images of Sample 8 show the matrix within the reef has a (dominant) pyrophyllite + chloritoid combination alongside sericite. Set within the matrix are silica-rich clasts. The small portion of internal quartzite within the reef without large quartz clasts was highly responsive to the pyrophyllite feature extraction in comparison to the matrix. The footwall had the highest response to the pyrophyllite feature suggesting higher amounts of pyrophyllite are found within the footwall unit. A moderate response to the sericite feature extraction was seen in the reef as well as a vein-like feature within the hangingwall. A low response was seen from the chlorite feature extraction, with almost no response seen from the hangingwall and footwall units. The response to the chloritoid feature extraction was moderate to high within the hangingwall and footwall, with a low to moderate response seen in the reef. This suggests that higher amounts of chloritoid are found within the hangingwall and footwall units in comparison to the reef. The mean depths for each feature extraction correlates well with what was seen in the spectral images (Table 3.18). As with Sample 3 and Sample 11, although the responses to the feature extractions are low the gold grade was very high (311.0 g/t).

Table 3.18: Spectral mean depths (nm) against the pyrophyllite, sericite, chlorite and chloritoid feature extractions as well as gold grade (g/t) for comparison – Sample 8.

Unit	Mean Depth				Gold grade (g/t)
	Pyrophyllite	Sericite	Chlorite	Chloritoid	
Hangingwall	22.426	0.132	0.014	6.403	0.2
No. 3 Facies	13.058	4.993	0.695	4.366	311.0
Footwall	29.616	0.152	0.105	8.001	0.5

The remaining tombstone samples can be referred to in Appendix 5 and Appendix 6. It was interesting to note for most of the tombstone samples that the higher gold grades were accompanied by lower responses to the feature extractions, with the lower gold grades accompanied by higher responses to the feature extractions.

Higher responses to the feature extractions may suggest alteration has taken place, further suggesting that in samples where alteration has taken place lower gold grades may be found. Lower responses indicate less alteration has taken place, and these samples are accompanied by higher gold grades.

3.4.2 Spectral Scanning Results (Borehole samples)

The spectral images for the boreholes have less detail than what was seen in the tombstone samples, but the spectral outcome is not affected. Smaller intervals were used during scanning, allowing for a spectral profile extending across several units within the borehole/borehole tray(s). The gold grades shown in the borehole spectral profiles are representative of the assay result determined during the initial sampling phase of the boreholes by AngloGold Ashanti. These have been used instead of the gold grades reported in Chapter 3.3 because most of the boreholes scanned were not available for resampling, thus limiting the number of boreholes with reported gold grade. The boreholes that were sampled and assayed by SGS for the purpose of this research have very similar, if not the same, gold grade reported in the spectral profiles.

The spectral images of Sample 30 (No. 1 Facies) can be seen in Table 3.19. The Carbon Leader Reef had both pyrophyllite + chlorite and pyrophyllite + sericite combinations (i.e. pyrophyllite dominant). The high response to the pyrophyllite feature extraction indicates a large presence of pyrophyllite within the reef. A moderate response to the sericite and chlorite feature extractions was seen, with very little to no response to the chloritoid feature extraction for the reef.

Microscopically and geochemically it was noted that there were chloritoid laths within Sample 30, and the chloritoid modal abundance was greater than that of chlorite, and on par with the pyrophyllite and sericitic muscovite content. In the spectral facies image, the hangingwall unit had chloritoid + pyrophyllite and chloritoid combinations with flat spectra which may be indicative of pyrophyllite, chloritoid, silica, chlorite or white mica. By referring to the feature extraction images it is most likely that the flat silica is representative of sericite or chloritoid within the hangingwall unit, as the images show the greatest responses to these feature extractions.

Within the spectral facies image, the footwall unit had predominantly chloritoid + pyrophyllite, with a pyrophyllite + sericite combination nearer to the contact with the Carbon Leader Reef. The feature extraction images suggest pyrophyllite as the dominant mineral alongside sericite and chlorite nearer to the contact with the reef. Pyrophyllite and chloritoid occur alongside

each other further away from the reef contact. As with the tombstone samples, the spectral profiles of the boreholes can be used to supplement the findings within the spectral image outputs of the boreholes (and vice versa).

Table 3.19: A spectral facies image as well as spectral responses to the pyrophyllite, sericite, chlorite and chloritoid feature extractions for Sample 30 – including the Green Bar (GB), Rice Pebble Marker (RPM), hangingwall (HW) and footwall (FW). The legend for the spectral facies image has been included below the images. Cooler colours (shades of dark purple and blue) indicate a low response to the feature extraction, and warmer colours (shades of green, orange and red) indicate a moderate to high response to the feature extraction.

Spectral Facies Image	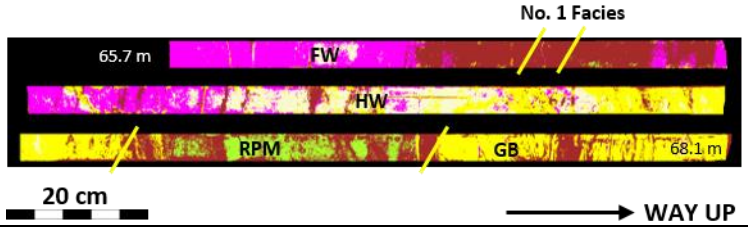
Pyrophyllite (λ=2165 nm)	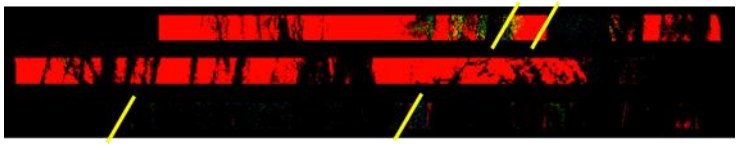
Sericite (λ=2200 nm)	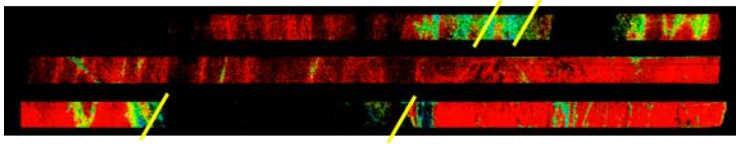
Chlorite (λ=2250 nm)	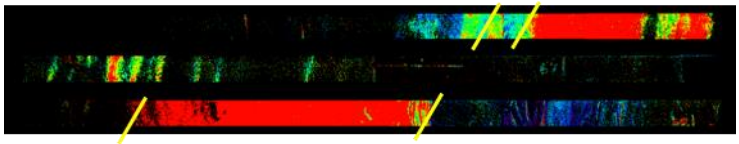
Chloritoid (λ=2390 nm)	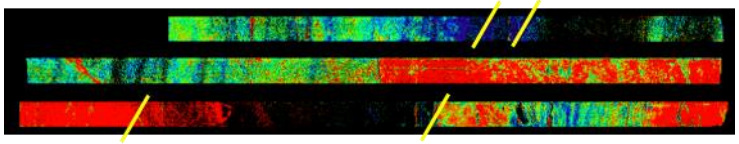
	

The spectral profiles of Sample 30 are shown in Figure 3.65. The highest mean depth for pyrophyllite was recorded for the No. 1 Facies, which correlates with what was noted in the spectral image. Moving from the footwall unit to the reef there was a drop in mean depth for sericite that increases at the hangingwall again. This corresponds to the red colouring (high

response) seen in the sericite spectral image either side of the reef. Chlorite had a zero mean depth, contradicting the moderate response seen against the chlorite feature extraction in the spectral image. This may be due to mineral mixtures within the spectral index (feature extraction) images (Harris, 2006b, p.101; Hauff, 2001, p.2). Mineral mixtures can change the spectral response in various ways and is commonly noted to result in suppressing the contrast which changes the depth characteristics of the spectra and ultimately affecting the representation of the spectral abundance of the sample (Harris, 2006b, p.101). Chlorite was noted microscopically and geochemically for Sample 30 within the Carbon Leader Reef however the response was extremely low in the spectral profile, suggesting there may be interference due to the mineral mixtures of the sample.

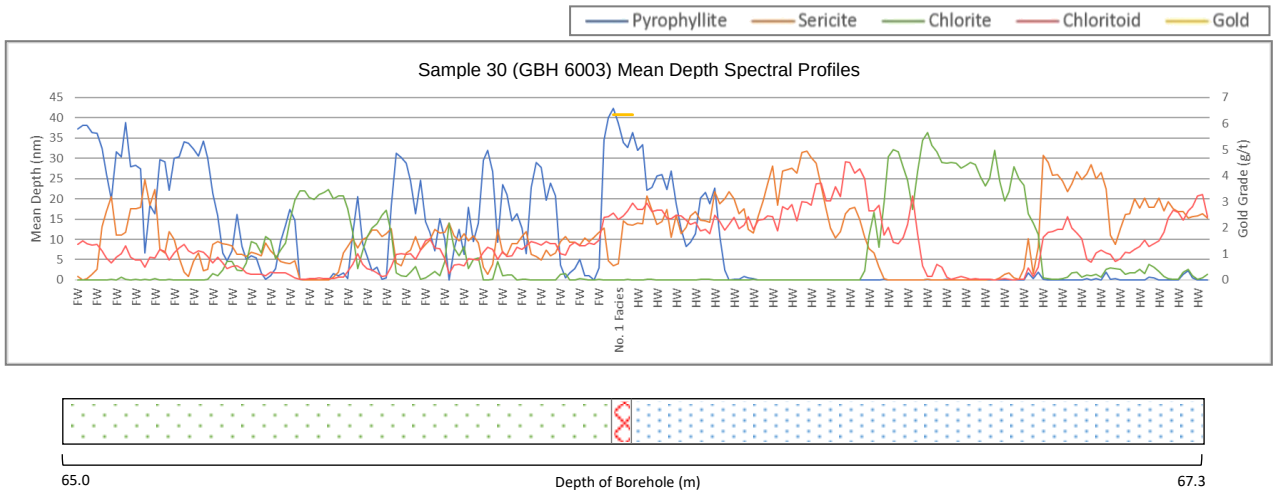

***Figure 3.65**: Spectral mean depth (nm) profiles against the pyrophyllite, sericite, chlorite and chloritoid feature extractions – Sample 30. The profiles include the underlying footwall (FW) unit and the overlying hangingwall (HW) unit. A borehole log to show the relative depth of the borehole and the sedimentological unit(s) underlies the spectral profiles.*

From the footwall to the hangingwall there was a gradual increase in the mean depth for chloritoid and this too contradicts the poor response seen against the chloritoid feature extraction. As with the tombstones, a much lower gold grade (6.4 g/t) was seen with higher responses to the feature extractions - particularly the pyrophyllite feature extraction.

The spectral image outputs for Sample 65 (No. 1 Facies) are shown in Table 3.20. The majority of the reef displayed flat spectra and silica responses with lessor amounts of chlorite, chlorite + sericite and sericite + chlorite combinations (i.e. chlorite dominant). Pyrophyllite had a low response in the reef and a high response within the footwall unit. The reef showed a moderate response to the sericite feature extraction in the centre portion of the unit, becoming more

responsive nearer to the footwall. The footwall unit had a high response to the sericite feature extraction closest to the reef-footwall contact, becoming gradually less responsive with proximity from the reef. The highest response to the chlorite feature extraction was noted immediately above the reef in the hangingwall unit, as well as slightly below the contact with the hangingwall. Overall, the reef was moderately responsive in comparison to the hangingwall and footwall, suggesting a higher amount of chlorite is present within the reef. The response to the chloritoid feature extraction was low in the reef, with a small moderate to high response nearer to the hangingwall contact. The hangingwall and footwall units both had higher responses to the chloritoid feature extraction, suggesting higher amounts of chlorite are present.

Table 3.20: A spectral facies image as well as spectral responses to the pyrophyllite, sericite, chlorite and chloritoid feature extractions for Sample 65 – including the hangingwall (HW) and the footwall (FW). The legend for the spectral facies image has been included below the images. Cooler colours (shades of dark purple and blue) indicate a low response to the feature extraction, and warmer colours (shades of green, orange and red) indicate a moderate to high response to the feature extraction.

Spectral Facies Image	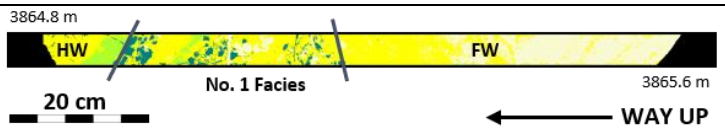
Pyrophyllite (λ=2165 nm)	
Sericite (λ=2200 nm)	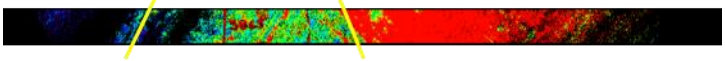
Chlorite (λ=2250 nm)	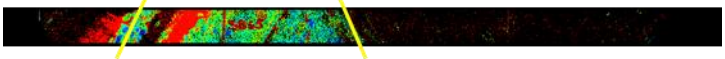
Chloritoid (λ=2390 nm)	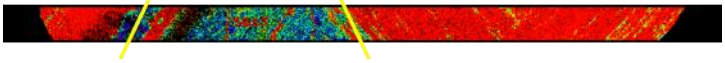
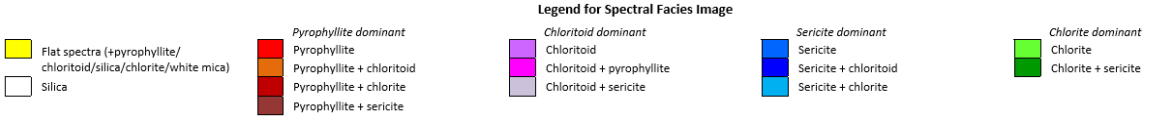	

The spectral profiles of Sample 65 are shown in Figure 3.66 (a). Both the Green Bar and Rice Pebble Marker are included in the spectral profiles however there are no corresponding spectral images to compare with.

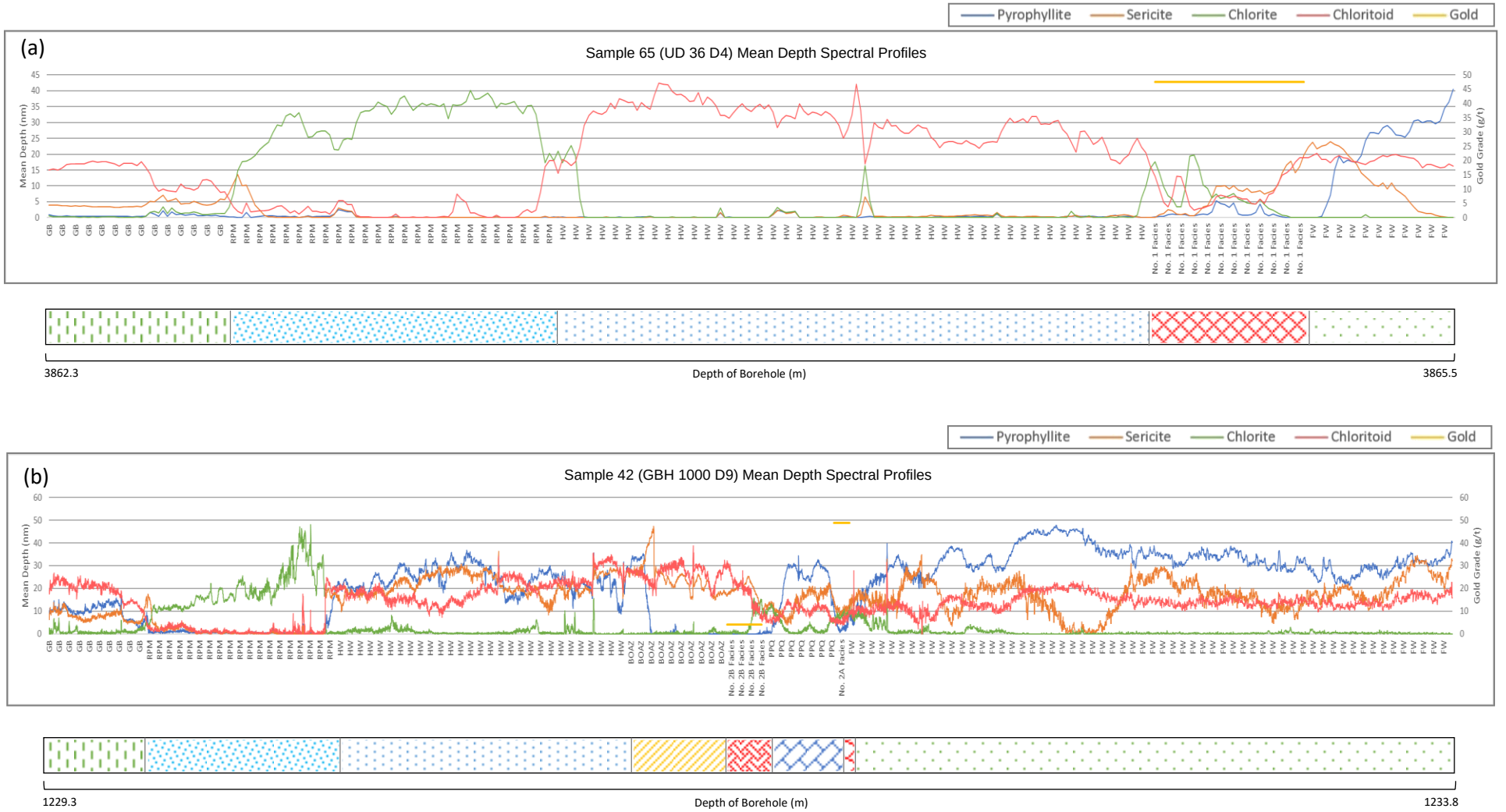

***Figure 3.66**: Spectral mean depth (nm) profiles against the pyrophyllite, sericite, chlorite and chloritoid feature extractions for (a) Sample 65 - the profiles include the Green Bar (GB), Rice Pebble Marker (RPM), hangingwall (HW) and footwall (FW); (b) Sample 42 – the profiles include the Rice Pebble Marker (RPM), hangingwall (HW), Brown-Orange Argillaceous Zone (BOAZ), Pale Pebbly Quartzite (PPQ) and footwall (FW). A borehole log to show the relative depth of the borehole and the sedimentological unit(s) underlies the spectral profiles.*

The highest mean depth for pyrophyllite was seen in the footwall, with a moderate mean depth seen in the reef and a very low mean depth in the hangingwall. This was similarly seen for sericite. The reef had the highest mean depth for chlorite. The hangingwall and footwall units had higher mean depths than the reef for chloritoid, with the hangingwall unit having greater mean depths than the footwall unit. The spectral profiles correlate well with what was seen in the spectral images. In terms of the gold grade, the mean depths were relatively low in comparison to the flanking hangingwall and footwall units. The gold grade was moderate (47.6 g/t) and the spectral profiles had similar patterns/characteristics to what was observed in the tombstones.

With reference to the Green Bar, the mean depths of both pyrophyllite and chlorite are both very low. Chloritoid had the highest mean depths across the Green Bar, suggesting there is an abundance of chloritoid. Pyrophyllite and sericite both had very low mean depths across the Rice Pebble Marker unit, with a peak in sericite closer to the Green Bar contact. Chloritoid had low mean depths and chlorite had the highest mean depths throughout the unit suggesting the Rice Pebble Marker unit has a higher abundance of chlorite than any of the other minerals scanned. No other methodologies were carried out to supplement the spectral findings of Sample 65, with the exception of macroscopic observations. This sample will be used in conjunction with the other samples that have been analysed throughout all the methodologies in close proximity to it (for example, Sample 22) to infer relationships.

The spectral images and spectral profiles for Sample 42 (No. 2 Facies) are shown in Table 3.21 and Figure 3.66 (b) respectively. Within the spectral facies image there are chloritoid + pyrophyllite and pyrophyllite combinations within both the No. 2A and No. 2B Facies. The No. 2B Facies was almost non-responsive to the pyrophyllite feature extraction whereas the No. 2A Facies had a slight response. The footwall, Pale Pebbly Quartzite, internal quartzite, and hangingwall units had a high response to the pyrophyllite feature extraction. Compared to the footwall, Pale Pebbly Quartzite and the Brown-Orange Argillaceous units the reef bands had a moderate response to the sericite feature extraction, with the No. 2B Facies having a slightly higher response than the No. 2A Facies. The Rice Pebble Marker had the highest response to the chlorite feature extraction, with a moderate to high response seen in the No. 2A and No. 2B Facies respectively. A low response to the chloritoid feature extraction was seen in the reef

bands, with the highest responses noted in the Brown-Orange Argillaceous Zone, internal quartzite, hangingwall and Rice Pebble Marker units.

Table 3.21: A spectral facies image as well as spectral responses to the pyrophyllite, sericite, chlorite and chloritoid feature extractions for Sample 42 – including the Rice Pebble Marker (RPM), hangingwall (HW), Brown-Orange Argillaceous Zone (BOAZ), Pale Pebbly Quartzite (PPQ) and the footwall (FW). The legend for the spectral facies image has been included below the images. Cooler colours (shades of dark purple and blue) indicate a low response to the feature extraction, and warmer colours (shades of green, orange and red) indicate a moderate to high response to the feature extraction.

Spectral Facies Image	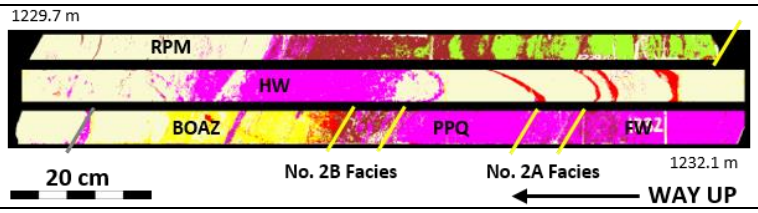
Pyrophyllite (λ=2165 nm)	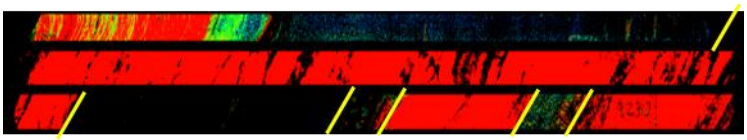
Sericite (λ=2200 nm)	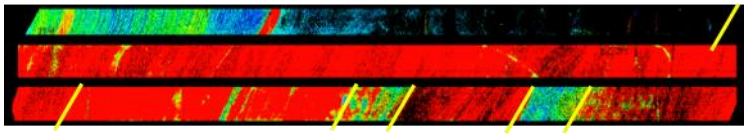
Chlorite (λ=2250 nm)	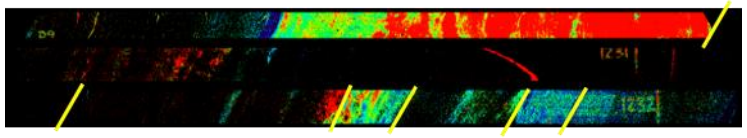
Chloritoid (λ=2390 nm)	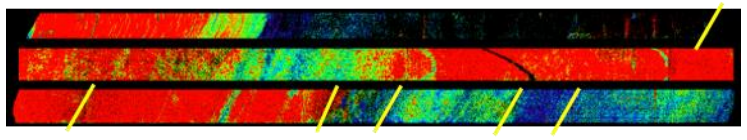
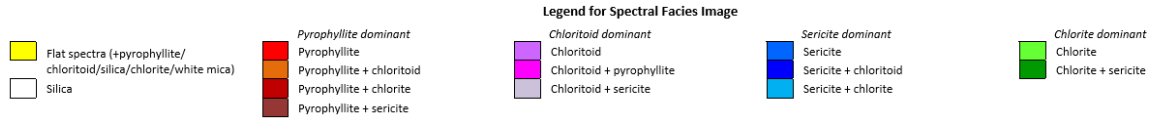	

Comparing the spectral profiles with the spectral images the chloritoid mean depths slightly contradict the spectral responses noted. The Brown-Orange Argillaceous Zone unit and both reef bands had mean depths greater than the Rice Pebble Marker although the Rice Pebble Marker was noted to have a higher response to the chloritoid feature extraction with proximity from the hangingwall. The mean depths for sericite, chlorite and pyrophyllite correspond to the

responses to the feature extractions in the spectral images. With reference to the gold grades, the No. 2A Facies (48.8 g/t) and the No. 2B Facies (3.9 g/t) had similar mean depths for pyrophyllite however the No. 2B Facies had higher mean depths for sericite, chlorite and chloritoid. As previously noted, it appears that the lower gold grade corresponds to higher mean depths and the higher gold grade corresponds to lower mean depths.

The spectral images for Sample 64 (No. 3 Facies) can be found in Table 3.22. The spectral profiles are shown in Figure 3.67 (a).

Table 3.22: A spectral facies image as well as spectral responses to the pyrophyllite, sericite, chlorite and chloritoid feature extractions for Sample 64 – including the hangingwall (HW), internal quartzite (IQ) and the footwall (FW). The legend for the spectral facies image has been included below the images. Cooler colours (shades of dark purple and blue) indicate a low response to the feature extraction, and warmer colours (shades of green, orange and red) indicate a moderate to high response to the feature extraction.

Spectral Facies Image	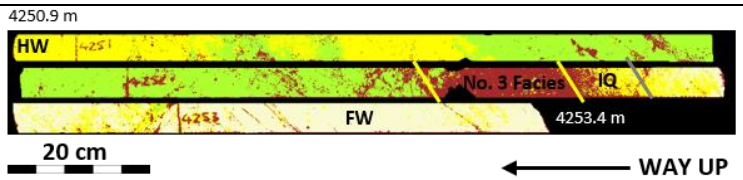
Pyrophyllite (λ=2165 nm)	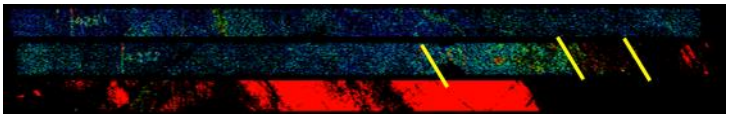
Sericite (λ=2200 nm)	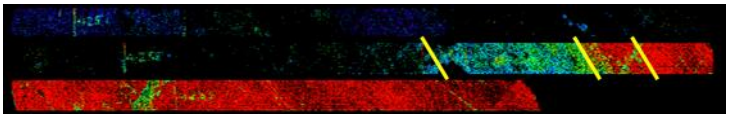
Chlorite (λ=2250 nm)	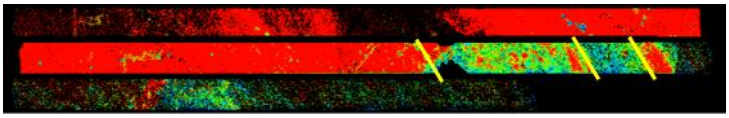
Chloritoid (λ=2390 nm)	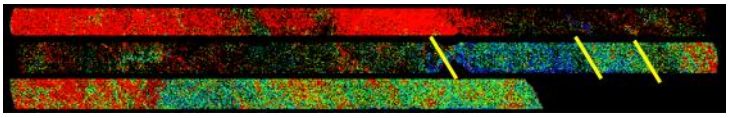
	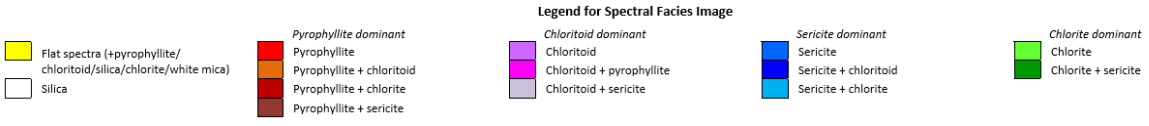

The reef is dominantly pyrophyllite + sericite with lessor amounts of chlorite and pyrophyllite. The reef had a low response to the pyrophyllite feature extraction. The highest response to the pyrophyllite feature was noted to be within the footwall unit.

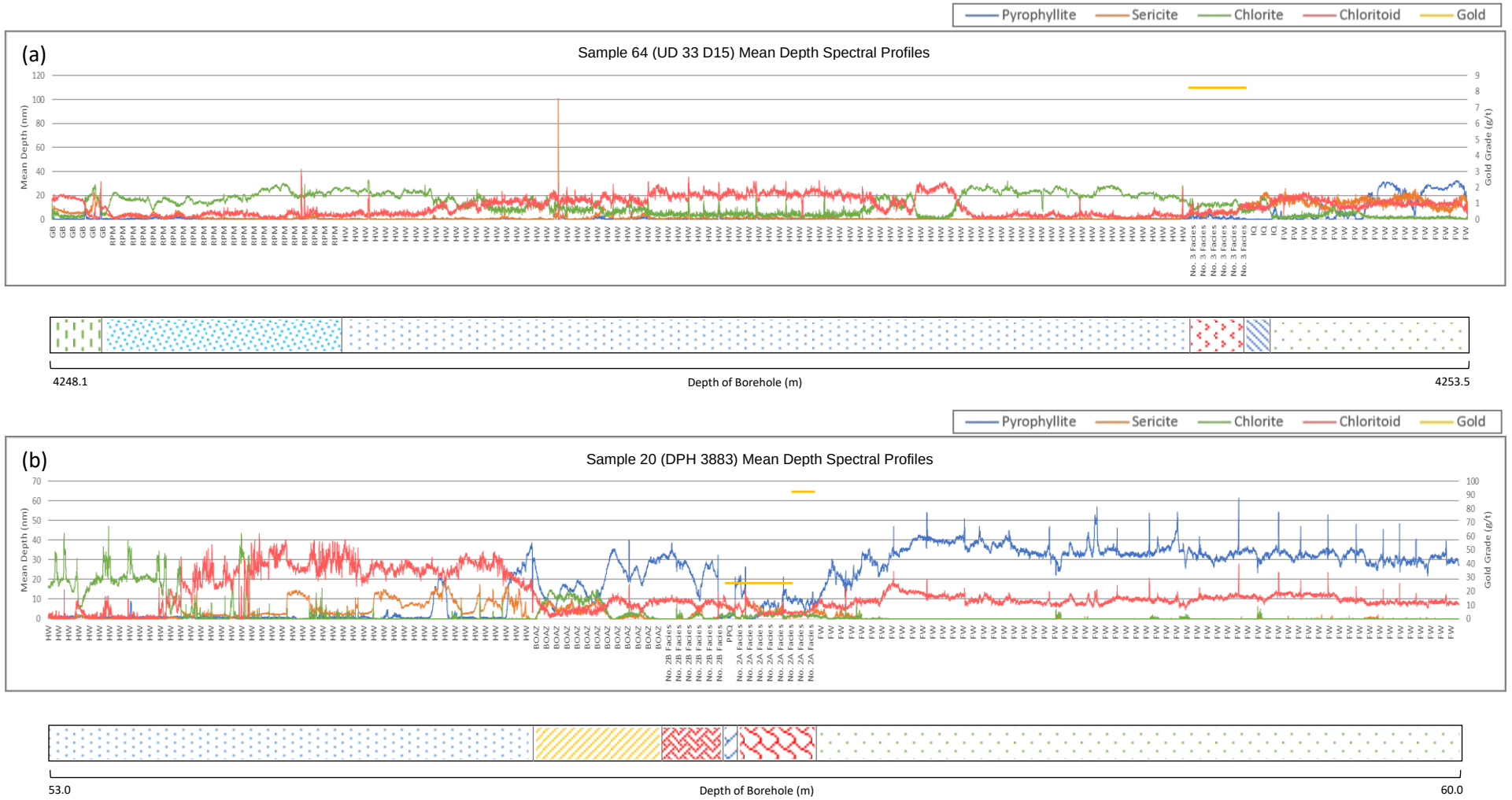

***Figure 3.67**: Spectral mean depth (nm) profiles against the pyrophyllite, sericite, chlorite and chloritoid feature extractions for (a) Sample 64 - the profiles include the Green Bar (GB), Rice Pebble Marker (RPM), hangingwall (HW), internal quartzite (IQ) and footwall (FW); (b) Sample 20 – the profiles include the hangingwall (HW), Brown-Orange Argillaceous Zone (BOAZ), Pale Pebbly Quartzite (PPQ) and footwall (FW). A borehole log to show the relative depth of the borehole and the sedimentological unit(s) underlies the spectral profiles.*

A moderate response to the sericite feature extraction was seen in the reef, and the response increases moving into the internal quartzite and footwall units below the reef. A high response to the chlorite feature extraction was noted within the internal quartzite portion above the reef, with a moderate response within the reef, lower internal quartzite unit and the top of the footwall unit. The reef shows a low response to the chloritoid feature extraction. The highest response to chloritoid feature extraction was noted to be within the upper portion of the internal quartzite unit above the reef as well as within the hangingwall quartzite. The spectral profiles include the Green Bar and Rice Pebble Marker units however there are no corresponding spectral images to compare with. The mean depths for pyrophyllite, sericite, chlorite and chloritoid throughout the borehole are relatively low however they correlate well with what was observed in the spectral images. The gold grade of the reef was low at 8.3 g/t. Compared to the surrounding units the reef appears to have smaller mean depths for sericite, chlorite and chloritoid however it should be noted that the pyrophyllite mean depths were higher in the No. 3 Facies compared to the hangingwall unit and increase significantly in the internal quartzite unit. This suggests the internal quartzite unit is pyrophyllite-rich in comparison to the reef unit. This is confirmed by both macroscopic and microscopic observations.

The spectral profiles for Sample 20 (No. 2 Facies) are shown in Figure 3.67 (b). No spectral image outputs were done for Sample 20 however the spectral profiles can be used alongside the macroscopic, microscopic and geochemical observations without the spectral image outputs. The mean depth for pyrophyllite was low within the No. 2A Facies and increases with proximity to the footwall contact and within the footwall unit itself. The pyrophyllite mean depth was also noted to increase near to the contact between the No. 2A Facies and the overlying Pale Pebbly Quartzite unit, becoming noticeable greater within the No. 2B Facies and the lower portion of the Brown-Orange Argillaceous Zone, and decreasing gradually further into the hangingwall unit. At the contact between the hangingwall unit and the Brown-Orange Argillaceous Zone there was a significant increase in the pyrophyllite mean depth, suggesting the immediate overlying hangingwall unit is pyrophyllite-rich in comparison to the underlying Brown-Orange Argillaceous Zone. Pyrophyllite was noted to occur within the matrix of the No. 2A Facies, occurring interstitially between quartz clasts.

Sericite had very little to no response to the sericite feature extraction within the footwall unit and increases slightly nearer to the No. 2A Facies contact and within the No. 2A Facies. The Pale Pebbly Quartzite had very little response to the sericite feature extraction, with a slight increase in response noted within the No. 2B Facies and Brown-Orange Argillaceous Zone. The greatest response to the sericite feature extraction was noted within the hangingwall unit. Sericite was noted to occur in the form of sericitic muscovite within the matrix of the No. 2A Facies, mixed with very fine pyrophyllite grains.

The underlying footwall and overlying Brown-Orange Argillaceous Zone as well as the hangingwall unit had greater responses to the chloritoid feature extraction in comparison to the No. 2A Facies, Pale Pebbly Quartzite and the No. 2B Facies. The response to the chlorite feature extraction was very low within the footwall unit, increasing gradually into the No. 2A Facies and the Pale Pebbly Quartzite, decreasing slightly within the No. 2B Facies, and increasing significantly within the upper portion of the Brown-Orange Argillaceous Zone. The upper hangingwall unit displayed the greatest response to the chlorite feature extraction in comparison to the remainder of the borehole. Within the No. 2A Facies, chlorite and chloritoid laths were noted in thin section.

The upper portion of the No. 2A Facies was sampled prior to the commencement of this research and exhibited a gold grade of 25.9 g/t. The lower portion of the No. 2A Facies had a gold grade of slightly above 92.5 g/t. The higher gold grade was accompanied by higher responses to the pyrophyllite feature extraction, with lower chlorite and sericite responses. The lower gold grade in the upper portion of the No. 2A Facies was noted to have lower responses to the pyrophyllite feature extraction in comparison to the lower portion of the No. 2A Facies, with higher chlorite and sericite responses. Chloritoid was noted to have a consistent response from the lower to the upper portion of the No. 2A Facies, with an increase noted nearer to the overlying Pale Pebbly Quartzite. This suggests a higher chloritoid abundance at the upper contact with the Pale Pebbly Quartzite, possibly due to the transition from one sedimentary unit to the next.

The remaining borehole samples with the spectral profiles and image outputs can be referred to in Appendix 7 and Appendix 8.

3.4.3 Discussion

When comparing both the spectral profiles and the spectral images there is valuable information that correlates well with what is seen macroscopically, microscopically and geochemically, however there are limitations in determining gold grade and carbon content from spectral profiles and spectral images.

In some instances there was contradicting information between the spectral profiles and the spectral image outputs, for example in Sample 30 a moderate response was seen against the chlorite feature extraction image however a zero mean depth was recorded in the spectral profile. Discrepancies between the spectral image outputs and the spectral profiles may be encountered and can possibly influence overall interpretations, however the accuracy of the spectral profile is greater than the visual images (The MathWorks Inc., 2005). The visual images are created by grouping similar features, wavelengths and mean depths which sometimes allows for the loss of spectral data, whereas the spectral profile is singled out per spectral index and variations can almost be pin-pointed (Harris, 2006b, p.101; The MathWorks Inc., 2005). A weakness of the spectral profile is if the spectral feature is unknown, it cannot be identified within the data (Harris, 2006b., p.101).

It is also possible that discrepancies can occur between the spectral image outcomes i.e. between the spectral facies image and the spectral index (feature extraction) images. Factors that should be taken into consideration include mineral mixtures of the sample (especially between pyrophyllite and sericitic muscovite which was evident in the microscopic observations), the presence of water, particle size effects, organic material, material orientation as well as sample texture (Harris, 2006b, p.100; Hauff, 2001, p.2). To overcome the noted discrepancies in some of the samples, the other methodologies – particularly microscopic and geochemical observations - can be referred to in order to confirm or reject the spectral findings.

Similar spectral responses were seen for the varying lithological units for most of the tombstone and borehole samples. The hangingwall quartzite had the highest response to the chloritoid and chlorite feature extractions, suggesting both chloritoid and chlorite are abundant. Pyrophyllite had the highest response to the pyrophyllite feature extraction within the footwall quartzite, indicating a higher abundance than sericite, chloritoid and chlorite. The

Pale Pebbly Quartzite unit had, on average, a slightly higher response to the pyrophyllite feature extraction than the Brown-Orange Argillaceous Zone unit. The Rice Pebble Marker had the highest response across the lithological units to the chlorite feature extraction, indicating an abundance of chlorite within the Rice Pebble Marker. The highest response recorded for the Green Bar was against the chloritoid feature extraction - this correlates with the mineralogical findings of Fletcher (2009) and McCarthy (2006).

A decrease in response (mean depth) to the different feature extractions was typically seen when moving from the overlying quartzite of the reef to the footwall quartzite. It was very rare to find any instance where the response of the reef to the feature extractions was greater than the surrounding lithology. This may be due to the reef comprising various clast types and sizes as well as varying mineralogy, which may affect the responses to the feature extractions.

The No. 2 Facies, in most of the samples, was noted to have very low to low responses to the pyrophyllite feature extraction, with high responses noted within Samples 31 and 39. Moderate responses to the pyrophyllite feature extraction within the No. 1 and No. 3 Facies samples were noted, particularly in the tombstone samples, with low to moderate responses in the borehole samples (with the exception of Sample 30 where a high response was recorded). The No. 1 Facies was noted to have low to moderate responses to the sericite feature extraction (with the exception of Sample 45), whereas the No. 2A, No. 2B and No. 3 Facies were noted to have moderate to high responses.

Very low to moderate responses to the chlorite and chloritoid feature extractions were noted within the No. 2 Facies samples. Very low to moderate responses to the chloritoid feature extraction were noted within the No. 1 and No. 3 Facies samples. The responses to the chlorite feature extraction were highest in the No. 3 Facies samples, with mostly low to moderate responses recorded in the No. 1 and No. 2 Facies.

Samples that were macroscopically noted to have a thin carbon seam or fly-speck carbon were seen to have a low to moderate response to the pyrophyllite and sericite feature extractions, with low responses to the chlorite and chloritoid feature extractions. In Samples 16, 17, 18 and 64 the response to the chlorite feature was notably high, however in these samples the gold grade was predominantly low with one very high gold grade recorded for Sample 18 (36.0, 15.4, 173.0 and 8.2 g/t respectively). Of the samples that had high gold grade and

microscopically noted carbon present, Sample 8 (311.0 g/t) had a low response to the pyrophyllite, chlorite and chloritoid feature extraction with a moderate response to the sericite feature extraction. Sample 3 (172.0 g/t) and Sample 10 (284.0 g/t) had moderate responses to the pyrophyllite feature extraction, with low responses to the sericite, chlorite and chloritoid feature extractions. Sample 11 (128.0 g/t) and Sample 13 (130.0 g/t) both had moderate responses to the pyrophyllite and sericite feature extractions, with low responses to the chlorite and chloritoid feature extractions. Sample 19 (141.0 g/t) had a very low response to the pyrophyllite feature extraction, with moderate responses to the sericite, chlorite and chloritoid feature extractions.

In terms of relating gold grade to the spectral observations it was noted that several tombstone and borehole samples with higher gold grades appeared to occur with lower spectral responses, and samples with lower gold grades appeared to occur with higher spectral responses to the respective feature extractions. This suggests that higher alteration levels may be associated with the lower gold grades and the lower alteration levels may be associated with the higher gold grades. However the reliability of this statement is inconsistent by only considering the spectral outputs and will have to be supplemented with the findings in the other methodologies.

In terms of relating carbon content to the spectral observations, it could only be noted that the response to the pyrophyllite feature extraction was predominantly moderate and the response to the sericite feature extraction ranges from low to moderate for samples noted to have carbon present (macroscopically and/or microscopically). It should be noted that organic matter within samples (i.e. carbon) may affect spectral readings (Hauff, 2001, p.2), which may be why no particular pattern could be identified.

Although spectral scanning is not a reliable process to follow to identify gold grade or carbon content, it most definitely can be used to determine varying amounts of alteration within samples. The summarised spectral outcomes (based on both the spectral profiles and spectral images, or in some instances only one or the other) of the reef intersections for all the tombstones and boreholes are found in Table 3.23, apart from Samples 4, 29, 33 and 34 that were not spectrally scanned.

Table 3.23: Spectral scanning output observations for all the reef samples (excluding Samples 4, 29, 33 and 34 that were not spectrally scanned). A red-yellow-green colour scale highlights the varying gold grades (red = high gold grade; yellow = intermediate gold grade; green = low gold grade). N/D: not determined.

Sample	Sample ID	Unit	Noted Spectral Observations				Gold grade (g/t)
			Pyrophyllite	Sericite	Chlorite	Chloritoid	
1	94-94 E1	No. 1 Facies	Moderate	Low	Low	Low	10.3
2	99-94 E2	No. 2A/2B Facies	Moderate	Low	Low	Low	40.1/41.2
3	104-88 W6	No. 1 Facies	Moderate	Low	Low	Low	172.0
5	112-83 W3	No. 1 Facies	Moderate	Low	Low	Low	73.6
6	112-83 W4	No. 1 Facies	Moderate	Low	Moderate	Low	119.0
7	114-78 E1	No. 1 Facies	Moderate	Low	Low	Low	21.1
8	120-55 W4	No. 3 Facies	Low	Moderate	Low	Low	311.0
9	120-77 S1	No. 3 Facies	Moderate	High	Low	Moderate	80.7
10	96-94 E2	No. 1 Facies	Moderate	Low	Low	Low	284.0
11	100-92 Wze	No. 2A Facies	Moderate	Moderate	Low	Low	128.0
12	104-88 E1A	No. 1 Facies	Moderate	Moderate	Moderate	Low	83.9
13	104-88 W7	No. 1 Facies	Moderate	Moderate	Low	Low	130.0
14	109-87 E2	No. 1 Facies	Moderate	Moderate	Low	Low	132.0
15	112-84 Rse	No. 1 Facies	Moderate	Moderate	Moderate	Low	79.5
16	120-55 NE7	No. 3 Facies	Moderate	Moderate	High	Low	36.0
17	120-55 W5	No. 3 Facies	Moderate	Moderate	High	Low	15.4
18	120-55 W7	No. 3 Facies	Moderate	Moderate	High	Low	173.0
19	120-70 W1	No. 3 Facies	Very low	Moderate	Moderate	Moderate	141.0
20	DPH 3883	No. 2A Facies	Low	Very low	Very low	Low	59.2
21	DPH 4057	No. 3 Facies	Moderate	Very low	Very low	Low	64.3
22	GBH 1000 D6	No. 2A/2B Facies	Moderate	Moderate	Low	Moderate	38.4/6.6
23	GBH 2788	No. 2A Facies	Very low	Low	Low	Low	183.9
24	GBH 3763	No. 1 Facies	Low to Moderate	Low to Moderate	Low	Low	39.0
25	GBH 3844	No. 3 Facies	Low to Moderate	Low	Low	Low to Moderate	12.0
26	GBH 3845	No. 3 Facies	Moderate	Low	Low	Low	19.0
27	GBH 4003	No. 1 Facies	Low to Moderate	Low to Moderate	Low	Low	86.8
28	GBH 6000	No. 1 Facies	Very low	Moderate	Low	Low	80.8
30	GBH 6003	No. 1 Facies	High	Moderate	Moderate	Very low	6.4
31	GBH 6004	No. 2A/2B Facies	Moderate to High	Low	Low	Low to Moderate	12.8
32	GBH 6014	No. 1 Facies	Low	Low	Low	Low	67.5
35	GBH 1000 D0	No. 2A/2B Facies	Very low	Low	Low	Low	27.4/9.2
36	GBH 1000 D1	No. 2B Facies	Low	Moderate	Low	Low	9.9
37	GBH 1000 D2	No. 2A/2B Facies	Low	Moderate	Very low	2B > 2A	110.0/7.6
38	GBH 1000 D4	No. 2A/2B Facies	Moderate	Moderate	Low	Moderate	20.2/2.9
39	GBH 1000 D5	No. 2A/2B Facies	High	High	Low	Moderate	44.5/12.5
40	GBH 1000 D7	No. 2A/2B Facies	Very low	High	Low	Low	24.4/7.3
41	GBH 1000 D8	No. 2A/2B Facies	2A > 2B	Moderate	Low	Moderate	16.3/8.3
42	GBH 1000 D9	No. 2A/2B Facies	2A > 2B	2B > 2A	2B > 2A	Low	48.8/3.9
43	GBH 1000 D10	No. 2A/2B Facies	2B > 2A	Moderate	2B > 2A	2A > 2B	100.2/5.8
44	GBH 1000 D11	No. 2A/2B Facies	Low	2B > 2A	2B > 2A	2B > 2A	96.0/9.3
45	GBH 6008	No. 1 Facies	Low	High	Low	Low	N/D
46	LIB 120 SW1 D0	No. 3 Facies	Low	Moderate	Moderate	Low	N/D
47	LVB 18 D0	No. 3 Facies	Low	High	Moderate	Low	N/D
48	LVBI D2	No. 2B Facies	Low	Moderate	Moderate	Moderate	19.7
49	LVBI D5	No. 2B Facies	Low	2A > 2B	2A > 2B	2B > 2A	2.1
50	LVBI D7	No. 2A Facies	Low	Moderate	Moderate	Low	22.4
51	LVBI D10	No. 2A Facies	Low	2A > 2B	2B > 2A	Low	11.5
52	LVBK D3	No. 2B Facies	Low	Moderate	Moderate	Low	10.4
53	LVBL D2	No. 2A Facies	Low	High	2A > 2B	Low	4.9
54	MPO LIB 2 D2	No. 3 Facies	Low	Moderate	Moderate	Low	N/D
55	MPO LIB 3 D2	No. 3 Facies	Low	Moderate	Moderate	Moderate	N/D
56	MPO LIB 3 D3	No. 3 Facies	Low	Moderate	Moderate	Low	N/D
57	UD 2 D0	No. 2A Facies	Low	Moderate	Moderate	Low	N/D
58	UD 2 D2	No. 2A Facies	Low	Low	High	Low	6.0
59	UD 5 D0	No. 2B Facies	2B > 2A	High	Moderate	2B > 2A	1.7
60	UD 13 D0	No. 3 Facies	Low	Moderate	High	Low	N/D
61	UD 15 D1	No. 2 Facies	Low	Moderate	Moderate	Low	N/D
62	UD 25 D11	No. 2A/2B Facies	Low	Moderate	Moderate	Low	7.0/1.1
63	UD 32 D8	No. 2A/2B Facies	Low	High	Low	High	N/D
64	UD 33 D15	No. 3 Facies	Low	Moderate	High	Low	8.2
65	UD 36 D4	No. 1 Facies	Low	Moderate	Moderate	Moderate	47.6
66	UD 36 D7	No. 1 Facies	Low	Low	Moderate	Low	N/D
67	UD 37 D1	No. 2A/2B Facies	Low	Low	Moderate	Low	N/D
68	UD 37 D5	No. 2A/2B Facies	Low	Low	Moderate	Low	N/D

3.5 GEOLOGICAL MODELLING OF THE CARBON LEADER REEF

Using the results from the macroscopic, microscopic and spectral observations, as well as gold assay and geochemical analyses, several geological models could be created. The outcomes for the individual models are discussed and were plotted relative to the mine boundaries, Carbon Leader Reef facies types as well as Carbon Leader Reef estimation domains. Geological modelling was carried out using Datamine's StudioRM® software that is currently licenced for use at AngloGold Ashanti.

3.5.1 Alteration Models of the Carbon Leader Reef

The borehole and tombstone samples used across all the methodologies are illustrated in Figure 3.68 (refer to Appendix 1: Sample Locality Map for the sample numbers). Some of the samples have information from each of the methods used, or a few of the methods used, and a subset samples have information from one method only (i.e. spectral results) – refer to Chapter 2, Table 2.1.

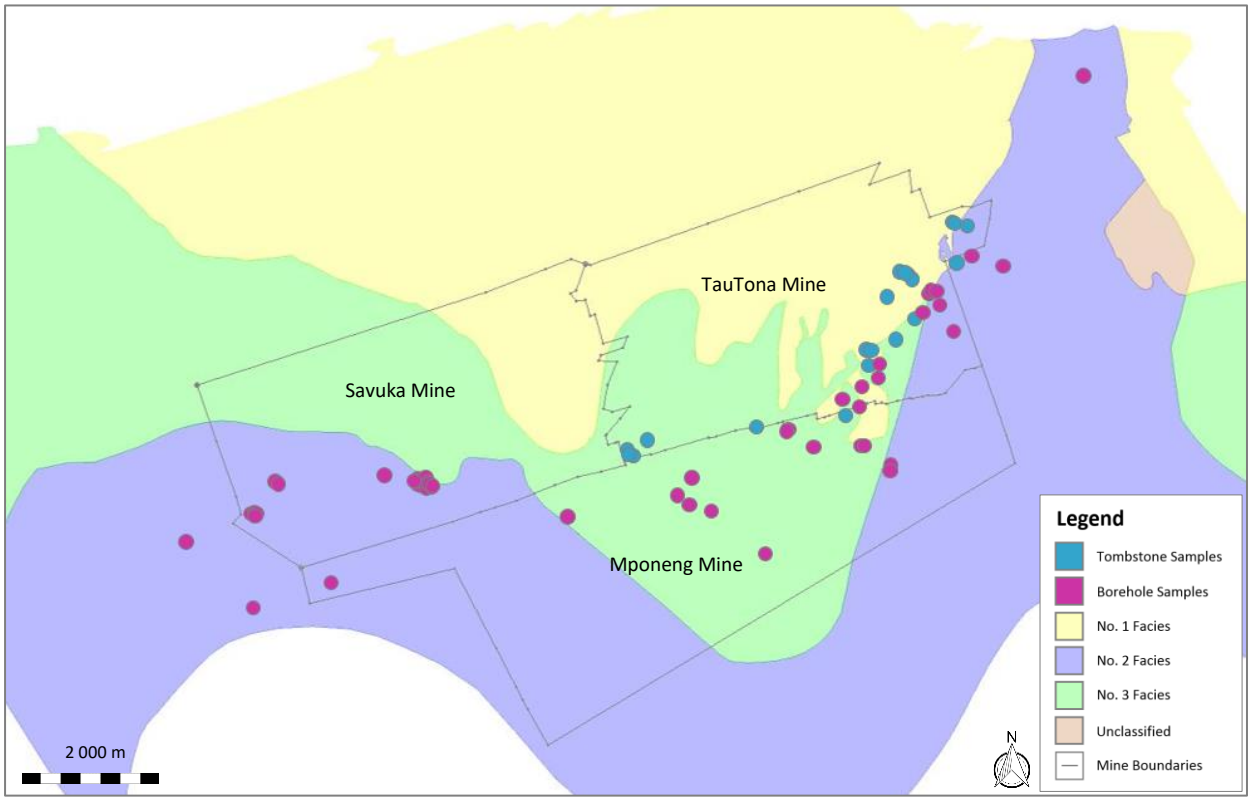

***Figure 3.68**: Sample locations for tombstone and borehole reef intersections relative to the Carbon Leader Reef facies type (In House Report, 2017).*

Three distinct styles of alteration were noted to occur throughout the reef samples: sericitic alteration, pyrophyllitic alteration and chloritisation (Table 3.24 and Figure 3.69).

Table 3.24: Overall findings of the various methodologies (including macroscopic observations, microscopic observations, geochemical analyses and spectral observations) were used to assign samples to an appropriate alteration group and to create an alteration model based on the major alteration groups. For the spectral observations, findings were ranked on a low, moderate (mod) and high response to a particular feature extraction. The feature extractions used for this research included pyrophyllite (prl), sericite (ser), chlorite (chl) and chloritoid (ctd). The gold grades used within this table are a combination of the gold grades reported for the purpose of this research, and in the absence of gold grade for the borehole samples, the gold assay grade of the borehole sample done prior to the commencement of this research was used. [(a)] No. 2A Facies; [(b)] No. 2B Facies; [(c)] No. 2A/2B Facies; [(d)] No. 2A and No. 2B Facies average. The samples are arranged from west to east across the West Wits Line.

Sample ID		Assigned Facies	Assigned Estimation Domain	Macroscopic Observations	Microscopic Observations	Geochemical Analyses	Spectral Observations	Gold grade (g/t)	Major Alteration Group
53	LVBL D2	No. 2 Facies	Savuka	Greenish discolouration of No. 2B Facies matrix			Low prl/high ser/mod chl/low ctd	4.9[(a)]	Chloritisation
52	LVBK D3	No. 2 Facies	Savuka				Low prl/mod ser/mod chl/low ctd	10.4[(b)]	Chloritisation
49	LVBI D5	No. 2 Facies	Savuka				Low prl/mod ser/mod chl/mod ctd	2.1[(b)]	Sericitic Alteration
50	LVBI D7	No. 2 Facies	Savuka				Low prl/mod ser/mod chl/low ctd	22.4[(a)]	Sericitic Alteration
48	LVBI D2	No. 2 Facies	Savuka				Low prl/mod ser/mod chl/mod ctd	19.7[(b)]	Sericitic Alteration
51	LVBI D10	No. 2 Facies	Savuka	Discolouration of Brown-Orange Argillaceous Zone			Low prl/mod ser/mod chl/low ctd	11.5[(a)]	Sericitic Alteration
58	UD 2 D2	No. 2 Facies	Savuka	Greenish discolouration of hangingwall			Low prl/low ser/high chl/low ctd	6.0[(a)]	Chloritisation
57	UD 2 D0	No. 2 Facies	Savuka				Low prl/mod ser/mod chl/low ctd		Chloritisation
62	UD 25 D11	No. 2 Facies	Savuka	Greenish discolouration of No. 2A Facies			Low prl/mod ser/mod chl/low ctd	7.0/1.1[(c)]	Chloritisation
23	GBH 2788	No. 2 Facies	Savuka	Discolouration of sulphides in No. 2B Facies	Sericitic alteration or oxidation	Sericite-rich	Low prl/low ser/low chl/low ctd	183.9[(a)]	Sericitic Alteration
39	GBH 1000 D5	No. 2 Facies	Savuka	Greenish discolouration of internal quartzite			High prl/high ser/low chl/low ctd	44.5/12.5[(c)]	Sericitic Alteration
37	GBH 1000 D2	No. 2 Facies	Savuka	Greenish discolouration of internal quartzite			Low prl/mod ser/low chl/mod ctd	110.0/7.6[(c)]	Sericitic Alteration
36	GBH 1000 D1	No. 2 Facies	Savuka				Low prl/mod ser/low chl/low ctd	9.9[(b)]	Sericitic Alteration
41	GBH 1000 D8	No. 2 Facies	Savuka				Mod prl/mod ser/low chl/mod ctd	16.3/8.3[(c)]	Sericitic Alteration
42	GBH 1000 D9	No. 2 Facies	Savuka				Mod prl/mod ser/mod chl/low ctd	48.8/3.9[(c)]	Sericitic Alteration
43	GBH 1000 D10	No. 2 Facies	Savuka				Mod prl/mod ser/mod chl/mod ctd	100.2/5.8[(c)]	Sericitic Alteration
38	GBH 1000 D4	No. 2 Facies	Savuka	Greenish discolouration of internal quartzite			Mod prl/mod ser/low chl/mod ctd	20.2	Sericitic Alteration
44	GBH 1000 D11	No. 2 Facies	Savuka				Low prl/mod ser/mod chl/mod ctd	96.0/9.3[(c)]	Sericitic Alteration
40	GBH 1000 D7	No. 2 Facies	Savuka				Low prl/high ser/low chl/low ctd	24.4/7.3[(c)]	Sericitic Alteration
35	GBH 1000 D0	No. 2 Facies	Savuka	Greenish discolouration of internal quartzite			Low prl/low ser/low chl/low ctd	27.4/9.2[(c)]	Sericitic Alteration
22	GBH 1000 D6	No. 2 Facies	Savuka	Greenish discolouration of hangingwall	Sericite-rich	Sericite-rich	Mod prl/mod ser/low chl/mod ctd	38.4/6.6[(c)]	Sericitic Alteration
60	UD 13 D0	No. 3 Facies	Peggy				Low prl/mod ser/high chl/low ctd		Chloritisation
18	120-55 W7	No. 3 Facies	Peggy	Greenish discolouration of upper No. 3 Facies	Possible Chloritisation	Chlorite/chloritoid-rich	Mod prl/mod ser/high chl/low ctd	173.0	Chloritisation
17	120-55 W5	No. 3 Facies	Peggy	Greenish discolouration along fault/shear edge in footwall unit at contact with reef	Sericite-rich	Chlorite/chloritoid-rich	Mod prl/mod ser/high chl/low ctd	15.4	Chloritisation
8	120-55 W4	No. 3 Facies	Peggy	Greenish discolouration of upper No. 3 Facies	Possible pyrophyllitic alteration	Sericite-rich	Low prl/mod ser/low chl/low ctd	311.0	Sericitic Alteration
16	120-55 NE7	No. 3 Facies	Peggy	Fly-speck carbon and pyrite stringers in No. 3 Facies	Sericite-rich	Chlorite/chloritoid-rich	Mod prl/mod ser/high chl/low ctd	36.0	Chloritisation
54	MPO LIB2 D2	No. 3 Facies	Peggy				Low prl/mod ser/mod chl/low ctd		Chloritisation
56	MPO LIB3 D3	No. 3 Facies	Peggy				Low prl/mod ser/mod chl/low ctd		Chloritisation
55	MPO LIB3 D2	No. 3 Facies	Peggy				Low prl/mod ser/mod chl/mod ctd		Sericitic Alteration
64	UD 33 D15	No. 3 Facies	Peggy	Thin carbon seam at base of No. 3 Facies			Low prl/mod ser/high chl/low ctd	8.2	Chloritisation
19	120-70 W1	No. 3 Facies	TauTona	Quartz veining in hangingwall; thin pyrite stringers mark base of No. 3 Facies	Possible sericitic alteration	Chlorite/chloritoid-rich	Low prl/mod ser/mod chl/mod ctd	141.0	Chloritisation
47	LVB 18 D0	No. 3 Facies	TauTona				Low prl/high ser/mod chl/low ctd		Sericitic Alteration
26	GBH 3845	No. 3 Facies	TauTona	Quartz veining in hangingwall	Pyrophyllite-rich	Sericite-rich	Mod prl/low ser/low chl/low ctd	19.0	Pyrophyllitic Alteration
25	GBH 3844	No. 3 Facies	TauTona	Greenish discolouration of No. 3 Facies matrix; thin carbon seam at the base	Possible sericitic alteration	Sericite-rich	Low prl/low ser/low chl/low ctd	31.4	Sericitic Alteration
46	LIB 120 SW1 D0	No. 3 Facies	TauTona				Low prl/mod ser/mod chl/low ctd		Chloritisation
28	GBH 6000	No. 1 Facies	TauTona	Greenish discolouration of hangingwall	Sericite-rich	Sericite-rich	Low prl/mod ser/low chl/low ctd	80.8	Sericitic Alteration

Table 3.24 – continued: Overall findings of the various methodologies (including macroscopic observations, microscopic observations, geochemical analyses and spectral observations) were used to assign samples to an appropriate alteration group and to create an alteration model based on the major alteration groups. For the spectral observations, findings were ranked on a low, moderate (mod) and high response to a particular feature extraction. The feature extractions used for this research included pyrophyllite (prl), sericite (ser), chlorite (chl) and chloritoid (ctd). The gold grades used within this table are a combination of the gold grades reported for the purpose of this research, and in the absence of gold grade for the borehole samples, the gold assay grade of the borehole sample done prior to the commencement of this research was used. [(a)] No. 2A Facies; [(b)] No. 2B Facies; [(c)] No. 2A/2B Facies; [(d)] No. 2A and No. 2B Facies average. The samples are arranged from west to east across the West Wits Line.

Sample ID		Assigned Facies	Assigned Estimation Domain	Macroscopic Observations	Microscopic Observations	Geochemical Analyses	Spectral Observations	Gold grade (g/t)	Major Alteration Group
9	120-77 S1	No. 3 Facies	TauTona		Pyrophyllite-rich	Sericite-rich	Mod prl/high ser/low chl/mod ctd	80.7	Sericitic Alteration
66	UD 36 D7	No. 1 Facies	TauTona				Low prl/low ser/mod chl/low ctd		Chloritisation
29	GBH 6001	No. 3 Facies	TauTona		Sericite-rich	Sericite-rich		36.4	Sericitic Alteration
65	UD 36 D4	No. 1 Facies	TauTona				Low prl/mod ser/mod chl/mod ctd	47.6	Chloritisation
32	GBH 6014	No. 1 Facies	TauTona	Thin carbon seam at base of No. 1 Facies	Sericite/Chlorite-rich	Chlorite/chloritoid-rich	Low prl/low ser/low chl/low ctd	67.5	Chloritisation
6	112-83 W4	No. 1 Facies	TauTona		Pyrophyllite-rich	Chlorite/chloritoid-rich	Mod prl/low ser/mod chl/low ctd	119.0	Chloritisation
7	114-78 E1	No. 1 Facies	TauTona	Thin carbon seam at base of No. 1 Facies	Pyrophyllite-rich	Sericite-rich	Mod prl/low ser/low chl/low ctd	21.1	Pyrophyllitic Alteration
5	112-83 W3	No. 1 Facies	TauTona	Disseminated pyrite along fractures in hangingwall	Pyrophyllite-rich	Sericite-rich	Mod prl/low ser/low chl/low ctd	73.6	Pyrophyllitic Alteration
21	DPH 4057	No. 3 Facies	TauTona	Sheared contact between No. 3 Facies and the footwall, discoloured milky quartz clast	Possible pyrophyllitic alteration	Sericite-rich	Mod prl/low ser/low chl/low ctd	64.3	Pyrophyllitic Alteration
33	GBH 6028	No. 1 Facies	TauTona	Greenish discolouration of No. 1 Facies matrix	Possible pyrophyllitic alteration	Sericite-rich		0.6	Pyrophyllitic Alteration
4	105-86 E2	No. 1 Facies	TauTona	Thin carbon seam at base of No. 1 Facies	Pyrophyllite-rich	Sericite-rich		227.0	Pyrophyllitic Alteration
68	UD 37 D5	No. 2 Facies	Driefontein				Low prl/low ser/mod chl/low ctd		Chloritisation
67	UD 37 D1	No. 2 Facies	Driefontein				Low prl/low ser/mod chl/low ctd		Chloritisation
15	112-84 Rse	No. 1 Facies	TauTona	Thin carbon seam at base of No. 1 Facies	Pyrophyllite-rich	Sericite-rich	Mod prl/mod ser/mod chl/low ctd	79.5	Pyrophyllitic Alteration
3	104-88 W6	No. 1 Facies	TauTona	Dark greenish discolouration of upper No. 1 Facies	Possible pyrophyllitic alteration	Sericite-rich	Mod prl/mod ser/low chl/low ctd	172.0	Pyrophyllitic Alteration
12	104-88 E1A	No. 1 Facies	TauTona	Thin carbon seam and pyrite stringer at base of No. 1 Facies	Sericite-rich	Sericite-rich	Mod prl/mod ser/mod chl/low ctd	83.9	Sericitic Alteration
24	GBH 3763	No. 1 Facies	TauTona		Pyrophyllite-rich	Pyrophyllite-rich	Low prl/low ser/low chl/low ctd	39	Pyrophyllitic Alteration
13	104-88 W7	No. 1 Facies	TauTona	Dark green to dark grey matrix of No. 1 Facies	Possible sericitic alteration	Sericite-rich	Mod prl/mod ser/low chl/low ctd	130.0	Sericitic Alteration
14	109-87 E2	No. 1 Facies	TauTona		Sericite-rich	Sericite-rich	Mod prl/mod ser/low chl/low ctd	132.0	Sericitic Alteration
34	GBH 6036	No. 1 Facies	TauTona		Pyrophyllite/Chlorite-rich	Chlorite/chloritoid-rich		29.6	Chloritisation
27	GBH 4003	No. 1 Facies	TauTona		Pyrophyllite/Chloritoid-rich	Sericite-rich	Low prl/low ser/low chl/low ctd	86.8	Pyrophyllitic Alteration
45	GBH 6008	No. 1 Facies	Driefontein				Low prl/high ser/low chl/low ctd		Sericitic Alteration
30	GBH 6003	No. 1 Facies	Driefontein		Low abundance of phyllosilicate minerals	Chlorite/chloritoid-rich	High prl/mod ser/mod chl/low ctd	6.4	Chloritisation
20	DPH 3883	No. 2 Facies	Driefontein	Greenish discolouration of hangingwall and quartz clasts in footwall	Sericite-rich	Sericite-rich	Low prl/low ser/low chl/low ctd	59.2[(a)]	Sericitic Alteration
1	94-94 E1	No. 1 Facies	TauTona	Greenish discolouration of No. 1 Facies matrix	Possible pyrophyllitic or sericitic alteration	Sericite-rich	Mod prl/low ser/low chl/low ctd	10.3	Pyrophyllitic Alteration
10	96-94 E2	No. 1 Facies	TauTona	Dark green to black matrix of No. 1 Facies	Possible pyrophyllitic or sericitic alteration	Sericite-rich	Mod prl/low ser/low chl/low ctd	284.0	Pyrophyllitic Alteration
63	UD 32 D8	No. 2 Facies	Driefontein	Greenish discolouration of Brown-Orange Argillaceous Zone			Low prl/high ser/low chl/high ctd		Sericitic Alteration
11	100-92 Wze	No. 2 Facies	Driefontein		Low abundance of phyllosilicate minerals	Chlorite/chloritoid-rich	Mod prl/mod ser/low chl/low ctd	128.0	Pyrophyllitic Alteration
2	99-94 E2	No. 2 Facies	TauTona		Pyrophyllite-rich	Sericite-rich	Mod prl/low ser/low chl/low ctd	40.1/41.2[(c)]	Pyrophyllitic Alteration
31	GBH 6004	No. 2 Facies	Driefontein		Possible pyrophyllitic, sericitic or chloritic alteration	Sericite-rich	Mod prl/low ser/low chl/low ctd	12.8[(d)]	Pyrophyllitic Alteration
61	UD 15 D1	No. 2 Facies	Driefontein	Quartz veining cutting No. 2B Facies			Low prl/mod ser/mod chl/low ctd		Chloritisation
59	UD 5 D0	No. 2 Facies	Driefontein	Greenish discolouration of No. 2B Facies matrix			Mod prl/high ser/mod chl/mod ctd	1.7[(b)]	Sericitic Alteration

The assignment of the style of alteration was done by combining the observations and findings across all the methodologies used for each sample.

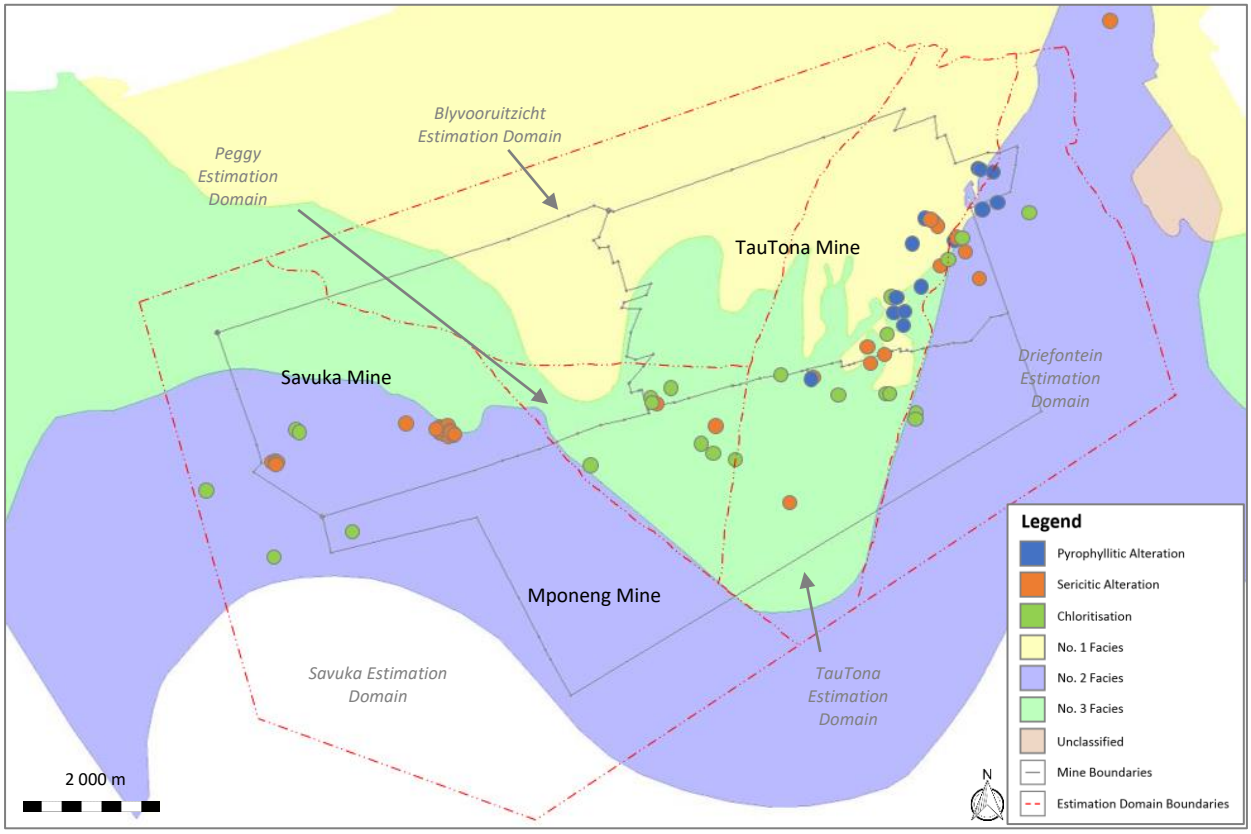

***Figure 3.69**: Three main types of alteration were noted for the reef intersections across the West Wits Line used within this research: pyrophyllitic alteration, sericitic alteration and chloritisation.*

The various reef intersection macroscopic descriptions for some of the samples did not align with the findings of Fletcher (2009) and Muller (1991). The No. 3 Facies typically has lesser amounts of hydrocarbons than the No. 1 Facies, which occurs as fly-speck carbon rather than an actual seam (Depiné *et al*., 2013; Fletcher, 2009; Janisch, 1986; Phillips and Law, 2000). The No. 3 Facies type is also seen to host high and persistent gold grades but less so than the No. 1 Facies because of the presence of a thin basal carbon seam that relates back to the gold-hydrocarbon-uranium relationship commonly noted within the Witwatersrand Basin (Agangi *et al.*, 2015; Depiné *et al*., 2013; Drennan and Robb, 2006; Muller, 1991; Phillips and Powell, 2015).

Several Carbon Leader Reef No. 3 Facies samples were noted to have a thin basal carbon seam (Sample 17, Sample 25 and Sample 64). Muller (1991) suggested that although the facies have been delineated into separate facies types, they are not definite boundaries and that there is a

transition from one facies into the next. By looking at the sample locations (refer to Appendix 1: Sample Locality Map), Sample 17 is well within the No. 3 Facies domain, as is Sample 64.

Sample 25 is near to the No. 1 Facies boundary however the sample had a gold grade of 31.4 g/t suggesting it is in the correct facies position in comparison to the No. 1 Facies samples according to Fletcher (2009) and Muller (1991). Additional to the noted thin basal carbon seam, Sample 25 also does not agree with the TauTona estimation domain characteristics that were proposed by Burnett *et al.* (2015) in the estimation domain model. The TauTona estimation domain typically has high gold grades, with high hydrothermal alteration in the north-east area indicated by dominance of pyrophyllite, with alteration becoming intermediate in the south-west area, indicated by an abundance of chloritoid (Burnett *et al*., 2015). Sample 25 had a low abundance of pyrophyllite and chloritoid, with a higher sericitic muscovite abundance as well as a low gold grade. This was confirmed in the microscopic observations as well as the geochemical analyses, suggesting sericitic alteration has taken place. In close proximity to Sample 25, is Sample 26 that is also representative of the No. 3 Facies and sits within the TauTona estimation domain. Sample 26 in contrast to Sample 25 had a higher abundance of pyrophyllite followed by sericitic muscovite (confirmed by microscopic observations and geochemical analyses) and its position was further south of Sample 25. According to Burnett *et al.* (2015) samples located in the south-west area of the TauTona estimation domain should be chloritoid-rich however this was not the case for Sample 25 and Sample 26. The gold grade for Sample 26 was 1.6 g/t, which aligns with the facies model in terms of lower gold grades expected in the No. 3 Facies samples, but the lower gold grade contradicts the estimation domain model.

It was also noted geochemically that the No. 3 Facies samples had higher overall gold grades and stronger relationships with major elements than the No. 1 Facies samples, which also disagrees with the Carbon Leader Reef facies model.

Across the West Wits Line, it was noted that several samples within the dataset, summarised in Table 3.25, did not agree with the Carbon Leader Reef facies model definitions set out by Fletcher (2009) and Muller (1991), and/or the estimation domain model definitions proposed by Burnett *et al*. (2015).

Table 3.25: Samples noted with discrepancies against the Carbon Leader Reef facies model definitions (Fletcher, 2009; Muller, 1991) and/or the estimation domain model definitions (Burnett *et al*., 2015).

Sample ID		Assigned Facies	Assigned Estimation Domain	Facies and/or Estimation Domain Model Discrepancy	Noted discrepancy
1	94-94 E1	No. 1 Facies	TauTona	Facies and estimation domain model	The gold grade (10.3 g/t) does not align to facies model or to the TauTona estimation domain.
2	99-94 E2	No. 2 Facies	TauTona	Facies and estimation domain model	The gold grade (40.1 g/t for No. 2A Facies and 41.2 g/t for No. 2B Facies) is not aligned to the TauTona estimation domain. The occurrence of carbon is not aligned to the facies model.
3	104-88 W6	No. 1 Facies	TauTona	Estimation domain model	Sample 3 has mineralogy to imply both sericitic and pyrophyllitic alteration has taken place. The dominant alteration mineral in the north-east portion of the TauTona estimation domain is pyrophyllite.
5	112-83 W3	No. 1 Facies	TauTona	Facies and estimation domain model	The gold grade (73.6 g/t) is lower than what is typically seen within the No. 1 Facies and TauTona estimation domain.
6	112-83 W4	No. 1 Facies	TauTona	Estimation domain model	The mineralogy does not align to the TauTona estimation domain.
7	114-78 E1	No. 1 Facies	TauTona	Facies and estimation domain model	The gold grade (21.1 g/t) is lower than what is typically seen within the No. 1 Facies and TauTona estimation domain.
8	120-55 W4	No. 3 Facies	Peggy	Facies and estimation domain model	Intermediate gold grades are typically seen within the Peggy estimation domain, with high grades in the No. 3 Facies however less so than within the No. 1 Facies. The gold grade for Sample 8 was the highest of all the samples at 311.0 g/t.
9	120-77 S1	No. 3 Facies	TauTona	Estimation domain model	Lower gold grade (80.7 g/t) than expected within the TauTona estimation domain.
11	100-92 Wze	No. 2A Facies	Driefontein	Facies and estimation domain model	The occurrence of carbon within the No. 2A Facies does not align to the facies model.
12	104-88 E1A	No. 1 Facies	TauTona	Estimation domain model	Samples in the north-east area of the TauTona estimation domain are typically pyrophyllite-rich. Sample 12 was noted to be sericite-rich. Gold grade (83.9 g/t) also does not align with typical grades of the TauTona estimation domain and No. 1 Facies.
13	104-88 W7	No. 1 Facies	TauTona	Estimation domain model	Samples in the north-east area of the TauTona estimation domain are typically pyrophyllite-rich. Sample 13 was noted to be sericite-rich.
14	109-87 E2	No. 1 Facies	TauTona	Estimation domain model	Samples in the north-east area of the TauTona estimation domain are typically pyrophyllite-rich. Sample 14 was noted to be sericite-rich.
15	112-84 Rse	No. 1 Facies	TauTona	Facies and estimation domain model	The gold grade (79.5 g/t) is lower than what is typically seen within the No. 1 Facies and TauTona estimation domain.
16	120-55 NE7	No. 3 Facies	Peggy	Facies and estimation domain model	The gold grade (36.0 g/t) is lower than what is typically seen within the No. 3 Facies and Peggy estimation domain.
17	120-55 W5	No. 3 Facies	Peggy	Facies and estimation domain model	Carbon Leader Reef unit characterised by a thin basal carbon seam, contradicting the descriptions of the facies model. Lower gold grade than typically noted within the No. 3 Facies and Peggy estimation domain.
18	120-55 W7	No. 3 Facies	Peggy	Estimation domain model	Intermediate gold grades are typically noted to occur within the Peggy estimation domain however Sample 18 had a reported gold grade of 173.0 g/t which is significantly high.
19	120-70 W1	No. 3 Facies	TauTona	Estimation domain model	Mineralogy of the reef is not aligned to the TauTona estimation domain.
20	DPH 3883	No. 2A Facies	Driefontein	Estimation domain model	Samples within the north-western portion of the Driefontein estimation domain are typically pyrophyllite dominant however Sample 20 was sericite-rich.
24	GBH 3763	No. 1 Facies	TauTona	Facies and estimation domain model	The gold grade (41.0 g/t) is lower than what is typically seen within the No. 1 Facies and the TauTona estimation domain.

Table 3.25 – continued: Samples noted with discrepancies against the Carbon Leader Reef facies model definitions (Fletcher, 2009; Muller, 1991) and/or the estimation domain model definitions (Burnett *et al*., 2015).

Sample ID		Assigned Facies	Assigned Estimation Domain	Facies and/or Estimation Domain Model Discrepancy	Noted discrepancy
25	GBH 3844	No. 3 Facies	TauTona	Facies and estimation domain model	The TauTona estimation domain typically hosts high gold grades with alteration varying from pyrophyllite-rich in the north-east area to chloritoid-rich in the south-west area. The gold grade for Sample 25 is low at 31.4 g/t and the sample was noted to have a higher sericitic abundance. The sample was also noted to have a thin basal carbon seam, contradicting the typical description of the No. 3 Facies.
26	GBH 3845	No. 3 Facies	TauTona	Facies and estimation domain model	A high abundance of pyrophyllite was noted within the sample however relative to its locality within the TauTona estimation domain, the sample should be chloritoid-rich. The gold grade was 1.6 g/t for the sample, which is significantly low for a sample within the TauTona estimation domain and within the No. 3 Facies.
28	GBH 6000	No. 1 Facies	TauTona	Estimation domain model	Mineralogy does not align with the TauTona estimation domain.
29	GBH 6001	No. 3 Facies	TauTona	Facies and estimation domain model	Sample 29 sits mid-way within the TauTona estimation domain and was noted to have a higher sericitic abundance compared to the typical pyrophyllite/chloritoid noted within the estimation domain. The gold grade was also low at 36.4 g/t.
30	GBH 6003	No. 1 Facies	Driefontein	Facies and estimation domain model	Gold grade (6.4 g/t) and mineralogy do not align to either the facies or estimation domain model.
32	GBH 6014	No. 1 Facies	TauTona	Facies and estimation domain model	The gold grade (67.5 g/t) is lower than typically seen within the No. 1 Facies and TauTona estimation domain. The mineralogy does not align with the TauTona estimation domain.
33	GBH 6028	No. 1 Facies	TauTona	Facies and estimation domain model	The gold grade (0.6 g/t) does not align to either the facies or the estimation domain model.
34	GBH 6036	No. 1 Facies	TauTona	Facies and estimation domain model	The gold grade (29.6 g/t) does not align to either the facies or the estimation domain model.
45	GBH 6008	No. 1 Facies	Driefontein	Estimation domain model	Samples within the Driefontein estimation domain are typically pyrophyllite-rich in the north-west portion. Sample 45 was noted to be sericite-rich.
46	LIB 120 SW1 D0	No. 3 Facies	TauTona	Estimation domain model	Samples to the south-west area of the TauTona estimation domain are typically chloritoid-rich. Sample 46 was noted to have a greater response to the chlorite feature extraction in comparison to the chloritoid feature extraction.
47	LVB 18 D0	No. 3 Facies	TauTona	Estimation domain model	Elevated abundance of chloritoid is typically noted within the south-west portion of the TauTona estimation domain however Sample 47 was noted to have a high response to the sericite feature extraction, suggestive of a higher sericite abundance within the sample.
63	UD 32 D8	No. 2 Facies	Driefontein	Estimation domain model	Samples within the north-western portion of the Driefontein estimation domain are typically pyrophyllite dominant however Sample 63 was sericite-rich.
64	UD 33 D15	No. 3 Facies	Peggy	Facies and estimation domain model	Carbon Leader Reef unit characterised by a thin basal carbon seam, contradicting the descriptions of the facies model. The low gold grade of 8.2 g/t does not align to the estimation domain or facies model.
65	UD 36 D4	No. 1 Facies	TauTona	Facies and estimation domain model	The gold grade (47.6 g/t) as well as the chloritisation within the sample does not align to either of the models.
66	UD 36 D7	No. 1 Facies	TauTona	Estimation domain model	Samples to the south-west area of the TauTona estimation domain are typically chloritoid-rich. Sample 66 was noted to have a greater response to the chlorite feature extraction in comparison to the chloritoid feature extraction.

The noted discrepancies in Table 3.25 indicate that although the localities of the sample(s) are within a particular facies type and/or estimation domain, the facies type definitions (particularly with regard to gold grade), the facies boundaries and/or the estimation domains (particularly with regard to mineralogy) may need to be updated.

Following the assignment of the three alteration styles to the samples, a structure model comprising faults and intrusions needed to be referred to. A structure model uses borehole logging as well as underground mapping of intrusions/faults and aids the mine planning processes that are undertaken at the mine. The structure model was used to note which samples have structural influences that may have altered the mineralogy rather than, or additionally to, alteration due to depositional processes. The most current structure model of the Carbon Leader Reef as well as the sample localities can be seen in Figure 3.70. One of the largest structures within the West Wits Line is the Pretorius Fault Zone, which dips at 65°NW at a strike of south-west to north-east across the south-eastern portion of TauTona Mine, extending into Mponeng Mine. The Pretorius Fault Zone ranges from 60 to 100 m in thickness and has a throw that exceeds 100 m in some places (Gibson *et al*., 2000).

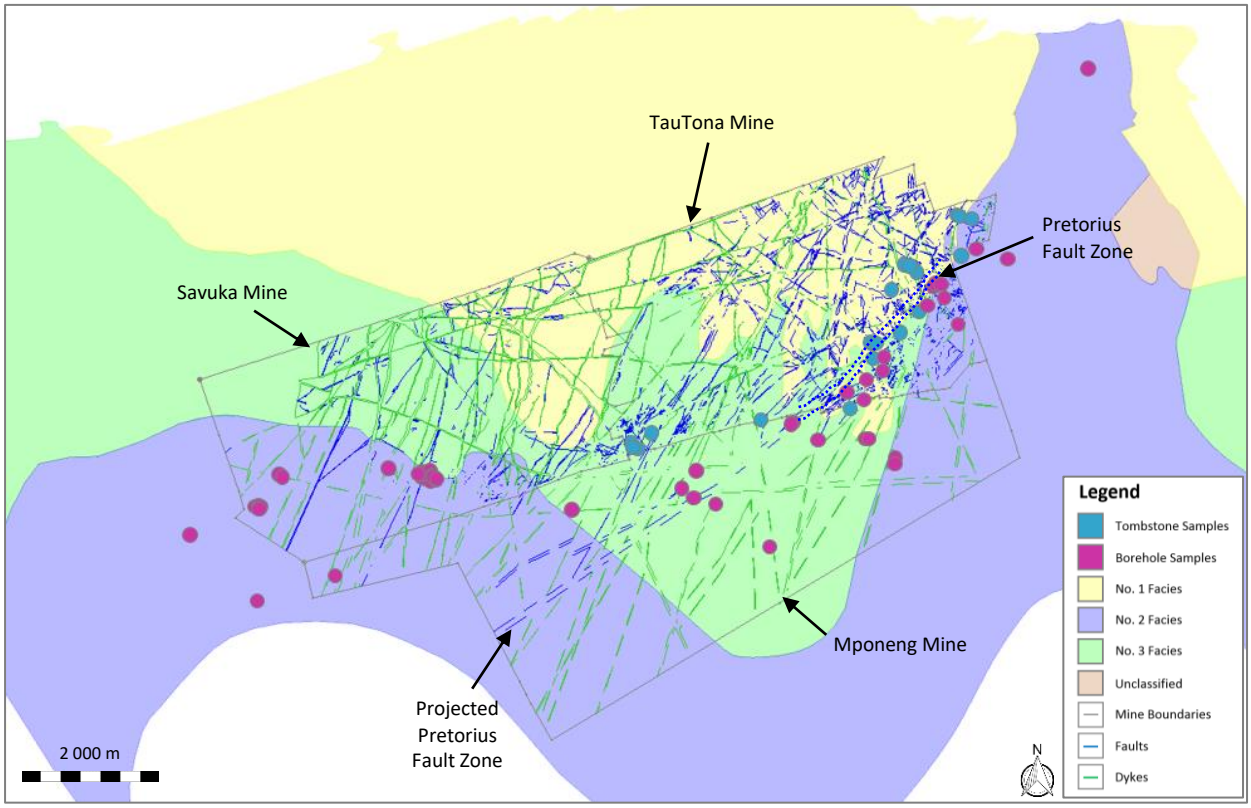

***Figure 3.70**: Sample locations for tombstone and borehole reef intersections relative to the current structure model of the Carbon Leader Reef (In House Report, 2017).*

Using a combination of the structure model and the various methodologies used to assign the predominant type of alteration of the reef, an alteration model could be created. The modelled alteration zones, based on the three major alteration styles, are shown in Figure 3.71. The samples proximal to structural influences (Samples 17, 20, 57 and 58 - mentioned in Chapter 3.1, Table 3.4) were removed for the purpose of creating the alteration zones.

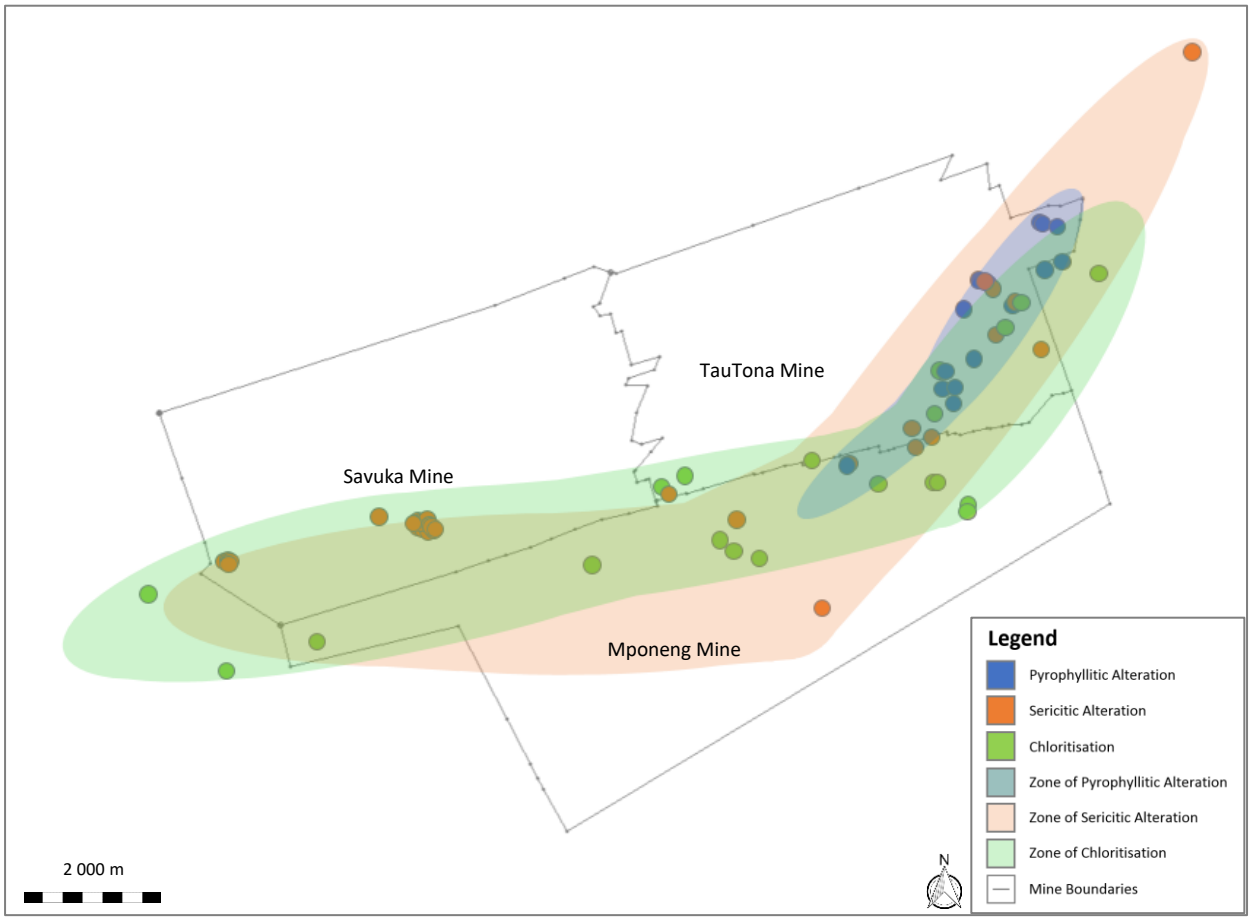

***Figure 3.71**: The proposed alteration model for the Carbon Leader Reef across the West Wits Line. Sericitic alteration had no definite trend and occurred across the mines; chloritisation occurred across all the mines however it extends further west than the sericitic alteration zone; pyrophyllitic alteration was concentrated on the north-eastern to the south-eastern and south portion of TauTona Mine.*

Post-modelling the samples that were removed due to possible structural influence were seen to suit the alteration zones in which they were located (Sample 17 – zone of chloritisation; Sample 20 – zone of sericitic alteration; Samples 57 and 58 – zone of chloritisation). This indicated that there was minimal influence from the structures on the respective sample's alteration mineralogy. This was most likely due to the small scale of the structures.

3.5.2 Discussion

The proposed alteration model discounts both the Carbon Leader Reef facies model and the estimation domain model as it only considers the major alteration style in which the sample(s) are located (based on the several methodologies carried out in this research). The alteration model reflects the samples used within this research and should be investigated further using a greater range of samples particularly in the northern and central areas of TauTona Mine, and the western and central areas of Mponeng Mine.

The chloritisation alteration zone extended across the West Wits Line from east to west and had no definite trend. The sericitic alteration zone extended further north-east and further south than the zone of chloritisation. The samples with pyrophyllitic alteration occurred in the north-eastern to the south portion of TauTona Mine. Sericitic alteration, pyrophyllitic alteration and chloritisation were noted within the No. 1 Facies samples, with higher gold grades accompanied by pyrophyllitic alteration and intermediate gold grades accompanied by sericitic alteration and chloritisation. The majority of the No. 2 Facies samples had undergone sericitic alteration, with only three samples having undergone pyrophyllitic alteration (Samples 2, 11 and 31) and eight samples having undergone chloritisation (Samples 52, 53, 57, 58, 61, 62, 67 and 68). Chloritisation, accompanied by intermediate gold grades, was the dominant alteration group within the No. 3 Facies samples. Pyrophyllitic alteration was noted in Samples 21 and 26. Sericitic alteration was noted in Samples 8, 25, 29, 47 and 55. Sample 8 had the highest gold grade (311.0 g/t) and has undergone sericitic alteration.

A west to east section of the gold grades of the samples versus the major alteration groups can be referred to in Figure 3.72. Samples that have undergone pyrophyllitic alteration were noted to have on average, the highest gold grades (78.3 g/t), followed by sericitic alteration (66.4 g/t) and chloritisation (53.3 g/t). The eastern portion of the West Wits Line had predominantly pyrophyllitic alteration becoming sericitic towards the western portion. Chloritisation was noted to occur inconsistently across the West Wits Line. Samples that are chlorite-rich are considered to have undergone the least amount of alteration whereas samples that are pyrophyllite-rich are considered to have undergone the greatest amount of alteration (Phillips, 1988). This suggests that the eastern portion of the West Wits Line is proximal to the main (hydrothermal) fluid source where the greatest amount of alteration has occurred, with increasing distance from the source in the central and western portions.

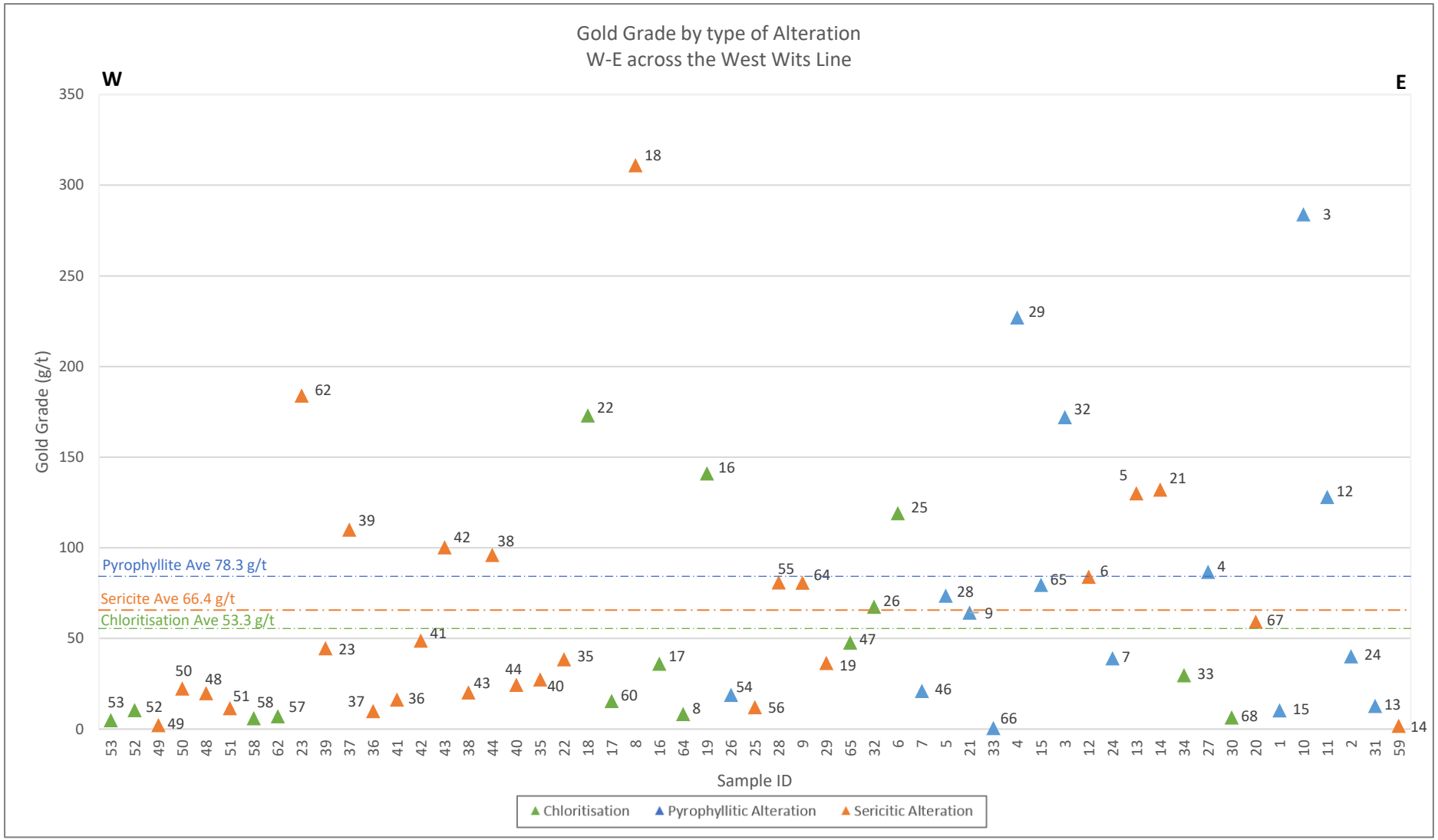

***Figure 3.72**: West to east section of the gold grades of the samples versus the major alteration groups. Pyrophyllitic alteration was predominant in the eastern portion of the West Wits Line suggesting these samples are proximal to the main (hydrothermal) fluid source. The samples were noted to have sericitic alteration in the western portions of the West Wits Line. The markers are annotated with a sample number.*

A comparison between the current Carbon Leader Reef facies model and the samples with noted discrepancies against the facies model suggest that the model needs to be revised and updated as new information becomes available. The latest model used on-site needs to be updated as this influences mine planning processes at the mine as well as the expected production output. The discrepancies have an influence on the expectant characteristics as well as the gold grades of the Carbon Leader Reef and understanding the deviations from the facies model becomes important. Although only four samples were noted to fall outside of the facies definitions proposed by Fletcher (2009) and Muller (1991), the likelihood of more samples not in agreement with the facies definitions is increased and should be investigated further. The noted discrepancies against the Carbon Leader Reef facies model are illustrated in Figure 3.73.

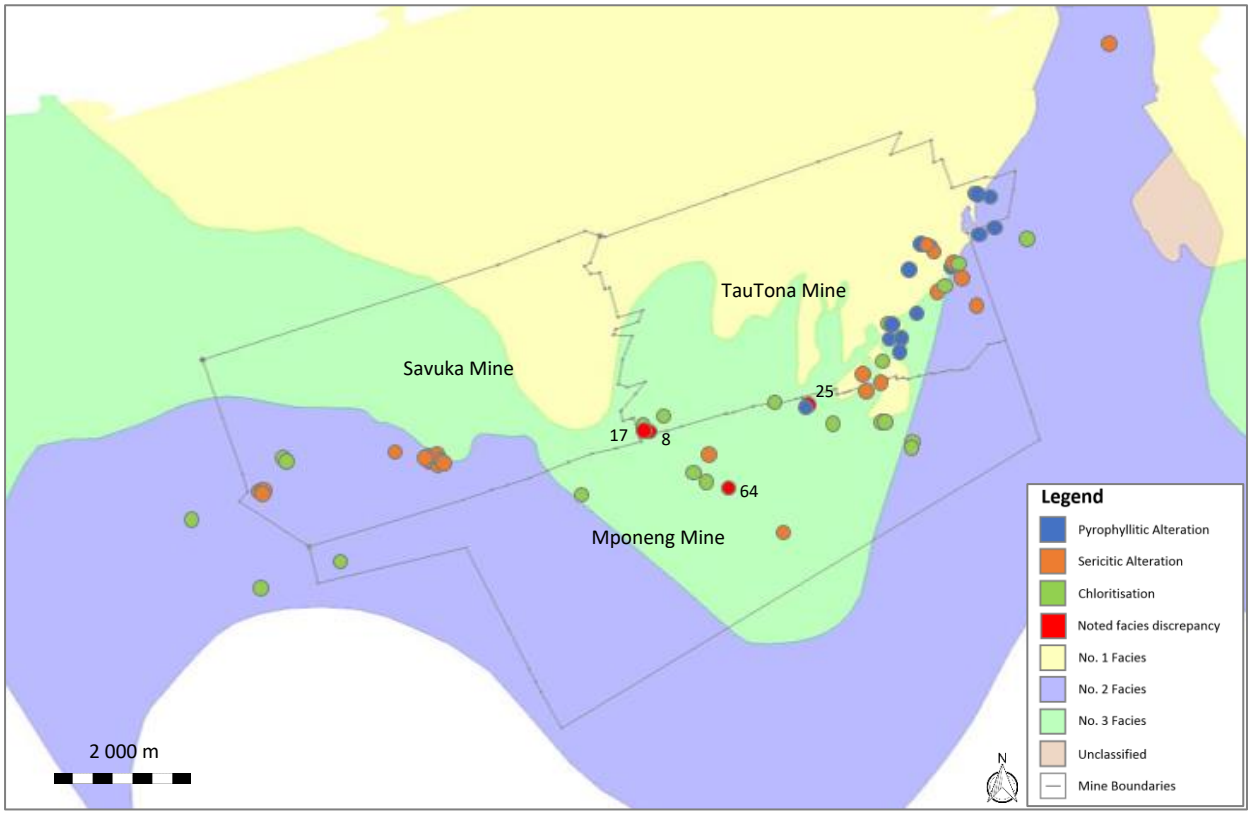

***Figure 3.73**: Three main types of alteration were noted for the reef intersections across the West Wits Line used within this research: pyrophyllitic alteration, sericitic alteration and chloritisation. Samples with discrepancies against the Carbon Leader Reef facies model are displayed in red and are annotated with a sample number.*

A recommendation would be to include a Carbon Leader Reef No. 3 Facies sub-type, based on Samples 8, 17, 25 and 64, within the facies descriptions and the model itself. Sample 8, with the highest gold grade (311.0 g/t) of all the samples used within this research, may not have had a thin basal carbon seam as Samples 17, 25 and 64 however considering the gold-hydrocarbon-

uranium relationship within the Witwatersrand Basin (Agangi *et al*., 2015; Depiné *et al.*, 2013; Drennan and Robb, 2006; Phillips and Powell, 2015) the area from which the sample was taken should be investigated further. A proposed facies model specific to the West Wits Line is illustrated in Figure 3.74. The No. 3 Facies sub-type was defined as samples falling outside of the No. 3 Facies definitions and included samples with a thin basal carbon seam and/or higher than average gold grades for the Carbon Leader Reef No. 3 Facies.

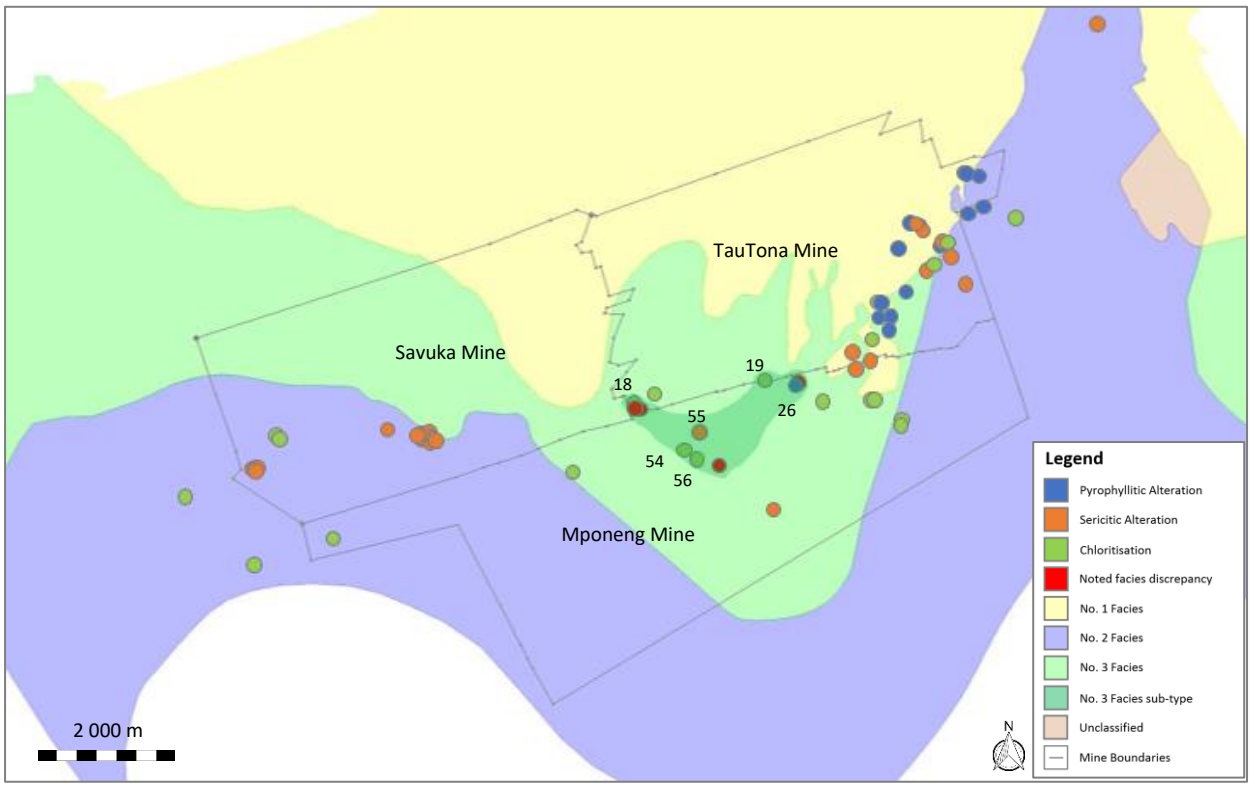

***Figure 3.74**: Proposed change to the Carbon Leader Reef facies model currently implemented at the West Wits Line. The No. 3 Facies sub-type includes samples with a thin basal carbon seam and/or higher than average gold grades for Carbon Leader Reef No. 3 Facies. Samples with discrepancies against the Carbon Leader Reef facies model are displayed in red and are annotated with a sample number.*

Sample 18 was included in the No. 3 Facies sub-type because of its higher than average gold grade at 173.0 g/t. Samples 54, 55 and 56 had little known about them including a gold grade and were included in the No. 3 Facies sub-type as they are proximal to Sample 64 that had a thin basal carbon seam. Sample 19 was also included in the sub-type because of its higher than average gold grade at 141.0 g/t. Sample 26 was included due to its proximity to Sample 25 which had a thin basal carbon seam. Samples 26, 54, 55 and 56 are borehole samples, and it is possible that there was a basal carbon seam however due to the drilling processes it may have been washed out.

Comparing the current estimation domain model and the samples with noted discrepancies against the estimation domain model suggest the model definitions need to be revised. The estimation domain model focuses on the mineralisation within the Carbon Leader Reef, particularly alteration mineralogy and variations in gold grade (Burnett *et al*., 2015). The noted discrepancies against the estimation domain model are illustrated in Figure 3.75.

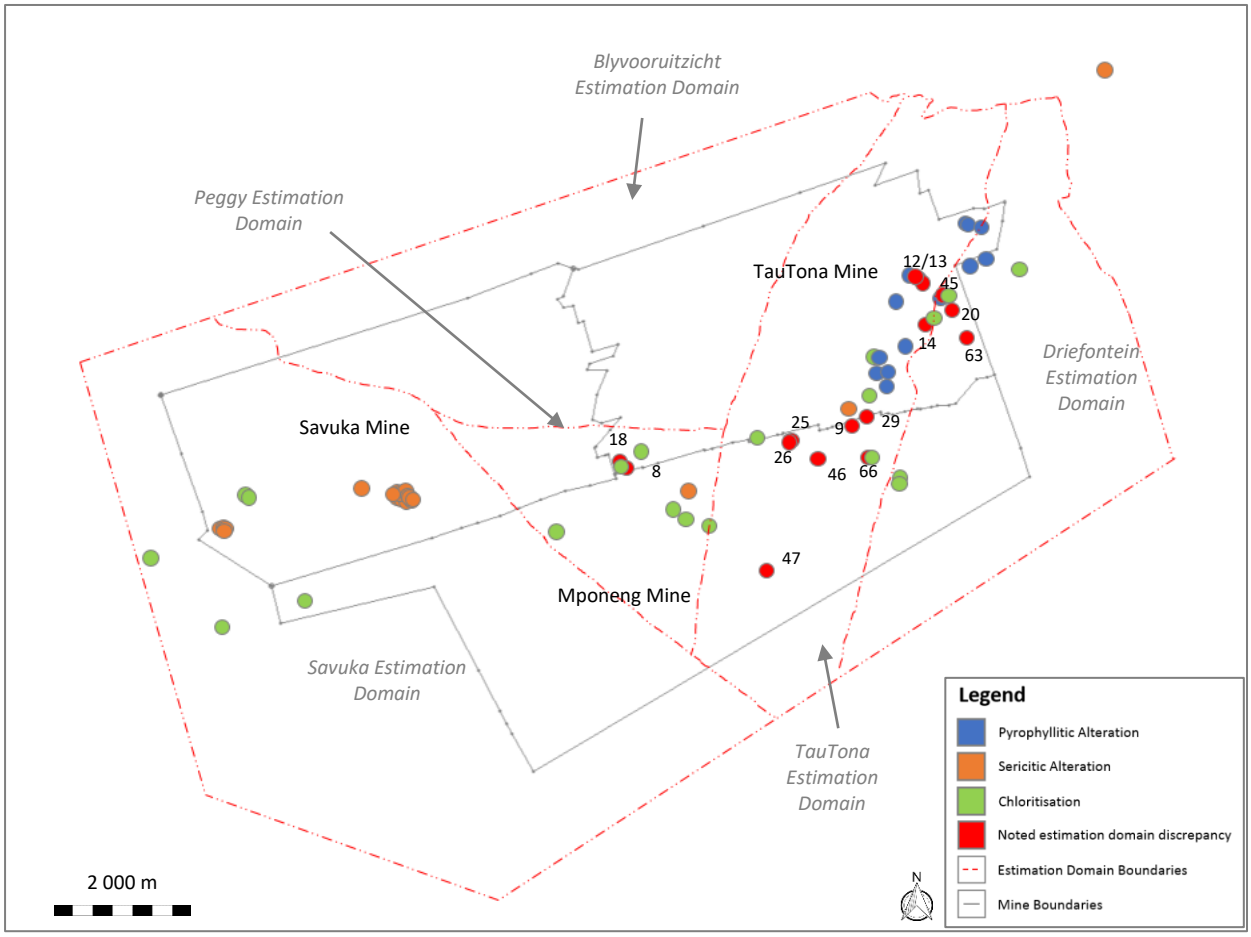

***Figure 3.75**: Three main types of alteration were noted for the reef intersections across the West Wits Line used within this research: pyrophyllitic alteration, sericitic alteration and chloritisation. Samples with discrepancies against the estimation domain model are displayed in red and are annotated with a sample number.*

Two discrepancies were noted within the Peggy estimation domain (Sample 8 and Sample 18). The Peggy estimation domain is reported to have intermediate gold values and it serves to separate the higher gold grades in the northern and eastern portions of the mines from the lower gold grades in the south-western areas of TauTona and the south-east areas of Savuka (Burnett *et al*., 2015). Sample 8 had the highest gold grade (311.0 g/t) of all the samples within this research. Sample 18 also had a considerably high gold grade (173.0 g/t) for a sample within the Peggy estimation domain. This suggests that the Peggy estimation domain may need to be re-looked at if its sole purpose is to separate higher gold grades from lower gold grades.

The Driefontein estimation domain is typically pyrophyllite-rich in the north-western portion of the estimation domain (Burnett *et al*., 2015) however Samples 20, 45 and 63 were noted to be sericite-rich. The TauTona estimation domain has relatively high gold grades and is dominated by pyrophyllite in the north-east area and has an abundance of chloritoid in the south-west area (Burnett *et al*., 2015). Samples 9, 12, 13, 14, 25, 29 and 47 were all noted to be sericitic. Sample 26 was noted to be pyrophyllitic however according to the estimation domain definitions its locality would suggest a higher chloritoid abundance. Samples 46 and 66 were less deviant to the definitions in that they were both chlorite-rich according to the spectral scanning, however samples in the south-west area of the TauTona estimation domain are typically chloritoid-rich and less chlorite-rich.

The differences in the above findings versus the estimation domain model definitions varies greatly, particularly with regards to the TauTona and Driefontein estimation domains. Similarly with the Peggy estimation domain, both the TauTona and Driefontein estimation domains should be re-looked at. The estimation domains need to be more accurate in terms of mineralogy and spatial placement of the generalised mineralogy to better understand the gold placement within the West Wits Line mines. The estimation domains should also be regularly checked and updated as more information becomes available (i.e. sampling and borehole data).

4 INTEGRATIVE DISCUSSION

The hangingwall samples of the Carbon Leader Reef were macroscopically similar across the West Wits Line. In hand specimen, some of the hangingwall samples exhibited a variation in colour from a light grey to a darker grey, and a light green to a darker green colour in other areas. This colour variation is not uncommon nearer to a contact between adjacent sedimentary packages as the contact most likely has acted as a conduit for post-depositional fluid flow (Tucker *et al*., 2016). A more distinct discolouration was noted in a few hangingwall samples on the outer edges of pyrite along foresets, pyrite lags as well as along fractures. The discolouration around the sulphides was initially proposed to be as a result of chloritisation, sericitic alteration or oxidation of sulphides.

The petrographic observations of the hangingwall samples with discolouration on the edges of sulphides (Samples 1, 5 and 10 overlying the No. 1 Facies; and Sample 8 overlying the No. 3 Facies) revealed an elevated pyrophyllite abundance, which suggested that pyrophyllitic alteration had taken place. Geochemically Samples 1, 8 and Sample 10 were noted to have a high $\%Al_2O_3$ (associated with the presence of muscovite and pyrophyllite), which overlaps with the possibility of pyrophyllitic alteration. Sample 5 had a higher $\%Fe_2O_3$ than $\%Al_2O_3$, which corresponds to the high pyrite abundance noted in both thin section and in hand specimen. This suggests that the discolouration within Sample 5 may be due to pyrophyllitic alteration however, the presence of sulphides may have influenced the alteration assemblage in comparison to the other hangingwall samples discussed.

When comparing the macroscopic observations, petrology and geochemical analyses with the spectral scanning results, Samples 1, 5, 8 and 10 have elevated pyrophyllite responses to the pyrophyllite feature extraction. The response to the pyrophyllite feature extraction for these samples is much greater than the responses to the chlorite, chloritoid or the sericite feature extractions, which corresponds well to what was observed in the preceding methodologies. Samples 1, 5 and 10 were noted to have the highest responses to the pyrophyllite feature. In thin section however, Sample 5 had the highest pyrophyllite abundance and both Samples 1 and 10 had slightly lower abundances albeit higher than the average for the hangingwall samples overlying the No. 1 Facies. Sample 8, overlying the No. 3 Facies, was noted to have the highest response to the pyrophyllite feature extraction out of all the hangingwall samples overlying the No. 3 Facies. This suggests that some form of alteration has taken place to alter the mineralogy. By referring to the petrology, the highest abundance of an alteration mineral is pyrophyllite in Sample 8. Combining the findings for Samples 1, 5, 8 and 10 of the hangingwall samples, it is very likely that pyrophyllitic alteration has taken place.

In terms of the associated gold grade, Sample 1 (0.2 g/t), Sample 5 (0.6 g/t) and Sample 8 (0.2 g/t) had low gold grades and Sample 10 had a gold grade of 2.7 g/t. Sample 10 was also noted to have the highest response to the pyrophyllite feature extraction however, it was further noted that Sample 10 was overlying a very high grade No. 1 Facies with a gold grade of 284.0 g/t. In this instance, it is very possible that gold from the No. 1 Facies has been remobilised into the overlying hangingwall unit. Overall it appears that higher responses to the pyrophyllite feature extraction, particularly in the hangingwall, correspond to lower gold grades. When

comparing the noted carbon in the hangingwall samples (Samples 1, 2 and 15) and the corresponding spectral scanning data, there were no distinct correlations. All 3 samples had higher responses to the pyrophyllite feature extraction, followed by chloritoid in Sample 1 (overlying the No. 1 Facies) and Sample 2 (overlying the No. 2 Facies), and chlorite in Sample 15 (overlying the No. 1 Facies).

Sample 19, another hangingwall sample overlying the No. 3 Facies, was noted in hand specimen to have a large 1 cm thick quartz vein cutting the hangingwall portion as well as the underlying reef, terminating at the footwall-reef contact. Petrographically the sample was noted to have a very low pyrophyllite abundance, with a higher sericitic muscovite abundance alongside chlorite and chloritoid. The combined chlorite and chloritoid abundance was higher than the sericitic muscovite abundance, suggesting that chloritisation has taken place. Geochemically Sample 19 was noted to have a high $\%Fe_2O_3$, followed by $\%Al_2O_3$ and then %MgO (associated with the presence of chlorite and chloritoid). This suggests sericitic alteration more so than chloritisation. The spectral data reveals the greatest response to the sericite feature extraction for Sample 19. Sample 19 was noted to have the lowest response to the pyrophyllite feature extraction and had a moderate response to the chlorite and chloritoid feature extractions. Combining all the methodologies, it appears that Sample 19 may have undergone sericitic alteration. The corresponding gold grade of Sample 19 is the highest of all the hangingwall samples at 8.0 g/t. The underlying No. 3 Facies unit has a high gold grade of 141.0 g/t. This suggests that gold may have been remobilised from the reef unit however it is also possible that Sample 19 is anomalously mineralised, as it is the highest gold grade of all the hangingwall samples. There appears to be no immediate relationship between alteration mineralogy and the associated gold grade for the hangingwall samples within this study.

Based on the accuracy of the spectral scanning when combined with the other methodologies used, a few other hangingwall samples that had notable alteration and were only observed in hand specimen were further supplemented by the spectral scanning data to determine the main type of alteration. These samples included Sample 20 (overlying the No. 2 Facies), Sample 22 (overlying the No. 2 Facies), Sample 26 (overlying the No. 3 Facies), Sample 28 (overlying the No. 1 Facies), Sample 53 (overlying the No. 2 Facies), Sample 58 (overlying the No. 2 Facies), Sample 61 (overlying the No. 2 Facies) and Sample 64 (overlying the No. 3 Facies).

Sample 20 and Sample 53 both had a greenish discolouration of the hangingwall quartzite on the outer edges of pyrite along foresets. It is possible that chloritisation or sericitic alteration has taken place. The spectral scanning data suggests that Sample 20 has undergone pyrophyllitic alteration and Sample 53 has undergone sericitic alteration. Quartz veining was noted in Sample 22, Sample 26 and Sample 64. Based on the findings that the hangingwall samples overlying the No. 3 Facies do not typically have a high response to the pyrophyllite feature extraction, the samples would likely display higher responses to the sericite, chlorite or chloritoid feature extractions. Sample 22 and Sample 26 were noted to have a high response to the pyrophyllite feature extraction, suggesting pyrophyllitic alteration has taken place. Sample 64 had a higher response to the chlorite feature extraction, suggesting chloritisation has taken place. Sample 28 and Sample 58 had a greenish discolouration of the hangingwall quartzite, and this discolouration may be as a result of chloritisation or sericitic alteration. The spectral scanning data revealed sericite to have the highest response in Sample 28 and chloritoid to have the highest response in Sample 58, suggesting sericitic alteration and chloritisation respectively. Sample 61 was noted to have a darkening grey colour with increasing proximity to the hangingwall-reef contact. The spectral data showed the highest response to the pyrophyllite feature extraction, suggesting a greater abundance of pyrophyllite within the hangingwall unit. This further suggests that pyrophyllitic alteration has taken place.

The gold grades were not determined for the hangingwall units from Sample 20 to Sample 64 and therefore no relationship could be determined between gold grade and alteration of the remainder of the hangingwall samples.

Overall, hangingwall samples overlying the No. 1 Facies typically showed higher responses to the pyrophyllite feature extraction in the north-east to central area of the TauTona estimation domain, with a higher chloritoid response noted within the south-west area of the TauTona estimation domain. The characteristics of the TauTona estimation domain are specific to the reef however alteration mineral similarities were noted within the hangingwall units. The hangingwall samples overlying the No. 2 Facies typically had higher responses to the pyrophyllite feature extraction in the north-west portion of the Driefontein estimation domain, and higher responses to the chlorite, chloritoid and sericite feature extractions in the Savuka estimation domain. As with the TauTona estimation domain, the characteristics of the Driefontein and Savuka estimation domains are specific to the reef however alteration mineral

similarities were noted within the hangingwall units. The hangingwall samples overlying the No. 3 Facies typically had higher responses to the pyrophyllite feature extraction in the north-east to central area of the TauTona estimation domain and higher responses to the chlorite and chloritoid feature extractions within the Peggy estimation domain. The Peggy estimation domain description proposed by Burnett *et al.* (2015) does not include any alteration minerals however using the results within this study it is possible that samples within this estimation domain have undergone chloritisation. This however can only be confirmed by the characteristics of the reef units within the Peggy estimation domain as the estimation domains are specific to the reef alteration and mineralogy. The hangingwall samples overlying the No. 1 and the No. 3 Facies had similar alteration mineralogy in comparison to the No. 2 Facies samples.

The footwall samples of the Carbon Leader Reef are also macroscopically similar across the West Wits Line. Sample 1, underlying the No. 1 Facies, was noted in hand specimen to have rounded (detrital) pyrite grains along fractures. In thin section Sample 1 had an elevated abundance of sericitic muscovite, with detrital pyrite grains occurring within the sericite-rich matrix. This suggests sericitic alteration may have taken place. Geochemically, Sample 1 had a very high $\%Al_2O_3$ which corresponds to the petrology. In terms of the spectral scanning data Sample 1 had a higher response to the pyrophyllite feature extraction, followed by the chloritoid feature extraction and only then the sericite feature extraction, suggesting a higher abundance of pyrophyllite and chloritoid in the footwall sample than sericitic muscovite. It is possible that the thin section taken from the footwall unit of Sample 1 may not have been 100% representative however the geochemical analyses corresponded to the petrology. This suggests that the spectral scanning may not have been carried out successfully for the footwall unit of Sample 1, i.e. specifically the footwall unit of the sample may have not dried fully prior to the scanning of the sample because the spectral scanning data for the remainder of Sample 1 (hangingwall and reef units) correspond to the petrology and geochemical analyses. The gold grade of Sample 1 was 0.1 g/t and no carbon was seen in thin section.

The footwall portion of Sample 17 exhibited a greenish discolouration of the quartzite on the outer edge of a fault/shear located at the contact between the reef and the footwall. The petrology of Sample 17 suggests sericitic alteration has taken place. Geochemically the $\%Al_2O_3$ is higher than the other oxides, further suggesting sericitic or pyrophyllitic alteration. When

referring to the spectral scanning data, the highest response is noted to be against the pyrophyllite feature extraction followed by the sericite feature extraction. This suggests that the footwall portion of Sample 17 has undergone pyrophyllitic alteration. The gold grade of Sample 17 was 0.9 g/t and no carbon was noted in thin section. For both Sample 1 and Sample 17, there appears to be no immediate relationship between gold grade and alteration noted within the footwall samples within this study.

Sample 18, with a gold grade of 135.0 g/t, was suggested to have been misidentified as a footwall sample rather than as part of the reef however when referring to the petrology the sample has similar modal abundances to the other footwall samples. Geochemically the sample exhibits similar oxide percentages as well as trace element concentrations, with the exception of U that is considerably higher in concentration, with the other footwall samples. However, when comparing the uranium concentrations within the footwall samples, samples underlying the No. 3 Facies seem to have much higher U concentrations than samples from the No. 1 and the No. 2 Facies. The higher U concentrations are associated with gold grade however these are not proportionate to one another i.e. higher U concentrations to do not yield higher gold grades in the footwall. This is seen in Sample $9^{(a)}$ which is representative of a footwall pebble band. The U, Ni, Th, Pb, U_3O_8 and Ba concentrations are much higher than the other footwall samples and are within the same range as Sample 18 however the gold grade of Sample $9^{(a)}$ is 2.8 g/t. This is also seen in Sample 19 that yields a gold grade of 26.8 g/t. By referring to the spectral scanning data of Sample 18, the footwall is distinctly different from the No. 3 Facies unit in the spectral scan. This suggests that the sample has been correctly identified as footwall. To further confirm this, the spectral profile can be referred to. The behaviour of the spectral responses of the hangingwall and reef portions of Sample 18 are similar in that they have a very low response to the pyrophyllite feature extraction. The spectral response to the pyrophyllite feature extraction in Sample 18 is higher in comparison to the Sample 19 that is also from the same facies type. This confirms that the footwall portion of Sample 18 is anomalously mineralised as the response to the pyrophyllite feature extraction would have been similar if not the same as the reef if it was indeed part of the reef and would have had a similar response to the pyrophyllite feature extraction as the footwall portion of Sample 19. In Sample 19, the spectral scan reveals a distinct separation between the reef and the footwall unit suggesting

that the higher gold grade within the footwall unit – as with Sample 18 – is as a result of remobilisation of gold from the overlying high grade reef units.

Based on the accuracy of the spectral scanning of the footwall samples and the overlaps with the other methodologies used within this research (with the exception of Sample 1) the spectral data was used to determine alteration within the footwall samples. Other footwall samples that were noted to have visible alteration in hand specimen with only spectral data to supplement the findings include Sample 20 (underlying the No. 2 Facies), Sample 22 (underlying the No. 2 Facies) and Sample 28 (underlying the No. 1 Facies).

Sample 20 was noted to have a greenish discolouration of several milky quartz clasts within a footwall pebble band. Fault-fill veining was also noted within the footwall unit. The highest response to a feature extraction for the footwall unit was to the pyrophyllite feature extraction. The next highest response was to the chloritoid feature extraction. It is possible that the major alteration that has taken place is pyrophyllitic alteration (fault-fill veining), with a minor occurrence of chloritisation that has allowed for the greenish discolouration of the milky quartz clasts. In Sample 22, the footwall quartzite was noted to become gradually darker with increasing proximity to the footwall-reef contact. When referring to the spectral data, particularly the spectral profiles, there is a gradual change from pyrophyllite to sericite having the highest response with increasing proximity to the footwall-reef contact. This suggests that there is localised sericitic alteration closer to the reef. Sample 28 was noted to have a greenish discolouration at the footwall-footwall pebble band contacts. The spectral profiles indicate a high response to the sericite feature extraction and a low response to the pyrophyllite feature extraction over the footwall pebble band. The footwall quartzite either side of the footwall pebble band exhibits a high response to both the sericite and pyrophyllite feature extraction. This suggests the greenish discolouration at the footwall-footwall pebble band contacts is due to sericitic alteration.

The gold grades were not determined for the footwall units from Sample 20 to Sample 64 and therefore no relationship could be determined between gold grade and alteration of the remainder of the footwall samples.

Overall, footwall samples underlying the No. 1 Facies typically showed higher responses to the pyrophyllite feature extraction. The alteration mineralogy of the footwall samples underlying

the No. 1 Facies coincides with the alteration mineralogy of the reef proposed by Burnett *et al*. (2015) within the north-east to central areas of the TauTona estimation domain as well as the north-west area of the Driefontein estimation domain. This also suggests pyrophyllitic alteration is common within the footwall underlying the No. 1 Facies. Footwall samples underlying the No. 2 Facies typically had higher responses to the pyrophyllite feature extraction (north-east portion of the TauTona estimation domain and north-west portion of the Driefontein estimation domain) or to the sericite feature extraction (within the Savuka estimation domain). As with the No. 1 Facies footwall samples, the No. 2 Facies footwall samples coincide with the alteration mineralogy of the reef proposed by Burnett *et al*. (2015). This suggests pyrophyllitic alteration in the north-eastern area of the West Wits Line, becoming sericitic towards the central to eastern area of the West Wits Line. The samples underlying the No. 3 Facies typically had higher responses to the pyrophyllite feature extraction, regardless of locality across the West Wits Mines. This suggests pyrophyllitic alteration is common within the footwall underlying the No. 3 Facies. Similarly to the hangingwall samples, the footwall samples for the No. 1 and the No. 3 Facies had similar alteration mineralogy in comparison to the samples underlying the No. 2 Facies.

The various facies types of the Carbon Leader Reef reveal noticeable differences across the West Wits Line with some similarities seen, particularly in the alteration of the reef packages. Alteration within the No. 1 Facies was mostly noted by a greenish discolouration of the matrix (Samples 1, 3, 10, 13 and 33). It was suggested that the alteration may be due to chloritisation. Sample 1 had an elevated pyrophyllite abundance followed by chlorite. Sample 3 and Sample 10 had no chlorite noted in thin section but had an elevated abundance of pyrophyllite followed closely by sericitic muscovite. Sample 13 had an elevated sericitic muscovite abundance followed by pyrophyllite and Sample 33 had an elevated abundance of pyrophyllite, followed by sericitic muscovite and had chlorite noted in thin section. Geochemically all these samples had high $\%Al_2O_3$ and this corresponded to the findings of sericitic muscovite and pyrophyllite in thin section. By referring to the spectral scanning data of these samples, Sample 1 and 10 had higher responses to the pyrophyllite feature extraction, and Samples 3 and 13 had higher responses to the sericite and pyrophyllite feature extractions. Sample 33 was not spectrally scanned however the gold grade was 0.6 g/t which is considerably low for a sample within the No. 1 Facies and within the TauTona estimation domain. The spectral scanning data

aligns somewhat to what was noted in thin section. The thin section is not always 100% representative of the mineralogy of the sample and should only be used as a guideline unless several thin sections of the same sample were cut and examined. The spectral scanning data of Samples 3 and 13 suggests the overall alteration is either sericitic or pyrophyllitic, or a combination of both, with Samples 1 and 10 having predominantly pyrophyllitic alteration. Samples 3 and 13 do not fully align to the TauTona estimation domain as the dominant alteration mineral seen within the reef in the north-east area of the TauTona estimation domain is pyrophyllite.

Samples within the No. 1 Facies with a noted basal carbon seam included Samples 4, 7, 12, 15 and 32. As the carbon was noted to occur at the base of the reef it was also possible to note the alteration mineralogy immediately at the contact with the footwall. The spectral responses however may not be accurate as organic matter may affect the responses to the feature extractions (Hauff, 2001, p.2). It should also be considered that because it is a contact between adjacent sedimentary units, the alteration may be due to the contact acting as a conduit for fluid flow (Tucker *et al*., 2016). Sample 4 (227.0 g/t) had the highest response to the pyrophyllite feature extraction, suggesting pyrophyllitic alteration has taken place. At the base of the reef unit there was no noticeable variation from the pyrophyllitic response. Sample 7 (21.1 g/t) was noted to have moderate responses to both the sericite and pyrophyllite feature extractions at the base of the reef, with a moderate response to the pyrophyllite feature extraction in the whole reef unit. Samples 12 and 15 were noted to have a moderate response to the sericite feature extraction at the base of reef however the whole reef unit for Sample 12 (83.9 g/t) also had a moderate response to the sericite feature extraction and the whole reef unit for Sample 15 (79.5 g/t) had a moderate response to the pyrophyllite feature extraction. Sample 32 (67.5 g/t) was noted to have a spike in the pyrophyllite response at the base of the reef unit with the remaining reef portion having a higher response to the chlorite and chloritoid feature extractions.

Samples 7, 12, 15 and 32 do not align with the facies model or the TauTona estimation domain as the gold grades are lower than what is usually expected for samples within the No. 1 Facies and TauTona estimation domain. Sample 12 was noted to be sericitic however samples in the north-east portion of the TauTona estimation domain are typically pyrophyllitic. Sample 32 was

noted to be chloritic which does not align with the typical mineralogy within the TauTona estimation domain proposed by Burnett *et al*. (2015).

Overall, the sample spectral scanning responses were able to reveal the major alteration mineralogy with a fair amount of accuracy for the samples that had undergone all the methodologies. Therefore, the remaining samples that had only been observed in hand specimen and spectrally scanned were assumed to have correct responses to the feature extractions. Samples from the No. 1 Facies were noted to have undergone sericitic alteration, pyrophyllitic alteration as well as chloritisation. The No. 1 Facies samples with the highest gold grades were noted to have pyrophyllitic alteration (Sample 3 at 172.0 g/t, Sample 4 at 227.0 g/t and Sample 10 at 284.0 g/t) however the samples with the lowest gold grades were also noted to have pyrophyllitic alteration (Sample 1 at 10.3 g/t and Sample 33 at 0.6 g/t). Samples with pyrophyllitic alteration were noted to occur within the north-east portion of the TauTona estimation domain. Samples with intermediate to high gold grades were noted to have undergone sericitic alteration and were found in the north-east to central portion of the TauTona estimation domain. Samples with intermediate gold grades were noted to have undergone chloritisation and were found in the central portion of the TauTona estimation domain.

Alteration within the No. 2 Facies was noted as a greenish discolouration within the matrix of the reef band(s) (Samples 53, 59 and 62), greenish discolouration of milky quartz clasts within the matrix of the reef (Samples 31 and 62) as well as discolouration of the Pale Pebbly Quartzite (Sample 23) and Brown-Orange Argillaceous Zone (Samples 51, 53 and 63) on the outer edges of pyrite lags. Sample 23 was noted to have a discolouration of the sulphides within the No. 2B Facies matrix. Sample 57 was noted to have broken and fragmented core possibly due to a proximal fault or fault zone. Sample 61 had a quartz vein cutting across both the reef and Brown-Orange Argillaceous Zone units.

The greenish discolouration within the matrix of the reef bands was suggested to be due to chloritisation. Samples 53, 59 and 62 were only observed in hand specimen and were spectrally scanned. The spectral scans for Sample 53 revealed higher responses to the sericite feature extraction for both the No. 2A and No. 2B Facies. The No. 2A Facies was highly responsive to both the sericite and chlorite feature extraction, suggesting higher abundances of sericite and chlorite within the reef band. This suggests that the discolouration of the matrix is due to

sericitic alteration within the No. 2B Facies and a combination of sericitic alteration and chloritisation within the No. 2A Facies. In Sample 59, the No. 2B Facies had a high response to both the sericite and the pyrophyllite feature extraction and the No. 2A Facies has a high response to the sericite feature extraction. This suggests a combination of sericitic and pyrophyllitic alteration within the No. 2B Facies, with sericitic alteration within the No. 2A Facies. In Sample 62, the No. 2A Facies and the No. 2B Facies were highly responsive to the sericite and chlorite feature extraction, suggesting that both sericitic alteration and chloritisation has taken place. The No. 2A Facies had a higher response to the chlorite feature extraction nearer to the footwall contact, suggesting a concentration of chlorite within the base of the No. 2A Facies. This further suggests that the greenish discolouration of the No. 2A Facies matrix as well as several milky quartz clasts within the No. 2A Facies may be due to chloritisation.

In Sample 31, the No. 2A Facies shows a greater response to the pyrophyllite feature extraction however there is a moderate response to both the chloritoid and chlorite feature extractions. This suggests that the main alteration may be pyrophyllitic, combined with chloritisation within the No. 2A Facies. The No. 2B Facies has a greater response to the pyrophyllite feature extraction, suggesting a higher abundance of pyrophyllite and further suggesting pyrophyllitic alteration has taken place. In thin section, the No. 2B Facies has a higher pyrophyllite abundance in comparison to sericitic muscovite, chlorite and chloritoid, and this aligns with the responses to the feature extractions for Sample 31. Geochemically, the No. 2B Facies had higher $\%Al_2O_3$ with %MgO below the lower detection limit. This further confirms that pyrophyllitic alteration may have taken place in the No. 2B Facies.

In Sample 23, the No. 2B Facies was noted in thin section to have a high abundance of sericitic muscovite in comparison to pyrophyllite, chlorite and chloritoid. The pyrite abundance was slightly above the average noted abundance for pyrite within the No. 2 Facies. This was also noted in the $\%Fe_2O_3$ for Sample 23. The $\%Al_2O_3$ was only slightly higher than the $\%Fe_2O_3$, and the $\%Fe_2O_3$ was greater than the %MgO suggesting a higher abundance of sulphides than chlorite and chloritoid within the sample. The spectral profiles for Sample 23 revealed a higher response to the sericitic feature extraction, followed by the chlorite and chloritoid feature extractions. It was suggested that Sample 23 had undergone oxidation, and this may be

possible due to the amount of sulphides within the sample, however it appears that the major alteration that has taken place within the No. 2B unit is sericitic.

Sample 57 appears to have undergone a combination of both sericitic alteration and chloritisation. This is suggested by the responses to the sericite and chlorite feature extractions. The feature extraction images suggest higher amounts of chloritisation particularly in the upper portion of the No. 2A Facies and the spectral profiles suggest higher amounts of sericitic alteration, with a slight decrease in the response in the upper portion of the reef. Sample 57 was noted to have fragmented core however the spectral responses align with the zone in which it lies, and the core may be fragmented due to blasting fractures prior to the hole having been drilled.

The spectral images for Sample 61 suggest that the quartz veining within the Brown-Orange Argillaceous Zone is sericitic. The quartz vein cutting across the unit to the No. 2B Facies is not visible within the images however the sericitic quartz veins are noted in the upper portion of the Brown-Orange Argillaceous Zone. It is then assumed that sericitic alteration has occurred primarily within and on the outer edges of the quartz veins. The major alteration that is noted within the No. 2B Facies is chloritisation, as the highest response is noted against the chlorite feature extraction.

The Pale Pebbly Quartzite of Sample 23 shows a very high response to the sericite feature extraction when referring to the spectral profiles, with lower responses to the chlorite and chloritoid feature extractions. The spectral images suggest a higher response to the pyrophyllite feature extraction however the spectral facies image shows a combination of chlorite and sericite, and the corresponding feature extraction images align to the spectral facies image and spectral profiles. This suggests that the alteration noted within the Pale Pebbly Quartzite unit is due to sericitic alteration that is concentrated (greater) on the outer edges of the pyrite lag.

Sample 51 shows a slight discolouration of the lower Brown-Orange Argillaceous Zone. In the lower portion of the unit, there is an increased response to the chlorite and chloritoid feature extractions within the spectral profiles. The spectral images suggest an increase in the chloritoid feature extraction. The overall alteration is sericitic in the unit as well as the

underlying No. 2B and No. 2A units, however the discolouration of the Brown-Orange Argillaceous Zone may be due to chloritisation.

Both Sample 53 and 63 have a greenish discolouration of the Brown-Orange Argillaceous Zone. Sample 53, with an overall sericitic alteration, shows an increase in chloritoid within the Brown-Orange Argillaceous Zone, suggesting a combination of sericitic alteration and chloritisation has occurred. This is similarly noted in Sample 63, where there is an increase in the chlorite and chloritoid responses, suggesting a combination of sericitic alteration (major alteration) and chloritisation has occurred.

As with the No. 1 Facies samples, a subset of No. 2 Facies samples did not align to the facies and/or the estimation domain model upon reviewing the microscopic, geochemical and/or spectral data. Sample 2, with a gold grade of 40.1 g/t for the No. 2A Facies and 41.2 g/t for the No. 2B Facies, has gold grades that do not align to the TauTona estimation domain as they are lower than what is typically noted within the estimation domain. The carbon that was noted in hand specimen and thin section for Sample 2 does not align with the facies model proposed for the No. 2 Facies. This is similarly noted for Sample 11 that also had carbon present. Sample 20 and Sample 63 within the north-west portion of the Driefontein estimation domain were noted to be sericitic, and samples within the area are typically pyrophyllite-rich.

Due to carbon occurring as fly-speck carbon it was not possible to pin-point variations in the spectral scanning results however due to the lack of the carbon in most of the samples, this would suggest greater accuracies with regards to the spectral scanning data as the organic matter is reduced significantly within the No. 2 Facies.

Overall, samples from the No. 2 Facies were noted to have undergone mostly sericitic alteration, with a few occurrences of chloritisation and only 3 samples with pyrophyllitic alteration. The No. 2 Facies samples with the highest gold grades were noted to have sericitic alteration (Sample 23 at 183.9 g/t, Sample 37 at 110.0 g/t and Sample 43 at 100.2 g/t) however the samples with the lowest gold grades were also noted to have sericitic alteration (Sample 59 at 1.7 g/t and Sample 49 at 2.1 g/t). The higher gold grades with sericitic alteration were noted to occur in the westernmost area of the West Wits Line within the Savuka estimation domain. Samples with intermediate to high gold grades were noted to have undergone pyrophyllitic alteration and were noted to occur within the north-east portion of the TauTona estimation

domain and the north-west of the Driefontein estimation domain. Samples with low gold grades were noted to have undergone chloritisation and were found in the central portion of the TauTona estimation domain as well as the western portion of the Savuka estimation domain.

Alteration within the No. 3 Facies was noted as a greenish discolouration within the matrix of the reef band (Samples 8, 18 and 25), greenish discolouration of milky quartz clasts within the matrix of the reef (Samples 21 and 25) as well as proximal to a sheared contact with the footwall quartzite (Sample 21).

Sample 8 in thin section was noted to have the greatest abundance of phyllosilicate material, specifically pyrophyllite, across all the reef samples regardless of facies type. Sericitic muscovite and chlorite were the next greatest in abundance. Geochemically it was noted that Sample 8 had the greatest $\%Al_2O_3$ at 10.10% as well as $\%Fe_2O_3$ at 7.23%. This aligns with the abundance of pyrophyllite and indicates a large presence of sulphides within the sample. The presence of sulphides and the large abundance of pyrophyllite within the sample is accompanied by a very high gold grade, the highest of the reef samples, of 311.0 g/t. The spectral scanning data suggests, similarly to the petrology and geochemical data, that pyrophyllite has a greater abundance than sericitic muscovite, chlorite and chloritoid. The hand specimen displayed a greenish discolouration in the uppermost part of the reef unit. When referring to the behavioural characteristics of the hangingwall spectral data, there appears to be a drastic increase of sericite from the hangingwall to the reef unit. This suggests that although the major alteration within the reef is possibly pyrophyllitic, the greenish discolouration may be due to sericitic alteration.

In Sample 18 the reef was also noted to have a greenish discolouration in the uppermost portion. In thin section the sample had low amounts of phyllosilicate material. The geochemical analyses revealed the sample to have a relatively low $\%Al_2O_3$ at 2.28%. This aligns with the low phyllosilicate content seen within the petrology of the sample. The spectral responses of the phyllosilicate minerals were also notably low in comparison to the other reef samples, aligning to what was seen in the other methodologies. The greatest response was noted to be against the sericite feature extraction, followed by the chlorite feature extraction. The overlying hangingwall unit was noted to have a high chlorite abundance in thin section and geochemically, as well a high response to the chlorite and chloritoid feature extractions. The

greenish discolouration in the upper region of the reef may be due to sericitic alteration of the reef, however the chloritisation of the hangingwall may have also affected the underlying reef unit. Sample 18 was accompanied by a high gold grade of 173.0 g/t.

Sample 25 was noted to have a higher abundance of sericitic muscovite, followed by pyrophyllite in thin section, although the total phyllosilicate material within the sample was low. Geochemically the sample had a low $\%Al_2O_3$ and %MgO content that coincides with the petrology. The spectral profile of Sample 25 suggests a higher abundance of pyrophyllite in the lower portion of the reef unit, becoming chloritoid and chlorite rich with increasing proximity to the hangingwall unit. This suggests that pyrophyllitic alteration is concentrated at the base of the reef nearer to the pyrophyllitic footwall unit and chloritisation has occurred in the remainder of the reef unit. The greenish discolouration of the reef matrix as well as the greenish discolouration of a few quartz clasts may, in this sample, be due to chloritisation.

The reef unit of Sample 21 shared a sheared contact with the footwall quartzite. A single milky quartz clast was noted to have a greenish discolouration within the matrix of the reef. In thin section, the reef was noted to have a greater amount of pyrophyllite, with lessor amounts of sericitic muscovite and chloritoid. No chlorite was observed in thin section for the reef unit of Sample 21. The geochemical analyses revealed a high $\%Al_2O_3$ at 6.94%, in comparison to the other reef samples used within this study. The spectral profiles for the reef unit indicated an abundance of pyrophyllite throughout the reef unit however becoming less pyrophyllitic and more chlorite and chloritoid-rich with increasing proximity to the hangingwall unit. This suggests that the greenish discolouration of the milky quartz clast may be due to chloritisation that occurred with the pyrophyllitic alteration. At the sheared contact between the reef and the footwall units the responses to the feature extractions are consistent and do not reveal any major changes in the pyrophyllitic alteration and chloritisation mineralogy. This suggests that the shearing took place prior to the alteration of the host rock.

Fly-speck carbon was noted in hand specimen for Sample 16 (36.0 g/t). A thin basal carbon seam was noted for Samples 17 (15.4 g/t), 25 (31.4 g/t) and 64 (8.2 g/t). Thin pyrite stringers were noted to mark the base of the reef unit in Sample 19 (141.0 g/t). No immediate differences were noted in the spectral scanning responses for Samples 16, 17 and 19. Sample 25 had a decrease in the pyrophyllite abundance and an increase in chloritoid at the contact, and Sample 64 had an increase in both chloritoid and pyrophyllite abundance at the contact

between the internal quartzite and footwall units at the carbon seam. Similarly to the No. 1 Facies samples, no correlation was noted between alteration type and carbon presence. Compared to the samples from the No. 1 Facies, the samples with a carbon seam in the No. 3 Facies had a considerably lower gold grade. This may be due to the lack of thickness and poor development of the basal carbon seam in the No. 3 Facies samples.

Of the samples that had notable macroscopic observations for the No. 3 Facies, Samples 8, 16, 17, 18, 25 and 64 do not align with either the facies model, estimation domain model or a combination of both. Sample 8 had the highest gold grade of all the reef samples at 311.0 g/t – this is unusual for a sample within the Peggy estimation domain that typically has intermediate gold grades, as well as within the No. 3 Facies. In contrast to Sample 8, Sample 16 had a lower gold grade than what is typically seen within the Peggy estimation domain and within the No. 3 Facies. Sample 17 had a basal carbon seam and a low gold grade, which is not typically seen within the Peggy estimation domain and within the No. 3 Facies. Sample 18, within the Peggy estimation domain, was noted to have a gold grade of 173.0 g/t which is significantly higher than the expected gold grades within the Peggy estimation domain. In Sample 25, the gold grade was low at 31.4 g/t, the sample was also noted to be sericitic and have a basal carbon seam. The characteristics do not align with the TauTona estimation domain that is pyrophyllite-rich in the north-east area to chloritoid-rich in the south-west area. The carbon seam and low gold grade are also not aligned to the facies model. Sample 64 has a gold grade of 8.2 g/t as well as thin carbon seam, which does not align to either the Peggy estimation domain or to the No. 3 Facies.

As with the No. 1 Facies and No. 2 Facies samples, a subset of No. 3 Facies samples did not align to the facies and/or the estimation domain model upon reviewing the microscopic, geochemical and/or spectral data. Sample 9, with a gold grade of 80.7 g/t has a gold grade that does not align to the TauTona estimation domain as it is lower than what is typically noted within the estimation domain. In Sample 19, the reef is sericitic which does not align to the typical mineralogy noted within the TauTona estimation domain. Sample 26 had a high abundance of pyrophyllite however relative to its locality within the TauTona estimation domain, the sample should be chloritoid-rich. The gold grade of 1.6 g/t for Sample 26 is significantly low for a sample within the TauTona estimation domain and within the No. 3 Facies. Sample 29 was sericitic, contradicting the typical mineralogy within the TauTona

estimation domain. The gold grade was low at 36.4 g/t and is not typically seen this low within the TauTona estimation domain and within the No. 3 Facies. Samples to the south-west of the TauTona estimation domain are typically chloritoid-rich. Sample 46 was noted to have a greater response to the chlorite feature extraction in comparison to the chloritoid feature extraction which does not align to the estimation domain. Sample 47, also within the south-west portion of the TauTona estimation domain had a higher response to the sericite feature extraction, suggesting a higher sericite abundance within the sample. This does not align to the typical findings within the TauTona estimation domain.

Overall, samples from the No. 3 Facies were noted to have undergone mostly chloritisation, with fewer occurrences of sericitic alteration and only 2 samples with pyrophyllitic alteration. The highest gold grade for a No. 3 Facies sample (Sample 8 at 311.0 g/t) was accompanied by sericitic alteration. Other high gold grades within the No. 3 Facies samples were noted to have undergone chloritisation (Sample 18 at 173.0 g/t and Sample 19 at 141.0 g/t) however the lowest gold grades were also noted to have chloritisation (Sample 17 at 15.4 g/t and Sample 64 at 8.2 g/t). The samples with sericitic alteration or chloritisation were noted to occur in the central area of the West Wits Line within the Peggy and TauTona estimation domains and ranged in gold grade from very low to very high. The 2 samples with pyrophyllitic alteration occurred in the central area of the TauTona estimation domain (Sample 21 at 64.3 g/t and Sample 26 at 19.0 g/t). There was no definite relationship between the gold grade of a sample and the type of alteration that had occurred within the No. 3 Facies.

By combining the observations of macroscopic, microscopic, geochemical analyses as well as spectral scanning it was possible to create an alteration model for the Carbon Leader Reef at the West Wits Line. Three main zones of alteration were suggested for the Carbon Leader Reef: sericitic alteration, pyrophyllitic alteration and chloritisation.

The reef samples with chloritisation present have no definite trend and the alteration zone extends across the West Wits Line from west to east. The average gold grade of samples that have undergone chloritisation was 53.3 g/t, with a greater frequency of chloritisation noted within the No. 3 Facies and the least amount of chloritisation noted within the No. 1 Facies. The sericitic alteration zone extends further north-east than the zone of chloritisation, suggesting the samples within this alteration zone are closer to the main (hydrothermal) fluid source than the samples within the chloritisation zone. The average gold grade of samples that

have undergone sericitic alteration was 66.4 g/t, with a greater frequency of sericitic alteration noted within the No. 2 Facies and the least amount of sericitic alteration noted within the No. 1 Facies. The reef samples with pyrophyllitic alteration occur on the north-eastern region, extending south-east to south of TauTona mine. The reef samples with the higher pyrophyllite content appear to have higher pyrophyllite content within the overlying hangingwall unit, suggesting intense alteration has occurred. This would indicate that these samples (and the north-eastern to southern region of TauTona) are proximal to the main fluid source. The average gold grade of the samples that have undergone pyrophyllitic alteration was 78.3 g/t, with a greater frequency of pyrophyllitic alteration within the No. 1 Facies and the least amount of pyrophyllitic alteration noted within the No. 3 Facies. Although the average gold grades per alteration zone suggest higher gold grades within the pyrophyllitic zone, it should be noted that the majority of the No. 1 Facies samples were within the pyrophyllitic zone thus increasing the average gold grade in comparison to the sericitic and chloritisation zones.

On a larger scale, with reference to Figure 3.70 and Figure 3.71 (Chapter 3.5), there appears to be an overlap between the amount and/or type of structural influences and the occurrence of an alteration style. Although the immediate structural influences for each sample were considered and subsequently excluded for geological modelling purposes, the samples may suggest the timing of faulting and intrusions based on the major type of alteration. Investigations into fluid evolution carried out by Drennan *et al*. (1999) revealed that several pulses of fluids occurred during the deposition of the Witwatersrand sediments. The earliest recognised fluids were noted to be associated with higher temperatures and were H_2O and H_2O-CO_2 dominated, whereas later fluids were associated with lower temperatures and were vapour-rich and hydrocarbon bearing (Drennan *et al*., 1999).

Various metamorphic temperature ranges in the Witwatersrand Basin have been proposed by means of various geothermometric techniques. Phillips and Law (1994) proposed pyrophyllite to be stable between 300°C and 400°C. A later study by Vidal *et al*. (2007) revised this range to begin at 350°C. The stable temperature of chloritoid as determined by Frimmel (1997a) was suggested to be greater than 300°C. Drennan *et al*. (1999) proposed chlorite to have a stable temperature of 280°C to 380°C. The lowest stable temperature is that of muscovite and was proposed to be greater than 200°C by Phillips and Law (1994). Based on these temperatures it is suggested that the presence of pyrophyllite indicates an earlier formational period at higher

temperatures, followed by chlorite, with muscovite indicative of a later event at lower formational temperatures.

The north-eastern to southern region of TauTona Mine was noted to have a greater amount of pyrophyllite in the samples. In this portion of TauTona Mine a large fault zone, referred to as the Pretorius Fault Zone, extends across the area. The style of alteration (pyrophyllitic) may be as a direct result of the extreme amount of fluid flow that would have occurred as a result of the multiple faulting events within the area. The area in which chloritisation is noted to occur within the West Wits Line coincides with the presence of faulting and fewer intrusions such as dykes and sills. This suggests that the chloritisation within this area is due to the occurrence of fluid flow from smaller faulting events more than the occurrence of the intrusions. Sericitic alteration is noted to occur predominantly in areas that have abundant intrusions, with fewer fault occurrences. This suggests that sericitic alteration within this area is due to intrusions, with a minimal influence from faults.

In terms of an estimated timeline based on geothermometric techniques, the Pretorius Fault Zone occurred initially. The occurrence of predominantly (smaller) faulting with lesser intrusions suggests an intermediate timing, with the occurrence of predominantly intrusions and lesser faulting indicative of a later occurrence. Overall, this may indicate that the intrusions are younger than the faults across the West Wits Line.

When comparing the overall outcomes of each facies type, it appears that there is very little correlation to the type of alteration and associated gold grade. Higher gold grades are often seen occurring within an alteration zone alongside lower gold grades and therefore no particular alteration pattern can be assigned as occurring with higher gold grades. There also appears to be no relationship between the alteration type and carbon within a sample, but this may be due to organic matter affecting the spectral outcomes for the reef, as suggested by Hauff (2001, p.2). Carbon and uranium content noted within a sample by means of petrology and geochemical analyses are more reliable indicators of higher, or rather, more favourable gold grades within the Carbon Leader Reef than alteration mineralogy.

In terms of spectral scanning, the results can indicate the dominant mineral type and further suggest major alteration that has taken place based on the response of the sample to the feature extractions. A definite trend cannot be identified between gold grade, carbon content

and the spectral scanning outputs however the other methodologies used within this study correlate well with the spectral scanning data.

5 CONCLUSION

This research was intended to investigate alteration in the Carbon Leader Reef and to investigate the possible association of alteration and gold mineralisation.

Observations and outcomes following this research include:

(i) *Lateral changes in mineralogy of the hangingwall, footwall and Carbon Leader Reef units:*

- The variations in the mineralogy of the Carbon Leader Reef did not align fully with the Carbon Leader Reef facies and/or the Carbon Leader Reef estimation domain models used at the AngloGold Ashanti West Wits Line.
- A new Carbon Leader Reef facies model, specific to the West Wits Line, was proposed to include a No. 3 Facies sub-type. The No. 3 Facies sub-type included and was based on samples that did not align fully with the No. 3 Facies definitions (i.e. samples with a thin basal carbon seam and/or higher than average gold grades for the No. 3 Facies).
- The samples used within this research also indicated that the TauTona, Driefontein and Peggy estimation domains need to be re-evaluated and revised on a continuous basis as more information becomes available.
- In both the TauTona and Driefontein estimation domain discrepancies were noted with the alteration styles for several samples. Several samples within the Driefontein estimation domain were noted to have sericitic alteration however typically the Driefontein estimation domain is supposed to be pyrophyllite-rich. The TauTona estimation domain characteristically ranges from pyrophyllite dominant in the north-east area to chloritoid in the south-west area, however several samples in the current investigation were noted to have sericitic alteration.
- The discrepancies within the Peggy estimation domain arise from variations in gold grades. The purpose of the Peggy estimation domain is to separate higher gold grades from lower gold grades (i.e. should consist of intermediate gold grades)

however two samples in the current investigation were noted to have very high gold grades.

(ii) Changes in alteration assemblages of the hangingwall, footwall and Carbon Leader Reef units:

- Elevated amounts of pyrophyllite were noted within the hangingwall, footwall and Carbon Leader Reef units in the north-east to southern portions of TauTona Mine.
- Chloritisation as well as sericitic alteration was noted to occur south of TauTona mine and within the western region of the West Wits Line.
- Sericitic alteration was noted to occur across the same area as chloritisation however it was noted to extend further south than chloritisation as well as further north-east than both pyrophyllitic alteration and chloritisation.

(iii) An alteration model depicting three alteration zones, based on major alteration styles, was produced to better understand the alteration processes that have occurred:

- Although the data was limited across the West Wits Line area, definite alteration styles were noted to occur: pyrophyllitic alteration, chloritisation and sericitic alteration.
- The assignment of the style of alteration was done by means of combining the observations and findings across all the methodologies used for each sample.
- The pyrophyllitic alteration zone was identified to extend from the north-eastern to the southern portion of TauTona Mine. The zone of chloritisation extended across the West Wits Line from east to west and the sericitic alteration zone extended further south and further north-east as compared to the zone of chloritisation.
- The pyrophyllitic alteration zone was noted to coincide with the Pretorius Fault Zone in the north-eastern to southern region of TauTona Mine. The zone of chloritisation was noted to coincide with smaller, more frequent faults and fewer intrusions, and the sericitic alteration zone was noted to coincide with a frequent occurrence of intrusions with lesser faults.

(iv) An estimated timeline based on geothermometric techniques was proposed for the main alteration styles:

- It was suggested that the Pretorius Fault Zone predates the occurrence of the smaller and more frequent faulting events with fewer intrusions. Furthermore, it has

been suggested that intrusions and lesser faulting correspond to the youngest structural events in the region.

- Overall, this suggested that the intrusions are younger than the faults across the West Wits Line, with the Pretorius Fault Zone having occurred before the smaller faults and associated intrusions.

(v) *Uranium and carbon content within the Carbon Leader Reef are more reliable indicators of favourable gold grade than alteration styles across the West Wits Line:*

- Investigations into other reefs that are non-carbon bearing, such as the Ventersdorp Contact Reef, may yield different results.

(vi) *Spectral scanning cannot be used to accurately predict gold grade within the Carbon Leader Reef:*

- Spectral scanning is however able to determine alteration products and alteration intensities within the host rock as reliably as petrological and geochemical analyses can predict.
- Spectral scanning is less time-consuming and presents accurate results, also contributing to the easy identification of sedimentological contacts where macroscopic observations are not as obvious.

6 RECOMMENDATIONS

Due to the limitations in the number of borehole samples that have undergone spectral scanning an accurate alteration model for the AngloGold Ashanti West Wits Line Carbon Leader Reef could not be produced. More boreholes should be scanned to cover the entire area to be able to better understand the alteration within the area as well as to produce a reliable reference for alteration of the Carbon Leader Reef. Although both the TauTona and Savuka Mines have been placed on care and maintenance, Mponeng Mine is planned to mine the Carbon Leader Reef. As a result, a reliable alteration model may be useful in predicting gold grade variations.

Another recommendation would be to carry out a similar project with a focus on the Ventersdorp Contact Reef – a non-carbon bearing reef. The Ventersdorp Contact Reef is the primary gold-bearing reef mined at Mponeng Mine, and there are Ventersdorp Contact Reef

(borehole) intersections at Savuka and TauTona Mines that could be used to supplement the Mponeng data.

The borehole spectral images may be more useful in terms of covering several stratigraphic units at one time however the tombstone samples offer more detail. It is recommended that a study be carried out with tombstone samples only. The tombstone samples should be sent for geochemical as well as gold assay analyses. It was noted that the tombstone samples yielded higher grades than the borehole samples and it is possible that this is due to the locations of the tombstone samples and/or because the tombstone samples retain softer carbon (containing gold grains) in comparison to borehole core from high pressured diamond drilling where carbon material is likely to be washed out during the drilling process.

Although gold grade trends could not be determined from the spectral scanning results, spectral scanning offers a quicker option to investigate alteration in both borehole and tombstone samples. Should alteration prove to have a direct relation to gold grade, following on from the above recommended studies, spectral scanning would be an ideal tool to determine gold grade/economic value of stratigraphic units prior to mining (using exploration borehole core) and during mining (from collected tombstone samples).

In terms of the estimation domain and facies model that are currently implemented at AngloGold Ashanti's West Wits Line, the data suggests both models need to be re-evaluated and revised. Gold grades for the models are categorised into high, intermediate and low gold grades and gold values, however, there is no quantitative reference to work with i.e. no numerical ranges for the gold grades and gold values - this may have influenced the overall results. Regardless of the gold grades, the mineralogy and Carbon Leader Reef characteristics for each estimation domain and facies type need to be revised.

7 REFERENCES

ASD Inc., 2008. *TerraSpec® User Manual*. ASD Inc., Document 600541 Rev. G., pp. 72.

Agangi, A., Hofmann, A., Rollion-bard, C., Marin-carbonne, J., Cavalazzi, B., Large, R. and Meffre, S., 2015. *Gold accumulation in the Archaean Witwatersrand Basin, South Africa — Evidence from concentrically laminated pyrite*. Earth Science Reviews, **140**, 27–53.

Allan, G.C. and Woodcock, J.T., 2001. *A Review of the Flotation of Native Gold and Electrum*. Minerals Engineering, **14** (9), 931-962.

Amelio, L. and Amelio, A., 2018. Classification Methods in Image Analysis with a Special Focus on Medical Analytics, in: Tsihrintzis, G., Sotiropoulos, D.N., Jain, L.C. (Eds). *Machine Learning Paradigms,* Intelligent Systems. Reference Library 149, Chapter 3, Springer International Publishing, 31-70.

Barnicoat, A.C., Henderson, I.H.C., Knipe, R.J., Yardley, B.W.D., Napier, B.W., Fox, N.P.C., Kenyon, A.K., Muntingh, D.J., Strydom, D., Winkler, K.S., Lawrence, S.R. and Cornford, C., 1997. *Hydrothermal gold mineralization in the Witwatersrand Basin*. Letters to Nature, **386**, 820–824.

Beach, A. and Smith, R., 2007. Structural geometry and development of the Witwatersrand Basin, South Africa, in: Ries, A.C., Butler, R.W.H. and Graham, R.H. (Eds). *Deformation of the Continental Crust: The Legacy of Mike Coward*. Geological Society, London, Special Publications, **272**, 533–542.

Brown, A., Walter, M. and Cudahy, T., 2004. *Short-Wave Infrared Reflectance Investigation of Sites of Paleobiological Interest: Applications for Mars Exploration.* Astrobiology, **4**, 359–376.

Burke, E.A.J., 2001. *Raman microspectrometry of fluid inclusions*. Lithology and Mineral Resources, **55**, 139–158.

Burnett, R.J., Orton, R., Chola, D., Lavery, R.K. and Linton, P., 2015. Carbon Leader Reef Estimation Domain Model (unpubl.), in: *AngloGold Ashanti Limited: Carbon Leader Reef Geoscience Project 2015*, 1-54.

Clark, R.N., 1995. *Reflectance Spectra*. U.S. Geological Survey, 178–188.

Clark, R.N., 1999. Spectroscopy of Rocks and Minerals, and Principles of Spectroscopy, in: Rencz, A. (Ed.). *Remote Sensing for the Earth Sciences: Manual of Remote Sensing*, U.S. Geological Survey, **1**, 3–58.

Coetzee, D.S., van Reenen, D.D. and Roering, C., 1988. *Metamorphism and metamorphic fluids in thrust systems along the north-west rim of the Witwatersrand Basin* (Abstract). Geological Society of South Africa, 109-112.

Coetzee, D.S., van Reenen, D.D. and Roering, C., 1995. *Quartz vein formation, metamorphism, and fluid inclusions associated with thrusting and bedding-parallel shear in the Witwatersrand quartzites, South Africa*. South African Journal of Geology, **98** (4), 371-381.

Crósta, A.P., 2010. Unveiling Mineralogical Information in Ore Deposits: the Use of Reflectance Spectroscopy for Mineral Exploration in South-America, in: *Proceedings of ASD and IEEE GRS; Art, Science and Applications of Reflectance Spectroscopy Symposium*, 1–20.

Dalm, M. and Buxton, M.W.N., 2018. *Ore-Waste Discrimination in Epithermal Deposits Using Near-Infrared to Short-Wavelength Infrared (NIR-SWIR) Hyperspectral Imagery*. Mathematical Geosciences, **Special Issue**, 1-27.

Depiné, M., Frimmel, H.E., Emsbo, P., Koenig, A.E. and Kern, M., 2013. *Trace element distribution in uraninite from Mesoarchaean Witwatersrand conglomerates (South Africa) supports placer model and magmatogenic source.* Mineralium Deposita, **48**, 423–435.

Drennan, G.R, Boiron, M.-C., Cathelineau, M. and Robb, L.J., 1999. *Characteristics of post-depositional fluids in the Witwatersrand Basin.* Mineralogy and Petrology, **66**, 83-101.

Drennan, G.R. and Robb, L.J., 2006. T*he nature of hydrocarbons and related fluids in the Witwatersrand Basin, South Africa: Their role in metal redistribution*. Geological Society of America Special Paper, **405**, 353–385.

England, G.L., Rasmussen, B., Krapež, B. and Groves, D.I., 2001. *The Origin of Uraninite, Bitumen Nodules, and Carbon Seams in Witwatersrand-Gold-Uranium-Pyrite Ore Deposits, Based on a Permo-Triassic Analogue*. Economic Geology, **96**, 1907-1920.

Fletcher, P., 2009. The Carbon Leader Reef (unpubl.), in: *AngloGold Ashanti Limited: TauTona Company Report 2009*, 1–30.

Frimmel, H.E., 1994. *Metamorphism of Witwatersrand Gold*. Exploration and Mining Geology, **3**, 1–16.

Frimmel, H.E., 1997a. *Chlorite Thermometry in the Witwatersrand Basin: Constraints on the Paleoproterozoic Geotherm in the Kaapvaal Craton, South Africa*. The Journal of Geology, **105**, 601-615.

Frimmel, H.E., 1997b. *Detrital origin of hydrothermal Witwatersrand gold - a review*. Terra Nova, **9**, 192–197.

Frimmel, H.E., 2014. *A Giant Mesoarchean Crustal Gold-Enrichment Episode: Possible Causes and Consequences for Exploration*. Society of Economic Geologists, Special Publication, **18**, 209–234.

Frimmel, H.E., Groves, D.I., Kirk, J., Ruiz, J., Chesley, J. and Minter, W.E.L., 2005. *The Formation and Preservation of the Witwatersrand Goldfields, the World's Largest Gold Province.* Economic Geology, **100th Anniversary**, 769–797.

Frimmel, H.E., Hallbauer, D.K. and Gartz, V.H., 1999. *Gold mobilizing fluids in the Witwatersrand Basin: composition and possible sources.* Mineralogy and Petrology, **66**, 55–81.

Frimmel, H.E. and Hennigh, Q., 2015. *First whiffs of atmospheric oxygen triggered onset of crustal gold cycle.* Mineralium Deposita, **50**, 5-23.

Frimmel, H.E. and Minter, W.E.I., 2002. *Recent Developments Concerning the Geological History and Genesis of the Witwatersrand Gold Deposits, South Africa*. Society of Economic Geologists, Special Publication, **9**, 17–45.

Fuchs, S., Williams-Jones, A.E., Jackson, S.E. and Przybylowicz, W.J., 2016. *Metal distribution in pyrobitumen of the Carbon Leader Reef, Witwatersrand Supergroup, South Africa: Evidence for liquid hydrocarbon ore fluids*. Chemical Geology, **426**, 45-59.

Gamby, A.N. and Katajainen, J., 2018. *Convex-Hull Algorithms: Implementation, Testing and Experimentation.* Algorithms, **11** (195), 1-28.

Gibson, M.A.S., Jolley, S.J. and Barnicoat, A.C. (2000). *Interpretation of the Western Ultra Deep Levels 3-D seismic survey.* South African Geophysical Association: The Leading Edge, 730-735.

Graton, L.C., 1930. *Hydrothermal origin of the Rand gold deposits. Part I: Testimony of the conglomerates*. Economic Geology, **25**, 1–185.

Grove, D. and Harris, C., 2010. *O- and H-isotope study of the Carbon Leader Reef and implications for the origin and evolution of Witwatersrand Basin fluids.* South African Journal of Geology, **113**, 73–86.

Guy, B.M., Beukes, N.J. and Gutzmer, J., 2010. *Paleoenvironmental controls on the texture and chemical composition of pyrite from non-conglomeratic sedimentary rocks of the Mesoarchean Witwatersrand Supergroup, South Africa*. South African Journal of Geology, **113**, 195–228.

Guy, B.M., Ono, S., Gutzmer, J., Lin, Y. and Beukes, N.J., 2014. *Sulfur sources of sedimentary " buckshot " pyrite in the Auriferous Conglomerates of the Mesoarchean Witwatersrand and Ventersdorp Supergroups , Kaapvaal Craton , South Africa*. Mineralium Deposita, **49**, 751–775.

Hauff, P.L., 2001. *Alteration Mineralogy of Alberta Kimberlites : PIMA Infrared Spectroscopic Analysis.* Alberta Geological Survey, Special Report, **12**, 1–74.

Hayward, C.L., Reimold, W.U., Gibson, R.L. and Robb, L.J., 2005. Gold mineralization within the Witwatersrand Basin, South Africa: evidence for a modified placer origin, and the role of the Vredefort impact event, in: McDonald, I., Boyce, A.J., Butler, I.B., Herrington, R.J. and Polya, D.A. (Eds.). *Mineral Deposits and Earth Evolution*. Geological Society, London, Special Publications, **248**, 31–58.

Harris, A.T., 2006a. *Spectral Mapping Tools from the Earth Sciences Applied to Spectral Microscopy Data*. International Society for Analytical Cytology, **69A**, 872-879.

Harris, P., 2006b. *Hyperspectral Core Imager: Processing Solution Operational System* (unpubl.). Anglo Operations Limited, 1-282.

Harris Geospatial Solutions, 2018a. *Decorrelation Stretch* (Online). Available at https://www.harrisgeospatial.com/docs/DecorrelationStretch.html (Accessed 20 February 2019).

Harris Geospatial Solutions, 2018b. *Hyperspectral Analysis: SAM and SFF Tutorial* (Online). Available at https://www.harrisgeospatial.com/docs/Whole-Pixel_Hyperspectral_Analysis_Tutorial.html (Accessed 14 February 2019).

Harris Geospatial Soultions, 2018c. *Recovering the continuum curve from the Continuum Removal process* (Online). Available at https://www.harrisgeospatial.com/Support/Maintenance-Detail/ArtMID/13350/ArticleID/19643/1826 (Accessed 14 February 2019).

Heinrich, C.A., 2015. *Witwatersrand gold deposits formed by volcanic rain, anoxic rivers and Archean life.* Nature Geoscience, **83** (3), 206-209.

Hutchinson, R.W. and Viljoen, R.P., 1987. *Re-evaluation of gold source in Witwatersrand ores.* South African Journal of Geology, **91**, 157–173.

In-house Report, 1998. *Module 12: Underground Geological and Cover Drilling* (unpubl.). AngloGold Geology Department, 1-14.

In-house Report, 2004a. *The 2004 Carbon Leader Reef geological model* (unpubl.). TauTona Mine Geology Department of AngloGold Ashanti Limited, 1-25.

In-house Report, 2004b. *Exploration Geochemistry: General protocols and procedures* (unpubl.). Quality control and Standards in Gold Exploration of AngloGold Ashanti Limited, 1-35.

In-house Report, 2008. *Mineral Resource Statement* (unpubl.). TauTona Mine Geology Department of AngloGold Ashanti Limited, 1-20.

In-house Report, 2017. *Current Carbon Leader Reef Facies Locations* (unpubl.). TauTona Mine Geology Department of AngloGold Ashanti Limited, 1.

Janisch, P.R., 1986. *Gold in South Africa*. Journal - South African Institute of Mining and Metallurgy, **86**, 273–316.

Jolley, S.J., Freeman, S.R., Barnicoat, A.C., Phillips, G.M., Knipe, R.J., Pather, A., Fox, N.P.C., Strydom, D., Birch, M.T.G., Henderson, I.H.C. and Rowland, T.W., 2004. *Structural controls on Witwatersrand gold mineralisation.* Journal of Structural Geology, **26**, 1067–1086.

Jolley, S.J., Henderson, I.H.C., Barnicoat, A.C. and Fox, N.P.C., 1999. Thrust-fracture network and hydrothermal gold mineralization: Witwatersrand Basin, South Africa, in: McCaffrey, K. J. W., Lonergan, L. and Wilkinson, J. J. (Eds.). *Fractures, Fluid Flow and Mineralization.* Geological Society, London, Special Publications, **155**, 153–165.

Jones, R.S. and Fleischer, M., 1969. *Gold in Minerals and the Composition of Native Gold.* U.S. Geological Survey Circular, **612**, 1-17.

Kao, T.C. and Knott, G.D., 1990. *An efficient and numberically correct algorithm for the 2D convex hull problem*. BIT Numerical Mathematics, **30** (2), 311-331.

Kerr, A., Rafuse, H., Sparkes, G., Hinchey, J. and Sandeman, H., 2011. *Visible/Infrared Spectroscopy (VIRS) as a research tool in Economic Geology: Background and Pilot Studies from Newfoundland and Labrador.* Geological Survey, **11**, 145–166.

Kositcin, N. and Krapež, B., 2004. *Relationship between detrital zircon age-spectra and the tectonic evolution of the Late Archaean Witwatersrand Basin, South Africa.* Precambrian Research, **129**, 141–168.

Koglin, K., Frimmel, H., Minter, W. and Brätz, H., 2010. *Trace-element characteristics of different pyrite types in Mesoarchaean to Palaeoproterozoic placer deposits*. Mineralium Deposita, **45** (3), 259-280.

Kruse, F.A., Lefkoff, A.B., Boardman, J.W., Heidebrecht, K.B., Shapiro, A.T., Barloon, P.J. and Goetz, A.F.H., 1993. *The Spectral Image Processing System (SIPS) - Interactive Visualisation and Analysis of Imaging Spectrometer Data*. Remote Sensing of Environment, **44**, 155-163.

Law, J.D.M. and Phillips, G.N., 2005. *Hydrothermal Replacement Model for Witwatersrand Gold*. Society of Economic Geologists, **100th Anniversary**, 1–12.

Malvern Panalytical Ltd., 2019. *ASD TerraSpec® 4 Hi-Res Mineral Spectrometer* (Online). Available at https://www.malvernpanalytical.com/en/products/product-range/asd-range/terraspec-range/terraspec-4-hi-res-mineral-spectrometer (Accessed 16 February 2019).

Mathur, R., Gauert, C., Ruiz, J. and Linton, P., 2013. *Lithos Evidence for mixing of Re – Os isotopes at <2.7 Ga and support of a remobilized placer model in Witwatersrand sulfides and native Au.* Lithos, **164-167**, 65–73.

McCarthy, T.S., 1994. *The tectono-sedimentary evolution of the Witwatersrand Basin with special reference to its influence on the occurrence and character of the Ventersdorp Contact Reef - A review.* South African Journal of Geology, **97**, 247–259.

McCarthy, T.S., 2006. *A revised stratigraphic framework for the Witwatersrand Supergroup, in: South African Committee for Stratigraphy: Lithostratigraphic Series, No. 42*, 1–7.

Meier, D.L., Heinrich, C.A.and Watts, M.A., 2009. *Mafic dikes displacing Witwatersrand gold reefs : Evidence against metamorphic-hydrothermal ore formation*. Geology, **37**, 607–610.

Mellor, E.T., 1916. *The conglomerates of the Witwatersrand*. Transactions of the Institution of Mining and Metallurgy, **25**, 226–348.

Mielke, C., Boesche, N.K., Rogass, C., Kaufmann, H. and Gauert, C., 2015. *New geometric hull continuum removal algorithm for automatic absorption band detection from spectroscopic data*. Remote Sensing Letters, **6** (2), 97-105.

Mossman, D.J., Minter, W.E.L., Dutkiewicz, A., Hallbauer, D.K., George, S.C., Hennigh, Q., Reimer, T.O. and Horscroft, F.D., 2008. *The indigenous origin of Witwatersrand "carbon".* Precambrian Research, **164**, 173–186.

Mossman, D.J., Reimer, T.O. and Durstling, H., 1999. *Microbial processes in gold migration and deposition: modern analogues to ancient deposits.* Geoscience Canada, **26**, 131–140.

Muller, C., 1991. The Occurrence of Carbon in the Carbon Leader Reef and some important considerations, in: *Gold Fields Oberholzer Geological Centre (Sedimentology Unit)* Reference: 990/29/73/SED, 61–64.

Murphy, R.J., 2015. *Evaluating simple proxy measures for estimating depth of the ~ 1900 nm water absorption feature from hypersepctral data acquired under natural illumination*. Remote Sensing of Environment, **166**, 22-33.

Murphy, R.J., Taylor, Z., Schneider, S. and Nieto, J., 2015. *Mapping clay minerals in an open-pit mine using hyperspectral and LiDAR data*. European Journal of Remote Sensing, **48** (1), 511-526.

Nesse, D., 2000. *Introduction to Mineralogy*. Oxford University Press: New York, pp. 442, 251-252; 356–376.

Nwaila, G., Frimmel, H.E. and Minter, W.E.L. (2017). *Provenance and Geochemical Variations in Shales of the Mesoarchean Witwatersrand Supergroup.* The Journal of Geology, **125**, 399-422.

Phillips, G.N., 1988. *Widespread fluid infiltration during metamorphism of the Witwatersrand goldfields: generation of chloritoid and pyrophyllite*. Journal of Metamorphic Geology, **6**, 311-332.

Phillips, G.N. and Powell, R., 2011. *Origin of Witwatersrand gold : a metamorphic devolatilisation – hydrothermal replacement model.* Applied Earth Science, **120**, 112–129.

Phillips, G.N. and Powell, R., 2015. *Hydrothermal alteration in the Witwatersrand goldfields*. Ore Geology Reviews, **65**, 245–273.

Phillips, N.G. and Law, J.D.M., 1994. *Metamorphism of the Witwatersrand gold fields: A review*. Ore Geology Reviews, **9**, 1–31.

Phillips, N.G. and Law, J.D.M., 2000. *Witwatersrand Gold Fields: Geology, Genesis, and Exploration.* Society of Economic Geologists Review, **13**, 439–500.

Robb, L.J., 2005. *Introduction to Ore-Forming Processes.* Blackwell Publishing Company: Oxford, 159-174.

Robb, L.J. and Robb, V.M., 1998. Gold in the Witwatersrand Basin, in: Wilson, M.G.C. and Anhaeusser, C.R. (Eds.).*The Mineral Resources of South Africa.* Council for Geoscience Handbook 16. Coucil for Geoscience, Pretoria, 294–349.

Sigernes, F., Syrjäsuo, M., Storvold, R., Foruna, J., Grøtte, M.E., and Johansen, T.A., 2018. *Do it yourself hyperspectral imager for handheld to airborne operations*. Optics Express, **26** (5), 1-15.

Simanovich, I.M., 2009. *Auriferous Precambrian conglomerates of Witwatersrand*. Lithology and Mineral Resources, **44**, 497–509.

Specim Spectral Imaging Ltd., 2013. sisuROCK® Datasheet, in: *Specim sisuROCK®*, 1-2.

Specim Spectral Imaging Ltd., 2015. sisuROCK® Overview, in: *Specim Sisu Systems,* 1–4.

Tappert, M.C., and Tappert, R., 2018. *Novel exploration tools: Using reflectance spectroscopy to detect hydation halos around kimberlites*. Northwest Territories Geological Survey - NWT Open Report 2018, **12**, 1-39.

The MathWorks Inc., 2005. *Image Processing Toolbox User's Guide* (Online). Available at https://www.mathworks.com/help/images/ (Accessed 20 February 2019).

Thompson, A.J.B., Hauff, P.L. and Robitaille, A.J., 1999. *Alteration Mapping in Exploration: Application of Short-Wave Infrared (SWIR) Spectroscopy.* Society of Economic Geologists (October), 15–27.

Tucker, R.F, Viljoen, R.P. and Viljoen, M.J., 2016. *A Review of the Witwatersrand Basin - The World's Greatest Goldfield.* Episodes: International Journal of Geosciences, **39** (2), 105–133.

van der Meer, F., 2004. *Analysis of spectral absorption features in hyperspectral imagery.* International Journal of Applied Earth Observation and Geoinformation, **5**, 55-68.

Vidal, O., Baldeyrou, A., Dubac, B., DeAndrade, V., Jullien, M. and Lanson, B., 2007. *Thermodynamics of pyllosilicates and low temperature thermometry*. Seminarios SEM, **3**, 75-84.

Warnsloh, J.M., 2015. TriAngle: A Microsoft Excel™ spreadsheet template for the generation of triangular plots. Journal of Mineralogy and Geochemistry, **192** (1), 101-105.

Zhang, G., Wasyliuk, K.E.N. and Pan, Y., 2001. *The Characterization and Quantitative Analysis of Clay Minerals in the Athabasca Basin, Saskatchewan: Application of Shortwave Infrared Reflectance Spectroscopy.* The Canadian Mineralogist, **39**, 1347–1363.

8 APPENDICES